UNIVERSITY OF COPENHAGEN
FACULTY OF SCIENCE

Master's Thesis

Kasper Ejdal Lund

Quantum Gates in Photonic Waveguides

Academic advisor: Anders S. Sørensen

Submitted: 30/09/2016

"Imagination is the Essence of Discovery"

Abstract

The field of quantum information is concerned with investigating the possibilities of using quantum phenomena for computational and communication purposes by using the sometimes counter intuitive behaviour of system described by quantum mechanics. This is a tremendous challenge, primarily due to the quantum systems' tendency to interact with the environment. Shielding these systems is thus an important part of the practical implementation of quantum technologies and this remains an active field of research within the field.
Quantum information systems are described by the qubit states $|0\rangle$ and $|1\rangle$ and can be formed in a linear superposition of these states, which is one of the main reasons for the strength of quantum information protocols. An important part in implementing quantum information protocols is to implement a two qubit gate, which is a controlled evolution of two coupled quantum states that are coupled together. This coupling is often mediated by some other physical entity (such as a propagating photon in a waveguide). One such gate in the *controlled phase gate*, which imprint a change of phase of $e^{-i\pi}$ onto the state where both qubits are in $|1\rangle$ but otherwise leaves the system unchanged. This thesis is concerned with investigating the possibilities of implementing a controlled phase gate using self-assembled quantum dot embedded in a nanophotonic waveguide.

This thesis provides a proposal to implement a controlled phase gate by using a strong interaction between three quantum dots. Two of these dots constitute the qubit, while the third auxiliary emitter is used to herald the gate. It is possible to control the dynamical change of phase of the qubits by illuminating the auxiliary quantum dot with a weak laser field. This will project the auxiliary quantum dot into a definite state, due to the nature of the dynamics. The primary source of error will project the auxiliary into another state; it is thus possible to check whether the gate has succeeded ot not by measuring the state of the auxiliary emitter, giving the gate an integrated error detection.
This thesis will report in a method to obtain a unity fidelity for this controlled phase gate and will report on the behaviour of the success probability. In addition, errors induced by variations in the physical parameters of the quantum dots are discussed and methods of mitigating these errors are presented.

Resumé

Mulighederne for at udnytte de til tider besynderlige kvantemekaniske fænomener til at udføre beregningsmæssige protokoller og for at implementere sikre kommunikationslinjer er nogle er de store mål inden for kvanteinformation. Dette er en besværlig opgave, da kvantemekaniske systemer har en tendens til at koble til diverse omgivelser. Det er derfor nødvendigt at beskytte disse systemer, og dette er en af hovedopgaverne inden for feltet.
Inden for kvanteinformation bliver fysiske tilstande beskrevet af qubit tilstandene $|0\rangle$ og $|1\rangle$. Disse systemer kan endda være i de såkaldte superpositioner, hvilket er en af grundene til styrken ved kvantemekaniske informationsprotokoller. Implementeringen af en to-qubit gate er en vigtig del ved udførslen af disse protokoller og er typisk udført ved at udnytte anden fysisk proces (for eksempel en photon, der bevæger sig fra en kvantemekanisk enhed til en anden) til at koble to systemer sammen. Disse gates er en kontrolleret tidlig udvikling af de kvantemekaniske systemer. Den *kontrollerede fase gate* er en vigtig to-qubit gate, som kan give en ændring af fasen af den bestemte tilstand, hvor begge qubits er i $|1\rangle$, og som ellers ikke ændrer systemet. Denne afhandling undersøger mulighederne for at implementere denne slags gate i et system bestående af tre groede kvantedots i en nanofotonisk bølgeleder.

Denne afhandling giver et forslag til udførslen af en kontrolleret fase gate ved at bruge en stærk kobling mellem tre kvantedots. To af disse dots bliver bruge til at lave de to qubits, mens at den trejde bruges til at styre gaten. Det er muligt at styre udviklingen af den tidligt udviklende ændring i fasen af de to qubits ved at belyse den såkaldte "hjælpemotor"med en svag laser, hvorved hjælpemotoren bliver projekteret ind i en bestemt tilstand. De primære fejlkilder for gaten vil derimod projektere hjælpemotoren hen i en anden tilstand. Det er dermed muligt at tjekke, om hvorvidt gaten har givet det korrekte output eller ej ved at måle på tilstanden af hjælpemotoren. Det giver dette forslag en integreret fejlsøgning.
Denne afhandling rappoterer en metode til at opnå en fidelity på 1 for den kontrollerede fase gate og vil desuden diskutere den resulterende opførsel af sandsynligheden for succes. Diverse variationer i de fysiske parameter kan opstå, når kvantedotsne bliver groet, og disse variationer kan have indflydelse på præstationen af gaten. Denne afhandling vil derfor også undersøge hvordan fidelitien of sandsynligheden for succesafhænger af disse variationer, og om der er muligt at minimere eller fjerne disse fejl.

Acknowledgements

I would first of all like to thank my supervisor Anders S. Sørensen for his invaluable help and guidance throughout this project, without which this project would not have been possible. To this end, I would also like to thank Sahand Mahmoodian for the plentiful and thoughtful discussions during this last year and for being willing to discuss my ideas and findings. Both have helped to steer me in the proper direction and have always been ready to give their helpful input.
In addition, I would like to thanks the rest of the Theoretical Quantum Optics Group for letting me tag along for the last year and it has been fascinating to listen to their presentations at the group meetings. Special thanks go to Luca, Sasha and Julia for their help in preparation to, and during, the DHL relay.
It has been fascinating to be part of the Quantum Optics and to get a taste of working with an active research field. I have enjoyed the friendly atmosphere that exists amongst the different groups, whether it has been through the cosy coffee breaks in the lounge, the friendly rivalry that exists for the DHL relay or the Christmas dinner.
I also want to thank the USG cross fit group for all the great sessions in the gym, which has helped me stay fit and focused for the duration of this thesis.
Lastly, I want to thank my parents and family for the support throughout the year.

Contents

List of Figures

Chapter 1

Introduction

The processing, storage and transmission of information have been a cornerstone of society throughout human history. This can be traced as far back as to the early Mesopotamian civilizations (most notably the Sumerian civilization) at 3600 BC who developed the first writing system to keep track of manufacturing and agricultural goods and for use in trading [19]. The advent of computers (analogue versions from the early 20th century and digital in the post war period) and modern cryptography heralded the modern information age and has allowed several fields to rapidly advance. Science has greatly benefited from using numerical simulation on digital computers, whereas society at large depend on modern communication methods and security protocols (e.g. the RSA protocol).

All of this has been accomplished by classical information theory which can be readily implemented using, in principle, simple physical systems (such as a voltage running through a capacitor for a digital computer) but these implementations face several challenges. Several problems, such as the travelling salesman and the factorization into prime numbers, are classified as computational hard. This means that the required time to solve these problems grows exponentially, whereas the solution for easy problems grow polynomial in time. The aforementioned RSA protocol is heavily dependent on this property. Note that is has not been proved that a classical and polynomial-time based solution for these problems do not exist.
It is possible to define a classical and completely secure encryption method. This is called the one-time pad method: Alice wants to send a message to Bob. To do this Alice writes her message as a sequence of binary numbers m and generates another sequence of binary number k through an ideal random number generator. This second sequence is called the key and is added (modulo two) to the message to scramble the information: $s = m \oplus k$. Alice then sends the message to Bob who can decrypt the message by adding the key again: $m = s \oplus k$. This has proven to be completely secure [12] but there exist certain constraints. Firstly, each key can only be used once, otherwise it is possible for eavesdroppers to extract information from various messages. This limits the use of this scheme for only extremely important uses. Secondly, Alive and Bob need to have a method for sharing the secret key. The only classically key distribution method is a trusted man with a suitcase, which may not be feasible.
Yet another example is simulation of quantum systems. Nature is, at the smallest length scales, governed by quantum mechanics. This includes collective effects like magnetism and superconductivity. Numerical simulation has proven to be an important tool in examining classical and small quantum systems but has difficulty in treating large quantum systems. This is due to the exponential increase in the number of parameters with the number of particles.

Lastly, there is a technological problem: Moors' law has a limit. The basic building block of any integrated circuit is the transistor. These transistors can be made on smaller dimensions as technology progresses, which allows integrated chips to include more and more transitions per square inch. This increase in number of transistors was first observed in 1965 by Intel co-founder Gordon Moore, who observed an exponential increase in the number of transistors per square inch on integrated circuits [15]. This poses a problem when these small structures begin to be governed by quantum mechanics. One such effect is tunneling, which allows particle to penetrate classically impassable potential barriers.
Classical computers operate with discrete *bits*, which are represented as the binary numbers 0 and 1. Bits can be physically implemented by various means and the most common example is the presence (the number 1) or absence (the number 0) of an electron in a circuit. There are fewer electrons per square inch of the chips as the components become smaller, which causes the probabilistic effect of tunneling to become apparent through its ability to change a bit from 0 to 1 (or vice versa). This is a non-deterministic change to the logical state of an operation, which can lead to computational errors, as classical algorithms assumes that classical bits are unchanged unless explicitly operated on.
This highlights the need to be able to control these quantum effects in order to mitigate the induced errors. Alternatively, it may be possible to use quantum effects for advanced problems. In fact, several advances has already been made in the field of *Quantum Information* and there exists theoretical proposals to solve classically hard problems(e.g. Shor's factorisation algorithm, quantum key distribution and quantum simulation [10].

This thesis focuses on a specific and crucial part of implementing a quantum computer: a heralded two-qubit controlled phase gate, where the qubits are represented by ground states in self-assembled quantum dots embedded in a nano-photonic wave guide. This is based on a recent proposal by Borregaard et al. [3], where the gate was implemented using three atoms in a cavity. This resulted in a CZ-gate with the possibility of attaining a unity fidelity. In addition, the gate has an integrated error detection, as a successful operation will project an auxiliary atom into a definite state, will a failed operation projects it into another state. The success, or failure, of the gate can be readily determined by measuring the state of the auxiliary atom without disturbing the state of the qubit. This work examines the possibilities of implementing this scheme in a system comprised of three self-assembled quantum dots embedded in a nanophotic crystal.
The main contributions of this work are:

- A theoretical description of the decay dynamics for several emitters coupled in a single-mode wave guide (Chapter (4)).
- A detailed calculation of the derivation of the success probability and the fidelity a heralded two-qubit controlled phase gate (Chapter (5)).
- The effects of changing various physical parameters, namely the dipole moments and positions of the qubits, on the success probability and the fidelity (Chapter (6)).

The outline of the thesis is

Chapter 1: (This chapter). This presents the motivation and objectives of this thesis.

Chapter 2: Provides a brief introduction to basic concepts of quantum mechanics and quantum information.

Chapter 3: Contains an introduction to the physical system under consideration in thus thesis. These systems are self-assembled quantum dots and photonic crystals.

Chapter 4: This gives a derivation of the decay dynamics of three coupled quantum emitters embedded in a photonic crystal waveguide.

Chapter 5: The dynamics of the three coupled quantum dots are derived and are used to implement a controlled phase gate. In addition, the success probability and fidelity is derived for the ideal case.

Chapter 6: The effects of changing the physical parameters of the qubit states are examined and methods for mitigating the detrimental effects on the fidelity of the gate are provided.

Chapter 7: Concludes on this work and provides an outlook for further research on this topic.

Chapter 2

Quantum Mechanics & Quantum Information

A system described by quantum mechanics can exhibit properties otherwise thought impossible by the laws of classical physics. This includes effects like quantum parallelism and entanglement and may be useful for information and computation purposes ([11]). This section will provide a basic introduction to concepts from quantum mechanics (Section (2.1)) and to the field of quantum information (Section (2.2)). This section is primarily based on [17] unless otherwise noted.

2.1 Basics of Quantum Mechanics

2.1.1 States

The complete description of a physical system is contained in a *state vector* $|\psi\rangle$ defined in the Hilbert space $\mathcal{H}$. This is a vector space over the complex numbers $\mathbb{C}$; it maps the inner product $\langle\phi|\psi\rangle$ between two states $|\psi\rangle$ and $|\phi\rangle$ to $\mathbb{C}$ with the following properties:

- Positivity: $\langle\phi|\psi\rangle \geq 0$.
- Linearity: $\langle\phi| \left(a\,|\psi_2\rangle + b\,|\psi_2\rangle\right) = a\,\langle\phi|\psi_1\rangle + b\,\langle\phi|\psi_2\rangle$.
- Skew symmetry: $\langle\phi|\psi\rangle = \langle\psi|\phi\rangle^*$.

Additionally, the Hilbert space is complete in its norm: $\|\psi\| = \langle\psi|\psi\rangle^{1/2}$. Any state can be expanded in the orthonormal basis states $|\{n\}\rangle$ spanned by the Hilbert space:

$$|\psi\rangle = \sum_n |n\rangle\,\langle n|\psi\rangle\,, \tag{2.1}$$

where $\langle n|\psi\rangle = c_n$ is the *expansion coefficient* c_n for the projection of $|\psi\rangle$ along $|n\rangle$. A normalised state $|\tilde{\psi}\rangle$ can be formed from $|\psi\rangle$ by

$$|\tilde{\psi}\rangle = \frac{1}{\sqrt{\langle\psi|\psi\rangle}}\,|\psi\rangle\,, \tag{2.2}$$

such that $\langle\tilde{\psi}|\tilde{\psi}\rangle = 1$. The norm of $|\psi\rangle$ can be found from Eq. (2.1):

$$\langle\psi|\psi\rangle = \sum_n |\langle n|\psi\rangle| = \sum_n |c_n|^2\,, \tag{2.3}$$

using that $|\{n\}\rangle$ is an orthonormal basis with the inner product $\langle n|n'\rangle = \delta_{n,n'}$. If $|\psi\rangle$ is a normalised state, then $\sum_n |c_n|^2 = 1$. This result is important for the statistical interpretation of quantum mechanics introduced below.

2.1.2 Observables and Measurement

An observable is a physical entity that can be measured and is represented by a self-adjoint (this is also denoted as hermitian) operator. An operator $\hat{M}$ is a linear map that takes vectors to vectors:

$$\hat{M} : |\psi\rangle \to \hat{M}\,|\psi\rangle\,, \quad \hat{M}\,(a\,|\psi\rangle + b\,|\phi\rangle) = a\hat{M}\,|\psi\rangle + b\hat{M}\,|\phi\rangle\,. \tag{2.4}$$

The adjoint $\hat{M}^\dagger$ of an operator is defined by:

$$\langle\phi|\hat{M}\psi\rangle = \langle\hat{M}^\dagger\phi|\psi\rangle\,, \tag{2.5}$$

for all vectors $|\psi\rangle\,, |\phi\rangle$. A hermitian operator satisfies $\hat{M} = \hat{M}^\dagger$, leading to the following property for $\hat{M}$: $\langle\phi|\hat{M}|\psi\rangle = \langle\psi|\hat{M}|\phi\rangle^*$, forming a real vector space. A measurement is a process where information about the system is gained; more specifically, information about the observable $\hat{M}$ is acquired and is represented by the real numbered *expectation value*:

$$\langle\hat{M}\rangle = \langle\psi|\hat{M}|\psi\rangle\,. \tag{2.6}$$

Any hermitian operator defined in A Hilbert space is diagonalisable, where its eigenstates form a complete orthonormal basis in $\mathcal{H}$. The operator can then be written in terms of the basis states $|\{n\}\rangle$ and its eigenvalues M_n by:

$$\hat{M} = \sum_n M_n\,|n\rangle\,\langle n|\,, \tag{2.7}$$

where $\hat{M}\,|n\rangle = M_n\,|n\rangle$. Writing $|\psi\rangle$ in terms of these basis states by Eq. (2.1) causes the expectation value to take the following form:

$$\langle\hat{M}\rangle = \sum_n M_n\,|c_n|^2\,, \tag{2.8}$$

where $|c_n|^2 = p_n$ is the probability to obtain the n'th eigenstate of $\hat{M}$ upon repeating the same measurement on a number of identically prepared systems. This statistical interpretation carries over to the state written in Eq. (2.1), highlighting one of the main differences between classical and quantum physics. According to the complimentary principle, the actual state of the system is in a superposition of the basis states $|\{n\}\rangle$ with a probability of measuring it in the n'th state of $|c_n|^2$. Only after a measurement can the state be said to be in a definite state, as it is projected into:

$$|\psi\rangle_{\text{After}} = \frac{M_n\,|n\rangle}{\|M_n\,|n\rangle\,\|}. \tag{2.9}$$

Repeated measurements will always return this state with probability 1. This interpretation of a quantum state provide the starting point of realising the strengths of quantum information processes and will be discussed in further detail in Section (2.2.2).

2.1.3 Time Evolution

The time evolution of physical systems remains important in the quantum mechanical formalism. The description of dynamics can be particularly involved when both the quantum states, the operators and the Hamiltonian depend on time; a variety of methods has thus been developed to solve this problem. The main methods (or pictures, as they are often referred to) are briefly discussed here. Note that the following assumes that there is no source of loss in the system; section Eq. (2.1.4) introduces the necessary corrections in the the presence of loss.

The Schrödinger Picture

The treatment of time evolution is simple if the Hamiltonian and operators are independent of time; all time dependence is thus only containing the in state vectors $|\psi(t)\rangle$. The time evolution is then governed by the Schrödinger equation:

$$i\hbar\frac{\mathrm{d}}{\mathrm{d}t}|\psi(t)\rangle = \hat{H}|(t)\rangle, \tag{2.10}$$

with the formal solution:

$$|\psi(t)\rangle = e^{-i\hat{H}t/\hbar}|\psi(t=0)\rangle, \tag{2.11}$$

where $\hat{U}(t) = e^{-i\hat{H}t/\hbar}$ is a *unitary* operator that evolves the state $|\psi(t=0)\rangle$ into $|\psi(t)\rangle$. It may often be more useful to collect all time evolution in the operators while leaving the state vectors stationary in time. This can be done in the Heisenberg picture;

The Heisenberg Picture

As stated above, the idea of the Heisenberg picture is to have all time evolution contained in the operators of the system, while the Hamiltonian and state vectors are independent in time. This can be accomplished by considering the expectation value of some operator $\hat{M}$ at time t (the factor of $\hbar$ has been omitted from the exponential function for brevity in the following):

$$\langle\psi(t)|\hat{M}|\psi(t)\rangle = \left\langle\psi_0 e^{iHt}\right|\hat{M}\left|e^{-iHt}\psi_0\right\rangle = \langle\psi_0|\hat{M}(t)|\psi_0\rangle, \tag{2.12}$$

where $|\psi_0\rangle = |\psi(t=0)\rangle$ and $\hat{M}(t) = e^{iHt}\hat{M}e^{-iHt} = \hat{O}^\dagger(t)\hat{M}\hat{O}(t)$. $\hat{O}(t) = e^{-i\hat{H}t}$ is a unitary operator that transforms the ssytem from the Schrödinger picture to the Heisenberg picture. Note that the operator $\hat{M}(t)$ is not the same operator as $\hat{M}$ in this formalism. The relevant equation of motion for $\hat{M}(t)$ can be straightforwardly derived:

$$\dot{M}(t) = i\left[\hat{H}, \hat{M}(t)\right] + \left(\partial_t\hat{M}\right)(t), \tag{2.13}$$

resulting in the Heisenberg equation of motion for $\hat{M}(t)$. Both this and the Schrödinger picture require that the Hamiltonian is independent of time, otherwise the interaction picture has to be used.

The Interaction Picture

This representation is introduced in order to treat the dynamics of a quantum system that is represented by a time dependent Hamiltonian. This Hamiltonian is split into two parts: the first is a time independent part $\hat{H}_0$ that is exactly solvable, while the second part is a time dependent perturbative interaction $\hat{V}(t)$:

$$\hat{H}(t) = \hat{H}_0 + \hat{V}(t). \tag{2.14}$$

The trivial time evolution from $\hat{H}_0$ can be removed from the dynamics by only including this part of the Hamiltonian in the unitary transformation: $\hat{O}(t) = e^{-i\hat{H}_0 t}$. This puts the time dependence into the operators and the states:

$$|\tilde{\psi}(t)\rangle = e^{i\hat{H}_0 t}|\psi\rangle \tag{2.15}$$

$$\tilde{M}(t) = e^{i\hat{H}_0 t}\hat{M}e^{-i\hat{H}_0 t}. \tag{2.16}$$

The dynamics of the system are described by equations of motion for the state vectors, operators and the density matrix:

$$i\frac{\mathrm{d}}{\mathrm{d}t}|\tilde{\psi}(t)\rangle = \tilde{V}(t)|\tilde{\psi}(t)\rangle \tag{2.17}$$

$$i\frac{\mathrm{d}}{\mathrm{d}t}\tilde{M}(t) = \left[\tilde{M}(t), \hat{H}_0\right] \tag{2.18}$$

$$i\frac{\mathrm{d}}{\mathrm{d}t}\tilde{\rho}(t) = \left[\tilde{V}(t), \tilde{\rho}(t)\right], \tag{2.19}$$

where the density matrix ρ will be introduced in Section (2.1.4). The perturbative part of the Hamiltonian is the only reference to time in this Schrödinger equation. The time evolution of the state $|\tilde{\psi}(t)\rangle$ can thus be described by a unitary operator $\hat{U}(t, t')$:

$$|\tilde{\psi}(t)\rangle = \hat{U}\left(t, t'\right)|\tilde{\psi}\left(t'\right)\rangle, \tag{2.20}$$

This operator is in general given by [4]

$$\hat{U}\left(t, t'\right) = T_t\left(\exp\left[-i\int_{t'}^{t}\mathrm{d}t''\left[\tilde{V}\left(t''\right)\right]\right]\right), \tag{2.21}$$

where T_t is a time ordering operator. The properties of, and relation to quantum information concepts (i.e. quantum gates), of these unitary operators are discussed in Section (2.2.3).

2.1.4 Non-Unitary Time Evolution & Quantum Jump Formalism

The description of time evolution of quantum systems presented in Section (2.2.6) is only valid no dissipative effects are at play between the quantum system and the outlying environment. In this case the time evolution is governed by the master equation

$$\dot{\rho} = -i\left[\hat{H}, \rho\right] + \mathcal{L}[\rho], \tag{2.22}$$

where $\rho = |\psi\rangle\langle\psi|$ is the density matrix for a pure state, $\hat{H}$ is the Hamiltonian governing the unitary evolution and $\mathcal{L}[\rho]$ is the Lindblad superoperator describing the dissipative processes. This is given by:

$$\mathcal{L}[\rho] = -\frac{1}{2}\sum_k\left(\hat{L}_k^\dagger\hat{L}_k\rho + \rho\hat{L}_k^\dagger\hat{L}_k - 2\hat{L}_k\rho\hat{L}^\dagger\right), \tag{2.23}$$

where the sum runs over the possible decay channels and the Lindblad operator $\hat{L}_k$ is an operator describing this process. As an example, a non-radiative decay from the excited state $|e\rangle$ in a quantum dot to some ground state $|0\rangle$ can be written as $\hat{L}_{\gamma'} = \sqrt{\gamma'}|0\rangle\langle e|$. It can be advantageous to rearrange the terms in Eq. (2.23) into:

$$\dot{\rho} = -i\left[\hat{H}_{\mathrm{NH}}, \rho\right] + \sum_k\hat{L}_k\rho\hat{L}_k^\dagger, \tag{2.24}$$

where the effective Hamiltonian $\hat{H}_{\mathrm{NH}}$ is given by the original Hamiltonian with the *no-jump* terms added to it:

$$\hat{H}_{\mathrm{NH}} = \hat{H} - \frac{i}{2}\sum_k \hat{L}_k^\dagger \hat{L}_k. \tag{2.25}$$

This non-hermitian Hamiltonian can be evolved directly using the Schrödinger equation, as long as $|\psi\rangle$ is a pure state. This has the formal solution:

$$i\frac{\partial}{\partial t}|\psi(t)\rangle = \hat{H}_{\mathrm{NH}}|\psi(t)\rangle \tag{2.26}$$

$$|\psi(t)\rangle = e^{-i\hat{H}_{\mathrm{NH}}t}|\psi(0)\rangle = e^{-i\hat{H}t}e^{-\frac{1}{2}\sum_k \hat{L}_k^\dagger \hat{L}_k}|\psi(0)\rangle, \tag{2.27}$$

where the no-jump terms gives rise to an exponential decay of the states and assuming that $\hat{H}$ commutes with the Lindblad operators. The effects of the *jump* term $2\sum_k \hat{L}_k\rho\hat{L}_k^\dagger$ can be included in the stochastic wavefunction approach [6] by projecting them onto $|\psi\rangle$ at discrete times.

Solving the master equation in Eq. (2.22) gives the complete description of the dynamics of an open quantum system. This method becomes impractical at best for large systems as open system involve both unitary and dissipative evolution. Various effects often cause the system to experience different time scales, which makes it possible to divide the Hilbert space into two separate subspaces; one for the rapidly evolving excited states and one for the (meta)stable ground states. It is then advantageous to eliminate the excited states to get a simpler description of the ground states.
The standard method is to adiabatically eliminate the excited states, provided that the time scale of the ground states is significantly slower than that for the excited states. This method can become rather impractical to carry out if the size of the system is large due to the large number of elements in the density matrix. Splitting the Hamiltonian governing the system and the interactions into subspaces for the ground states and excited states makes it possible to obtain an effective master equation [18] involving only the dynamics of the ground states:

$$\dot{\rho} = -i\left[\hat{H}_{\mathrm{eff}},\rho\right] + \sum_k \hat{L}^k_{\mathrm{eff}}\rho\left(\hat{L}^k_{\mathrm{eff}}\right)^\dagger - \frac{1}{2}\left(\left(\hat{L}^k_{\mathrm{eff}}\right)^\dagger \hat{L}^k_{\mathrm{eff}}\rho - \rho\left(\hat{L}^k_{\mathrm{eff}}\right)^\dagger \hat{L}^k_{\mathrm{eff}}\right), \tag{2.28}$$

with the effective Hamiltonian and Lindblad operator:

$$\hat{H}_{\mathrm{eff}} = -\frac{1}{2}\hat{V}_-\left[\hat{H}^{-1}_{\mathrm{NH}} + \left(\hat{H}^{-1}_{\mathrm{NH}}\right)^\dagger\right]\hat{V}_+ + \hat{H}_{\mathrm{g}} \tag{2.29}$$

$$\hat{L}^k_{\mathrm{eff}} = \hat{L}_k\hat{H}^{-1}_{\mathrm{NH}}V_+, \tag{2.30}$$

where V_+ (V_-) is the perturbative (de)excitation of the system , $\hat{H}_g$ is the ground state Hamiltonian and $\hat{H}_{\mathrm{NH}}$ is a slightly modified version of the non-hermitian Hamiltonian introduced above:

$$\hat{H}_{\mathrm{NH}} = \hat{H}_{\mathrm{e}} - \frac{i}{2}\sum_k \hat{L}_k^\dagger \hat{L}_k, \tag{2.31}$$

where the unitary part of the non-hermitian Hamiltonian is only given in terms of the excited state Hamiltonian $\hat{H}_{\mathrm{e}}$. This formalism will be used in Chapters (5) and (6) to derive the effective operators describing the time evolution of the qubit states for the proposed controlled phase gate. A full derivation of this formalism is given in Appendix (A).

2.2 Quantum Computation

2.2.1 DiVicenzo's Criteria

There is a list of 5+2 requirements identified by David DiVicenzo in [7] that any system has to full fill in order to build a general purpose quantum computer. The +2 denotes two additional conditions that have to be met in order to implement a quantum communication network. These conditions will be listed here and their implementation in two distinct physical systems will be discussed. These systems are the ion trap [5] and self-assembled quantum dots embedded in a nano-photonic wave guide. The former due to the already highly successful implementation and the later due to it being the focus of this work.

2.2.2 Qubits

Information carriers in classical information theory are *bits*. These are typically represented by the absence or presence of a physical entity and take the distinct values 0 and 1, respectively. The equivalent entity for quantum information theory is the *qubit* and are represented by the state vectors $|0\rangle$ and $|1\rangle$. The most general form of a qubit is described trough the computational basis and takes the form:

$$|\psi\rangle = \alpha\,|0\rangle + \beta\,|1\rangle\,, \tag{2.32}$$

which is a linear superposition of the two qubit states, where α and β are complex coefficients satisfying $|\alpha|^2 + |\beta|^2 = 1$ to ensure that the qubit state is normalised. The superposition of $|0\rangle$ and $|1\rangle$ sets qubits apart from the definite valued classical bits which is further highlighted by the probabilistic nature of a measurement on the qubit. This *quantum parallelism* enables the construction of quantum algorithms that operates on several inputs simultaneously, leading to higher computational power of a quantum computer. Only the relative phase between the two vectors in the qubits state is physically significant; the global phase does not contribute to any meaningful physical observable.
Several qubits are often needed for any realistic application of quantum information. The vectors $|\psi\rangle_1$ and $|\psi_2\rangle$ describing the two qubits are defined in separate two-dimensional Hilbert spaces $\mathcal{H}_1$ and $\mathcal{H}_2$, where the total Hilbert space $\mathcal{H}$ is a tensor product between the smaller Hilbert spaces: $\mathcal{H} = \mathcal{H}_1 \otimes \mathcal{H}_2$. The combined state for the two qubits is then a tensor product between the individual qubit states: $|\psi\rangle_{\text{TwoQubits}} = |\psi\rangle_1 \otimes |\psi\rangle_2$. If $|\psi\rangle_j = \alpha_j\,|0\rangle_j + \beta_j\,|1\rangle_j$ then the combined qubit state takes the form:

$$\begin{aligned} |\psi\rangle_{\text{TwoQubits}} = |\psi\rangle_1 \otimes |\psi\rangle_2 &= (\alpha_1\,|0\rangle_1 + \beta_1\,|1\rangle_1) \otimes (\alpha_2\,|0\rangle_2 + \beta_2\,|1\rangle_2) && (2.33)\\ &= c_{00}\,|11\rangle + c_{01}\,|01\rangle + c_{10}\,|10\rangle + c_{11}\,|11\rangle\,, && (2.34)\end{aligned}$$

where $|00\rangle$ is a shorthand notation for the product state $|0\rangle_1 \otimes |0\rangle_2$. This notation is used throughout the thesis. The coefficients in Eq. (2.34) are defined as $c_{00} = \alpha_1\alpha_2, c_{01} = \alpha_1\beta_2, c_{10} = \beta_1\alpha_2$ and $c_{11} = \beta_1\beta_2$. Note that it is the newly defined coefficients c_{kl} that evolve when the two-qubit state is evolved in time.

A simple physical example of a qubit is the spin states of any spin-1/2 particle. A spin-1/2 particle has a spin magnitude of $S = 1/2$ with projection $m_S = \pm 1/2$. It is then possible to define $|0\rangle \equiv |s = 1/2, m_S = 1/2\rangle = |\downarrow\rangle$ and $|1\rangle \equiv |S = 1/2, m_S = -1/2\rangle = |\uparrow\rangle$. Other simple examples include the excited and ground states of a two level atom or the polarization degree of freedom of a photon. These simple systems (except from the photon polarization) are often not useful for practical applications due to the four other DiVincenzo criteria.

Trapped atoms constitutes a working application of a quantum computer. This is largely due to the well developed ability to control the state of atoms and the well documented knowledge about the internal structure of various atoms. The majority of experimental methods for manipulating the internal states of atoms involve illuminating the atoms with lasers. The discrete nature of the atomic energy levels ensures that any transition between two states can only be driven if the laser is on resonance with the frequency of the transition. In addition, transition rules dictate that only light fields with a particular polarization can drive the transition. This polarization is defined by the combined angular momentum (i.e. the sum of orbital L, electronic spin S and nuclear spin I angular momentum) of the two states. Illuminating the atom with a light field with a particular energy (i.e. frequency) and polarization ensures that only transitions between two specific levels are driven. These two levels can then be directly mapped to the two qubit states.
Consider a number of $^9Be^+$ ions confined in a trap (it is advantageous to use ions due to their charge. The charge makes it possible to use various time-varying electric fields to trap the ions). These ions have a nuclear spin of $I = 3/2$ which gives a hyperfine splitting in the level structure. The hyperfine states $|0\rangle = |F = 1, m_F = \pm 1\rangle$ and $|1\rangle = |F = 1, m_F = \pm 2\rangle$ for the $^2S_{1/2}$ fine structure ground state constitutes a good choice for a qubits, as these states are well defined and shielded (i.e. they have no allowed transitions that they can decay through). Interactions between these two states can be readily implemented using Raman transitions using $|F = 2, m_F = \pm 1\rangle$ as a virtual state. Note that a chain of ions will undergo a vibrating motion due to the Coulomb force that each ion exert on the other ions in the chain. It is thus necessary to cool the ions into the motion ground state before any quantum information process can be implemented. Methods for initializing this qubit (both driving into the qubit states and cooling the vibrational motion) will be discussed in Section (2.2.4).
It is possible to use confined electronic states in quantum dots for the implementation of qubits. The so-called trion provides a suitable physical platform for this purpose, as it has a stable ground state consisting of the two magnetic spin states of an electron. Section (3.3) discusses this in more depth.

Another important consideration is the need to be able to make a quantum system *scalable* in order to make practical use of quantum information protocols. This is evident for the ion trap, as it gets progressively harder to add ions into the trap and to keep them on a straight line. This can be accomplished by generating entanglement between the ions and then teleporting the qubit to various points in the chain [2].
The scalability of self assembled quantum dots in nanohpotonic crystals is an active area of research but it is still a considerable challenge to attaining the same level of control of a system with several quantum dots linked together, compared to that demonstrated for a single quantum dot. One proposal involves using the quantum dots as nodes in a quantum communication network, using the near-unity on-demand single-photon generation that these structures are promising candidates for.

2.2.3 Universal Quantum Gates

Any logical gate, classical or quantum, is implemented by changing the physical state of a (qu)bit by taking a set of inputs and deterministically change them to an output (or several outputs for certain gates). This process is described through Boolean algebra. The basic classical gates include the AND, OR and NOT gates. It can be shown [23] that any Boolean operation can be performed using just AND and NOT gates. Furthermore, the NAND gate can implement both of these gates; the NAND gate is thus referred to as an *universal gate* from which any Boolean

function can be performed. Note that certain classical gates (such as the AND, OR and NAND) gates are logically irreversible as it is not possible to determine unique inputs for certain output. As an example, take the output 0 from an OR gate. This output can be the result from inputs of the form 00, 01 and 10.
Quantum gates perform similarly as classical gates: they take a physical entity, i.e. the qubit, as an input, and evolves it according to some logical operation, producing the output qubit. The evolution of the qubit $|\psi\rangle$ must follow the laws of quantum mechanics and is governed by the Schrödinger equation (typically represented in the interaction picture) $i\hbar\partial|\psi\rangle/\partial t = \hat{H}|\psi\rangle$, where $\hat{H}$ is the Hamiltonian that specifies the fields at work. This time evolution, and by extension quantum gate that gives rise to the evolution, is described through unitary operators $\hat{U} = \exp\left(-i\hat{H}t/\hbar\right)$, as long as no measurements take place and that unwanted interactions with the environment are suppressed. Any state, starting from an initial time t' will then evolve to the final time t by

$$|\psi(t)\rangle = \hat{U}\left(t, t'\right)|\psi\left(t'\right)\rangle. \tag{2.35}$$

Unitary matrices thus provide the mathematical description of quantum gates. A matrix is said to be unitary when $\hat{U}^{-1} = \hat{U}^\dagger$ and it has the following properties:

- $\hat{U}^\dagger\hat{U} = \hat{U}\hat{U}^\dagger = \mathbb{1}$
- $\langle\phi\hat{U}^\dagger|\hat{U}\psi\rangle = \langle\phi|\psi\rangle$ - The inner product is preserved when the vectors are multiplied by the unitary matrix
- $|\det(U)| = 1$
- $\hat{U} = V\hat{D}V^*$ - $\hat{U}$ is diagonalizable, where $\hat{D}$ is a diagonal and unitary matrix and V is an unitary matrix.
- The columns and rows of $\hat{U}$ form an orthonormal set of vectors
- For a fixed column: $\sum_{i=1}^{2^n}|U_{ij}|^2 = 1$ and for a fixed row: $\sum_{j=1}^{2^n}|U_{ij}|^2 = 1$

The evolution of a quantum state can be reversed by multiplying Eq. (2.35) by $\hat{U}^\dagger$ and using $\hat{U}^\dagger\hat{U} = \mathbb{1}$. Any qubit gate is thus logically reversible, in contrast to the classical gates mentioned above. There do exist logically reversible classical gates (such as the NOT and TOFFOLI gates). The matrix representation for these gates are given by permutation matrices, whereas unitary matrices provide a sufficient representation for quantum gates. The two sums $\sum_{i=1}^{2^n}|U_{ij}|^2 = 1$ and $\sum_{j=1}^{2^n}|U_{ij}|^2 = 1$ ensure that any normalised initial state is evolved into a normalised final state.

Consider the following matrix:

$$H = \frac{1}{\sqrt{2}}\begin{pmatrix} 1 & 1 \\ 1 & -1 \end{pmatrix} \tag{2.36}$$

This is the so called Hadamard gate that changes a computational basis state in to the superposition: $H|0,1\rangle = (|0\rangle \pm |1\rangle)/\sqrt{2}$. This is the basic workhorse of quantum computing due to its ability to turn a single input state into a superposition. Consider a situation where N qubits are prepared in $|0\rangle$ and where a Hadamard gate is applied to each qubit in parallel:

$$H^{\otimes N}|0\rangle^{\otimes N} = \frac{1}{2^{N/2}}(|0\rangle + |1\rangle)\otimes(|0\rangle + |1\rangle)\otimes\cdots\otimes(|0\rangle + |1\rangle) = \frac{1}{2^{N/2}}\sum_{j=1}^{2^N-1}|j\rangle, \tag{2.37}$$

where $|j\rangle$ is a number written in binary notation. This creates an equal superposition of all integer states between 0 and $2^N - 1$ by loading just N qubits into the system. This makes the Hadamard gate a key component in a number of quantum algorithms, including the Grover search algorithm and the Deutsch-Jozsa algorithm.

It is possible to make a geometrical representation of a qubit using the Bloch sphere picture. The qubit can be thought of a a vector pointing to the surface of a unit sphere described by the three polar coordinates: the radius r, the polar angle $\theta \in [0, \pi]$ and the azimuthal angle $\phi \in [0, 2\pi]$. The chosen frame of reference is such that the North pole is located at the coordinates $(1, 0, 0)$ and the South pole at the coordinates $(1, \pi, 0)$. The polar coordinates can be related to Cartesian through the usual transformations:

$$x = r \sin(\theta) \cos(\phi) \tag{2.38}$$
$$y = r \sin(\theta) \sin(\phi) \tag{2.39}$$
$$z = r \cos(\theta). \tag{2.40}$$

The qubit takes the general form $|\psi\rangle = \cos\left(\frac{\theta}{2}\right)|0\rangle + e^{i\phi} \sin\left(\frac{\theta}{2}\right)|1\rangle$. The full description of the qubit includes an addition phase $e^{i\eta}$ multiplied unto both terms in $|\psi\rangle$ but, as mentioned before, this phase holds no physical significance. Rotations about the three axes can be readily expressed as Euler rotations [20]:

$$R_x(\theta) = \exp(-i\theta\sigma_z/2) = \begin{pmatrix} \cos(\theta/2) & -i\sin(\theta/2) \\ -i\sin(\theta/2) & \cos(\theta/2) \end{pmatrix} \tag{2.41}$$
$$R_y(\theta) = \exp(-i\theta\sigma_y/2) = \begin{pmatrix} \cos(\theta/2) & -\sin(\theta/2) \\ \sin(\theta/2) & \cos(\theta/2) \end{pmatrix} \tag{2.42}$$
$$R_z(\phi) = \exp(-i\phi\sigma_z/2) = \begin{pmatrix} e^{-i\phi/2} & 0 \\ 0 & e^{i\phi/2} \end{pmatrix} \tag{2.43}$$
$$R_{ph}(\eta) = e^{i\eta}\mathbb{1}. \tag{2.44}$$

These rotations can be readily implemented using e.g. laser fields for Rabi oscillations. Note that two full rotations are needed in order to return a qubit to its original state. Any single-qubit quantum gate can be written in terms of these rotation matrices, which can be seen by considering $\left|\det\left(\hat{U}\right)\right| = 1$. It is sufficient to use the special unitary matrix V that is defined by $\hat{U} = R_{ph}(\eta) V$. This matrix has a relaxed condition: $\det(V) = 1$ and has the general form:

$$V = \begin{pmatrix} \alpha & -\bar{\beta} \\ \beta & \bar{\alpha} \end{pmatrix}, \tag{2.45}$$

from which the determinant is readily calculated: $\det(V) = |\alpha|^2 + |\beta|^2 = 1$. A general choice for the parameters that satisfies this equation is $\alpha = e^{i\kappa}\cos(\theta/2)$ and $\beta = e^{i\epsilon}\sin(\theta/2)$. The special unitary matrix can then be expressed in the Block sphere picture as:

$$V = \begin{pmatrix} e^{i\kappa}\cos(\theta/2) & e^{-i\epsilon}\sin(\theta/2) \\ e^{i\epsilon}\sin(\theta/2) & e^{-i\kappa}\cos(\theta/2) \end{pmatrix} \tag{2.46}$$

This matrix can, in addition, also be constructed as the product

$$R_z(\epsilon - \kappa) \cdot R_y(\theta) \cdot R_z(-[\epsilon + \kappa]) \tag{2.47}$$

with the geometrical interpretation that any rotation on the Bloch sphere can be decomposed into a sequence of three rotations; one about the z-axis followed by a rotation around the y-axis and end with another rotation about the z-axis. A simple example is the decomposition of a rotation about the x-axis into three small rotations by:

$$R_x(\theta) = R_z(\pm\pi/2)\, R_y(\theta)\, R_z(\mp\pi/2)\,. \tag{2.48}$$

This has a significant implication for the application of quantum gates: any quantum gate is represented by a unitary matrix which acts on the qubit by rotating it three times as given by Eq. (2.47). Each of these rotations are only about a single axis and can be implemented through standard experimental techniques, such as the effective Hamiltonian arising when performing Raman transitions between two ground states via a virtual excited state (though it is rotations about the x- and z axis in this case.) Another, and a more specific, example is the decomposition of the Hadamard gate into:

$$H = R_z(0) \cdot R_y(\pi/2) \cdot R_z(\pi) \cdot R_{ph}(\pi/2)\,. \tag{2.49}$$

Single-qubit gates are not enough for quantum computational purposes. Gates that operate between several qubits are also needed. It is sufficient to use two-qubit gates for this; gates between more than two qubits can be made by chaining several two-qubit and single-qubit gates together between various qubit pairs. In fact, any kind of quantum gate can be implemented using just a two-qubit gate and a number of single-qubit gates. These form a set of *universal* quantum gates from which any quantum computation can be implemented. The fact that only a few gates are needed for any computation greatly simplifies the task of engineering specific interactions between several qubits.

Two-qubit gates are typically implemented by using some physical property to mediate interactions between the two qubits. This can be the quantized vibrational modes that exists in a chain of trapped ions, or it can be through the emission and absorption of photon by two quantum dots embedded in a waveguide.

The controlled phase gate $U_\pi^{(2)}$ and the CNOT gate $U_{\mathrm{CNOT}}^{(2)}$ are often used to form one of these universal sets. The superscripts denotes that these are two-qubit gates. The controlled phase gate imparts a change of phase (this is often chosen to be such that the imprinted phase is $e^{-i\pi} = 1$) of both input qubits are in state $|1\rangle$ but it leaves the other three input states unchanged. The CNOT gate changes the state of the second qubit only if the first qubit is in state $|1\rangle$ and leaves it unchanged otherwise. These gates are summarized in Table. (2.1). The CNOT gate can be related to the controlled phase gate by the use of a sequence of Hadamard gates by:

$$U_{\mathrm{CNOT}}^{(2)} = (\mathbb{1}_1 \otimes H_2)\, U_\pi^{(2)}\, (H_1 \otimes H_2)\,, \tag{2.50}$$

where the subscripts refer to the specific qubit that the gate operates on. This thesis is concerned with the possibility of created a heralded controlled phase gate with an integrated error detection by exploiting the interaction between several quantum dots embedded in a nanophotonic wave guide.

CNOT				Controlled Phase			
Input		Output		Input		Output	
Control	Target	Control	Target	Control	Target	Control	Target
$\|0\rangle$	$\|0\rangle$	$\|0\rangle$	$\|0\rangle$	$\|0\rangle$	$\|0\rangle$	$\|0\rangle$	$\|0\rangle$
$\|0\rangle$	$\|1\rangle$	$\|0\rangle$	$\|1\rangle$	$\|0\rangle$	$\|1\rangle$	$\|0\rangle$	$\|1\rangle$
$\|1\rangle$	$\|0\rangle$	$\|1\rangle$	$\|1\rangle$	$\|1\rangle$	$\|0\rangle$	$\|1\rangle$	$\|0\rangle$
$\|1\rangle$	$\|1\rangle$	$\|1\rangle$	$\|0\rangle$	$\|1\rangle$	$\|1\rangle$	$\|1\rangle$	$-\|1\rangle$

Table 2.1: Truth tables describing the operation of the CNOT gate and the Controlled Phase gate

2.2.4 Initialization

Any quantum computation protocol involves the deterministic time evolution of the quantum mechanical system of choice and the subsequent measurement of the final state. These processes depend on the initial state of the system; consider the simple case of a $\pi/2$ rotation about the $\hat{y}$-axis for the three initial states $|\downarrow\rangle_z, |\uparrow\rangle_z$ and $|\uparrow\downarrow\rangle_z \equiv (|\uparrow\rangle_z + |\downarrow\rangle_z)/\sqrt{2}$:

$$R_y(\pi/2)|\uparrow\rangle_z = \frac{1}{\sqrt{2}}(|\uparrow\rangle_z + |\downarrow\rangle_z) = |\uparrow\rangle_x \tag{2.51}$$

$$R_y(\pi/2)|\downarrow\rangle_z = \frac{1}{\sqrt{2}}(|\uparrow\rangle_z - |\downarrow\rangle_z) = |\downarrow\rangle_x \tag{2.52}$$

$$R_y(\pi/2)|\uparrow\downarrow\rangle_z = |\uparrow\rangle_z = \frac{1}{\sqrt{2}}(|\uparrow\rangle_x + |\downarrow\rangle_x), \tag{2.53}$$

where the spin states also have been decomposed into the basis states for the spin along the $\hat{x}$ axis. A measurement along the $\hat{z}$-axis of the first two final states have a probability of 1/2 to return either $|\uparrow\rangle_z$ or $|\downarrow\rangle_z$, whereas the same measurement for the last final state is guaranteed to return $|\uparrow\rangle_z$. Changing the measurement axis to be along the $\hat{x}$-axis changes the results, such the the result for the first two states are always $|\uparrow\rangle_x$ and $|\downarrow\rangle_x$, respectively. This simple example highlights the need to be a to *initialize* the system into a well known initial state in order to deterministically evolve the system during the computation operation.
The ground state $|0\rangle = |F = 1, m_F = -1\rangle$ for the ion trap introduced in Section (2.2.2) can be prepared using the method of optical pumping. This is implemented by continuously pumping the optical transition between the $^2S_{1/2}, F = 2$ and the $^2P_{1/2}, F = 2$ states. This needs to be done using a laser with σ^- polarization, such that only processes for which $M_{\text{Excited}} = M_{\text{Ground}} - 1$ are induced by the laser; this ensures that the target state is not excited by the laser field. The continuous pumping causes the undesired long lived states to be excited to some short lived excited states; subsequent spontaneous emission will relax the system into the desired state $|0\rangle$ in the steady state situation. In addition, tuning the laser along the lower vibrational sideband [5] ensures that the ions are cooled into the vibrational ground state, completing the initialization process.
A proposed initialisation scheme for a qubit in a self-assembled quantum dot comprised of the electronic ground state of a trion is described in Section (3.3).

The system will always have some interaction with the outlying environment, which may introduce errors into any quantum computation protocol. There exists protocols that can detect

and correct these errors (see Section (2.2.8) for an example if one such protocol). The efficient implementation of these protocols often needs a continuous supply of ground states in order to function properly. The need to implement a continuous initialization process is a substantial experimental challenge, making integrated error detection schemes highly desirable. The implementation for a controlled phase gate found in this thesis has one such integrated error detection, thereby bypassing the needed for a continuous initialization process.

2.2.5 A Qubit Specific Measurement Capability

The reliable method for obtaining the final result of a quantum computation is needed in order to make the protocol useful; this requires being able to perform a measurement on a specific qubit. This can be reliably implemented in the ion trap by applying a σ^- polarised laser field on the ${}^2\mathrm{S}_{1/2}, F = 2$ to the ${}^2\mathrm{P}_{3/2}, F = 3$ states. The resulting photon cascade from spontaneous emission can be measured. The transition is chosen such that there is only one allowed optical transition for spontaneous emission and that only one of the qubit states (in this example it would be the state $|1\rangle$) is illuminated by the laser. A cascade of photons will be measured the qubit is in $|1\rangle$ due to repeated excitation and emission, whereas none are measured in the case where the qubit is in $|0\rangle$. Similar measurement schemes exist for probing the optical properties fo quantum dots, namely resonance florescence and photoluminescence spectroscopy. Alternatively, the approach used in [8] can be employed.
In addition to measure the final result of a quantum computation, several protocols in the field of quantum information relies on the ability to perform a qubit specific measurement. These protocols include quantum teleportation, which relies on performing Bell measurements to imprint the information stored in the input state to the output state, or to encode additional information into the input state, respectively.

2.2.6 Long Decoherence Times

Section (2.1.4) introduced the master equation in order to treat the non-unitary dynamics that is introduced by the coupling of a quantum system to the environment. This can introduce unwanted changes in the qubit states, ruining the deterministic evolution needed by quantum information protocols. In addition, the quantum mechanical properties of the system are washed out, leaving the qubit described by the statistical mixture $\rho = |a|^2 |0\rangle \langle 0| + |b|^2 |1\rangle \langle 1|$. In this situation there will always be a probability of $|a|^2$ to measure the qubit in $|0\rangle$, regardless of the measurement axis chosen.
This unwanted evolution happens on a time scale set by the *decoherence time* T_2, which will be introduced in Section (3.2.3). The detrimental effects of decoherence can be minimised by having the time of the gate operation be significantly short than the decoherence time. This is easily achievable in the ion trap implementation, due to the long life time of hyperfine states and their insensitivity to the electric fields that trap the ions. The decoherence processes are more pronounced for quantum dots, as they are mesoscopic emitters embedded in a solid state environment. These include interactions with phonons in the photonic crystal and charge fluctuations from lattice defects. These processes are one of the main causes for errors in the controlled phase gate described in this thesis; these errors and the possibilities of removing them are discussed in Chapters (5) and (6). The detrimental effects of pure dephasing is also presented in these chapters..

2.2.7 Transmission of Flying Qubtis & the Ability to Interconvert Stationary and Flying Qubits

The five points outlined above constitute a sufficient set of requirements that need to be satisfied in order to build a quantum computer. Two additional conditions has to be met in order to build a suitable platform for quantum communication. This topic is outside of the scope of this thesis and will only be briefly discussed. Stationary qubits, like those discussed in Section (2.2.2), are well suited for computational purposes but are confined to a particular lab due to their tendency of interacting with the environment. Flying qubits thus describe qubits that are well suited for transmission purposes; photons are a particular useful choice as they interact weakly with the environment and the transmission of photons is readily available using optical fibres as a technological baseline. This introduces a new decoherence effect, as the probability to lose the photon scales exponentially with distance; various schemes exist to remedy this problem through, an example is a network of quantum repeaters. Quantum dots in a nanophotonic crystal provide a promising platform for the efficient generation of coherent single photons due to the new-unity observed β-factor, high achievable Purcell factors and long decoherence times. These concepts are introduced in Section (3).

2.2.8 Quantum Error Correction

The practical realisation of the quantum gates discussed above have some risk to produce an erroneous qubit state as the output due to e.g. the coupling to the environment. These errors are detrimental to the performance of any computational protocol. Various methods for detecting and correcting these errors have thus been produced in order to protect the implementation of quantum information against these errors. One such method is Shor's nine qubit code, which can correct a single *bit flip* and a number of *phase flips* of a qubit state. These errors are defined as, for a pure qubit state:

$$|\psi\rangle = \alpha\,|0\rangle + \beta\,|1\rangle \underset{\text{Error}}{\rightarrow} \begin{cases} \alpha\,|1\rangle + \beta\,|0\rangle\,, & \text{Bit flip} \\ \alpha\,|0\rangle - \beta\,|1\rangle\,, & \text{Phase flip} \end{cases} \tag{2.54}$$

The basic idea is to make a correction scheme similar to a classical repetition code. This is complicated by the no-clone theorem, which forbids the possibility of encoding $|\psi\rangle$ as $|\psi\rangle\,|\psi\rangle\,|\psi\rangle$. Instead, each of the two basis states in $|\psi\rangle$ are encoded onto eight additional qubits giving rise to the following state:

$$|\psi\rangle \underset{\text{Encode}}{\rightarrow} \begin{cases} \alpha\dfrac{(|000\rangle + |111\rangle)\,(|000\rangle + |111\rangle)\,(|000\rangle + |111\rangle)}{2\sqrt{2}} \\ +\beta\dfrac{(|000\rangle - |111\rangle)\,(|000\rangle - |111\rangle)\,(|000\rangle - |111\rangle)}{2\sqrt{2}} \end{cases} \tag{2.55}$$

Each parenthesis in Eq. (2.55) organises the encoded state into three blocks, each consisting of three qubit states of the form:

$$\alpha\frac{|000\rangle + |111\rangle}{\sqrt{2}} + \beta\frac{|000\rangle - |111\rangle}{\sqrt{2}}, \tag{2.56}$$

where the first qubit of each block is encoded onto two others with respect to bit flip errors. The correction of errors then follow a simple procedure, as long as there is one bit flip in only one of the blocks. Consider the following specific example where there is a phase flip in the second

block and a bit flip on the fourth qubit:

$$\begin{aligned}&\alpha\frac{(|000\rangle+|111\rangle)(|010\rangle-|101\rangle)(|000\rangle+|111\rangle)}{2\sqrt{2}}\\&+\beta\frac{(|000\rangle-|111\rangle)(|010\rangle-|101\rangle)(|000\rangle-|111\rangle)}{2\sqrt{2}}\end{aligned}\tag{2.57}$$

Running the bit flip code will return the following three binary numbers: $00, 10, 00$. The first and third represents that there are no errors in the respective blocks, whereas 10 informs that there is a bit flip error on the second qubit in block two. Correcting the error results in the following state:

$$\begin{aligned}&\alpha\frac{(|000\rangle+|111\rangle)(|000\rangle-|111\rangle)(|000\rangle+|111\rangle)}{2\sqrt{2}}\\&+\beta\frac{(|000\rangle-|111\rangle)(|000\rangle+|111\rangle)(|000\rangle-|111\rangle)}{2\sqrt{2}}\end{aligned}\tag{2.58}$$

The phase flip code is applied to this state, which yields a single binary number. The output is in this case 10, representing the phase flip error in the second block. Correcting this error results in the original state of Eq. (2.55), which can be decoded into $|\psi\rangle = \alpha|0\rangle + \beta|1\rangle$ by running the encoding procedure in reverse.
The main drawback of this procedure is the need to load eight additional ground states in order to implement the error correction code. This, as mentioned in Section (2.2.4), can be experimentally cumbersome, especially if the error correction has to be implemented several times. This makes quantum gates with integrated error detection and correction a highly valuable alternative.

Chapter 3

Basics of Nanophotonic Structures

The physical structures that are considered in this work are the so called self-assembled quantum dots embedded in nanophotonic structures that have opened up new avenues for research into the fields of quantum electrodynamics and quantum optics. Both are concerned with the interaction between matter and light at the quantum level. It is therefore a great advantage to be able to tailor the light-matter interaction and nanophotonic structures provide a platform that is well suited for this task. These structures exhibit a number of advantages compared to the traditional use of atoms for experiments in quantum optics., which includes the ability to strongly enhance the light-matter interaction. Modern nanofabrication methods have enabled the possibility to build photonic crystals (PhC) where the optical properties enhance the interaction between a photon and a quantum emitter by inhibiting the coupling into the vast array of unwanted optical modes and/or enhance the coupling to one particular preferred mode. These single-photon emitters, the quantum dots, can be grown directly in the nanophotonic structures and, due to the nature of solid-state systems, do not need the trapping and cooling techniques used in atomic systems. Their optical properties can be tailored by the well developed growth methods. This section reviews the basics of the photonic crystals in Section (3.1) and Section (3.2) provides an overview of the concepts and properties of the epitaxially grown III-V semiconductor quantum dots. Section (3.3) provides a proposal for the initialisation of two qubit state needed for the implementation of the controlled phase gate presented in this thesis. This chapter is largely based on the review article from [13].

3.1 Nanophotonic Waveguides

3.1.1 Structural Properties

A photonic crystal is an inhomogeneous dielectric material with a periodically modulated refractive index. The propagation of light is strongly affected by optical Bragg scattering, if the periodicity of the refractive is on the order of the optical wavelength. This is analogous to the electronic Bragg scattering in crystallographic experiments in solids and is the key to the desired optical properties employed in nanophotonic QED. These materials are highly dispersive and can support a wealth of Bloch modes. A photonic band gap, in which no Bloch modes exist, can open up in the band diagram for the material, provided that the Bragg scattering is sufficiently powerful. The typical devices used are 2D membranes, where the propagation of light is suppressed in two dimensions by the band gap and is confined in the third dimension through total internal reflection at the semiconductor-air interface, similar to the reflection of light in optical fibres. A suppression in all three dimensions would be ideal but there are substantial technological challenges associated with the production of 3D modulated structures. In addition,

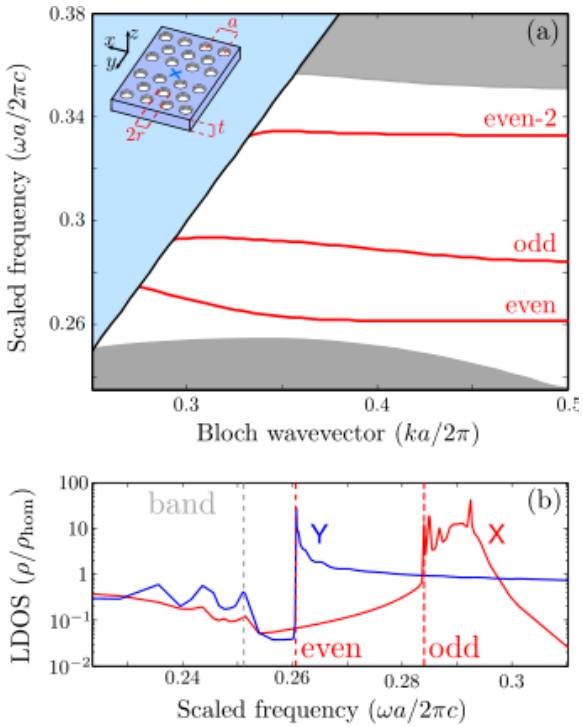

Figure 3.1: Dispersion diagram and frequency dependence of the LDOS in a photonic crystal waveguide. (a) Dispersion diagram of the TE-modes of a W1 waveguide in a photonic crystal. Three waveguide modes appear in the band gap; it is typically the lowest frequency mode that is employed in experiments. The grey areas show contain extended Bloch modes and leaky radiation modes. The insert shows a sketch of the crystals with a triangular lattice with lattice constant a and hole radius r. (b) Frequency dependence of the LDOS, normalised to that for a homogeneous medium. The red line corresponds to a x-dipole while the y-dipole is represented by the blue line; both dipoles are placed at the cross i the insert of (a). The dashed vertical lines mark the emergence of the frequency region of the extended Bloch modes. The expression for the two LDOS are given in Eqs. (3.3) and (3.4). This figure is reprinted from [13]

2D membranes provide a convenient method for probing emitters with laser excitation from the top of the membrane. GalliumArsenide (GaAs) has proven to be well suited for quantum optics experiments due to the ease of growing InGaAs quantum dots in the crystals and due to the highly advanced and precise fabrication methods. A 2D GaAs structure is shown in Fig. (3.1) with air holes of radius r. These holes are arranged in a triangular pattern with lattice constant a. The size and central frequency og the band gap can be controlled by modifying the values of r and a. The typical values for the radius of the holes is $r = a/3$ and the structure has a thickness of $t = 2a/3$.

3.1.2 Optical Properties

The local density of states, LDOS, quantifies the local light-matter interaction strength. It specifies the number of optical states at frequency ω per frequency bandwidth and mode volume as experienced by the emitter. The LODS and the corresponding radiative decay rate, is given by:

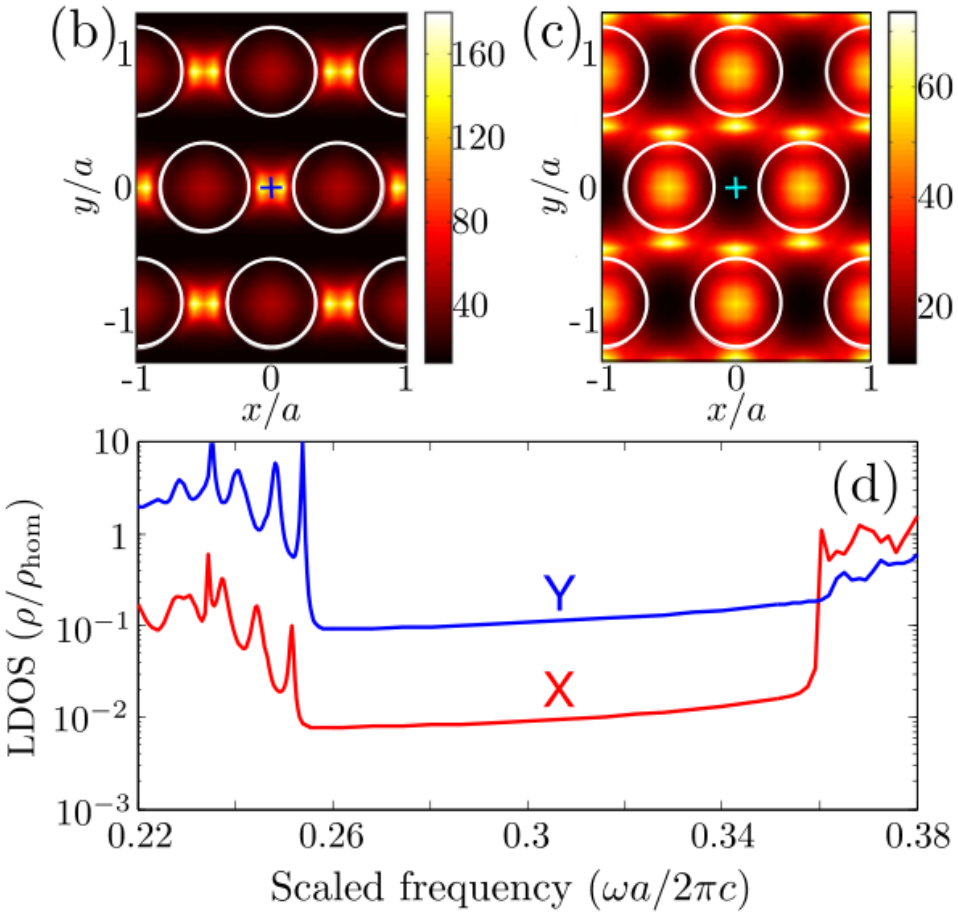

Figure 3.2: (b) and (c) shows a spatial map in the $x-y$ plane of the LDOS ρ of an x- and y-dipole, respectively. The LDOS is normalised to the LDOS ρ/ρ_{Hom} for a homogeneous GaAs structure. (d) Frequency dependence of ρ/ρ_{Hom} for a x-dipole (red curve) and a y-dipole (blue curve). These dipoles are placed at the crosses in (b) and (c). This figure is an exert from Fig. (8) from [13].

$$\rho\left(\mathbf{r}_0,\omega,\hat{\mathbf{e}}_{\mathbf{d}}\right)=\sum_{\mathbf{k}}\left|\hat{\mathbf{e}}_{\mathbf{d}}\cdot\hat{\mathbf{u}}_{\mathbf{k}}\left(\mathbf{r}_0\right)\right|^2\delta\left(\omega-\omega_{\mathbf{k}}\right) \tag{3.1}$$

$$\gamma_{\mathrm{rad}}\left(\mathbf{r}_0,\omega_0,\hat{\mathbf{e}}_{\mathbf{d}}\right)=\frac{\pi\omega_0}{\epsilon_0\hbar}\left|\mathbf{d}\right|^2\rho\left(\mathbf{r}_0,\omega,\hat{\mathbf{e}}_{\mathbf{d}}\right), \tag{3.2}$$

where $\mathbf{r}_0$ is the position of the emitter, $\mathbf{k}$ is the Bloch wave vector and $\hat{\mathbf{e}}_d$ is a unit vector pointing in the direction of the transition dipole moment $\mathbf{d}$ of the quantum dot. The LDOS for a homogeneous medium and for a W1 waveguide for the interaction with a single quantum dot are given by:

$$\rho_{\mathrm{Hom}}=\frac{n\omega^2}{3\pi^2c^3} \tag{3.3}$$

$$\rho_{\mathrm{W1}}\left(\mathbf{r}_{\mathrm{n}},\omega,\mathbf{e}_{\mathbf{d}}\right)=\frac{a}{\pi v_g}\frac{f\left(\mathbf{r}\right)}{\epsilon\left(\mathbf{r}\right)V_{\mathrm{Eff}}}\left|\hat{\mathbf{e}}\left(\mathbf{r}\right)\cdot\hat{\mathrm{e}}_{\mathrm{d}}\right|^2, \tag{3.4}$$

where n is the refractive index of the waveguide, v_g is the group velocity, $f\left(\mathbf{r}\right)$ is a dimensionless function describing the spatial mismatch between the emitter and waveguide-mode field, V_{Eff} is the effective mode volume and e_{d} is a unit vector poiting along the dipole. The expression for

the waveguide and the various functions are explained in greater detail in Chapter (4). Fig. (3.1) shows a calculated LDOS for as a function of frequency for a GaAs membrane. A strong suppression of the LDOS in the band gap region is clearly seen, leaving any radiation of a dipole oriented in the plane of the dipole to only be of the form of the weakly radiating non-guided modes found above the light line of the band diagram. A suppression up to a factor of a 160 can be seen from Fig. (3.2), relative to the LDOS found from a homogeneous medium of GaAs. This results in a strongly suppressed decay rate for these modes, as is seen from Eq. (3.2). This large suppression the coupling to the unwanted modes eliminates one of the main sources of loss and is the main strength of the photonic crystals. Note that any other source of loss, such as absorption of the transmitted light, is detrimental to the functionality of the crystal.

It is also possible to enhance the strength of the coupling to a particular preferred mode, in addition to the suppression of the coupling to the unwanted modes detailed above, to greatly enhance the light-matter interaction. The W1 waveguide can be readily implemented in a photonic crystal by leaving out a row of holes i the Γ-K direction of a triangular lattice. This allows a limited numbed of bands to appear in the band gap, making it possible for certain modes of light to propagate through the waveguide. These modes are highly dispersive, which can give rise to a strong slow-down effect og the propagating light through the group velocity $v_g(\omega) = |\nabla_{\mathbf{k}\omega}|$. Losses are ideally eliminated, as the bands appear below the light line of the band diagram, but fabrication imperfections will allow a small leakage through a vertical coupling. The band diagram and frequency dependence of the LDOS are shown in Fig. 3.1 for a W1 waveguide of GaAs. Three guided modes are formed inside the band gap and the slow-light effect is clearly seen from the vanishing slopes of the dispersion curves. This effect is the most pronounced at the edge og the guided mode, where the group velocity tends to zero, and the corresponding group index $n_g = c/v_g$ diverges. Additionally, the mode in the waveguide is confined to a small spatial volume, which causes the electric field to have an additional component, directed along the propagation direction. It is possible to couple the x- and y-dipoles to the odd and even mode, respectively, by placing the emitter in a high-symmetry point. This gives the y-dipole a wide range of possible frequencies with an enhanced LDOS; this makes the even mode the most commonly used mode for experiments. The x-dipole, on the other hand, has a shorter range of frequencies with several sharp peaks for the LDOS, due to a vanishing group velocity at several frequencies. The effect of the band gap region is also seen in the frequency region $\omega a/2\pi = (0.255, 0.26)$ which shows a suppressed LDOS.
The effect of slow light enhances the interaction between the guided modes and a quantum emitter embedded in the waveguide. This enhancement is quantified by the Purcell factor, which for a PhC waveguides is given by:

$$F_{\mathrm{P}}^{\max}(\omega) = \left(\frac{3}{4\pi n}\frac{\lambda^2/n^2}{V_{\mathrm{eff}}/a}\right) n_g(\omega), \tag{3.5}$$

where $V_{\mathrm{eff}} \sim a(\lambda/n)^2/3$ is the effective mode volume for a W1 waveguide and λ/n is the wavelength of the light inside the waveguide, with n a the refractive index of the waveguide. The mode volume varies weakly over the waveguide band, which leaves the group index as the primary contributor to the Purcell factor. Values of $n_g \sim 300$ for a silicon based W1 waveguide [22] has been achieved experimentally, which gives a Purcell factor of 120, whereas the group index approaches $n_g \sim 50$ for GaAs waveguides [1]. Fig. (3.3) shows the spatial dependence of the Purcell factor and the β-factor (introduced below) in both the fast light ($n_g = 5$)- and the slow-light ($n_g = 58$) regime.
An additional advantage of PhC waveguide is that they are open systems, which allows a quantum emitter to directly channel an emitted photon into the waveguide. This is in contrast to

cavity based systems, where the single photons are coupled to localized modes and needs to be coupled out of the cavity. This makes PhC waveguides prime candidates for the use in quantum information processes that requires the interaction between stationary and flying qubits. The coupling between the quantum dot and the waveguide is quantified by the β-factor:

$$\beta = \frac{\gamma_{\mathrm{wg}}}{\gamma_{\mathrm{wg}} + \gamma_{\mathrm{ng}} + \gamma_{\mathrm{nrad}}}, \tag{3.6}$$

where γ_{wg} is the emission rate into the waveguide, γ_{ng} is the loss rate to non-guided modes and γ_{nrad} is the loss rate to various non-radiative losses of the quantum dot. Recent experiments have determined a near-unity β-factor > 0.98 [1] due to the strong suppression of γ_{ng} by the photonic band gap. The main limiting factor for the β-factor is from the intrinsic loss rate γ_{nrad} of the quantum dot.

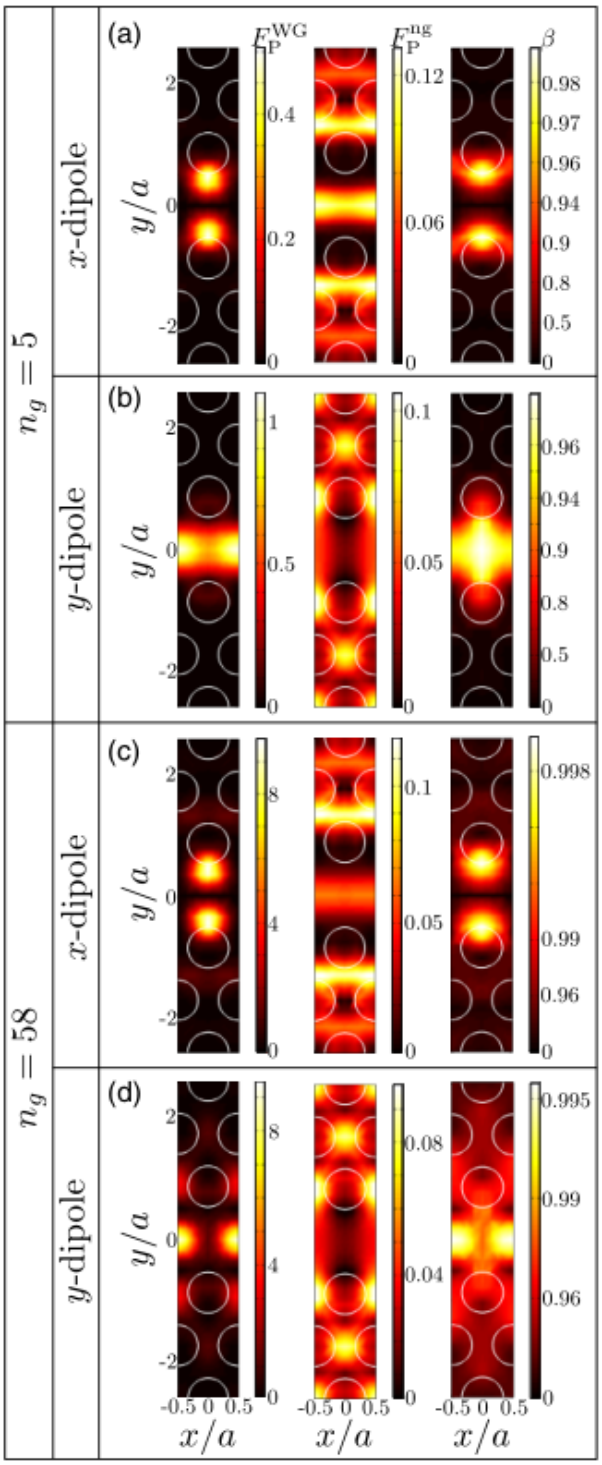

Figure 3.3: Spatial dependence of the Purcell factor and β-factor in a photonic waveguide. The left panel shows the overall Purcell factor, while the center panel shows the Purcell enhancement of emission into nonradiative modes. The panel to the right shows the enhancement of the radiative β factor. (a) is for a x-dipole with $n_g = 5$, while (b) is for a y-dipole with the same group index. (c) and (d) shows plots for a x- and y-dipole respectively with $n_g = 58$. This figure is reprinted from [13].

3.2 Quantum Dots

3.2.1 Basic Properties

Self-assembled semiconductor quantum dots provide a suitable platform for an implementation of quantum emitters into a PhC waveguide. These structures contain thousands of individual atoms that collectively display similar optical properties to natural atoms, due to the quantum confinement of electrons on a nanometer length scale. This confinement can be implemented by sandwiching a lower-band gap semiconducting material between two pieces of another semiconducting material with a higher band gap. The regions with the lower band gap acts as a trapping potential and strongly changes the electronic density of states (E), depending on the number of confined dimensions:

$$\text{No confinement: Bulk material } - g_{3\mathrm{D}} = \frac{m_{\mathrm{eff}}}{\pi^3\hbar^2}\sqrt{2m_{\mathrm{eff}}\left(E-E_0\right)} \tag{3.7}$$

$$\text{Confinement in 1D: Quantum well} - g_{2\mathrm{D}} = \frac{m_{\mathrm{eff}}}{\pi\hbar^2}\sum_j \theta\left(E-E_j\right) \tag{3.8}$$

$$\text{Confinement in 2D: Quantum wire} - g_{1\mathrm{D}} = \frac{\sqrt{2m_{\mathrm{eff}}}}{\pi\hbar}\sum_j \frac{\theta\left(E-E_j\right)}{\sqrt{E-E_j}} \tag{3.9}$$

$$\text{Confinement in 3D: Quantum dot} - g_{0\mathrm{D}} = 2\delta\left(E-E_j\right), \tag{3.10}$$

where E_j denotes discrete energy levels. The discrete structure of the electronic density of states allows quantum dots to emit single photons when an correlated election-hole pair (also called an exciton) recombine. An energetic electron-hole pair can be generated at the GaAs band gap by absorption of a photon. The pair can then relax into the confinement potential of the quantum dot through nonradiative processes. This correlated pair will eventually recombine, thereby emitting a single photon. This emission process can be measured using photoluminescence spectroscopy, which reveals a sharp peak at the emission frequency, similar to that of an atom. The electron occupancy can be directly controlled by varying the gate voltage over the heterojunction[21]. This also makes it possible to control the interaction strength between the quantum dot and the guided mode by enhancing the overlap of the envelope functions. These are introduced in Section (3.2.2).

One common approach for growing quantum dots is the Stranski-Krastanov method, which relies on the self assembly of InAs quantum dots on a GaAs surface due to the mismatch between lattice constants in the two materials. This leads to a truncated pyramidal shape due to material intermixing and further leads to an inhomogeneous indium distribution and a spatially varying strain. The typical height of a quantum dot is $1-10$ nm with an in-plane size of $10-70$ nm. This leads to aspect ratios relatively larger than unity with a quantization axis in the growth direction. Each quantum dot needs to be tuned differently from others due to inevitable differences in the size of quantum dots from the same growth run.
The tetrahedral bonds and zinc-blende crystal structure for InAs, GaAs and InGaAs quantum dots results in the formation of three degenerate energy bands in the valence band. The split-off band gets shifted to a lower energy level by including spin-orbit couplings, while the degeneracy between the heavy- and light-hole bands gets lifted by the aspect ratio of these quantum dots. This energy spacing is sufficiently large that the lowest energy transition is between the conduction band and the heavy-hole band. The unfilled orbital shells of Ga, In and As are $4s^2 4p, 5s^2 5p$ and $4s^2 4p^3$, which results in the conduction band exhibiting s-symmetry while the valence band shows p-symmetry. Additionally, the heterojunctions of InGaAs embedded in GaAs (as well as GaAs in AlGaAs) have type-I energy bands alignments, which ensures that carriers are confined

in both the conduction and valence bands. This is crucial for the efficient interaction with light for the formation of quantized states of elections and holes.

3.2.2 Effective Mass Theory & the Transition Matrix Element

Quantum dots can be reliably described through the effective mass theory, provided that the energy-level spacing of carries is large compared to the confinement potential such that the potential can be treated as a perturbation. In addition, only a small region in **k**-space is assumed to contribute to the interaction and that only small carrier populations is involved with the interaction. Lastly, the larger than unity aspect ration for the relevant quantum dots shift the light-hole band energy far enough away from the heavy hole band energy that only the latter is needed for a sufficient description of the quantum dot. Note that this assumption relies heavily on the large aspect ratio and can easily break down. The wave function for an electron in the conduction band c or valence band v can be split into three parts:

$$|\psi_{\mathrm{c,v}}\rangle = |\chi_{\mathrm{c,v}}\rangle\,|u_{\mathrm{c,v}}\rangle\,|\alpha_{\mathrm{c,v}}\rangle\,, \tag{3.11}$$

where $|\chi_{\mathrm{c,v}}\rangle$ is the envelope wave function, $|u_{\mathrm{c,v}}\rangle$ is the electronic Bloch function and $|\alpha_{\mathrm{c,v}}\rangle$ is the spin wave function. The envelope function is obtained from the time independent effective-mass Schrödinger equation:

$$\left(\frac{-\hbar^2}{2m_0}\nabla\frac{1}{m_e\left(\mathbf{r}\right)}\nabla - V_{\mathrm{c,v}}\left(\mathbf{r}\right)\right)|\chi_{\mathrm{c,v}}\left(\mathbf{r}\right)\rangle = \left(E - E_{\mathrm{c,v}}\right)|\chi_{\mathrm{c,v}}\left(\mathbf{r}\right)\rangle\,, \tag{3.12}$$

and describes the modulation of the Bloch function to give the full wave function. E is the electron eigenenergy, $E_{\mathrm{c,v}}$ is the band edge energy, $V_{\mathrm{c,v}}\left(\mathbf{r}\right)$ is the confinement potential, m_0 is the electron rest mass and $m_e\left(\mathbf{r}\right) = \hbar^2\left(\partial^2 E/\partial\left(\mathbf{k}\right)^2\right)^{-1}$ is the effective mass. This Schrödinger equation can be cast into a form that resembles the equation for a hydrogen atom by assuming that the effective mass is isotopic (which is a reasonable approximation for type III-V semiconductors) and using an attractive Coulombic potential between the electron and hole: $V\left(\mathbf{r}\right) = -e^2/\left(4\pi\epsilon_0\epsilon\left|\mathbf{r}_e - \mathbf{r}_h\right|\right)$. Here e is the elementary charge, ϵ_0 is the vacuum permittivity, ϵ is the permittivity of the material and $|\mathbf{r}_e - \mathbf{r}_h|$ is the distance between the election and the hole. The complicated potential profile of the unit cell has been merged into the effective mass, which can be accurately determined from experiments. These assumptions greatly simplifies the problem of solving the Schrödinger equation and allows to find the discrete energy levels of the quantum dot.

The minimal coupling Hamiltonian H_c induces optical transitions and is in the Coulomb gauge given by:

$$H_c = -\frac{e}{m_0}\mathbf{p}\cdot\mathbf{A}\left(\mathbf{r}_0, t\right), \tag{3.13}$$

where $\mathbf{p} = -i\hbar\nabla$ is the momentum operator and $\mathbf{A}\left(\mathbf{r}_0, t\right)$ is the vector potential of the electromagnetic field and is evaluated at the position of the quantum dot. This Hamiltonian is written in the dipole approximation, which is valid when the wavelength of light is significantly larger than spatial extent of the quantum dot. This Hamiltonian enter into the decay rate for spontaneous emission, which is given by Fermi's golden rule:

$$\Gamma\left(\omega\right) = \frac{\pi e^2}{\hbar\omega m_0^2\epsilon_0}\left|\langle f|\mathbf{p}|i\rangle\right|^2\rho\left(\mathrm{r}_0, \omega, \hat{e}_{\mathbf{p}}\right), \tag{3.14}$$

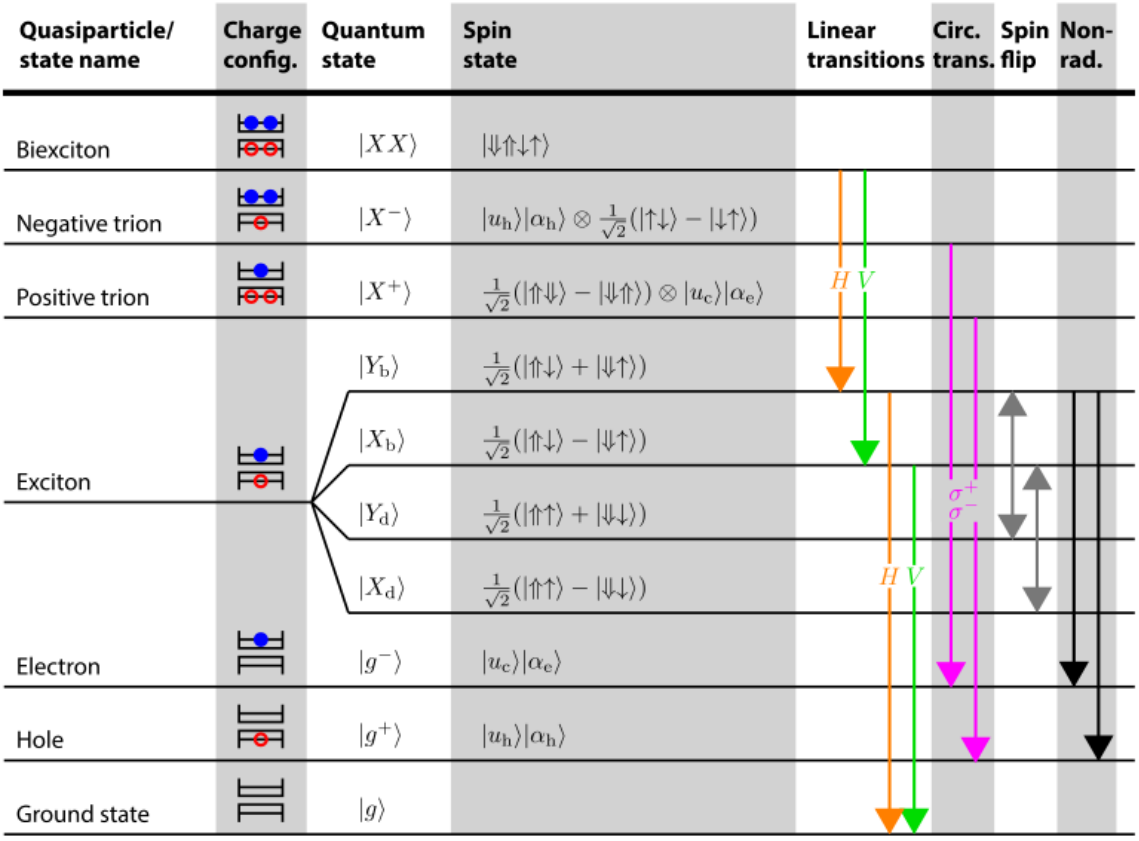

Figure 3.4: The transition for the lowest-energy confined states in a quantum dot. The full blue (empty red) circles represent the electron (hole) configuration in the conduction (valence) bands. Reprinted from [13]

where $|f\rangle$ and $|i\rangle$ represent final and initial states, respectively. The crucial component is the transition dipole matrix element $\mathbf{P} = \langle\psi_v|\mathbf{p}|\psi_c\rangle$ which, when using Eq. (3.11), takes the following form:

$$\mathbf{P} = \langle F_v|F_c\rangle \langle u_v|\mathbf{p}|u_c\rangle \langle \alpha_v|\alpha_c\rangle \,, \tag{3.15}$$

which reveals three selection rules for optical transitions: (i) the envelope functions must have the same parity, (ii) the Bloch functions must have opposite parity, and (iii) the electron spin must be unchanged. These selection rules, along with the respective s- and p-symmetry of the conduction- and valence band, makes it possible to determine the polarization of the optical transitions. The electron pseudospin states are defined as

$$|\uparrow\rangle \equiv |u_c\rangle\,|\uparrow_e\rangle = |u_s\rangle\,|\uparrow_e\rangle \tag{3.16}$$

$$|\downarrow\rangle \equiv |u_c\rangle\,|\downarrow_e\rangle = |u_s\rangle\,|\downarrow_e\rangle \tag{3.17}$$

and the hole pseudospin states are

$$|\Uparrow\rangle \equiv |u_v\rangle\,|\uparrow_h\rangle = -\frac{1}{\sqrt{2}}\left(|u_x\rangle + i\,|u_y\rangle\right)|\uparrow_h\rangle \tag{3.18}$$

$$|\Downarrow\rangle \equiv |u_v\rangle\,|\downarrow_h\rangle = \frac{1}{\sqrt{2}}\left(|u_x\rangle - i\,|u_y\rangle\right)|\uparrow_h\rangle \,, \tag{3.19}$$

where $|u_{\rm s}\rangle, |u_{\rm x}\rangle$ and $|u_{\rm y}\rangle$ denotes functions with even parity, odd parity along x and odd parity along y, respectively. It is easy to see that the states $|\Uparrow\uparrow\rangle$ and $|\Downarrow\downarrow\rangle$ have optically forbidden transitions, as the relevant matrix s are given by the inter products $\langle\uparrow_{\rm e}\,|\uparrow {\rm h}\rangle = \langle\downarrow_{\rm e}\,|\downarrow {\rm h}\rangle = 0$. These definitions makers it possible to evaluate the matrix element for the transition dipole; this is simplified by assuming that the magnitude of the two odd parity Bloch function are equal and differ only bu the direction of their circular polarization. The transition matrix elements for an electron-hole pair is then given by:

$$\langle g|\mathbf{p}|\Uparrow\downarrow\rangle = -\frac{1}{\sqrt{2}}\langle F_{\mathbf{v}}|F_{\rm v}\rangle\langle u_{\rm x}|\mathbf{p}|u_{\rm s}\rangle(\hat{e}_{\rm x} + i\hat{e}_{\rm y}) \tag{3.20}$$

$$\langle g|\mathbf{p}|\Downarrow\uparrow\rangle = \frac{1}{\sqrt{2}}\langle F_{\mathbf{v}}|F_{\rm v}\rangle\langle u_{\rm x}|\mathbf{p}|u_{\rm s}\rangle(\hat{e}_{\rm x} - i\hat{e}_{\rm y}), \tag{3.21}$$

where the inner product between the spin states have been implicitly evaluated to one. The optical transition for an electron-hole pair is evidently circular polarized. The most general electron-hole states are linear superpositions of the optically allowed states listened in Eqs. (3.16) through (3.19). These bright exciton states are defined as

$$|X_{\rm b}\rangle = \frac{1}{\sqrt{2}}(|\Uparrow\downarrow\rangle - |\Downarrow\uparrow\rangle) \tag{3.22}$$

$$|Y_{\rm b}\rangle = \frac{1}{\sqrt{2}}(|\Uparrow\downarrow\rangle + |\Downarrow\uparrow\rangle). \tag{3.23}$$

The optical transitions for these two exciton states are linearly polarized along x and y respectively, which is easily seen from Eqs. (3.20) and (3.21). The dark exciton states are defined as:

$$|X_{\rm b}\rangle = \frac{1}{\sqrt{2}}(|\Uparrow\Downarrow\rangle - |\Downarrow\Uparrow\rangle) \tag{3.24}$$

$$|Y_{\rm b}\rangle = \frac{1}{\sqrt{2}}(|\Uparrow\Downarrow\rangle + |\Downarrow\Uparrow\rangle), \tag{3.25}$$

and are related to the bright states through spin-flip processes. There exist several other excitonic states, such as the trion states (with two holes in the valence band and a single electron in the conductance band for the positive trion or a single hole and two electrons for the negative trion) and the biexciton, which is comprised of two correlated electron-hole pairs. The negative and positive trion decay to a single electron and hole, respectively, while the biexciton can decay to either of the bright exciton states. The various excitonic states, their pseudospin representation and their allowed optical transitions are summarized in Fig. (3.4).

3.2.3 Optical Properties of Quantum Dots

The ground states of an exciton in comprised of an electron with spin and spin projection $S = 1/2, M_{\rm S} = \pm 1/2$ in the conduction band and a heavy hole with angular momentum $J = 3/2$ and projections $M_{\rm J} = \pm 3/2$ in the valence band. The light hole band can often be neglected, as it is separated in energy from the heavy-hole band due to strain effects and the large aspect ratio of the quantum dot. The total angular momentum of the exciton is thus $J_{\rm ex} = \pm 2$ for the dark excitons of Eqs. (3.24) and (3.25), while $J_{\rm ex} = \pm 1$ is associated with the bright excitons defined in Eqs. (3.22) and (3.23). The Coulomb exchange energy induce an energy-splitting between the dark and bright states of $\Delta E_{\rm fss} \sim 10 - 100\mu$eV and they are coupled through spin-flip processes, as mentioned above, at a rate of γ_{sf}. An additional effect of the exchange energy is a splitting of the two dark states on the order of 1μeV.

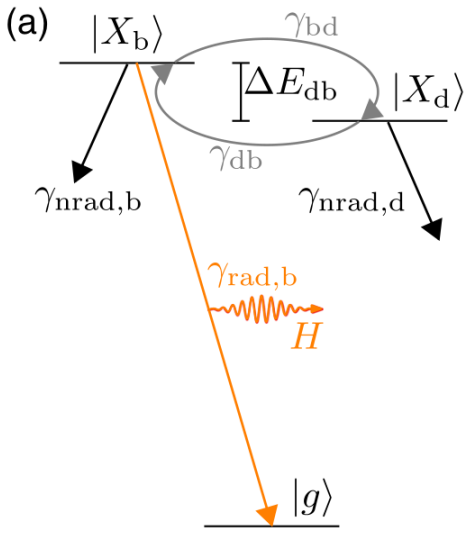

Figure 3.5: Basic level scheme for the exciton. The bright exciton can decay through radiative and nonradiative processes, while the dark exciton only decay nonradiatively. Spin-flip processes between the two states can occur at the rate γ_sf. This is an excerpt from Fig. 4 in [13].

The bright states can, in addition to the radiative transitions with decay rate γ_rad discussed above, decay through nonradiative transitions with a rate of γ_nrad, while the dark states can only decay through decay nonradiantly. The spin-flip processes typically takes place over longer time scales than the radiative decay, and transition between $|X_\mathrm{b,d}\rangle$ and $|Y_\mathrm{b,d}\rangle$ require the simultaneous change of spin on both the electron and the hole. It is therefore sufficient to only include the spin flip processes between $|X_\mathrm{b}\rangle$ and $|X_\mathrm{d}\rangle$, as well as between $|Y_\mathrm{b}\rangle$ and $|Y_\mathrm{d}\rangle$. Consider the level scheme in Fig. (3.5) for the decay dynamics of the bright and dark exciton. The exciton follows a bi-exponential decay in the case of non-resonant excitation and with evenly distributed populations in the dark and bright state $\rho_\mathrm{b}(0) = \rho_\mathrm{d}(0) = 1/2$. The population of the bright state then decay as:

$$\rho_\mathrm{b} = A_\mathrm{f} e^{-\gamma_\mathrm{f} t} + A_\mathrm{s} e^{-\gamma_\mathrm{s} t}, \tag{3.26}$$

with fast and slow decay rates and amplitudes

$$\gamma_\mathrm{f,s} = \frac{\gamma_\mathrm{rad}}{2} + \gamma_\mathrm{nrad} + \gamma_\mathrm{sf} \pm \sqrt{\frac{\gamma_\mathrm{rad}^2}{4} + \gamma_\mathrm{sf}^2} \tag{3.27}$$

$$A_\mathrm{f,z} = \rho_\mathrm{b}(0)\left(1 + \pm\frac{\gamma_\mathrm{rad}}{\gamma_\mathrm{f} - \gamma_\mathrm{s}}\right) \mp \rho_\mathrm{d}(0)\frac{\gamma_\mathrm{sf}}{\gamma_\mathrm{f} - \gamma_\mathrm{s}}. \tag{3.28}$$

This bi-exponential decay makes it possible to map out the radiant, nonradiant and spin-flip decay rates for a single quantum dot through time resolved photoluminescence spectroscopy. This must be done for each single quantum dot in an ensemble, as random processes during fabrication can result in considerable differences in the spin-flip and nonradiative decay rates. Note that trions and biexcitons do not have a fine structure. The carrier population will thus follow a single-exponential decay for these excitonic states with no direct way of accessing the spin-flip and nonradiant decay rates.

The mesocopic nature of quantum dots and the solid state structure of the photonic crystals that they are embedded in gives rise to various decoherence processes, including interactions with phonons in the crystal, interactions with charge fluctuations due to lattice defects and coupling to spin fluctuations in the nuclei of the lattice atoms all give rise to the non-radiative decay and to dephasing, where the processes due to dephasing can reduce the coherence of the quantum dot without affecting the population of the excitonic states. High coherence is needed in order to efficiently implement quantum information protocols. The simplest approach is to assume that the dephasing processes are Markovian and can be described by a single decay rate γ_{dp}. This decay can be phenomenologically introduced into the equations of motion for the off-diagonal element of the master equation. The resulting lifetime can be decomposed in to a contribution from spontaneous emission and from dephasing processes:

$$\frac{1}{T_2} = \frac{1}{2T_1} + \frac{1}{T_2^*}, \tag{3.29}$$

where T_2 is the total coherence time, T_1 is the inverse of the total decay rate of the emitter and $T_2^* = \gamma_{\mathrm{dp}}^{-1}$ is the dephasing time. The existence of dephasing causes the coherence to decay faster than the population and can introduce additional errors in quantum information protocols. Dephasing times up to $T_2^* = 0.6$ns have been reported for a photonic crystal cavity [14]. The effects of charge noise can be reduced by resonantly exciting the quantum dot, whereas the effects imposed by interactions with phonons can be reduced by cooling the quantum dot down to near absolute zero temperatures, as can be seen from Fig. (3.6). Fig. (3.6) shows the emission spectrum of a quantum dot coupled to a longitudinal acoustic (LA) phonon reservoir for various temperatures. This demonstrates that LA phonons constitute a significant broadband source of dephasing with an asymmetrical broadening of the linewidth of the emission spectrum.
The detrimental effects of the pure dephasing processes on the proposed controlled phase gate are discussed in Sections (5) and (6).

The interaction strength is determined by the transition matrix element, as introduced above. This in an intrinsic, immutable property of atoms but can be manipulated in quantum dots. This is quantified by the oscillator strength f, defined as the ratio of the radiative decay rate in a homogeneous medium and the decay rate of a classical harmonic oscillator of elementary charge. The oscillator strength is given by:

$$f = \frac{2}{\hbar\omega_0 m_0} |\mathbf{P}|^2 = \frac{E_p}{\hbar m_0} \left|\langle F_{\mathrm{v}}|F_{\mathrm{c}}\rangle\right|^2, \tag{3.30}$$

where E_P is the Kane energy and is of the order of $E_P \sim 25$eV for InAn and GaAs. It is seen that the oscillator strength can be maximized by increasing the overlap between the conduction band and valence band envelope functions. These can be changed by tuning the trapping potential barrier of the quantum dot and it is thus possible to increase the light-matter interaction directly through the emitter, in contrast to the case with atomic system, where the light-matter interaction strength can only be increased by changing the LDOS of electromagnetic modes that the atom can couple to. It is possible to further increase the light-matter interaction for the quantum dot by embedding it in a W1 waveguide in a PhC, thereby inhibiting the continuum of unwanted modes and enhancing the coupling to a desired guided mode, as described in Section (3.1).

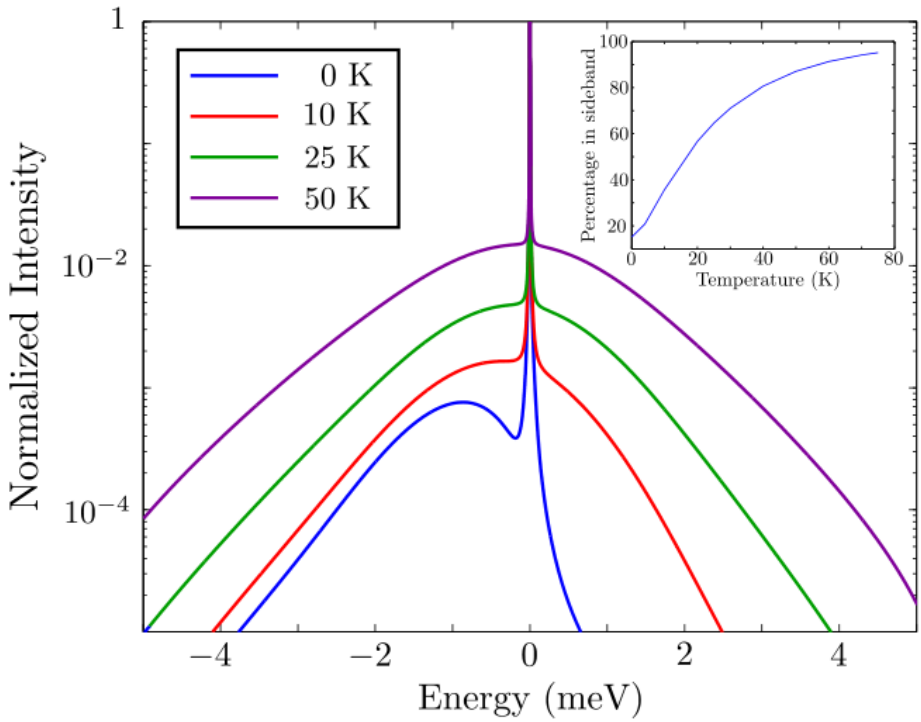

Figure 3.6: Broadening of the normalised emission spectrum of a quantum dot coupled to a LA phonon reservoir. The strong dependence on temperature is observed with a high degree of asymmetry in the sidebands at low temperatures. Reprinted from [13].

3.3 Initialization of Qubit States

The properties of quantum dots and waveguides embedded in photonic crystals provide a promising platform for implementing quantum information protocols. Any successful implementation requires that the qubits are represented by long lived quantum states, as explained in Section (2.2.2). The bright exciton described above is not a useful physical entity for this purpose, due to the emptiness of the ground state. The biexciton is unsuited for the same reason, as it decays to the either of the bright excitons. Instead, consider the structure of the negatively charged trion: it consists of two electrons in a singlet with a heavy hole. The trion is denoted by $|\downarrow\uparrow\Uparrow\rangle$ ($|\downarrow\uparrow\Downarrow\rangle$) and has the spin projections $M_S = 3/2$ ($M_S = -3/2$). This is coupled to a ground state consisting of an electron $|\uparrow\rangle$ ($|\downarrow\rangle$) with spin projection $M_S = 1/2$. ($M_S = -1/2$). The optical transition between the trion and the electron is circularly polarised (see Fig. (3.4)) with a decay rate of γ^{1D} into the guided mode. It is possible to use the states $|\uparrow\rangle$ and $|\downarrow\rangle$ for the electron as qubit states due to the lack for optical transitions for an electron and the trapping of the electron in the confinement potential; they will thus be denoted as $|\uparrow\rangle = |1\rangle$ and $|\downarrow\rangle = |0\rangle$. These qubits can be initialised following the procedure from [8], which is highlighted below.
The four states listed above each undergo a different energy shift when an external magnetic field is applied along the z axis. Transitions from the state $|\downarrow\uparrow\Downarrow\rangle$ can be neglected if a σ^+ polarised laser at Rabi frequency Ω_R is introduced at the optical transition, as the coupling strength is reduced by a factor of 10^3 for magnetic fields larger than 60mT. The laser has a detuning of $\Delta\omega = \omega_0 - \omega_L$, where ω_0 is the transition frequency of the trion and ω_L is the laser frequency. The Hamiltonian describing the system is

$$\hat{H} = \hat{H}_{\text{Hyp}} + \hat{H}_{\text{Charge}} + \hat{H}_{\text{Phonon}} + \hat{H}_{\text{Int,rad}} + \hat{H}_{\text{Zeeman}}, \tag{3.31}$$

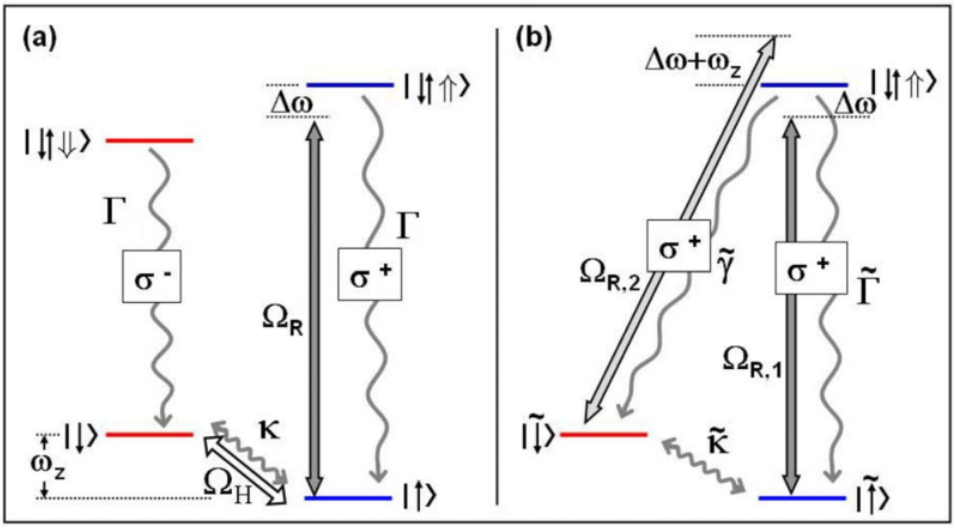

Figure 3.7: (a). Four-level system for the negatively charged trion. A magnetic field is applied along the growth direction, which induces a Zeeman splitting $\hbar\omega_z$ of the electron and trion states. A laser with Rabi frequency $\Omega_{\mathring{R}}$ is introduced along the σ^+ transition. Ω_{H} and κ denote coherent and incoherent spin-flip processes, respectively. (b) Dressed state picture formed by eliminating Ω_{H}. The laser field has been split up into $\Omega_{\mathrm{R},1}$ and $\Omega_{\mathrm{R},2}$, while a weak decay rate $\tilde{\gamma}$ has been introduced. Reprinted from [8]

where the first three terms describe coupling to the nuclear spin (i.e. the hyperfine effect), electron gas and phonons, respectively. In addition, this scheme suppresses the decay rate for nonradiative decay processes between $|\uparrow\downarrow\Uparrow\rangle$ and $|\downarrow\rangle$. The interaction with the radiation field is treated in Chapter (4) and results in dissipative evolution of the quantum dot with a decay rate of $\gamma^{1\mathrm{D}}$. Coherent and dissipative dipole-dipole interactions exist in a structure containing several quantum dots, which may exert an influence on the initialisation scheme presented here. In addition, the coupling to the phonons and electron gas can be treated as dissipative processes in the Born Markov approximation, leaving $\hat{H}_{\mathrm{Hyp}}$ and $\hat{H}_{\mathrm{Zeeman}}$ as the only unitary processes of Eq. (3.31).

The magnetic field is given by $\mathbf{B} = \mathbf{B}_{\mathrm{Ext}} + \mathbf{B}_{\mathbf{N}}$, where $\mathbf{B}_{\mathrm{Ext}} = (0, 0, B_z)$ is the external magnetic field aligned along the z axis and $\mathbf{B}_{\mathbf{N}}$ is the nuclear magnetic field. The hyperfine Hamiltonian is given by:

$$\hat{H}_{\mathrm{Hyp}} = \hbar\Omega_H\hat{\sigma}_x, \tag{3.32}$$

$$\hbar\Omega_H = \frac{g_e\mu_B\sqrt{B_{N,x}^2 + B_{N,y}^2}}{2}, \tag{3.33}$$

where g_e is the quantum dot electron g factor, μ_B is the Bohr magneton and $B_{N,\{x,y\}}$ is the x and y component of the nuclei magnetic field. Ω_{H} describes a coherent spin-flip process between the two electronic ground states due to fluctuations in the nuclei magnetic field. This will typically be much lower than the effect from the external magnetic field. The z component $B_{N,z}$ is not included here as it leads to a Zeeman shift; it is thus included in the Hamiltonian for the Zeeman

effect:

$$\hat{H}_{\text{Zeeman}} = \hbar\omega_z\hat{\sigma}_z + g_h\mu_B B_z \cdot \hat{J}_z, \tag{3.34}$$

$$\omega_z = g_e\mu_B \left(B_z + B_{N,z}\right), \tag{3.35}$$

where g_h is the quantum dot hole g factor, $\hat{\sigma}_i$ are Pauli spin operators for the electronic ground states and $\hat{J}_z$ is the z component of the hole spin operator. The spin-reservoir couplings leads to a weak mixing between $|\downarrow\rangle$ and $|\uparrow\rangle$ and between the two trion states; the mixing rate κ between the electronic state can be suppressed using sufficiently low gate voltages, whereas mixing between the trion is neglected due to the low probability for the system to be in these excited states.
The Hamiltonian is Eq. (3.34) can be cast in a more intuitive picture by transforming to the dressed state picture. The new dressed states are:

$$|\tilde{0}\rangle \equiv \cos\theta\,|0\rangle - \sin\theta\,|1\rangle \tag{3.36}$$

$$|\tilde{1}\rangle \equiv \sin\theta\,|0\rangle + \cos\theta\,|1\rangle \tag{3.37}$$

$$|e\rangle \equiv |\downarrow\uparrow\Uparrow\rangle, \tag{3.38}$$

where $\theta = \Omega_H/\omega_z$ is the mixing angle. This can be taken as $\theta \ll 1$ for the experimental parameters in [8], leading to the dressed state Hamiltonian:

$$\tilde{H} = \hbar\omega_z\,|\tilde{0}\rangle\langle\tilde{0}| + \Delta\omega\,|e\rangle\langle e| + \Omega_{R,0}\left(|\tilde{0}\rangle\langle e| + |e\rangle\langle\tilde{0}|\right) + \Omega_{R,1}\left(|\tilde{1}\rangle\langle e| + |e\rangle\langle\tilde{1}|\right). \tag{3.39}$$

This leads to a system that is diagonal in the dressed ground states $|\tilde{0}\rangle$ and $|\tilde{1}\rangle$. The single laser field is in this basis represented by two laser fields, $\Omega_{R,0}$ and $\Omega_{R,1}$, that couple the excited state to $|\tilde{0}\rangle$ and $|\tilde{1}\rangle$, respectively. In addition, the spontaneous emission is split into two distinct channels with emission rates $\tilde{\gamma}^{1\text{D}}$ and $\tilde{\gamma}$. The relevant parameters for the interactions between $|\tilde{1}\rangle$ and $|e\rangle$ are:

$$\tilde{\gamma}^{1\text{D}} = \gamma^{1\text{D}}, \quad \Omega_{R,1} = \Omega_R, \quad \Delta\omega_0 = \Delta\omega, \tag{3.40}$$

while the parameters for the $|\tilde{0}\rangle \leftrightarrow |e\rangle$ subsystem are:

$$\tilde{\gamma} = \theta^2\gamma^{1\text{D}}, \quad \Omega_{R,0} = \theta\Omega_R, \quad \Delta\omega_1 = \Delta\omega + \omega_z \tag{3.41}$$

This creates an effective Raman transition between two dressed ground states when a resonant laser is applied on the $|\tilde{1}\rangle \leftrightarrow |e\rangle$. The absence of an external magnetic field equalises the two subsystems, leading to a random mixed spin: $\rho_{\tilde{0}\tilde{0}}\left(t=\infty, B_z=0\right) = \rho_{\tilde{1}\tilde{1}}\left(t=\infty, B_z=0\right) = 1/2$, leading to a mixed state $\rho = 1/2\left(|0\rangle\langle 0| + |1\rangle\langle 1|\right)$ unsuited as a starting point for quantum information processes. On the other hand, keeping the external magnetic field non-zero inhibits the transfer rate from $\rho_{\tilde{0}\tilde{0}}$ to $\rho_{\tilde{1}\tilde{1}}$, where ρ is the density matrix formed from the three dressed states in Eqs. (3.36) through (3.38). This makes it possible to prepare the population of the spins to be solely in ρ_{00} for a strong external magnetic field in the steady state, while keeping the population of the excited state empty. Keeping the external magnetic field at a value of $B_z \sim 60\text{mT}$ leads to a coherent population transfer with $\rho_{\tilde{0}\tilde{0}}\left(t=\infty, B_z\sim 60\right) = \rho_{\tilde{1}\tilde{1}}\left(t=\infty, B_z\sim 60\right) = 1/2$. Choosing the dressed ground states as the qubit states will then make it possible to prepare the following superposition state:

$$|\psi\rangle = \frac{1}{\sqrt{2}}\left(|\tilde{0}\rangle + |\tilde{1}\rangle\right) \tag{3.42}$$

$$\approx \frac{1}{\sqrt{2}}\left(|0\rangle + |1\rangle\right), \tag{3.43}$$

for mixing angles $\theta \ll 1$. Repeating this scheme for a second qubit gives the product state:

$$|\Psi\rangle = |\psi\rangle_{\text{q},1} \otimes |\psi_{\text{q},2}\rangle = \frac{1}{2}\left(|00\rangle + |01\rangle + |10\rangle + |11\rangle\right), \tag{3.44}$$

from which the derivation of the controlled phase gate in Chapter (5) starts from.

Chapter 4

Decay Properties of Coupled Quantum Emitters

A strong interaction between a number of quantum emitters is a necessary condition in order to implement a two-qubit quantum gate. This interaction is typically mediated by some other physical entity. This chapter will formalise the interaction between three self assembled quantum dots embedded in a Q1 waveguide in a GaAs photonic crystal. The quantum dots acts as the quantum emitters, where the interaction between them is mediated by photons propagating in the waveguide. Section (4.1) introduces the model for the three-level quantum emitters, while the simplified case of three coupled two-level emitters is discussed in Section (4.2) as a staring point. The full treatment of the coupled three-level emitters is given in Section (4.3).

4.1 Defining the System

It is possible to use the dipole-dipole interaction between three quantum emitters to implement a controlled phase gate. Two of the emitters are used to represent the actual qubit states, while the third auxiliary emitter is used to probe the system and for implementing an integrated error detection. This chapter will explore the decay properties of three coupled quantum dots embedded in a W1 photonic waveguide. All three emitters couple to the waveguide through optical transitions between the excited state and the optical ground state. In addition, a weak laser field $\hat{V}$ is directed at a forbidden transition for the auxiliary emitter. The level scheme of the auxiliary and qubit emitters is shown in Fig. (4.1) and can be represented by the following Hamiltonian in the dipole approximation and in a proper rotating frame:

$$\hat{H} = \hbar\Delta_{\mathrm{A}} \left|\mathrm{E}\right\rangle_{\mathrm{A}} \left\langle\mathrm{E}\right| + \hbar \sum_{n=1}^{2} \delta_{\mathrm{n}} \left|\mathrm{e}\right\rangle_{\mathrm{n}} \left\langle\mathrm{e}\right| + \frac{\Omega}{2} \left[\left|\mathrm{E}\right\rangle_{\mathrm{A}} \left\langle\mathrm{g}\right| + \left|\mathrm{g}\right\rangle_{\mathrm{A}} \left\langle\mathrm{E}\right|\right] \tag{4.1}$$

$$+ \hbar \sum_{\mathbf{k}} \left[g_{\mathbf{k}}^{(\mathrm{A})} \hat{\sigma}_{+}^{(\mathrm{A})} a_{\mathbf{k}} e^{i(\Delta_{\mathrm{A}} - \omega_{\mathbf{k}})t} + \sum_{n=1}^{2} g_{\mathbf{k}}^{(\mathrm{n})} \hat{\sigma}_{+}^{(\mathrm{n})} a_{\mathbf{k}} e^{i(\delta_{\mathrm{n}} - \omega_{\mathbf{k}})t} \right] + H.C. \tag{4.2}$$

where $\Delta_{\mathrm{A}} = \omega_{\mathrm{E}} - \omega_{\mathrm{g}} - \omega_{\mathrm{L}}$ is the detuning between the laser and the transition energy of the forbidden transition for the auxiliary emitter. $\delta_{\mathrm{n}} = \Delta_{\mathrm{A}} + \omega_{\mathrm{e,n}} - \omega_{1,\mathrm{n}}$ is a detuning for the qubits formed from the choice of rotating frame. ω_{L} is the frequency of the laser, while ω_x denotes the frequency for level x, Ω is the strength of the laser and $a_{\mathbf{k}}$ is the annihilation operator of a photon with wave vector $\mathbf{k}$ and frequency $\omega_{\mathbf{k}}$. The auxiliary emitter is not included in the sums in the equations above, as it may have different optical properties from the qubit emitters. The coupling constant $g_{\mathbf{k}}$ is defined from the interaction Hamiltonian between the dipole operator

$\hat{\mathbf{d}} = \mathbf{d}\left(\hat{\sigma}_+ + \hat{\sigma}_-\right)$ and a reservoir of photonic states through the quantized electric field $\hat{E}$. The electric field is written in terms of the photonic annihilation and creation operators as:

$$\hat{\mathbf{E}}\left(\mathbf{r}, t\right) = i \sum_{\mathbf{k}} \left[\mathbf{E}_{\mathbf{k}}\left(\mathbf{r}\right) a_{\mathbf{k}} - H.C.\right], \tag{4.3}$$

where the electric field is expanded in the normalized mode functions $\mathbf{u}_{\mathbf{k}}\left(\mathbf{r}\right)$ by:

$$\mathbf{E}_{\mathbf{k}}\left(\mathbf{r}\right) = \hbar\sqrt{\frac{\omega_{\mathbf{k}}}{2\hbar\varepsilon_0}}\mathbf{u}_{\mathbf{k}}\left(\mathbf{r}\right). \tag{4.4}$$

The interaction Hamiltonian is then given by:

$$\hat{H}_{\mathrm{I}} = -\sum_{n=1}^{3} \hat{\mathbf{d}}^{(\mathrm{n})} \cdot \hat{\mathbf{E}}\left(\mathbf{r}, t\right) \tag{4.5}$$

$$\approx \hbar \sum_{n=1}^{3} \sum_{\mathbf{k}} \left[g_{\mathbf{k}}^{(\mathrm{n})} \hat{\sigma}_+^{(\mathrm{n})} a_{\mathbf{k}} + H.C.\right], \tag{4.6}$$

in the dipole approximation and rotating wave approximation. The coupling constant for the n'th emitter has been defined as:

$$g_{\mathbf{k}}^{(\mathrm{n})} = \sqrt{\frac{\omega_{\mathbf{k}}}{2\hbar\varepsilon_0}} d^{\mathrm{n}} \mathbf{e}_{\mathbf{d}} \cdot \mathbf{u}_{\mathbf{k}}\left(\mathbf{r}\right), \tag{4.7}$$

where ε_0 is the vacuum permittivity, $d^{(\mathrm{n})}$ is the magnitude of the dipole moment for emitter n and $\mathbf{e}_{\mathbf{d}}$ is a unit vector pointing in the direction of the dipole.

4.2 Decay Dynamics for Three Two-Level Quantum Emitters

This section develops a formal derivation of the decay dynamics of three two-level emitters in an arbitrary dielectric material, whose electromagnetic properties are described though the Green tensor $G\left(\mathbf{r}, \omega, \hat{\mathbf{e}}_{\mathbf{d}}\right)$. In addition, this section will elaborate upon Eqs. (3.1) and (3.2) that were introduced in Chapter (3.1.2) and will expand upon the discussion presented is this chapter.

4.2.1 General Formalism

A strong interaction between several quantum emitters is needed in order to make a functioning two-qubit quantum gate. This interaction will be modified by the optical properties by the material, in which the emitter is embedded, as well as the properties of the emitters. This section will describe a general theory for the spontaneous emission of three coupled emitters embedded in an arbitrary dielectric material and will specialize this to a W1 waveguide in a photonic crystal. In addition, the effects if super- and subradiance will be introduced.
Only the levels coupled to the radiation continuum in Fig. (4.1) will be considered in this section. The Hamiltonian governing the system is written in the non-rotated frame:

$$\hat{H} = \hat{H}_{\mathrm{S}} + \hat{H}_{\mathrm{I}} = \sum_{n=1}^{3} \frac{1}{2}\hbar\omega_0^{(n)} \hat{\sigma}_{\mathrm{z}}^{(\mathrm{n})} + \sum_{\mathbf{k}} \hbar\omega_{\mathbf{k}} \left(\hat{a}_{\mathbf{k}}^{\dagger}\hat{a}_{\mathbf{k}} + \frac{1}{2}\right) + \hbar \sum_{n=1}^{3} \sum_{\mathbf{k}} \left[g_{\mathbf{k}}^{(n)} \hat{\sigma}_+^{(\mathrm{n})} \hat{a}_{\mathbf{k}} + H.C.\right], \tag{4.8}$$

where $\omega_0^{(n)}$ is the transition energy for emitter n and $\sigma_{\pm}^{(n)}$ and $\sigma_z^{(n)}$ are the emitter (de-)excitation and population operators.

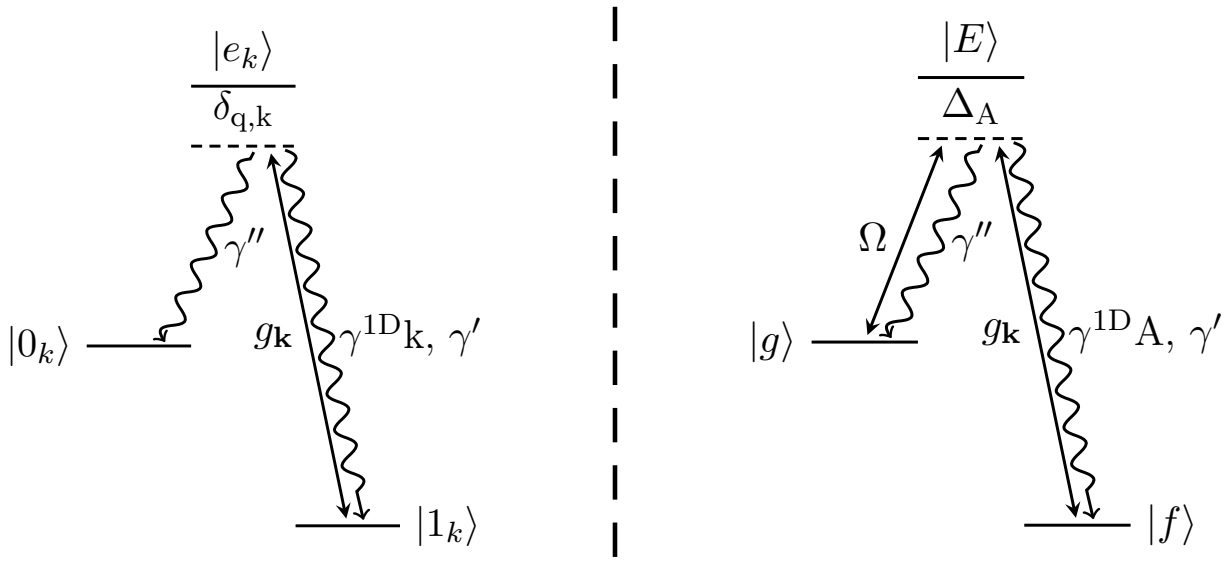

Figure 4.1: Left panel: Level structure of the qubit quantum dot, where only the transition between $|e\rangle$ and $|1\rangle$ couple to the waveguide with a decay rate of $\gamma^{1\mathrm{D}}$. This transition also includes a nonradiative decay with γ'. Another nonradiative decay processes with a rate of γ'' between $|e\rangle$ and $|0\rangle$ is also shown. Right Panel: Level structure of the auxiliary quantum dot and the transitions driven by the weak laser Ω and by the coupling to the waveguide $g_{\mathbf{k}}$. Only $|f\rangle$ couples to the waveguide. The nonradiative decay rate of γ'' will be assumed to be neglible in this work.

The (de-)excitation and population operators for the emitters satisfy the commutation relation:

$$\left[\hat{\sigma}_{\pm}^{(\mathrm{n})},\hat{\sigma}_{\mathrm{z}}^{(\mathrm{m})}\right]=\mp2\hat{\sigma}_{\pm}^{(\mathrm{n})}\delta_{\mathrm{nm}} \tag{4.9}$$

$$\left[\hat{\sigma}_{+}^{(\mathrm{n})},\hat{\sigma}_{-}^{(\mathrm{m})}\right]=\pm\hat{\sigma}_{\mathrm{z}}^{(\mathrm{n})}\delta_{\mathrm{nm}}. \tag{4.10}$$

where $\hat{\sigma}_{+}^{(\mathrm{n})}=|\mathrm{e}\rangle_{\mathrm{n}}\langle g|,\hat{\sigma}_{-}^{(\mathrm{n})}=\left(\hat{\sigma}_{+}^{(\mathrm{n})}\right)^{\dagger}$ and $\hat{\sigma}_{\mathrm{z}}^{(\mathrm{n})}=|\mathrm{e}\rangle_{\mathrm{n}}\langle e|-|\mathrm{g}\rangle_{\mathrm{n}}\langle g|$. The annihilation and creation operators for the photons satisfy:

$$\left[a_{\mathbf{k}},a_{\mathbf{k}'}^{\dagger}\right]=\delta_{\mathbf{k},\mathbf{k}'} \tag{4.11}$$

$$\left[a_{\mathbf{k}},a_{\mathbf{k}}\right]=\left[a_{\mathbf{k}}^{\dagger},a_{\mathbf{k}}^{\dagger}\right]=0. \tag{4.12}$$

The treatment is simplified by changing to the interaction picture using the unitary operator $\hat{O}(t)=e^{-i\hat{H}_{\mathrm{S}}t/\hbar}$, which reduces the Schrödinger equation to:

$$i\hbar\frac{\mathrm{d}}{\mathrm{d}t}|\psi(t)\rangle=\tilde{H}_{\mathrm{I}}|\psi(t)\rangle, \tag{4.13}$$

where the interaction Hamiltonian is given by:

$$\tilde{H}_{\mathrm{I}}=\hbar\sum_{n=1}^{3}\sum_{\mathbf{k}}\left[g_{\mathbf{k}}^{(n)}\hat{\sigma}_{+}^{(\mathrm{n})}e^{-i\Delta_{\mathbf{k}}t}\hat{a}_{\mathbf{k}}+H.C.\right] \tag{4.14}$$

$$=\hbar\sum_{\mathbf{k}}\left[S_{+}e^{-\Delta_{\mathbf{k}}t}\hat{a}_{\mathbf{k}}+H.C.\right]. \tag{4.15}$$

Here $\Delta_{\mathbf{k}}^{(n)} = \omega_0^{(n)} - \omega_{\mathbf{k}}$. It will be assumed in this treatment that the transition frequency is the same for the three emitters, such that $\Delta_{\mathbf{k}}^{(n)} = \Delta_{\mathbf{k}}^{(m)}$. An arbitrary state of the system is expanded in terms of the basis states:

$$|\psi(t)\rangle = \sum_{\mathbf{k}} c_{f,\mathbf{k}}(t)\,|fff\rangle \otimes |\{\mathbf{k}\}\rangle + \left(c_{e,1}(t)\,|eff\rangle + c_{e,2}(t)\,|fef\rangle + c_{e,3}(t)\,|ffe\rangle\right) \otimes |\{0\}\rangle\,, \tag{4.16}$$

where $|eff\rangle = |e\rangle_1 \otimes |f\rangle_2 \otimes |f\rangle_3$ is a short hand notation for the tensor product between the three emitter states. $|\{\mathbf{k}\}\rangle$ is the state describing a single photon with wavenumer $\mathbf{k}$, while $|\{0\}\rangle$ is the photon vacuum state.

4.2.2 Dynamics in the Interaction Picture

The right hand side of Eq. (4.13) can be written as:

$$\left.\begin{aligned}\hat{H}_{\mathrm{I}}\,|\psi(t)\rangle = &\sum_{\mathbf{k}} \left[g_{\mathbf{n}}^{(1)}\,|eff\rangle + g_{\mathbf{k}}^{(2)}\,|fef\rangle + g_{\mathbf{k}}^{(3)}\,|ffe\rangle\right] c_{f,\mathbf{k}}(t)\,e^{-i\Delta_{\mathbf{k}}t} \otimes |\{0\}\rangle \\ &+ \left[g_{\mathbf{k}}^{(1)^*} c_{e,1}(t) + g_{\mathbf{k}}^{(2)^*} c_{e,2}(t) + g_{\mathbf{k}}^{(3)^*} c_{e,3}(t)\right] e^{i\Delta_{\mathbf{k}}t}\,|fff\rangle \otimes |\{\mathbf{k}\}\rangle\end{aligned}\right\} \tag{4.17}$$

It is now possible to find equations of motion for the expansion coefficients in Eq. (4.16) by projecting the basis states onto Eq. (4.17):

$$\dot{c}_{f,\mathbf{k}} = -i \sum_{n=1}^{3} \sum_{\mathbf{k}} \left(g_{\mathbf{k}}^{(n)}\right)^* c_{e,n}(t)\,e^{i\Delta_{\mathbf{k}}t} \tag{4.18}$$

$$\dot{c}_{e,n} = -g_{\mathbf{k}}^{(n)} c_{f,\mathbf{k}}(t)\,e^{-i\Delta_{\mathbf{k}}t}, \quad n = 1,2,3. \tag{4.19}$$

The equations of motion for $c_{e,n}(t)$ can be decoupled from $c_{f,\mathbf{k}}(t)$ by formally integrating Eq. (4.18), using the initial condition $c_{f,\mathbf{k}}(t=0) = 0$:

$$c_{f,\mathbf{k}}(t) = -i \sum_{n=1}^{3} \sum_{\mathbf{k}} \left(g_{\mathbf{k}}^{(n)}\right)^* \int_0^t \mathrm{d}t' \left[c_{e,n}\left(t'\right) e^{i\Delta_{\mathbf{k}}t'}\right]. \tag{4.20}$$

Substituting this expression into Eq. (4.19) gives an equation of motion for the expansion coefficient for the n'th excited state:

$$\dot{c}_{e,n} = -\sum_{\mathbf{k}} \sum_{m=1}^{3} g_{\mathbf{k}}^{(n)} \left(g_{\mathbf{k}}^{(m)}\right)^* \int_0^t \mathrm{d}t' \left[c_{e,m}\left(t'\right) e^{-i\Delta_{\mathbf{k}}(t-t')}\right]. \tag{4.21}$$

This term describes interactions between the two emitters that are mediated by photons propagating in the medium. It is possible to write Eq. (4.21) in terms of the local density of states by introducing the expression for the coupling constants: $g_{\mathbf{k}}^{(n)} = d^{(n)}\sqrt{\frac{\omega_{\mathbf{k}}}{2\hbar\epsilon_0}}\mathbf{e_d} \cdot \mathbf{u_k}(\mathbf{x}_n)$ and multiplying by $1 = \int_{-\infty}^{\infty} \mathrm{d}\omega\,\delta(\omega - \omega_{\mathbf{k}})$. The LDOS is given by:

$$\rho(\mathbf{x}_{\mathrm{n}}, \mathbf{x}_{\mathrm{m}}, \omega, \mathbf{e_d}) = \sum_{\mathbf{k}} \mathbf{e_d} \cdot \mathbf{u_k}(\mathbf{x}_{\mathrm{m}})\,\mathbf{u}_{\mathbf{k}}^*(\mathbf{x}_{\mathrm{m}}) \cdot \mathbf{e_d}\,\delta\left(\omega - \omega_{\mathbf{k}_{\mathrm{R,L}}}\right) = \frac{2}{\pi\omega}\mathbf{e_d}\mathrm{Im}\left[\mathrm{G}(\mathbf{x}_{\mathrm{n}}, \mathbf{x}_{\mathrm{m}}; \omega)\right]\mathbf{e_d}, \tag{4.22}$$

and was introduced in Section (3.1). The LDOS has been written in terms of Green's tensor $\mathrm{G}\left(\mathbf{x}_\mathrm{n}, \mathbf{x}_\mathrm{m}; \omega\right)$ projected along the orientation of the dipole emitter [16]. Eq. (4.21) can then be written in the form:

$$\dot{c}_{e,n} = -\frac{d^{(n)} d^{(m)}}{2\hbar\epsilon_0} \int_{-\infty}^{\infty} \mathrm{d}\omega \omega \rho\left(\mathbf{x}_\mathrm{n}, \mathbf{x}_\mathrm{m}, \omega, \mathbf{e_d}\right) \int_0^t \mathrm{d}t' c_{e,m}\left(t'\right) e^{-i\Delta_\mathbf{k}(t-t')} \tag{4.23}$$

$$= -\sum_{m=1}^{3} \int_0^{\infty} \mathrm{d}t' c_{e,m}\left(t'\right) K_e\left(\mathbf{x}_\mathrm{n}, \mathbf{x}_\mathrm{m}, t-t'\right), \tag{4.24}$$

where the memory kernel $K_e\left(\mathbf{x}_\mathrm{n}, \mathbf{x}_\mathrm{m}, t-t'\right)$ has been introduced:

$$K_e\left(\mathbf{x}_\mathrm{n}, \mathbf{x}_\mathrm{m}, t-t'\right) = \frac{d^{(n)} d^{(m)}}{2\hbar\epsilon_0} \int_{-\infty}^{\infty} \mathrm{d}\omega e^{-i\Delta_\mathbf{k}(t-t')} \omega \rho\left(\mathbf{x}_\mathrm{n}, \mathbf{x}_\mathrm{m}, \omega, \mathbf{e_d}\right) \tag{4.25}$$

This function expresses how previous times t' can contribute to $c_e^n(t)$. Eq. (4.23) is a crucial result that relates the dynamics quantum emitter to the photonic environment for an arbitrary homogeneous, dielectric medium. The imaginary part of Green's tensor determines the LDOS, which is the sole contributor to the dynamics of the emitter.

4.2.3 Wigner-Weisskopf Theory for a W1 PhC Waveguide

Wigner-Weisskopf theory constitutes a simple, special case of the formalism outlined above, where $\omega\rho\left(\mathbf{x}_\mathrm{n}, \mathbf{x}_\mathrm{m}, \omega, \mathbf{e_d}\right)$ is assumed to change slowly compared to $e^{-i\Delta_\mathbf{k}(t-t')}$. The memory kernel then becomes:

$$K_e\left(\mathbf{x}_\mathrm{n}, \mathbf{x}_\mathrm{m}, t-t'\right) \approx \frac{d^{(n)} d^{(m)}}{2\hbar\epsilon_0} \omega_0 \rho\left(\mathbf{x}_\mathrm{n}, \mathbf{x}_\mathrm{m}, \omega_0, \mathbf{e_d}\right) \int_{-\infty}^{\infty} \mathrm{d}\omega e^{-i\Delta_\mathbf{k}(t-t')} \tag{4.26}$$

$$= \frac{\pi d^{(n)} d^{(m)}}{\epsilon_0 \hbar} \omega_0 \rho\left(\mathbf{x}_\mathrm{n}, \mathbf{x}_\mathrm{m}, \omega_0, \mathbf{e_d}\right) \delta\left(t-t'\right) \tag{4.27}$$

$$= \gamma_\mathrm{nm} \delta\left(t-t'\right) \tag{4.28}$$

The singular behaviour of the memory kernel implies that the reservoir of radiation modes is memoryless. This is also know as the Markoff approximation. In addition, the decay rate γ_nm to the radiation reservoir has been defined as:

$$\gamma_\mathrm{nm} \equiv \frac{\pi d^{(n)} d^{(m)}}{\epsilon_0 \hbar} \omega_0 \rho\left(\mathbf{x}_\mathrm{n}, \mathbf{x}_\mathrm{m}, \omega_0, \mathbf{e_d}\right) = 2\frac{d^{(n)} d^{(m)}}{\epsilon_0 \hbar} \mathbf{e_d} \cdot \mathrm{Im}\left[\mathrm{G}\left(\mathbf{x}_\mathrm{n}, \mathbf{x}_\mathrm{m}, \omega_0, \mathbf{e_d}\right)\right] \cdot \mathbf{e_d}. \tag{4.29}$$

The time integral in Eq. (4.24) can then be evaluated:

$$\dot{c}_{e,n} = -\sum_{m=1}^{3} \int_0^{\infty} \mathrm{d}t' c_{e,m}\left(t'\right) K_e\left(\mathbf{x}_\mathrm{n}, \mathbf{x}_\mathrm{m}, t-t'\right) \tag{4.30}$$

$$= -\sum_{m=1}^{3} \gamma_\mathrm{nm} \int_0^{\infty} \mathrm{d}t' c_{e,m}\left(t'\right) \delta\left(t-t'\right) \tag{4.31}$$

$$= -\sum_{m=1}^{3} \frac{\gamma_\mathrm{nm}}{2} c_{e,m}\left(t\right), \tag{4.32}$$

where γ_{nn} is the standard decay rate of the n'th emitter into a continuum of radiation modes, while $\gamma_{nm}, n \neq m$ is an additional decay that arises from the dipole-dipole interaction and is mediated by the radiation reservoir. Both of these decay rates depend only on the magnitude of the dipole moment $d_{\mathrm{n,m}}$ and on the photonic environment through the LDOS. Both of the properties can be readily tailored for a self-assembled quantum for and photonic crystals, respectively.

This formalism can be specialized to the case where the dielectric material is a W1 waveguide, as those discussed in Section (3.1) using the procedure from [24]. The basis functions for a single band in the dispersion relation of the photonic waveguide are Bloch modes of the form:

$$\mathbf{u}_{\mathbf{k}}(\mathbf{x}) = \sqrt{\frac{a}{L}}\mathbf{b}_{\mathbf{k}}(\mathbf{x})\, e^{ikx}, \tag{4.33}$$

where a is the lattice constant, L is the length of the waveguide and $\mathbf{b}_{\mathbf{k}}(\mathbf{x})$ is a function that is periodic in the direction of the waveguide. It is often a sufficient assumption to only consider a single band due to the frequency spacing of the three bands being larger than the transition energy between the conduction band and the lowest valence band. Green's tensor can then be expressed as:

$$G(\mathbf{x}_{\mathrm{n}}, \mathbf{x}_{\mathrm{m}}; \omega) = \sum_{\mathbf{k}} \omega^2 \frac{\mathbf{u}^*_{\mathbf{k}}(\mathbf{x}_{\mathrm{m}}) \cdot \mathbf{u}_{\mathbf{k}}(\mathbf{x}_{\mathrm{n}})}{\omega^2_{\mathbf{k}} - \omega^2} \tag{4.34}$$

$$\approx \frac{a}{4\pi L v_g} \int \mathrm{d}\omega_{\mathbf{k}} \frac{\omega}{\omega_{\mathbf{k}} - \omega - i\epsilon} \mathbf{b}_{\mathbf{k}}(\mathbf{x}_{\mathrm{n}})\, \mathbf{b}^*_{\mathbf{k}}(\mathbf{x}_{\mathrm{m}})\, e^{ik(x_n - x_m)}, \tag{4.35}$$

where the sum has been converted into an integral by $\sum_{\mathbf{k}} = \frac{1}{2\pi}\int \mathrm{d}\mathbf{k}$ and where $\omega^2_{\mathbf{k}} - \omega^2 - i\epsilon \approx (\omega_{\mathbf{k}} - \omega - i\epsilon)^2 \approx 2\omega(\omega_{\mathbf{k}} - \omega - i\epsilon)$ when $\omega_{\mathbf{k}}$ is near the pole $\omega_{\mathbf{k}} \sim \omega$. The slowdown of light is described by the group index n_g and the group velocity $v_g = \mathrm{d}\omega_{\mathbf{k}}/\mathrm{d}\mathbf{k} = cn_g$. The small parameter ϵ has been introduced to keep the integral convergent, which can be solved by considering the two different cases of $x_{\mathrm{n}} - x_{\mathrm{m}} < 0$ and $x_{\mathrm{n}} - x_{\mathrm{m}} > 0$ yielding:

$$\left.\begin{aligned} G_{\mathrm{W1}}(\mathbf{x}_{\mathrm{n}}, \mathbf{x}_{\mathrm{m}}; \omega) = &\frac{ia\omega}{2v_g} \mathbf{b}_{\mathbf{k}}(\mathbf{x}_{\mathrm{n}})\, \mathbf{b}^*_{\mathbf{k}}(\mathbf{x}_{\mathrm{m}})\, e^{ik(x_n - x_m)} \Theta(x_{\mathrm{n}} - x_{\mathrm{m}}) \\ &+ \frac{ia\omega}{2v_g} \mathbf{b}^*_{\mathbf{k}}(\mathbf{x}_{\mathrm{n}})\, \mathbf{b}_{\mathbf{k}}(\mathbf{x}_{\mathrm{m}})\, e^{-ik(x_n - x_m)} \Theta(x_{\mathrm{m}} - x_{\mathrm{n}}) \end{aligned}\right\} \tag{4.36}$$

which defines the forward- and backward propagating modes through the Heaviside function Θ. The LDOS can then be written as:

$$\rho_{\mathrm{W1}}(\mathbf{x}_{\mathrm{n}}, \mathbf{x}_{\mathrm{m}}, \omega, \mathbf{e}_{\mathbf{d}}) = \frac{a}{2\pi v_g} \cos\left[k(x_n - x_m)\right] \cdot \left\{ \begin{array}{c} \mathbf{b}_{\mathbf{k}}(\mathbf{x}_{\mathrm{n}})\, \mathbf{b}^*_{\mathbf{k}}(\mathbf{x}_{\mathrm{m}})\, \Theta(x_n - x_m) \\ +\mathbf{b}^*_{\mathbf{k}}(\mathbf{x}_{\mathrm{n}})\, \mathbf{b}_{\mathbf{k}}(\mathbf{x}_{\mathrm{m}})\, \Theta(x_m - x_n) \end{array} \right\} \tag{4.37}$$

This equation can be rewritten into

$$\rho_{\mathrm{W1}}(\mathbf{x}_{\mathrm{n}}, \mathbf{x}_{\mathrm{m}}, \omega, \mathbf{e}_{\mathbf{d}}) = \frac{a}{2\pi v_g} \cos\left[k(x_n - x_m)\right] \cdot \left\{ \begin{array}{c} \frac{f_{\mathrm{R}}(\mathbf{x}_{\mathrm{n}}, \mathbf{x}_{\mathrm{m}})\, \Theta(x_n - x_m)}{V_{\mathrm{eff,R}} \sqrt{\varepsilon(\mathbf{x}_{\mathrm{n}})\, \varepsilon(\mathbf{x}_{\mathrm{m}})}} \\ +\frac{f_{\mathrm{L}}(\mathbf{x}_{\mathrm{n}}, \mathbf{x}_{\mathrm{m}})\, \Theta(x_m - x_n)}{V_{\mathrm{eff,L}} \sqrt{\varepsilon(\mathbf{x}_{\mathrm{n}})\, \varepsilon(\mathbf{x}_{\mathrm{m}})}} \end{array} \right\}, \tag{4.38}$$

where

$$f_{\mathrm{R}}(\mathbf{x}_{\mathrm{n}}, \mathbf{x}_{\mathrm{m}}) = \sqrt{\varepsilon(\mathbf{x}_{\mathrm{n}})\, \varepsilon(\mathbf{x}_{\mathrm{m}})} \mathbf{b}_{\mathbf{k}}(\mathbf{x}_{\mathrm{n}})\, \mathbf{b}^*_{\mathbf{k}}(\mathbf{x}_{\mathrm{m}})\, V_{\mathrm{eff,R}} \left[\mathbf{e}^*_{\mathbf{d}} \cdot \mathbf{e}_{\mathbf{k}}(\mathbf{x}_{\mathrm{n}}) \cdot \mathbf{e}^*_{\mathbf{k}}(\mathbf{x}_{\mathrm{m}}) \cdot \mathbf{e}_{\mathbf{d}}\right] \tag{4.39}$$

is a dimensionless function describing the spatial mismatch between the emitter field maximum and that of the waveguide mode. The subscripts R and L refer to the forwards- and backwards propagating mode, respectively. It additionally takes the alignment of the dipole with the Bloch mode into account through the product of the unit vectors $\mathbf{e_d}$ and $\mathbf{e}^*_{\mathbf{k}}(\mathbf{x}_\mathrm{m})$. The effective mode volume per unit cell is defined through $V^{-1}_{\mathrm{eff,R}} = \max\left[\sqrt{\varepsilon(\mathbf{x}_\mathrm{n})\varepsilon(\mathbf{x}_\mathrm{m})}\mathbf{b_k}(\mathbf{x}_\mathrm{n})\mathbf{b_k}(\mathbf{x}_\mathrm{m})\right]$ for the forward propagating mode. The equivalent definition for the mode volume for the backward propagating mode is then straightforward to write down. The LDOS for a diagonal element takes the simpler form:

$$\rho_{\mathrm{W1}}(\mathbf{x}_\mathrm{n}, \mathbf{x}_\mathrm{n}, \omega, \mathbf{e_d}) = \frac{a}{2\pi v_g}\frac{f(\mathbf{x}_\mathrm{n})}{V_{\mathrm{Eff}}\varepsilon(\mathbf{x}_\mathrm{n})}\left|\mathbf{e_k}(\mathbf{x}_\mathrm{n})\cdot\mathbf{e_d}\right|^2, \tag{4.40}$$

where the alignment of the dipole and waveguide Bloch mode unit vectors have been explicitly extracted from $f(\mathbf{x}_\mathrm{n})$.
The decay rates for radiative decay into the two guides modes can then be calculated:

$$\gamma^{\mathrm{nm}}_{\mathrm{R,L}} = \frac{\pi d^{(n)}d^{(m)}}{\epsilon_0\hbar}\omega_0\rho_{W1}(\mathbf{x}_\mathrm{n}, \mathbf{x}_\mathrm{m}, \omega_0, \mathbf{e_d}) \tag{4.41}$$

$$= \frac{a d^{(n)}d^{(m)}}{2\epsilon_0\hbar v_g}\omega_0\cos\left[k(x_n - x_m)\right]_{\mathrm{R,L}} \tag{4.42}$$

$$\Rightarrow \gamma^{\mathrm{nm}} = \gamma^{\mathrm{nm}}_0\cos\left[k(x_n - x_m)\right]\left[\Theta(x_n - x_m) + \Theta(x_m - x_n)\right], \tag{4.43}$$

where the sum over Bloch mode functions have been omitted for brevity. The dissipative single dipole decay rate γ^{nn} has a constant value set by the magnitude of the dipole moment, while the decay rate from dipole-dipole interactions display spatial oscillations with a maximum amplitude of

$$\gamma^{\mathrm{nm}}_0 = \frac{a d^{(n)}d^{(m)}}{2\epsilon_0\hbar v_g}\omega_0. \tag{4.44}$$

The oscillations can be seen as an effect of interference between the radiation fields and will be discussed in further detail in Section (4.2.4).
Eqs. (4.38) and (4.43) reveal the primary methods for enhancing the light-matter though the W1 waveguide: the LDOS increases with small mode volumes and for slow light. Both of these requirements are met for photonic waveguides, as was discussed in Section (3.1.2). The enhancement of the optical LDOS will then enhance the spontaneous decay rate into the preferred mode for both the forwards and backwards propagating mode. This is quantified by the Purcell factor by taking the ratio of the LDOS for one of the modes and the LDOS for a homogeneous medium and was introduced in Section (3.1.2). It is printed here again for convenience:

$$F_{\mathrm{P}}(\omega) = \left(\frac{3}{4\pi n}\frac{\lambda^2/n^2}{V_{\mathrm{eff}}/a}\right)n_g(\omega). \tag{4.45}$$

This enhancement is shown in Fig. (3.3). This also show the enhancement of the $\beta-$factor for a single quantum dot in a W1 waveguide:

$$\beta = \frac{\sum_{\mathrm{n,m}}\gamma^{\mathrm{nm}}}{\sum_{\mathrm{n,m}}\gamma^{\mathrm{nm}} + \gamma_{\mathrm{ng}} + \gamma'}, \tag{4.46}$$

where γ_{ng} is the decay rate into non-guided modes and γ' is the nonradiative decay rate. The sum over the various γ^{nm} gives the total decay rate into the guided modes. It is possible to obtain

values exceeding $\beta > 98\%$ [1] for the case of a single quantum dot in a waveguide, demonstrating that these systems provides a promising platform for implementing single photon sources. The β-factor is primarily limited by the nonradiative decay processes with γ'. The decay rates into the non-guided modes will thus be set to zero in this thesis. The cooperativity C of the system is defined as the ratio between the decay rate γ^{1D} (in the case of a single quantum dot in the system) into the guided mode and the nonradiative decay:

$$C \equiv \frac{\gamma^{1D}}{\gamma'}, \tag{4.47}$$

and can be related to the β-factor by

$$C = \frac{1}{1 - \frac{1}{\beta}}. \tag{4.48}$$

4.2.4 Superradiance

It is now possible to complete the equations of motion in Eq. (4.32) by summing over the three emitters. This is done for the case where the emitters are embedded in a W1 waveguide introduced in the precious section. The decay dynamics can be expressed as the following matrix equation for the expansion coefficients of the excited states $c_{e,n}$ of the three emitters:

$$\begin{pmatrix} \dot{c}_{e,1} \\ \dot{c}_{e,2} \\ \dot{c}_{e,3} \end{pmatrix} = \hat{H}_{\text{int}} \cdot \begin{pmatrix} c_{e,1}(t) \\ c_{e,2}(t) \\ c_{e,3}(t) \end{pmatrix} \tag{4.49}$$

$$= \frac{1}{2} \begin{pmatrix} \gamma^{11}(\mathbf{x}_1, \mathbf{x}_1) & \gamma_{\text{L}}^{12}(\mathbf{x}_1, \mathbf{x}_2) & \gamma_{\text{L}}^{13}(\mathbf{x}_1, \mathbf{x}_3) \\ \gamma_{\text{R}}^{21}(\mathbf{x}_2, \mathbf{x}_1) & \gamma^{22}(\mathbf{x}_2, \mathbf{x}_2) & \gamma_{\text{L}}^{23}(\mathbf{x}_2, \mathbf{x}_3) \\ \gamma_{\text{R}}^{31}(\mathbf{x}_3, \mathbf{x}_1) & \gamma_{\text{R}}^{32}(\mathbf{x}_3, \mathbf{x}_2) & \gamma^{33}(\mathbf{x}_3, \mathbf{x}_3) \end{pmatrix} \cdot \begin{pmatrix} c_{e,1}(t) \\ c_{e,2}(t) \\ c_{e,3}(t) \end{pmatrix}, \tag{4.50}$$

where the matrix is represented by $\hat{H}_{\text{int}}$. This thesis considers two distinct cases: the first is when all matrix elements in Eq. (4.50) are equal, whereas the second is where two of the emitters are equal (say emitter 2 and 3) and different from the third. These cases can be related to the eigenvalues of the matrix, as described below. It is also assumed that the each emitter's self-interaction couples identically to the two modes (i.e. $\gamma_{\text{R}}^{(\text{nn})} = \gamma_{\text{L}}^{(\text{nn})}$). This matrix can then be written as (while also absorbing the factor of 1/2 into the matrix elements:)

$$\hat{H}_{\text{int}}^{(1)} = \begin{pmatrix} \gamma_{\text{A}} & \gamma_{\text{Aq}} & \gamma_{\text{Aq}} \\ \gamma_{\text{Aq}} & \gamma_{\text{q}} & \gamma_{\text{qq}} \\ \gamma_{\text{Aq}} & \gamma_{\text{qq}} & \gamma_{\text{q}} \end{pmatrix}, \tag{4.51}$$

where γ_{A} and γ_{q} are the decay rates of the single *auxiliary* emitter and γ_{q} is the decay rate of either of the two *qubit* emitters. γ_{Aq} and γ_{qq} is the two-body decay rates between the auxiliary and qubit emitters; and between the two qubit emitters, respectively. Diagonalization of the matrix in Eq. (4.51) yields the three following eigenvalues:

$$\gamma_{\pm} = \frac{\gamma_{\text{A}} + \gamma_{\text{q}} + \gamma_{\text{qq}}}{2} \pm \frac{1}{2}\sqrt{(\gamma_{\text{A}} - \gamma_{\text{q}} - \gamma_{\text{qq}})^2 + 8\gamma_{\text{Aq}}^2} \tag{4.52}$$

$$\gamma_0 = \gamma_{\text{q}} - \gamma_{\text{qq}}, \tag{4.53}$$

with the corresponding eigenvectors:

$$|\psi_{\pm}\rangle = \frac{1}{\sqrt{3}}\left(|eff\rangle + |fef\rangle \pm |ffe\rangle\right) \tag{4.54}$$

$$|\psi\rangle_0 = \mathcal{N}\left(A_+ |eff\rangle + A_- |fef\rangle\right), \tag{4.55}$$

where the coefficients $A_{\pm}$ for $|\psi_0\rangle$ are given at the end of this section. Notably, the eigenvalue γ_+ is linked to the eigenstate that is a symmetric superposition of the excited states, while γ_- and γ_0 are associated with the two non-symmetric superpositions. $\mathcal{N}$ is a normalization constant. Further inside is gained by considering the ideal limit where all decay rates are equal: $\gamma^{\mathrm{nm}} = \gamma_{\mathrm{A}}$. The eigenstates and eigenvalues are then given by:

$$\gamma_+ = 3\gamma_{\mathrm{A}}, \qquad |\psi_+\rangle = \frac{1}{\sqrt{3}}\left(|eff\rangle + |fef\rangle + |ffe\rangle\right) \tag{4.56}$$

$$\gamma_- = 0, \qquad |\psi_-\rangle = \frac{1}{2}\left(-2\,|eff\rangle + |fef\rangle + |ffe\rangle\right) \tag{4.57}$$

$$\gamma_0 = 0, \qquad |\psi_0\rangle = \frac{1}{\sqrt{2}}\left(|eff\rangle - |fef\rangle\right). \tag{4.58}$$

The effect of super- and subradiance is evident from Eqs. (4.52) through (4.58): It is possible to project the excited states into either the symmetric state or the two anti-symmetric states by varying the optical properties of the emitters. This can primarily be done in two distinct manners: the decay rate of the three emitters γ_{A} and γ_{q} can tailored, typically by varying the gate voltage over the heterostructure, see Section(3.2.2). In addition, the value of the two-body decay rates γ_{Aq} and γ_{qq} can be changed by varying the distance between the three emitters. The last effect induces interference between the radiation emitted from the quantum dots with an oscillation set by $\gamma_{\mathrm{nm}} \sim \cos\left[k\left(x_n - x_m\right)\right]$. This has a frequency $\omega_k = v_g k$ set by the guided mode and amplitude by the relative values of the magnitude of the dipole moments of the auxiliary and qubit emitters.
The coefficients for the eigenvectors are given by:

$$A_{\pm} = \frac{2\gamma_{\mathrm{Aq}}}{\frac{-\gamma_{\mathrm{A}}+\gamma_{\mathrm{q}}+\gamma_{\mathrm{qq}}}{2} \pm \frac{1}{2}\sqrt{\left(\gamma_{\mathrm{A}} - \gamma_{\mathrm{q}} - \gamma_{\mathrm{qq}}\right)^2 + 8\gamma_{\mathrm{Aq}}^2}} \tag{4.59}$$

4.3 Full Time Evolution

The discussion presented in Section (4.2) shows a simplified version of the full dynamics by considering the coupling between a number of two-level emitters to a single electromagnetic mode. The method used is cumbersome to apply when the external drive and nonradiative decay is included and a more detailed method is needed. The Hamiltonian in Eqs. (4.1) and (4.2) has been written in the rotating frame defined by the unitary operator $\hat{O}(t) = \hat{O}_2(t)\,\hat{O}_1(t)$, where

$$\hat{O}_1(t) = \exp\left(-i\hat{H}_{\mathrm{g}} t\right) \tag{4.60}$$

$$\hat{O}_2(t) = \exp\left[i\left(\Delta_{\mathrm{A}} |E\rangle\langle E|\right) + \sum_{n_q=1}^{2} \delta_{\mathrm{n_q}} |e\rangle_{n_q}\langle e|\right], \tag{4.61}$$

where the sum runs over the two qubit emitters. The rotated Hamiltonian can then be written as:

$$\tilde{H} = \hat{H}_{\mathrm{e}} + \tilde{V} + \tilde{H}_{\mathrm{int}}(t) \tag{4.62}$$

$$\hat{H}_{\mathrm{e}} = \sum_{n}^{3} \Delta_{\mathrm{n}} |e\rangle_n \langle e|, \quad \hat{V} = \frac{\Omega}{2}\left(|E\rangle_{\mathrm{A}} \langle g| + |g\rangle \langle E|\right) \tag{4.63}$$

$$\tilde{H}_{\mathrm{int}}(t) = \sum_{\mathrm{n}=1}^{3} \sum_{\mathbf{k}} \left[g_{\mathbf{k}}^{(\mathrm{n})} \hat{\sigma}_{+}^{(\mathrm{n})} a_{\mathbf{k}} e^{i(\Delta_{\mathrm{n}} - \omega_{\mathbf{k}})t} + H.C. \right], \tag{4.64}$$

where the sum is over all three emitters. Note that Δ_{n} can take the form Δ_{A} or $\delta_{\mathrm{n_q}}$ depending on whether the terms in the sum is for the auxiliary- or on e of the qubit emitters, respectively. The nonradiative decay γ' is governed by the Lindblad superoperator

$$\mathcal{L}[\rho] = -\frac{\gamma'}{2} \sum_{n=1}^{3} \left[\rho \hat{\sigma}_{+}^{(\mathrm{n})} \hat{\sigma}_{-}^{(\mathrm{n})} + \hat{\sigma}_{+}^{(\mathrm{n})} \hat{\sigma}_{-}^{(\mathrm{n})} \rho - 2\hat{\sigma}_{-}^{(\mathrm{n})} \rho \hat{\sigma}_{+}^{(\mathrm{n})} \right]. \tag{4.65}$$

The commutation relations for the emitters are written here again for convenience:

$$\left[\hat{\sigma}_{\pm}^{(\mathrm{n})}, \hat{\sigma}_{\mathrm{z}}^{(\mathrm{m})} \right] = \mp 2\hat{\sigma}_{\pm}^{(\mathrm{n})} \delta_{\mathrm{nm}} \tag{4.66}$$

$$\left[\hat{\sigma}_{+}^{(\mathrm{n})}, \hat{\sigma}_{-}^{(\mathrm{m})} \right] = \pm \hat{\sigma}_{\mathrm{z}}^{(\mathrm{n})} \delta_{\mathrm{nm}}. \tag{4.67}$$

and the commutation relation for the electromagnetic creation- and annihilation operators are:

$$\left[a_{\mathbf{k}}, a_{\mathbf{k}'}^{\dagger} \right] = \delta_{\mathbf{k},\mathbf{k}'} \tag{4.68}$$

$$[a_{\mathbf{k}}, a_{\mathbf{k}}] = \left[a_{\mathbf{k}}^{\dagger}, a_{\mathbf{k}}^{\dagger} \right] = 0. \tag{4.69}$$

The equation of motion for the annihilation operator (and by extension, the creation operator) can be found from Heisenberg's equation of motion:

$$\dot{a}_{\mathbf{k}} = i \left[\hat{H}, a_{\mathbf{k}} \right] = -i \sum_{n=1}^{3} \left(g_{\mathbf{k}}^{\mathrm{n}} \right)^* \hat{\sigma}_{-}^{(\mathrm{n})} e^{-i\Delta_{\mathrm{n},\mathbf{k}} t}, \tag{4.70}$$

where $\Delta_{\mathrm{n},\mathbf{k}} = \Delta_{\mathrm{n}} - \omega_{\mathbf{k}}$. The equations of motion for the coherences $\hat{\sigma}_{+}^{(\mathrm{n})}$ and population $\hat{\sigma}_{\mathrm{z}}^{(\mathrm{n})}$ can be found in a similar manner:

$$\dot{\sigma}_{+}^{(\mathrm{n})} = -2i\Delta_{\mathrm{n}} \hat{\sigma}_{+}^{(\mathrm{n})} - i \sum_{\mathbf{k}} \left(g_{\mathbf{k}}^{\mathrm{n}} \right)^* a_{\mathbf{k}}^{\dagger} \hat{\sigma}_{\mathrm{z}}^{(\mathrm{n})} e^{-i\Delta_{\mathrm{n},\mathbf{k}} t} \tag{4.71}$$

$$\dot{\sigma}_{\mathrm{z}}^{(\mathrm{n})} = -2i \sum_{\mathbf{k}} \left[g_{\mathbf{k}}^{\mathrm{n}} \hat{\sigma}_{+}^{(\mathrm{n})} a_{\mathbf{k}} e^{i\Delta_{\mathrm{n},\mathbf{k}} t} \right] + H.C. \tag{4.72}$$

These equations can be simplified by eliminating the field operators. This is done by formally integrating Eq. (4.70) and substituting the result into Eqs. (4.71) through (4.72):

$$\dot{\sigma}_{+}^{(\mathrm{n})} = 2i\Delta_{\mathrm{n}} \hat{\sigma}_{+}^{(\mathrm{n})} - \sum_{m=1}^{3} \sum_{\mathbf{k}} g_{\mathbf{k}}^{(\mathrm{m})} \left(g_{\mathbf{k}}^{(\mathrm{n})} \right)^* \int_{0}^{t} \mathrm{d}t' \left[\hat{\sigma}_{+}^{(\mathrm{m})}(t') e^{i(\Delta_{\mathrm{m}} t' - \Delta_{\mathrm{n}} t)} \right] \hat{\sigma}_{\mathrm{z}}^{(\mathrm{n})} \tag{4.73}$$

$$= 2i\Delta_{\mathrm{n}} \hat{\sigma}_{+}^{(\mathrm{n})} - \int_{-\infty}^{\infty} \mathrm{d}\omega \int_{0}^{t} \mathrm{d}t' \left[\sum_{m=1}^{3} \hat{\sigma}_{+}^{(\mathrm{m})}(t') K_{\mathrm{e}}(\mathbf{x}_{\mathrm{n}}, \mathbf{x}_{\mathrm{n}}, t - t') \right] \hat{\sigma}_{\mathrm{z}}^{(\mathrm{n})} \tag{4.74}$$

$$\tag{4.75}$$

$$\dot{\sigma}_{\mathrm{z}}^{(\mathrm{n})} = -2\left\{\begin{array}{l} \displaystyle\sum_{m=1}^{3} \hat{\sigma}_{+}^{(\mathrm{n})} \int_{-\infty}^{\infty} \mathrm{d}\omega \int_{0}^{t} \mathrm{d}t' \left[K_e\left(\mathbf{x}_{\mathrm{n}}, \mathbf{x}_{\mathrm{n}}, t-t'\right) \hat{\sigma}_{-}^{(\mathrm{m})}\left(t'\right)\right] \\ + \displaystyle\sum_{m=1}^{3} \int_{-\infty}^{\infty} \mathrm{d}\omega \int_{0}^{t} \mathrm{d}t' \left[K_e^{*}\left(\mathbf{x}_{\mathrm{n}}, \mathbf{x}_{\mathrm{n}}, t-t'\right) \hat{\sigma}_{+}^{(\mathrm{m})}\left(t'\right)\right] \hat{\sigma}_{-}^{(\mathrm{n})} \end{array}\right\}, \tag{4.76}$$

where the memory kernel $K_e\left(\mathbf{x}_{\mathrm{n}}, \mathbf{x}_{\mathrm{n}}, t-t'\right)$ has been introduced as in Section (4.2.3).
Note that there is no contribution from the freely propagating input field due to the choice of rotating frame. These equations show that the evolution of the coherences and populations are non-local, i.e. the evolution at time t depend on the value of the coherences and populations at an earlier time t' and is defined by the form of memory kernel. The system will be assumed to be Markovian in the rest of the thesis (i.e. $\int \mathrm{d}\omega K_e\left(t-t'\right) \sim \delta\left(t-t'\right)$) in order to simplify the treatment but non-Markovian processes can be prevalent and should be considered in future treatments.

The evolution described by Eqs. (4.74) and (4.3) are governed by the Hamiltonian and Lindblad superoperator in the Markovian approximation:

$$\hat{H} = \sum_{n=1}^{3}\left(\Delta_{\mathrm{n}} \left|\mathrm{E}\right\rangle_{\mathrm{n}} \left\langle\mathrm{E}\right| + \frac{\Omega\delta_{\mathrm{nA}}}{2}\left[\left|\mathrm{E}\right\rangle_{\mathrm{n}} \left\langle\mathrm{g}\right| + \left|\mathrm{g}\right\rangle_{\mathrm{n}} \left\langle\mathrm{E}\right|\right]\right) + \sum_{n,m=1}^{3} J^{nm} \hat{\sigma}_{+}^{(\mathrm{n})} \hat{\sigma}_{-}^{(\mathrm{m})} \tag{4.77}$$

$$\mathcal{L}\left[\rho\right] = \sum_{n,m=1}^{3} \frac{\gamma'\delta_{\mathrm{n,m}} + \gamma^{nm}}{2}\left[\rho\hat{\sigma}_{+}^{(\mathrm{n})}\hat{\sigma}_{-}^{(\mathrm{m})} + \hat{\sigma}_{+}^{(\mathrm{n})}\hat{\sigma}_{-}^{(\mathrm{m})}\rho - 2\hat{\sigma}_{-}^{(\mathrm{n})}\rho\hat{\sigma}_{+}^{(\mathrm{m})}\right], \tag{4.78}$$

where the coherent and dissipative dipole-dipole interaction are given by

$$J^{nm} = \frac{1}{\hbar\varepsilon_0}\mathbf{d}_{\mathrm{n}}^{*} \cdot \mathrm{Re}\left[\mathrm{G}\left(\mathbf{x}_{\mathrm{n}}, \mathbf{x}_{\mathrm{m}}; \omega_0\right)\right] \cdot \mathbf{d}_{\mathrm{m}} \propto -\frac{a d^{(\mathrm{n})} d^{(\mathrm{m})}}{2\hbar\varepsilon_0 v_g}\omega_0 \sin\left[k\left(x_n - x_m\right)\right] \tag{4.79}$$

$$\gamma^{nm} = \frac{2}{\hbar\varepsilon_0}\mathbf{d}_{\mathrm{n}}^{*} \cdot \mathrm{Im}\left[\mathrm{G}\left(\mathbf{x}_{\mathrm{n}}, \mathbf{x}_{\mathrm{m}}; \omega_0\right)\right] \cdot \mathbf{d}_{\mathrm{m}} \propto \frac{a d^{(\mathrm{n})} d^{(\mathrm{m})}}{\hbar\varepsilon_0 v_g}\omega_0 \cos\left[k\left(x_n - x_m\right)\right], \tag{4.80}$$

respectively. The exact expression for Green's function for a W1 waveguide in a photonic crystal is given by Eq. (4.36) and includes the coupling to the forwards- and backwards propagating guided modes. The evolution can be described by the non-hermitian Hamiltonian $\hat{H}_{\mathrm{NH}}$ introduced in Section (2.1.4) if the jump terms in $\mathcal{L}\left[\rho\right]$ can be neglected. The non-hermitian Hamiltonian is then given by [9]:

$$\hat{H}_{\mathrm{NH}} = \hat{H}_{\mathrm{e}} - i\sum_{n,m=1}^{3} \frac{\gamma'\delta_{\mathrm{n,m}} + iJ^{\mathrm{nm}} - \gamma^{\mathrm{nm}}}{2}\hat{\sigma}_{+}^{(\mathrm{n})}\hat{\sigma}_{-}^{(\mathrm{m})} \tag{4.81}$$

$$= \hat{H}_{\mathrm{e}} - i\sum_{n,m=1}^{3} \frac{\gamma'\delta_{\mathrm{n,m}} + \gamma_0^{\mathrm{nm}} e^{-ik(x_n - x_m)}}{2}\hat{\sigma}_{+}^{(\mathrm{n})}\hat{\sigma}_{-}^{(\mathrm{m})}, \tag{4.82}$$

where γ_0^{nm} is equal to the maximum magnitude of γ^{nm}, as defined in Eq. (4.44) and where $\hat{H}_{\mathrm{e}}$ is the same as in Eq. (4.63). The exponential factor in the interaction term in Eq. (4.82) describes how an emitter at site n picks up a change in phase upon being excited by a photon emitted into

the waveguide by an emitter at site m. This change in phase depends on the distance travelled by the photon and is dominated by dissipative dipole-dipole interactions for $x_n - x_m = n\pi$ while it is dominated by coherent interactions for $x_n - x_m = k\pi/2$ for $k \in \mathbb{N}$.
The non-hermitian Hamiltonian in Eq. (4.82) provides a sufficient description of the dynamics of the presented system for deriving the proposed controlled phase gate. It is, however, necessary to use another approximation to reduce the complexity of the equation of motion that can be derived from this Hamiltonian. This is done by performing adiabatic elimination of the excited states of the system. The formal framework for this method is presented in Appendix (A). The derivation of the success probability and fidelity of the CZ gate is presented in Chapter (5) for the ideal case where the matrix elements γ^{nm} are equal, while Chapter (6) treats the case where the matrix elements can take different values as the dipole moments and positions for the qubit emitters are varied.

Chapter 5

Ideal CZ-Gate

This chapter describes the implementation of the controlled phase gate proposed in [3] in a nanophotonic environment in the ideal case and how to judge its performance. Section (5.1) discusses the preliminary considerations, while Section (5.2) provides the description of the gate operation and the derivation of the success probability and the fidelity of the gate. This section also discusses how to optimise the fidelity. Lastly, Section (5.3) provides the criteria needed to ensure that the adiabatic treatment remains valid.

5.1 Preliminaries

The system described in Chapter (4) can be used to implement a controlled phase gate for the two-qubit state $|\psi\rangle$. This state, and the ideal output state $|\Psi\rangle$, have the forms

$$|\psi\rangle = \frac{1}{2}\left(|00\rangle_{\mathrm{q}} + |01\rangle_{\mathrm{q}} + |10\rangle_{\mathrm{q}} + |11\rangle_{\mathrm{q}}\right) \tag{5.1}$$

$$|\Psi\rangle = \frac{1}{2}\left(|00\rangle_{\mathrm{q}} + |01\rangle_{\mathrm{q}} + |10\rangle_{\mathrm{q}} - |11\rangle_{\mathrm{q}}\right), \tag{5.2}$$

and can be implemented using the $|1\rangle = |S = 1/2, M_{\mathrm{S}} = 1/2\rangle$ and $|0\rangle = |S = 1/2, M_{\mathrm{S}} = -1/2\rangle$ electron ground states of the trion conduction band as the qubit states, as described in Sections (2.2.2) and (3.3). A third emitter quantum dot is included in this description; this is the auxiliary emitter and is used to drive the system and to implement an integrated error detection. The auxiliary emitter is also implemented using the ground states of the trion state: $|f\rangle = |S = 1/2, M_{\mathrm{S}} = 1/2\rangle$ and $|g\rangle = |S = 1/2, M_{\mathrm{S}} = -1/2\rangle$.

The level scheme is shown in Fig. (4.1) and the time evolution of $|\psi\rangle$ is governed by the non-hermitian Hamiltonian $\hat{H}_{\mathrm{NH}}$ that takes both coherent and dissipative evolution of the quantum states into account. The non-hermitian Hamiltonian derived in Section (4.3) is for the case where both qubit emitters are coupled to the waveguide.

$$\hat{H}_{\mathrm{NH}}\Big|_{n=2} = \begin{array}{c} \\ |11E\rangle \\ |e1f\rangle \\ |1ef\rangle \end{array} \begin{array}{c} \begin{array}{ccc} \langle 11E| & \langle e1f| & \langle 1ef| \end{array} \\ \begin{pmatrix} \Delta_{\mathrm{A}} - \frac{i}{2}\left(\gamma_A^{1\mathrm{D}} + \gamma'\right) & -\frac{i}{2}\gamma_{Aq}^{1\mathrm{D}} & -\frac{i}{2}\gamma_{Aq}^{1\mathrm{D}} \\ -\frac{i}{2}\gamma_{Aq}^{1\mathrm{D}} & \delta_{\mathrm{q_1}} - \frac{i}{2}\left(\gamma_{q_1}^{1\mathrm{D}} + \gamma'\right) & -\frac{i}{2}\gamma_{qq}^{1\mathrm{D}} \\ -\frac{i}{2}\gamma_{Aq}^{1\mathrm{D}} & -\frac{i}{2}\gamma_{qq}^{1\mathrm{D}} & \delta_{\mathrm{q_1}} - \frac{i}{2}\left(\gamma_{q_2}^{1\mathrm{D}} + \gamma'\right) \end{pmatrix} \end{array} \tag{5.3}$$

The braket notation on the outside of the matrix indicates how to write the matrix in the Dirac notation. These kets describes the combined state of the tqo qubit emitters and the auxiliary

quantum dot: $|\psi\rangle_{\mathrm{q_1}} \otimes |\psi\rangle_{\mathrm{q2}} \otimes |\psi\rangle_{\mathrm{A}}$ It is possible that only one of the qubit emitters is coupled to the waveguide. The non-hermitian Hamiltonian for each of these cases is:

$$\hat{H}_{\mathrm{NH}}\Big|_{n=1,q_1} = \begin{array}{c} \\ |10E\rangle \\ |e0f\rangle \end{array} \begin{array}{c} \begin{array}{cc} \langle 10E| & \langle e0f| \end{array} \\ \begin{pmatrix} \Delta_{\mathrm{A}} - \frac{i}{2}\left(\gamma_A^{1\mathrm{D}} + \gamma'\right) & -\frac{i}{2}\gamma_{Aq}^{1\mathrm{D}} \\ -\frac{i}{2}\gamma_{Aq}^{1\mathrm{D}} & \delta_{\mathrm{q_1}} - \frac{i}{2}\left(\gamma_{q_1}^{1\mathrm{D}} + \gamma'\right) \end{pmatrix} \end{array} \tag{5.4}$$

$$\hat{H}_{\mathrm{NH}}\Big|_{n=1,q_2} = \begin{array}{c} \\ |01E\rangle \\ |0ef\rangle \end{array} \begin{array}{c} \begin{array}{cc} \langle 01E| & \langle 0ef| \end{array} \\ \begin{pmatrix} \Delta_{\mathrm{A}} - \frac{i}{2}\left(\gamma_A^{1\mathrm{D}} + \gamma'\right) & -\frac{i}{2}\gamma_{Aq}^{1\mathrm{D}} \\ -\frac{i}{2}\gamma_{Aq}^{1\mathrm{D}} & \delta_{\mathrm{q_2}} - \frac{i}{2}\left(\gamma_{q_2}^{1\mathrm{D}} + \gamma'\right) \end{pmatrix} \end{array} \tag{5.5}$$

These two Hamiltonians may be different from each other, depending on the values of the parameters of the quantum dot. The non-Hermitian takes the following form, when none of the qubits interact with the guided mode:

$$\hat{H}_{\mathrm{NH}}\Big|_{n=0} = \left(\Delta_{\mathrm{A}} - \frac{i}{2}\left(\gamma_A^{1\mathrm{D}} + \gamma'\right)\right)|00E\rangle\langle 00E| \tag{5.6}$$

These Hamiltonians can be combined into one single Hamiltonian by:

$$\begin{pmatrix} \hat{H}_{\mathrm{NH}}\Big|_{n=2} & & & \\ & \hat{H}_{\mathrm{NH}}\Big|_{n=1,\mathrm{q_1}} & 0 & \\ & & \hat{H}_{\mathrm{NH}}\Big|_{n=1,\mathrm{q_2}} & \\ & 0 & & \hat{H}_{\mathrm{NH}}\Big|_{n=1} \end{pmatrix} \tag{5.7}$$

Here $\Gamma'_{\mathrm{A,q}} = \gamma_{\mathrm{A,q}} + \gamma'$. $\gamma_{\mathrm{A,q}}$ is the single-emitter decay rate for the auxiliary and qubit emitters while γ_{Aq} and γ_{qq} are the two-emitter decay rates between the auxiliary- and qubit emitters, and between the two qubit emitters respectively. These rates are for decay into the guided mode in the waveguide, while γ' is the decay rate for nonradiative decay. Only nonradiative decay processes along the optical transition is considered in the following. Δ_{A} and $\delta_{\mathrm{q_1}}$ are the detuning of the auxiliary and qubit emitters. The evolution of the system can be simplified using adiabatic elimination, which results in the effective master equation with a set of effective operators [18]:

$$\dot{\rho} = -i\left[\hat{H}_{\mathrm{eff}}, \rho(t)\right] - \frac{1}{2}\sum_{k,l}\left[\left(\hat{L}_{\mathrm{eff}}^k\right)^\dagger \hat{L}_{\mathrm{eff}}^l \rho(t) + \rho(t)\left(\hat{L}_{\mathrm{eff}}^k\right)^\dagger \hat{L}_{\mathrm{eff}}^l - 2\hat{L}_{\mathrm{eff}}^k \rho(t)\left(\hat{L}_{\mathrm{eff}}^l\right)^\dagger\right] \tag{5.8}$$

$$\hat{H}_{\mathrm{eff}} = -\frac{1}{2}\hat{V}_-\left[\hat{H}_{\mathrm{NH}}^{-1} + \left(\hat{H}_{\mathrm{NH}}^{-1}\right)^\dagger\right]\hat{V}_+ + \hat{H}_{\mathrm{g}} \tag{5.9}$$

$$\hat{L}_{\mathrm{eff}}^k = \hat{L}_k \hat{H}_{\mathrm{NH}}^{-1}\hat{V}_+. \tag{5.10}$$

This chapter will describe the mathematical foundation for the implementation of the controlled phase gate and will quantify the effectiveness of the implementation through the success probability P_{S} and the Fidelity F of the gate, while Chapter (6) will discus the effect of lifting the approximations that lead to the ideal case.

5.2 Ideal CZ Gate

The ideal case involves three main approximations:

- The quantum dots are placed exactly in the regions of maximal constructive interference
- The coupling constants of the three quantum dots are equal
- The resonance frequency of the three dots are equal

The spatial phase factors can then be set to 1 and all decay rates can be set to γ^{1D} using these three approximations. This leads to the simple case discussed in this chapter and greatly simplifies the mathematical treatment. In addition, it is assumed that nonradiative decay processes are suppressed along the $|\mathrm{E}\rangle_{\mathrm{A}} \leftrightarrow |\mathrm{f}\rangle_{\mathrm{A}}$ transition for the auxiliary emitter and along the $|\mathrm{e}\rangle_{\mathrm{q_k}} \leftrightarrow |0\rangle_{\mathrm{q_k}}$ transitions for the qubit emitters. The approximation also sets the two single-qubit non-hermitian Hamiltonians to be equal: $\hat{H}_{\mathrm{NH}}\Big|_{n=1,q_1} = \hat{H}_{\mathrm{NH}}\Big|_{n=1,q_2}$. In addition, the detuning of the qubits will be set to zero: $\delta_{\mathrm{q},1} = \delta_{1,2} = 0$. The effective operators for the four different blocks will be derived separately in the following section.

5.2.1 Effective Operators

The matrix representation of the non-hermitian Hamiltonian is given by Eq. (5.7) and is used to derive the effective operators for the system. More details about the calculations can be found in Appendix. (B). This results in the following effective operators, where the sum is over the number n of qubits in the ground state:

$$\hat{H}_{\mathrm{eff}} = \sum_{n=0}^{2} -\frac{\Omega^2}{\gamma'}\frac{\Delta_{\mathrm{A}}}{\gamma'}\frac{(nC+1)^2}{\left(2\frac{\Delta_{\mathrm{A}}}{\gamma'}\right)^2(nC+1)^2 + ([n+1]C+1)^2}|\mathrm{g}\rangle_{\mathrm{A}}\langle\mathrm{g}| \otimes \hat{P}_{\mathrm{n}} \tag{5.11}$$

$$= \sum_{n=0}^{2} \Delta_n |\mathrm{g}\rangle_{\mathrm{A}}\langle\mathrm{g}| \otimes \hat{P}_{\mathrm{n}} \tag{5.12}$$

$$\hat{L}^{A}_{\mathrm{eff}} = \sum_{n=0}^{2} \sqrt{C+1}\frac{\Omega}{\sqrt{\gamma'}}(nC+1)\frac{2\frac{\Delta_{\mathrm{A}}}{\gamma'}(nC+1) + i([n+1]C+1)}{\left(2\frac{\Delta_{\mathrm{A}}}{\gamma'}\right)^2(nC+1)^2 + ([n+1]C+1)^2}|\mathrm{f}\rangle_{\mathrm{A}}\langle\mathrm{g}| \otimes \hat{P}_{\mathrm{n}} \tag{5.13}$$

$$= \sum_{n=0}^{2} r_{\mathrm{A},n}|\mathrm{f}\rangle_{\mathrm{A}}\langle\mathrm{g}| \otimes \hat{P}_{\mathrm{n}} \tag{5.14}$$

$$\hat{L}^{q_j}_{\mathrm{eff}} = \sum_{n=1}^{2} -\sqrt{C}\frac{\Omega}{\sqrt{\gamma'}}C\frac{2\frac{\Delta_{\mathrm{A}}}{\gamma'}(nC+1) + i([n+1]C+1)}{\left(2\frac{\Delta_{\mathrm{A}}}{\gamma'}\right)^2(nC+1)^2 + ([n+1]C+1)^2}|\mathrm{f}\rangle_{\mathrm{A}}\langle\mathrm{g}| \otimes \hat{P}_{\mathrm{n}} \tag{5.15}$$

$$= \sum_{n=1}^{2} r_{\mathrm{q}_j,n}|\mathrm{f}\rangle_{\mathrm{A}}\langle\mathrm{g}| \otimes \hat{P}_{\mathrm{n}} \tag{5.16}$$

where $r_{\mathrm{q}_j,0} = 0$, $C \equiv \gamma^{1D}/\gamma'$ is the cooperativity and $\hat{P}_{\mathrm{n}}$ are projection operators that project onto the qubit ground states. The only dynamical change stems from $\hat{H}_{\mathrm{eff}}$, which project the auxiliary quantum dot into $|\mathrm{g}\rangle_{\mathrm{A}}$ and introduces an effective AC Stark shift of the ground states, while the parameters $r_{\mathrm{A},n}$ and $r_{\mathrm{q}_j,n}$ describe the effective decay processes. Free evolution of the system while applying the weak laser field $\hat{V}$ then imprints a phase shift of Δ_n on the state $|\mathrm{g}\rangle_{\mathrm{A}} \otimes \hat{P}_{\mathrm{n}}$. This dynamical phase shift can be used to implement a controlled phase gate with

the truth table from Tab. (2.1) by, naively, applying the laser field for a time of $t_g = \frac{\pi}{|\Delta_2|}$. The implementation the CZ gate will be examined more closely in Sec. (5.2.3).
The only effect of any effective decay process is to project the auxiliary emitter into $|\mathrm{f}\rangle_{\mathrm{A}} \otimes \hat{P}_{\mathrm{n}}$, as can be read off from Eqs. (5.13) and (5.15). These errors are detectable through measuring the state of the auxiliary emitter using the methods mentioned discussed in Section (2.2.5) after the gate operation has been implemented. The effects of these decay processes on the fidelity can be removed by conditioning the gate on measuring the auxiliary emitter in $|\mathrm{g}\rangle_{\mathrm{A}}$, though they will still have a detrimental effect on the success probability. This, and additional errors, will be discussed in further detail in Section (5.2.3).
Expressions for the success probability and fidelity can be derived by solving the effective master equation and comparing the ideal density matrix $\rho_{\mathrm{I}} = |\Psi\rangle\langle\Psi|$ to the one describing the actual output state $\rho_{\mathrm{q}}(t_{\mathrm{g}}) = |\psi(\mathrm{t_g})\rangle_{\mathrm{q}}\langle\psi(t_{\mathrm{g}})|$. The success probability can be found by tracing over the density matrix for the qubits at time t_{g}:

$$P_{\mathrm{S}} = \mathrm{Tr}\left\{\rho_{\mathrm{q}}(t_{\mathrm{g}})\right\} = \sum_{n=0}^{2} \mathrm{Tr}\left\{\rho_{\mathrm{q}}(t_{\mathrm{g}})\,\hat{P}_{\mathrm{n}}\right\}, \tag{5.17}$$

and the fidelity is found by projecting the ideal output state $|\Psi\rangle$ onto $\tilde{\rho}(t_{\mathrm{g}})(t_{\mathrm{g}})$ and normalizing with P_{S}:

$$F = \frac{1}{P_{\mathrm{S}}}\,{}_{\mathrm{A}}\langle\mathrm{g}|\langle\Psi|\tilde{\rho}(t_{\mathrm{g}})\,\rho_{\mathrm{q}}(t_{\mathrm{g}})\,|\Psi\rangle\,|\mathrm{g}\rangle_{\mathrm{A}}. \tag{5.18}$$

Both the fidelity and success probability in conditioned upon measuring the auxiliary emitter in $|\mathrm{g}\rangle_{\mathrm{A}}$. The expressions for the success probability and the fidelity are derived in Section (5.2.3) while the density matrix $\rho_{\mathrm{q}}(t)$ is found by solving the effective master equation.

5.2.2 Solving the Effective Master Equation

The effective master equation can be solved by plugging the coefficients from Eqs. (5.11) through (5.15) into Eq. (5.8) and then project states onto the equation to obtain the equations of motion for the sixteen matrix elements of $\rho(t)$. The gate operation is only concerned with the evolution of the qubit states, so the density matrix used in the following in the reduced density matrix found by tracing over the auxiliary emitter:

$$\rho = \mathrm{Tr}_{\mathrm{A}}\left\{\rho_{\mathrm{Full}}\right\}, \tag{5.19}$$

where $\rho_{\mathrm{Full}} = |\Psi\rangle_{\mathrm{q}}|\psi\rangle_{\mathrm{A\,q}}\langle\Psi|_{\mathrm{A}}\langle\psi|$. The jump terms in the effective master equation are all proportional to the population of the excited state; these states are emptied by the initialisation procedure, making possible to neglect the evolution imposed by the jump terms in the following treatment.
The details of solving the effective master equation can be found in Appendix. (D). Luckily, all the differential equations are decoupled, thereby making the system solvable. The equation of motion for any matrix element $\rho_y^x(t)$ is given by:

$$\dot{\rho}_y^x = i(\Delta_y - \Delta_x)\,\rho_y^x(t) - \frac{1}{2}(\Gamma_x + \Gamma_y)\,\rho_y^x(t), \quad x = \left\{\underset{n=0}{00}, \underset{n=1}{01}, \underset{n=1}{10}, \underset{n=2}{11}\right\}, \tag{5.20}$$

where the notation underneath each element in the definition of x and y indicates the number of qubits in $|1\rangle_{\mathrm{q}}$. This differential equation has the straightforward solution:

$$\rho_x^y(t) = \rho_x^y(t=0)\,e^{i(\Delta_y - \Delta_x)t}e^{-\frac{1}{2}(\Gamma_x+\Gamma_y)t}. \tag{5.21}$$

Here Γ_n denote the decay rate of the combined system of three emitters when n qubits are in state $|1\rangle$. These decay rates are defined by the coefficients of the dissipative terms in the effective master equation and take the following form:

$$\Gamma_0 \equiv \left|r_0^{\mathrm{A}}\right|^2 \tag{5.22}$$

$$\begin{aligned}\Gamma_1 &\equiv \left|r_1^{\mathrm{A}}\right|^2 + \left|r_1^{\mathrm{q}}\right|^2 + r_1^{\mathrm{A}}\left(r_1^{\mathrm{q}}\right)^* + r_1^{\mathrm{q}}\left(r_1^{\mathrm{A}}\right)^* \\ &= \left|r_1^{\mathrm{A}}\right|^2 + \left|r_1^{\mathrm{q}}\right|^2 + r_1^{\mathrm{A}}\left(r_1^{\mathrm{q}}\right)^*\end{aligned} \tag{5.23}$$

$$\begin{aligned}\Gamma_2 &\equiv \left|r_2^{\mathrm{A}}\right|^2 + 4\left|r_2^{\mathrm{q}}\right|^2 + 2r_2^{\mathrm{A}}\left(r_2^{\mathrm{q}}\right)^* + 2r_2^{\mathrm{q}}\left(r_2^{\mathrm{A}}\right)^* \\ &= \left|r_2^{\mathrm{A}}\right|^2 + 4\left|r_2^{\mathrm{q}}\right|^2 + 4r_2^{\mathrm{A}}\left(r_2^{\mathrm{q}}\right)^*,\end{aligned} \tag{5.24}$$

as the cross terms for each n are equal in the ideal case. These three expressions can be collected together as:

$$\Gamma_n = \left|r_{\mathrm{n}}^{\mathrm{A}}\right|^2 + n^2\left|r_{\mathrm{n}}^{\mathrm{q}}\right|^2 + 2n \cdot r_{\mathrm{n}}^{\mathrm{A}}\left(r_{\mathrm{n}}^{\mathrm{q}}\right)^*. \tag{5.25}$$

It can be readily seen from Eq. (5.21) that the decay rate of the four diagonal elements is given by Eqs. (5.22) through (5.24). The non-diagonal elements have a time-dependent change in phase and a decay rate that is constructed from the decay rates of the diagonal elements. Plugging in the expressions for the Lindblad coefficients from Eqs. (5.13) and (5.15) yields the following expressions for the decay rates (assuming that the detuning is $\Delta_E \propto \sqrt{\gamma^{1\mathrm{D}}\gamma'} = \sqrt{C}\gamma'$). The three different terms in Eqs. (5.23) and (5.24) are given by, where the $C \gg 1$ limit is done for the terms in the square root of Eq. (5.30) for brevity:

$$\left|r_{\mathrm{n}>0}^{\mathrm{A}}\right|^2 = \frac{\Omega^2}{\gamma'}\frac{(C+1)\left(nC+1\right)^2}{\left(2\frac{\Delta_{\mathrm{A}}}{\gamma'}\right)^2\left(nC+1\right)^2 + \left(\left[n+1\right]C+1\right)^2} \tag{5.26}$$

$$= \frac{\Omega^2}{\gamma'}\frac{n^2C^3 + \left(2n+n^2\right)C^2 + (1+2n)C + 1}{\left(2\frac{\Delta_{\mathrm{A}}}{\gamma'}\right)^2\left(nC+1\right)^2 + \left(\left[n+1\right]C+1\right)^2} \tag{5.27}$$

$$\left|r_{\mathrm{n}>0}^{\mathrm{q}}\right| = \frac{\Omega^2}{\gamma'}\frac{C^3}{\left(2\frac{\Delta_{\mathrm{A}}}{\gamma'}\right)^2\left(nC+1\right)^2 + \left(\left[n+1\right]C+1\right)^2} \tag{5.28}$$

$$r_{\mathrm{n}>0}^{\mathrm{A}}\left(r_{\mathrm{n}>0}^{\mathrm{q}}\right)^* = -\frac{\Omega^2}{\gamma'}\frac{\sqrt{(C+1)C}C\left(nC+1\right)}{\left(2\frac{\Delta_{\mathrm{A}}}{\gamma'}\right)^2\left(nC+1\right)^2 + \left(\left[n+1\right]C+1\right)^2} \tag{5.29}$$

$$\underset{C\gg1}{\cong} -\frac{\Omega^2}{\gamma'}\frac{nC^3 + C^2}{\left(2\frac{\Delta_{\mathrm{A}}}{\gamma'}\right)^2\left(nC+1\right)^2 + \left(\left[n+1\right]C+1\right)^2}. \tag{5.30}$$

The three decay rates can then be calculated:

$$\Gamma_{n>0} = \frac{\Omega^2}{\gamma'} \frac{n^2C^2 + (1+2n)\,C + 1}{\left(2\frac{\Delta_\mathrm{A}}{\gamma'}\right)^2 (nC+1)^2 + ([n+1]\,C+1)^2} \tag{5.31}$$

$$\underset{C\gg 1}{\rightarrow} \frac{\Omega^2}{\gamma'} \frac{n^2C^2}{4n^2\left(\frac{\Delta_\mathrm{A}}{\gamma'}\right)^2 C^2} \tag{5.32}$$

$$= \frac{\Omega^2}{\gamma'} \frac{1}{4\left(\frac{\Delta_\mathrm{A}}{\gamma'}\right)^2} \tag{5.33}$$

$$\Gamma_0 = \frac{\Omega^2}{\gamma'} \frac{(C+1)}{\left(2\frac{\Delta_\mathrm{A}}{\gamma'}\right)^2 + [C+1]^2} \tag{5.34}$$

$$\underset{C\gg 1}{\rightarrow} \frac{\Omega^2}{\gamma'} \frac{1}{C}. \tag{5.35}$$

It is seen from Eq. (5.33) that the decay rate for a system comprised of the auxiliary quantum dot coupled to either one of or both the qubits dots depends on the detuning of the weak perturbative driving field. Note that the effective decay rate is the same for any $n > 0$. The choice of detuning has a pronounced effect on the fidelity and success probability of the gate operation and is the most direct manner of reducing errors. The decay rate for $n = 2$ and $n = 1$ are equal in the ideal case.

5.2.3 Effective Phase Evolution for $C \gg 1$

The coefficients for the effective Hamiltonian is given by Eq. (5.11) and can be greatly simplified by considering the limit where $\gamma^{1\mathrm{D}} \gg \gamma' \Rightarrow C \gg 1$ and by only include the dominant term in the denominator. Choosing the same form of detuning as in Section. (5.2.2) causes the first term in the denominator to scale as C^3 for $n > 0$. The energy shift can then be expressed as:

$$\begin{aligned}\Delta_{n>0} &\underset{C\gg 1}{\rightarrow} -\frac{\Omega^2}{\gamma'} \frac{(\Delta_\mathrm{A}/\gamma')\,(nC+1)^2}{(\Delta_\mathrm{A}/\gamma')^2\,(nC+1)^2} \\ &= -\frac{\Omega^2}{\gamma'} \frac{1}{4\,(\Delta_\mathrm{A}/\gamma')}\end{aligned} \tag{5.36}$$

Note that the induced energy shift is the same for any $n > 0$. The second term in the denominator dominates for $n = 0$:

$$\Delta_0 = -\frac{\Omega^2}{\gamma'} \frac{(\Delta_\mathrm{A}/\gamma')}{(C+1)^2} \tag{5.37}$$

The scaling causes Δ_0 to vanish significantly faster than $\Delta_{n>0}$, which ensures that the ground state remain unshifted under any gate operation. Choosing a gate time of $t_g = \frac{\pi}{|\Delta_n|}$ will not enable the implementation of a controlled phase gate, as the remaining three qubit states acquires an identical phase shift. This can be mitigated by employing the following single-qubit rotations on all four states at the end of the gate operation (each vertical line of arrows represents the effect of a single qubit rotation. The first line of arrows thus represent the rotation that removed the dynamical change of phase from $|00\rangle_\mathrm{w}$, while the second i for removing the phase change

from $|10\rangle_{\mathrm{q}}$ and $|01\rangle_{\mathrm{q}}$):

$$
\begin{aligned}
&e^{-i\Delta_0 t}\,|00\rangle_{\mathrm{q}} \to |00\rangle_{\mathrm{q}} \\
&e^{-i\Delta_1 t}\,|01\rangle_{\mathrm{q}} \to e^{-i(\Delta_1-\Delta_0)t}\,|01\rangle_{\mathrm{q}} \to |01\rangle_{\mathrm{q}} \\
&e^{-i\Delta_1 t}\,|10\rangle_{\mathrm{q}} \to e^{-i(\Delta_1-\Delta_0)t}\,|10\rangle_{\mathrm{q}} \to |10\rangle_{\mathrm{q}} \\
&e^{-i\Delta_2 t}\,|11\rangle_{\mathrm{q}} \to e^{-i(\Delta_2-\Delta_0)t}\,|11\rangle_{\mathrm{q}} \to e^{-i(\Delta_2-2\Delta_1+\Delta_0)t}\,|11\rangle_{\mathrm{q}}\,.
\end{aligned}
$$

Choosing a gate time of

$$
t_{\mathrm{g}} = \frac{\pi}{|\Delta_2 - 2\Delta_1 + \Delta_0|} \approx \frac{4\pi\gamma'\sqrt{C}}{\Omega^2} \tag{5.38}
$$

thus ensures the correct phase evolution of state $|11\rangle_{\mathrm{q}}$ while keeping the three remaining terms unshifted, thereby completing the gate operation for the controlled phase gate. The success of the gate is, as explained above, conditioned on measuring the auxiliary quantum dot in state $|\mathrm{g}\rangle_{\mathrm{A}}$. The success probability P_{S} can then be calculated as a trace over the density matrix ρ_{q} describing the two qubits:

$$
P_{\mathrm{S}} = \mathrm{Tr}\left\{\rho_{\mathrm{q}}\left(t_{\mathrm{g}}\right)\right\} = \sum_{n=0}^{2} \mathrm{Tr}\left\{\rho_{\mathrm{n}}\left(t_{\mathrm{g}}\right)\hat{P}_{\mathrm{n}}\right\} = \sum_{n=0}^{2} \mathrm{Tr}\left\{e^{-\Gamma_n t_{\mathrm{g}}}\rho_{\mathrm{n}}\left(t=0\right)\hat{P}_{\mathrm{n}}\right\}, \tag{5.39}
$$

where the projection operator has been explicitly extracted to keep track of the effects from either both, only one or none qubits in the ground state. It will be assumed that the initial values of all the matrix elements in the density operator is $\rho_y^x\left(t=0\right) = \frac{1}{4}$. The detuning is initially chosen to take the value $\Delta_{\mathrm{A}} = \sqrt{C}\gamma'$. The energy shifts and decay rates are then given by:

$$
\Delta_0 = -\frac{\Omega^2}{\gamma'}\frac{1}{3/2} \qquad \Gamma_0 = \frac{\Omega^2}{\gamma'}\frac{1}{C} \tag{5.40}
$$

$$
\Delta_{n>0} = -\frac{\Omega^2}{\gamma'}\frac{1}{\sqrt{C}} \qquad \Gamma_{n>0} = \frac{\Omega^2}{\gamma'}\frac{1}{4C}, \tag{5.41}
$$

where Γ_1 and Γ_2 will both be denoted as Γ_2 in the following. The success probability defined in Eq. (5.17) can then be calculated:

$$
\begin{aligned}
P_{\mathrm{S}} &= \frac{1}{4}\left(\exp\left[-\Gamma_0 t_{\mathrm{g}}\right] + 3\exp\left[-\Gamma_2 t_{\mathrm{g}}\right]\right) && (5.42)\\
&= \frac{1}{4}\left(\exp\left[-\frac{4\pi}{\sqrt{C}}\right] + 3\exp\left[-\frac{\pi}{\sqrt{C}}\right]\right) && (5.43)\\
&\approx 1 - \frac{7\pi}{4\sqrt{C}} && (5.44)
\end{aligned}
$$

The fidelity of the gate is defined as the projection of the ideal output state $|\Psi\rangle$ projected onto the actual output density matrix $\tilde{\rho}_{\mathrm{q}}\left(t_{\mathrm{g}}\right)$ after the gate operation and is normalized by the success probability:

$$
F = \frac{1}{P_{\mathrm{S}}}\,{}_{\mathrm{A}}\langle \mathrm{g}|\,\langle\Psi|\,\tilde{\rho}_{\mathrm{q}}\left(t_{\mathrm{g}}\right)|\Psi\rangle\,|\mathrm{g}\rangle_{\mathrm{A}}\,, \tag{5.45}
$$

The density operator in Eqs. (5.42) and (5.45) is the solution to the effective master equation and its matrix elements are given by Eq. (5.21).

The fidelity is at an arbitrary time t given by Eq. (6.15) and will simplify to the following expression in the simple, ideal case considered here:

$$F(t) = \frac{F_0(t) + 2F_1(t) + F_2(t)}{\frac{1}{4}\left(\exp\left[-\Gamma_0 t\right] + 2\exp\left[-\Gamma_2 t\right]\right)}, \tag{5.46}$$

where the functions $F_n(t)$ are shorthand functions that collect the contribution to the fidelity from the matrix elements of $\rho(t)$. The subscript n correspond to the contribution when to when n qubits are in $|1\rangle_{\mathrm{q}}$:

$$F_0(t) = \frac{1}{16}\left(e^{-\Gamma_0 t} + 2e^{-\frac{1}{2}(\Gamma_0+\Gamma_2)t} - e^{-i\Delta_2' t}e^{-\frac{1}{2}(\Gamma_0+\Gamma_2)t}\right) \tag{5.47}$$

$$F_1(t) = \frac{1}{16}\left(e^{-\frac{1}{2}(\Gamma_2+\Gamma_0)t} + 2e^{-\Gamma_2 t} - e^{-i\Delta_2' t}e^{-\Gamma_2 t}\right) \tag{5.48}$$

$$F_2(t) = \frac{1}{16}\left(-e^{i\Delta_2' t}e^{-\frac{1}{2}(\Gamma_2+\Gamma_0)t} - 2e^{i\Delta_2' t}e^{-\Gamma_2 t} + e^{-\Gamma_2 t}\right). \tag{5.49}$$

Note that the term $2F_1(t)$ in Eq. (5.46) will be split into two terms in the general case due to possible difference between the decay rates of either of the qubits. Adding the function above then gives:

$$F(t_{\mathrm{g}}) = \frac{1}{4}\frac{e^{-\Gamma_0 t} + 5e^{-\Gamma_2 t} + 4e^{-\frac{1}{2}(\Gamma_0+\Gamma_2)t} - 2e^{-i\Delta_2' t}\left[2e^{-\Gamma_2 t} + e^{-\frac{1}{2}(\Gamma_0+\Gamma_2)t}\right]}{e^{-\Gamma_0 t} + 3e^{-\Gamma_2 t}} \tag{5.50}$$

Here $\Delta_2' = \Delta_2 - \Delta_{1,1} - \Delta_{1,2}$ is the phase shift of the $|11\rangle_{\mathrm{q}}$ state after the single-qubit rotations have been performed. All the complex exponential functions evaluate as -1 at the chosen gate time $t_{\mathrm{g}} = \pi/|\Delta_2'|$. The fidelity simplifies to the following expression in the ideal case:

$$F(t_{\mathrm{g}}) = \frac{1}{4}\frac{e^{-\Gamma_0 t_{\mathrm{g}}} + 6e^{-\frac{1}{2}(\Gamma_0+\Gamma_2)t_{\mathrm{g}}} + 9e^{-\Gamma_2 t_{\mathrm{g}}}}{e^{-\Gamma_0 t_{\mathrm{g}}} + 3e^{-\Gamma_2 t_{\mathrm{g}}}} \tag{5.51}$$

$$= \frac{1}{4}\left(1 + 3\frac{1 + e^{\frac{1}{2}(\Gamma_0-\Gamma_2)t_{\mathrm{g}}}}{\cosh\left[\frac{1}{2}\left(\Gamma_0 - \Gamma_2\right)t_{\mathrm{g}}\right] + e^{\frac{1}{2}(\Gamma_0-\Gamma_2)t_{\mathrm{g}}}}\right) \tag{5.52}$$

$$\approx \frac{1}{4}\left(1 + 3\left[1 - \frac{1}{4}\left(\frac{1}{2}\left(\Gamma_0 - \Gamma_2\right)t_{\mathrm{g}}\right)^2\right]\right) \tag{5.53}$$

$$= 1 - \frac{27\pi^2}{64}\frac{1}{C}. \tag{5.54}$$

The success probability and the fidelity of the gate with detunings $\Delta_E = \sqrt{C}\gamma'$ and $\delta_1 = \delta_2 = 0$ have thus been found as:

$$P_S(t_{\mathrm{g}}) = 1 - \frac{7\pi}{4}\frac{1}{\sqrt{C}} \tag{5.55}$$

$$F(t_{\mathrm{g}}) = 1 - \frac{27\pi^2}{64}\frac{1}{C}. \tag{5.56}$$

The effect of these errors on the success probability and fidelity are shown in Fig. (5.1), demonstrating the importance of being able to obtain a high cooperativity to overcome the influence of the various errors that can occur during the gate operation.
These errors can be explained by the different values for Γ_0 and $\Gamma_{n>0}$. This changes the relative weight of the qubit states in Eq. (5.50) leading to the errors in the fidelity of order $\mathcal{O}\left(C^{-1}\right)$ derived above. Additional errors will arise from higher order corrections from the energy shifts

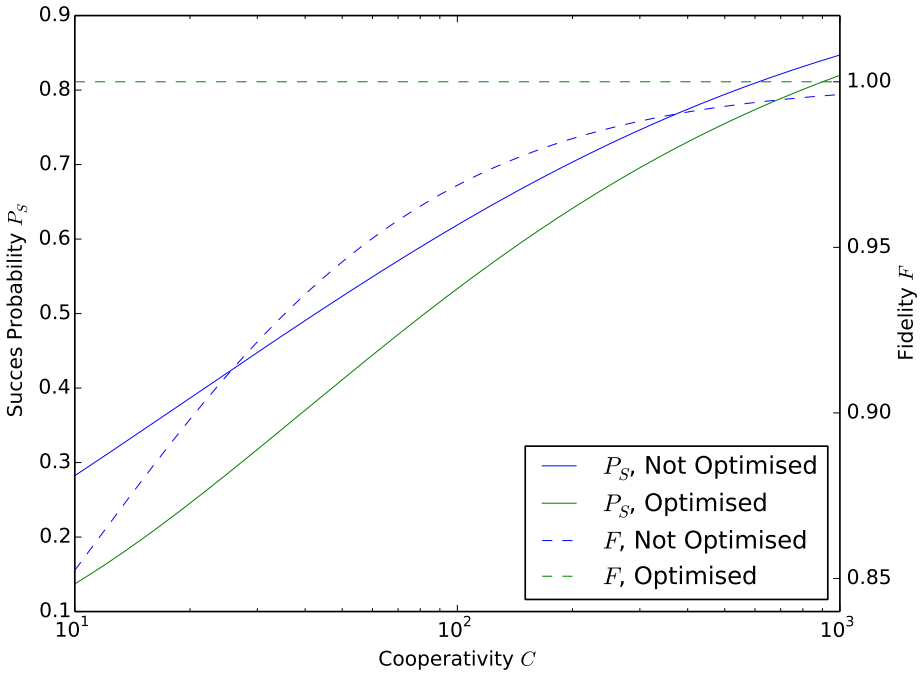

Figure 5.1: Plot of the probability (solid lines) and the fidelity (dashed lines)of the CZ gate as a function of cooperativity. Both the non-optimised case with $\Delta_{\mathrm{A}} = \gamma'\sqrt{C}$ (blue lines) and the optimised case $\Delta_{\mathrm{A}} = \gamma'\sqrt{C}/2$ (green lines) are included. It is clearly seen that the errors due to the uneven weights of the qubit basis states can be removed with a proper choice of detuning, at the cost of lowering the success probability.

Δ_n. The energy shift used above all scale as $\Delta_{n>0} \sim \Omega^2/\left(4\gamma\sqrt{C}\right)$ while the higher order corrections are of order $\mathcal{O}\left(\Omega^2/C^{3/2}\right)$. This leads to an uneven phase evolution dependent on the number of qubits in state $|1\rangle$ of order $\mathcal{O}\left(C^{-1}\right)$. These errors in the fidelity will then scales as $\mathcal{O}\left(C^{-2}\right)$.
Any errors for the gate operation that stem from the effective decay processes through Eqs. (5.13) and (5.15) are, as described in Section (5.2.1), detectable upon measuring the state of the auxiliary quantum dot. These errors will not affect the fidelity if the gate is conditioned upon measuring the auxiliary emitter in $|\mathrm{g}\rangle_{\mathrm{A}}$ but the success probability will be negatively affected, as the system is projected into some erroneous state. Any gate operation that has failed in this manner will be detected by the measurement on the auxiliary emitter. Discarding the present gate operation and repeating the process until a successful measurement is performed makes it possible to produce the desired output state with a high fidelity. The errors will thus only affect the bit rate through the sub-unity probability.

The dominant source of errors for the gate operation thus comes from the difference in the rate Γ_n of detectable errors, due to the $\mathcal{O}\left(C^{-1}\right)$ scaling of the infidelity. These errors can be mitigated by standardizing the decay rates such that $\Gamma_0 = \Gamma_1 = \Gamma_2 \equiv \Gamma$. This can be done by choosing a specific form of the detuning for the auxiliary emitter Δ_{A} while keeping δ_1 and δ_2 at zero. The success probability is then given by:

$$P_S\left(t_{\mathrm{g}}\right) = e^{-\Gamma t_{\mathrm{g}}} \tag{5.57}$$
$$\tag{5.58}$$

It is then easily from Eq. (5.50) that this leads to the *optimised* case where the fidelity becomes:

$$F\left(t_{\mathrm{g}}\right) = \frac{4e^{-\Gamma t_{\mathrm{g}}}}{e^{-\Gamma t_{\mathrm{g}}}} = 1. \tag{5.59}$$

Setting $\Delta_{\mathrm{A}} = \gamma'\sqrt{C}/2$ is sufficient to eliminate the errors due to the different relative weights of the qubit states. The standardized decay rate and gate time are in this case given by:

$$\Gamma_0 = \Gamma_{n>0} = \frac{\Omega^2}{\gamma'}\frac{1}{C}, \quad t_{\mathrm{g}} = \frac{\gamma'}{\Omega^2}2\pi\sqrt{C} \tag{5.60}$$

with the success probability and fidelity:

$$P_S\left(t_{\mathrm{g}}\right) = e^{-\Gamma_0 t_{\mathrm{g}}} = e^{-\frac{2\pi}{\sqrt{C}}} \approx 1 - \frac{2\pi}{\sqrt{C}} \tag{5.61}$$
$$F\left(t_{\mathrm{g}}\right) = 1. \tag{5.62}$$

The optimised success probability and fidelity are included in Fig (5.1). Note that the this choice of detuning results in a lower success probability than in the non optimised case, leading to a lower bit rate for the gate operation than in the non-optimised case.
The dynamics of the ground states of the three quantum dots, that are described by the effective operators in Eqs. (5.11) through (5.15), completely mimic the dynamics of the three atoms in Borregaard et al. in [3]. In addition, the behaviour of the success probability and fidelity of the CZ gate follows the same dependence on the cooperativity for the non-optimising choice of detuning and it is possible to optimise the fidelity in a manner similar to that employed in Borregaard's proposal with the same integrated error detection scheme. A brief discussion about the advantages and disadvantages of both systems is presented at the end of Chapter (6) when the effects of lifting the approximations listed in Section (5.2) have been examined.

5.3 Criteria for the Driving Field

5.3.1 Satisfying the Adiabatic Condition

It is necessary to put certain constraints of the drive field in order for the adiabatic elimination to be valid. This can be satisfied by setting $\Delta_n^2/\Omega^2 \ll 1$ [3], giving the following constraint on Ω:

$$\Omega \ll 4\pi\Delta_{\mathrm{A}} = 2\pi\gamma'\sqrt{C}, . \tag{5.63}$$

using $\Delta_{\mathrm{A}} = \gamma'\sqrt{C}/2$. This condition can be satisfied for a driving of the form

$$\Omega \sim a2\pi\gamma'\sqrt{C}, \qquad a \ll 1, \tag{5.64}$$

where the value of a sets the size of the errors induced from non-adiabatic effects. Numerical treatment of the master equation has shown that setting $a = 0.25$ is sufficient to reduce the errors induced by the adiabatic treatment.
In addition to this, the effect of the driving when no qubits needs to be taken into consideration.

In this case, the driving field and the coupling to the waveguide creates a Raman transition between $|\mathrm{g}\rangle_\mathrm{A}$ and $|\mathrm{f}\rangle_\mathrm{A}$ governed by the Hamiltonian:

$$\hat{H} = \Delta_0 |\mathrm{E}\rangle_\mathrm{A} \langle \mathrm{E}| + \Omega \left(|\mathrm{E}\rangle_\mathrm{A} \langle \mathrm{g}| + |\mathrm{g}\rangle_\mathrm{A} \langle \mathrm{E}| \right) + \sum_\mathbf{k} g_\mathbf{k} \left(|\mathrm{E}\rangle_\mathrm{A} \langle \mathrm{f}| a_\mathbf{k} + |\mathrm{f}\rangle_\mathrm{A} \langle \mathrm{E}| a_\mathbf{k}^\dagger \right) \tag{5.65}$$

$$= \Delta_0 |\mathrm{E}\rangle_\mathrm{A} \langle \mathrm{E}| + |\mathrm{E}\rangle_\mathrm{A} \left[\Omega \, {}_\mathrm{A}\langle \mathrm{g}| + \sum_\mathbf{k} g_\mathbf{k} \, {}_\mathrm{A}\langle \mathrm{f}| a_\mathbf{k} \right] + \left[\Omega |\mathrm{g}\rangle_\mathrm{A} + \sum_\mathbf{k} g_\mathbf{k} |\mathrm{f}\rangle_\mathrm{A} \, a_\mathbf{k}^\dagger \right] {}_\mathrm{A}\langle \mathrm{E}|. \tag{5.66}$$

The excited state couple to the bright state $|\psi\rangle_\mathrm{B} = \mathcal{N} \left(\Omega |\mathrm{g}\rangle_\mathrm{A} + g |\mathrm{f}\rangle_\mathrm{A} \right)$ but adiabatic evolution makes it possible for the system to enter the dark state:

$$|\psi\rangle_\mathrm{D} = \mathcal{N} \left(\sum_\mathbf{k} g_\mathbf{k} |\mathrm{g}, 0\rangle_\mathrm{A} - \Omega |\mathrm{f}, 1\rangle_\mathrm{A} \right) \tag{5.67}$$

$$= \cos\theta |\mathrm{g}, 0\rangle_\mathrm{A} - \sin\theta |\mathrm{f}, 1\rangle_\mathrm{A}, \tag{5.68}$$

with the mixing angle

$$\theta = \frac{\Omega}{\sum\limits_\mathbf{k} g_\mathbf{k}} = \frac{a 2\pi\gamma' \sqrt{C}}{\sum\limits_\mathbf{k} g_\mathbf{k}}, \tag{5.69}$$

where the number in the state vectors represent the number of photons in the waveguide. The dark state is an eigenstate of the Hamiltonian in Eq. (5.65) with an eigenvalue of zero. It is possible to project thus emitter into $|\psi\rangle_\mathrm{D}$ during the adiabatic evolution, unless the mixing angle is sufficiently small to eliminate $|\mathrm{f}\rangle_\mathrm{A}$ from $|\psi\rangle_\mathrm{D}$:

$$\theta = \frac{\Omega}{\sum\limits_\mathbf{k} g_\mathbf{k}} \ll 1 \Rightarrow \Omega \ll \sum_\mathbf{k} g_\mathbf{k} \tag{5.70}$$

$$\Rightarrow \frac{a\gamma' \sqrt{C}}{\sum\limits_\mathbf{k} g_\mathbf{k}} \ll 1. \tag{5.71}$$

This condition can be met by suppressing the nonradiative decay processes(preferentially only to the guided mode) and by choosing a low value for a.

5.3.2 Effects of Dephasing

Dephasing constitutes another potential source of errors by letting the coherences decay without affecting the population of the qubit states. This effect can readily be incorporated into the formalism for the CZ gate by phenomenologically including a dephasing rate γ_dp into the equations of motion for the off-diagonal elements of the density matrix:

$$\dot{\rho}_y^x = i \left(\Delta_y - \Delta_x \right) \rho_y^x (t) - \frac{1}{2} \left(\Gamma_x + \Gamma_y \right) \rho_y^x (t) - \gamma_\mathrm{dp} \rho_y^x (t), \qquad n \neq m. \tag{5.72}$$

This can be readily solved:

$$\rho_x^y (t) = \rho_x^y (t = 0) \, e^{i(\Delta_y - \Delta_x)t} e^{-\frac{1}{2}\left(\Gamma_x + \Gamma_y + \gamma_\mathrm{dp}\right)t}, \qquad x \neq y. \tag{5.73}$$

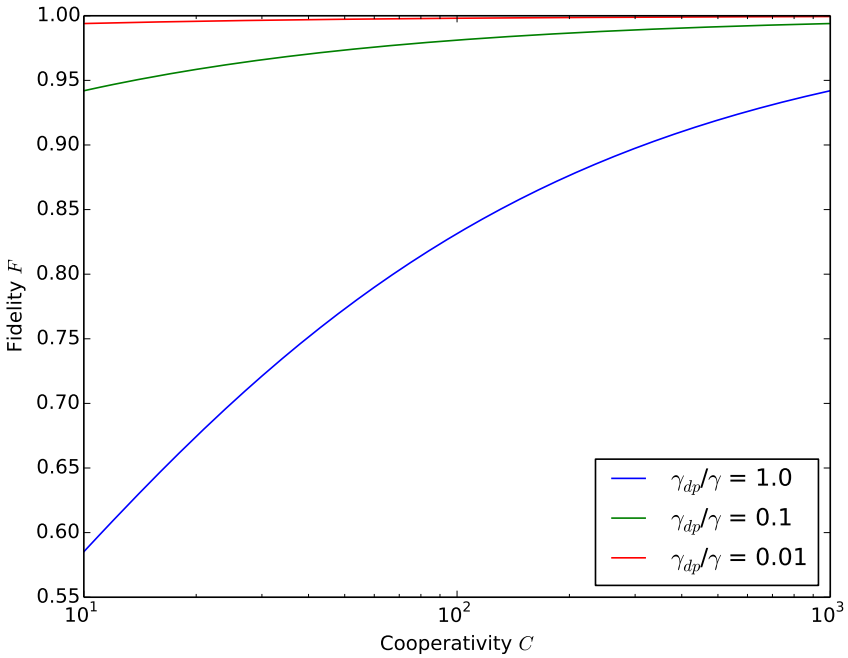

Figure 5.2: The fidelity plotted against the cooepratvity in the presence of pure dephasing processes. The strong dependence on the dephasing rate compared to the nonradiative decay rate is observed.

This does not have an effect on the success probability, but dephasing processes have a substantial the fidelity, in the optimized case:

$$F = \frac{1}{4}\frac{e^{-\Gamma t} + 3e^{-(\Gamma+\gamma_{\mathrm{dp}})t}}{e^{-\Gamma t}} \tag{5.74}$$

$$= \frac{1}{4} + \frac{3}{4}e^{-\gamma_{\mathrm{dp}} t} \tag{5.75}$$

$$\underset{t=t_{\mathrm{g}}}{=} \frac{1}{4} + \frac{3}{4}\exp\left[-\frac{2\pi\gamma'\gamma_{\mathrm{dp}}\sqrt{C}}{\Omega^2}\right]. \tag{5.76}$$

Eq. (5.76) shows that dephasing can lead to a fidelity of $F = 1/4$ as $C \gg 1$. The detrimental effect of dephasing can be neglected if the dephasing time $t_{\mathrm{dp}} = \gamma_{\mathrm{dp}}^{-1}$ is longer than the gate time. This gives the following constraint:

$$t_{\mathrm{g}}\gamma_{\mathrm{dp}} \ll 1 \tag{5.77}$$

$$\Rightarrow \frac{\gamma_{\mathrm{dp}}}{2\pi\gamma'}\frac{1}{a^2\sqrt{C}} \ll 1, \tag{5.78}$$

when using Eq. (5.64) for the drive field Ω in order to reduced non-adiabatic errors. Eq. (5.78) shows that there exists a trade off between the non-adiabatic errors and the errors induced by pure dephasing processes. Reducing the non-adiabatic errors will increase the dephasing errors and vice versa. This behaviour is shown in Fig. (5.2). It may be possible to choose a more intricate drive in order to reduce both of these detrimental effects but this is beyond the scope of this work.

It is thus possible to implement a controlled two qubit phase gate by performing the single-qubit rotations at the end of a driving pulse with a duration of $t_{\mathrm{g}} = \pi / |\Delta_2'|$ on the auxiliary emitter. Choosing a detuning between laser frequency and the transition frequency of $\Delta_{\mathrm{A}} = \gamma' \sqrt{C}$ ensures that the gate operation can be performed with a unity fidelity and a sub-unity probability set by the cooperativity.
Conditioning the gate operation on measuring the auxiliary emitter in $|\mathrm{g}\rangle_{\mathrm{A}}$ will eliminate the effects of dissipative errors due to the high fidelity. Any other error will only have a negative effect on the bit rate, due to having to repeat the gate operation until a desired outcome is obtained by reinitializing the system upon detecting a failed gate operation. This integrated error detection removes the need for using more complicated techniques, such as entanglement purification and quantum error correction, and may be directly implemented in quantum circuits. In addition it is possible to completely eliminate the disruptive effect of dephasing by satisfying the criteria outlined in Section (5.3).
Additional errors will be introduced when the approximations outlined in Section (5.2) are relaxed. These, and the possibilities for mitigating them, are discussed in Chapter (6).

Chapter 6

Non-Ideal CZ Gate

Chapter (5) has introduced the possibility of implementing a controlled phase gate using the superradiative effect of the dipole-dipole interaction between three coupled quantum dots. In addition, a number of errors has been identified and mitigated by conditioning the gate on measuring the auxiliary emitter in state $|\mathrm{g}\rangle_{\mathrm{A}}$ and by standardizing the decay rates. A number of assumptions has been made in order to simplify the treatment:

- The detuning δ_{q} of the two qubits were set to zero
- The three emitters were assumed to have the same coupling constant $g_{\mathbf{k}}$
- Three three emitters were placed with a perfect displacement, such that no subradient effects were present.

The last two assumptions will generally not hold for self-assembled quantum dots due to the random nature of the growth process and will reintroduce errors to the relative weights of the qubit states. The effect of these errors will be discussed in this chapter and the possibility of mitigating them by letting δ_{q} be non-zero will be explored. This is done in Sections (6.1) and (6.2), while Section (6.3) discusses the detrimental effects of dephasing processes and the criteria that has to be fulfilled in order to reduce errors from non-adiabatic effects. In this chapter, the ideal case will refer to the case explored in Chapter (5) while the optimized case will refer to any system where it is possible to remove part of the infidelity by changing the detuning of the emitters.

6.1 Variable Qubit Dipole Moment

Each quantum dot in the chain can have a dipole moment that is different from that of the other two emitters due to variations in the vertical and in-plane composition of the quantum dot. A simple way of treating this is to parametrise the magnitude of the dipole moments of the two qubits in terms of the one from the auxiliary emitter:

$$d_{\mathrm{q}_1} = \kappa d_{\mathrm{A}}, \quad d_{\mathrm{q}_2} = \eta d_{\mathrm{A}}, \tag{6.1}$$

leading to the following non-hermitian Hamiltonian for the case of both qubits interacting with the waveguide:

$$\hat{H}_{\mathrm{NH}}\Big|_{n=2} = \begin{array}{c} \\ |11E\rangle \\ |e1f\rangle \\ |1ef\rangle \end{array} \begin{array}{c} \begin{array}{ccc} \langle 11E| & \langle e1f| & \langle 1ef| \end{array} \\ \begin{pmatrix} \Delta_{\mathrm{A}} - \frac{i}{2}\left(\gamma_A^{1\mathrm{D}} + \gamma'\right) & -\frac{i}{2}\kappa\gamma_A^{1\mathrm{D}} & -\frac{i}{2}\eta\gamma_A^{1\mathrm{D}} \\ -\frac{i}{2}\kappa\gamma_A^{1\mathrm{D}} & \delta_{\mathrm{q}} - \frac{i}{2}\left(\kappa^2\gamma_A^{1\mathrm{D}} + \gamma'\right) & -\frac{i}{2}\kappa\eta\gamma_A^{1\mathrm{D}} \\ -\frac{i}{2}\eta\gamma_A^{1\mathrm{D}} & -\frac{i}{2}\kappa\eta\gamma_A^{1\mathrm{D}} & \delta_{\mathrm{q}} - \frac{i}{2}\left(\eta^2\gamma_A^{1\mathrm{D}} + \gamma'\right) \end{pmatrix} \end{array} \tag{6.2}$$

where $\gamma_A^{1\mathrm{D}}$ is the decay rate in to the guided mode for the auxiliary quantum dot and the detuning of the two qubit emitters has been set to the same value of δ_{q}. It is straightforward to write up the non-Hermitian for the case where $n = 1$ and $n = 0$. Note that the two 2×2 matrices representing the $\hat{H}_{\mathrm{NH}}$ for $n = 1$ will now be different due to the different parametrization constants. This splits Γ_1 into two different decay rates, one for each qubit. The decay rates are in this general case given by summing up the contributions from the various Lindblad coefficients from the dissipative part of the effective master equation:

$$\Gamma_0 \equiv \left|r_0^{\mathrm{A}}\right|^2 \tag{6.3}$$

$$\Gamma_{1,1} \equiv \left|r_{1,1}^{\mathrm{A}}\right|^2 + \left|r_{1,1}^{\mathrm{q}}\right|^2 + r_{1,1}^{\mathrm{A}}\left(r_{1,1}^{\mathrm{q}}\right)^* + r_{1,1}^{\mathrm{q}}\left(r_{1,1}^{\mathrm{A}}\right)^* \tag{6.4}$$

$$\Gamma_{1,2} \equiv \left|r_{1,2}^{\mathrm{A}}\right|^2 + \left|r_{1,2}^{\mathrm{q}}\right|^2 + r_{1,2}^{\mathrm{A}}\left(r_{1,2}^{\mathrm{q}}\right)^* + r_{1,2}^{\mathrm{q}}\left(r_{1,2}^{\mathrm{A}}\right)^* \tag{6.5}$$

$$\left.\begin{aligned}\Gamma_2 \equiv\ & \left|r_2^{\mathrm{A}}\right|^2 + \left|r_{2,1}^{\mathrm{q}}\right|^2 + \left|r_{2,1}^{\mathrm{q}}\right|^2 + r_{2,1}^{\mathrm{q}}\left(r_{2,2}^{\mathrm{q}}\right)^* + r_{2,2}^{\mathrm{q}}\left(r_{2,1}^{\mathrm{q}}\right)^* \\ & + r_2^{\mathrm{A}}\left(r_{2,1}^{\mathrm{q}}\right)^* + r_2^{\mathrm{A}}\left(r_{2,1}^{\mathrm{q}}\right)^* + r_{2,1}^{\mathrm{q}}\left(r_2^{\mathrm{A}}\right)^* + r_{2,2}^{\mathrm{q}}\left(r_2^{\mathrm{A}}\right)^*\end{aligned}\right\} \tag{6.6}$$

where the letter in the subscript denotes whether the Lindblad coefficient comes from the Auxiliary or Qubit emitter, the first number denotes the number of qubits in $|1\rangle_{\mathrm{q}}$ and, in the case of only one connected qubit, the second number determines which particular qubit is contributing. The jump terms from the effective Hamiltonian does not contribute in this case due to the initialisation of the three quantum dots in the electronic ground states. The effective Hamiltonian, Lindblad operators and decay rates now takes the form:

$$\hat{H}_{\mathrm{eff}} = \left[\Delta_0\hat{P}_0 - \sum_{n=1}^{2}\frac{\Omega^2}{\gamma'}\frac{4\tilde{\Delta}_{\mathrm{A}}\tilde{\delta}_{\mathrm{q}}^2 + f_{H,n}(\kappa,\eta)C^2\tilde{\delta}_{\mathrm{q}} + g_{H,n}(\kappa,\eta)C^2\tilde{\Delta}_{\mathrm{A}}}{4\tilde{\delta}_{\mathrm{q}}^2C^2 + h_n(\kappa,\eta)\tilde{\Delta}_{\mathrm{A}}\tilde{\delta}_{\mathrm{q}}C^2 + j_n(\kappa,\eta)\tilde{\Delta}_{\mathrm{A}}^2C^2 + k_n(\kappa,\eta)C^2}\hat{P}_{\mathrm{n}}\right] \otimes |\mathrm{g}\rangle_{\mathrm{A}}\langle\mathrm{g}| \tag{6.7}$$

$$= \sum_{n=0}^{2}\Delta_n|\mathrm{g}\rangle_{\mathrm{A}}\langle\mathrm{g}| \otimes \hat{P}_{\mathrm{n}} \tag{6.8}$$

$$\hat{L}_{\mathrm{eff}}^{A} = \sum_{n=0}^{2} r_{\mathrm{n}}^{\mathrm{A}}(C,\kappa,\eta)|\mathrm{f}\rangle_{\mathrm{A}}\langle\mathrm{E}| \otimes \hat{P}_{\mathrm{n}} \tag{6.9}$$

$$\hat{L}_{\mathrm{eff}}^{q_j} = \sum_{n=1}^{2} r_{\mathrm{n}}^{\mathrm{q_j}}(C,\kappa,\eta)|\mathrm{f}\rangle_{\mathrm{A}}\langle\mathrm{E}| \otimes \hat{P}_{\mathrm{n}} \tag{6.10}$$

$$\Gamma_{n>0} = \frac{\Omega^2}{\gamma'}\frac{4\tilde{\delta}_{\mathrm{q}}^2C + f_{\Gamma,n}(\kappa,\eta)C^3 + g_{\Gamma,n}(\kappa,\eta)C^2}{4\tilde{\delta}_{\mathrm{q}}^2C^2 + h_n(\kappa,\eta)\tilde{\Delta}_{\mathrm{A}}\tilde{\delta}_{\mathrm{q}}C^2 + j_n(\kappa,\eta)\tilde{\Delta}_{\mathrm{A}}^2C^2 + k_n(\kappa,\eta)C^2} \tag{6.11}$$

$$\Gamma_0 = \frac{\Omega^2}{\gamma'}\frac{1}{C}, \tag{6.12}$$

where $\Delta_0 = -\Omega^2/\left(\gamma' C^{-3/2}\right)$. The dimensionless detunings $\tilde{\Delta}_{\mathrm{A}} = \Delta_{\mathrm{A}}/\gamma'$ and $\tilde{\delta}_{\mathrm{q}} = \delta_{\mathrm{q}}/\gamma'$ has been introduced to ease the notation. The end of Section (5.2.3) described errors in the fidelity due to the omission of the $\mathcal{O}(C)^{-3/2}$ terms. It is necessary to include these terms in the expressions above in order to include the effects of δ_{q} when optimising the decay rates.

Note that there is a separate term for each of the two qubits for $n = 1$ in the sum. The various functions in Eqs. (6.7) and (6.11) are defined in Appendix (B.2) and depend only on the parametrization parameters κ and η. It has been assumed that the two qubits are tuned in the

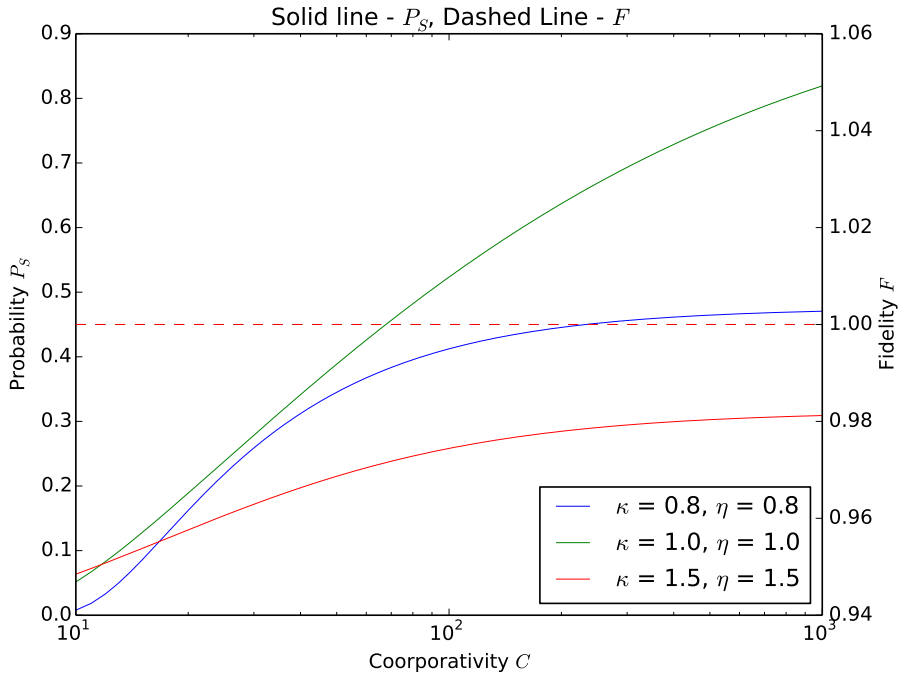

Figure 6.1: The success probability (solid lines) and fidelity (dashed lines) plotted against the cooperativity C for various values of $\kappa = \eta$. This has been plotted for the case of complete optimisation from Eqs. (6.26) and (6.27), leading to a fidelity of $F = 1$ for all three cases. Note the strong fall off in the success probability when $\kappa \neq 1$.

same manner, $\delta_{q_1} = \delta_{q_2}$. The effective Hamiltonian and Lindblad operators above show that the different values of κ and η only change the values of the energy shift and decay rates, while leaving the essential dynamics of the system unchanged. The gate operation can thus be implemented using the same procedure as described in Chapter (5) by letting the auxiliary emitter be illuminated by a weak laser drive for a duration of $t_g = \pi/|\Delta'_A|$. Here $\Delta'_A = \Delta_2 - \Delta_{1,1} - \Delta_{1,2} + \Delta_0$ is the dynamical change in phase of the state $|11\rangle_1$ after the sequence of single-qubit rotations detailed in chapter (5) has been applied at the end of the gate operation.
The variation in the coupling constants change the decay rates, which reintroduces the infidelity from the different weights of the qubit state, as can be seen in the general expression for the fidelity in Eq. (6.15). Fig. (6.2) shows that this leads to a rapid drop off in the fidelity and the success probability for $\kappa, \eta \neq 1$. This is plotted for both the unoptimised case where $\Delta_A = \gamma'\sqrt{C}$ and for the simple optimisation scheme where $\Delta_A = \gamma'\sqrt{C}/2$ and $\delta_q = 0$, highlighting that the detunings derived in Chapter (5) are insufficient to reduce the errors in the non-ideal cases.

Success Probability & Fidelity

The success probability and fidelity are defined as in Chapter (5):

$$P_S = \mathrm{Tr}\left\{\rho_q\left(t_g\right)\right\} = \sum_{n=0}^{2} \mathrm{Tr}\left\{\rho_n\left(t_g\right)\hat{P}_n\right\} = \sum_{n=0}^{2} \mathrm{Tr}\left\{e^{-\Gamma_n t_g}\rho_n\left(t=0\right)\hat{P}_n\right\}, \tag{6.13}$$

$$F = \frac{1}{P_S}\,{}_A\langle g|\,\langle\Psi|\,\tilde{\rho}\left(t_g\right)|\Psi\rangle\,|g\rangle_A\,, \tag{6.14}$$

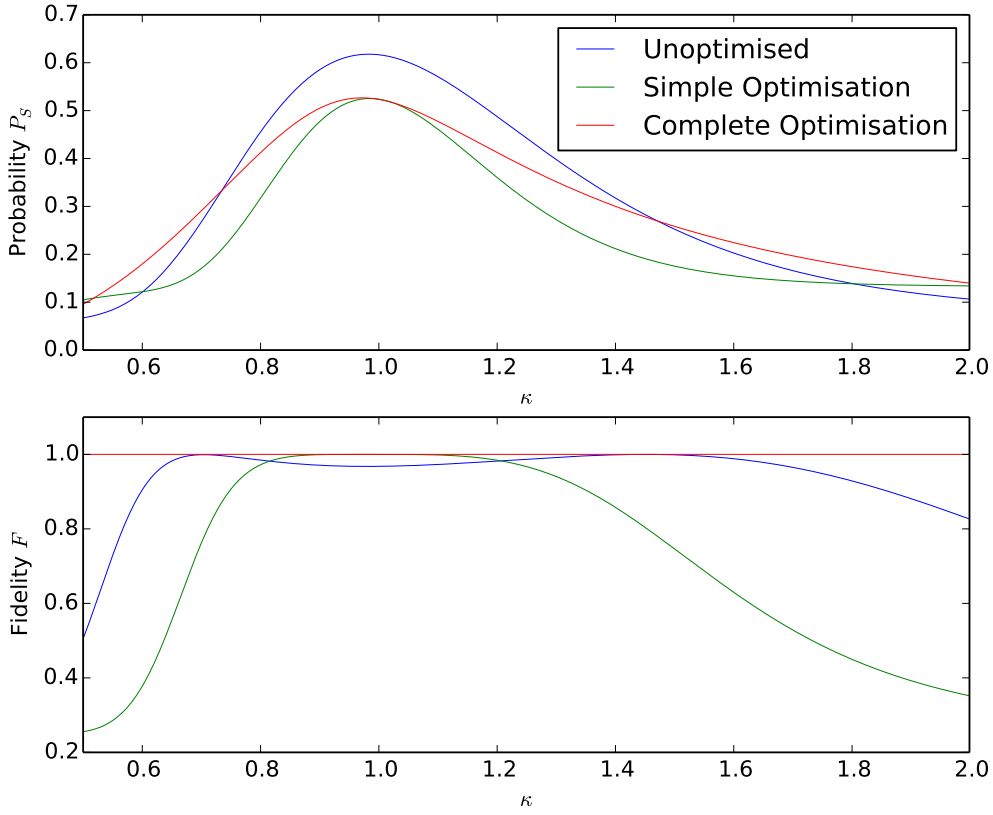

Figure 6.2: The success probability and fidelity plotted against the parametrization constant κ in three distinct cases. The first is the unoptimised case where $\Delta_{\mathrm{A}} = \gamma'\sqrt{C}$ and $\delta_{\mathrm{q}} = 0$. The second is the simple case where $\Delta_{\mathrm{A}} = \gamma'\sqrt{C - 1/2}/2$ and $\delta_{\mathrm{q}} = -7\gamma'/8\sqrt{C}$ leading to the fidelity being optimized only for the ideal case where $\kappa = 1$. The last is the completely optimised case where Δ_{A} and δ_{q} are given by Eqs. (6.26) and (6.27), respectively. This optimises the fidelity for any value of κ and leads to a slightly higher success probability. All cases are plotted for a cooperativity of $C = 100$. Note the high success probability and the peaks in the fidelity for the unoptimised case.

where $|\Psi\rangle = |00\rangle_{\mathrm{q}} + |01\rangle_{\mathrm{q}} + |10\rangle_{\mathrm{q}} - |11\rangle_{\mathrm{q}}$ is the ideal output of a CZ gate, up to a normalization and $\rho_{\mathrm{n}}(t=0) = 1/4$ is the initial value of the diagonal elements in the density matrix. The success probability then becomes a sum over four exponential functions, one for each Γ_n, whereas the fidelity at an arbitrary time t is given by:

$$F(t) = \frac{F_0(t) + F_{1,1}(t) + F_{1,2}(t) + F_2(t)}{\frac{1}{4}\left(\exp\left[-\Gamma_0 t\right] + \exp\left[-\Gamma_{1,1} t\right] + \exp\left[-\Gamma_{1,2} t\right] + \exp\left[-\Gamma_2 t\right]\right)}. \tag{6.15}$$

The functions $F_n(t)$ are shorthand functions that collect the contribution to the fidelity from the n'th column from the density matrix:

$$\begin{aligned}
F_0(t) &= {}_{\mathrm{q}}\langle 00|\rho(t)|00\rangle_{\mathrm{q}} + {}_{\mathrm{q}}\langle 00|\rho(t)|01\rangle_{\mathrm{q}} + {}_{\mathrm{q}}\langle 00|\rho(t)|10\rangle_{\mathrm{q}} - {}_{\mathrm{q}}\langle 00|\rho(t)|11\rangle_{\mathrm{q}} && (6.16)\\
&= \frac{1}{16}\left(e^{-\Gamma_0 t} + e^{-\frac{1}{2}(\Gamma_0+\Gamma_{1,1})t} + e^{-\frac{1}{2}(\Gamma_0+\Gamma_{1,2})t} - e^{-i\Delta_2' t}e^{-\frac{1}{2}(\Gamma_0+\Gamma_2)t}\right) && (6.17)\\
F_{1,1}(t) &= {}_{\mathrm{q}}\langle 01|\rho(t)|00\rangle_{\mathrm{q}} + {}_{\mathrm{q}}\langle 01|\rho(t)|01\rangle_{\mathrm{q}} + {}_{\mathrm{q}}\langle 01|\rho(t)|10\rangle_{\mathrm{q}} - {}_{\mathrm{q}}\langle 01|\rho(t)|11\rangle_{\mathrm{q}} && (6.18)\\
&= \frac{1}{16}\left(e^{-\frac{1}{2}(\Gamma_{1,1}+\Gamma_0)t} + e^{-\Gamma_{1,1} t} + e^{-\frac{1}{2}(\Gamma_{1,1}+\Gamma_{1,2})t} - e^{-i\Delta_2' t}e^{-\frac{1}{2}(\Gamma_{1,1}+\Gamma_2)t}\right) && (6.19)\\
F_{1,2}(t) &= {}_{\mathrm{q}}\langle 10|\rho(t)|00\rangle_{\mathrm{q}} + {}_{\mathrm{q}}\langle 10|\rho(t)|01\rangle_{\mathrm{q}} + {}_{\mathrm{q}}\langle 10|\rho(t)|10\rangle_{\mathrm{q}} - {}_{\mathrm{q}}\langle 10|\rho(t)|11\rangle_{\mathrm{q}} && (6.20)\\
&= \frac{1}{16}\left(e^{-\frac{1}{2}(\Gamma_{1,2}+\Gamma_0)t} + e^{-\frac{1}{2}(\Gamma_{1,2}+\Gamma_{1,1})t} + e^{-\Gamma_{1,2} t} - e^{-i\Delta_2' t}e^{-\frac{1}{2}(\Gamma_{1,2}+\Gamma_2)t}\right) && (6.21)\\
F_2(t) &= -{}_{\mathrm{q}}\langle 11|\rho(t)|00\rangle_{\mathrm{q}} - {}_{\mathrm{q}}\langle 11|\rho(t)|01\rangle_{\mathrm{q}} - {}_{\mathrm{q}}\langle 11|\rho(t)|10\rangle_{\mathrm{q}} + {}_{\mathrm{q}}\langle 11|\rho(t)|11\rangle_{\mathrm{q}} && (6.22)\\
&= \frac{1}{16}\left(-e^{i\Delta_2' t}e^{-\frac{1}{2}(\Gamma_2+\Gamma_0)t} - e^{i\Delta_2' t}e^{-\frac{1}{2}(\Gamma_2+\Gamma_{1,1})t} - e^{i\Delta_2' t}e^{-\frac{1}{2}(\Gamma_2+\Gamma_{1,2})t} + e^{-\Gamma_2 t}\right), && (6.23)
\end{aligned}$$

after having projected $|\mathrm{g}\rangle_{\mathrm{A}}$ onto the density matrix. It is, as in the ideal case, possible to minimize this effect by choosing specific values for Δ_{A} and δ_{q}. Consider the simplified case of $\kappa = \eta$ where the coupling constants of the two qubits are equal. The decay rates for $n > 0$ are then:

$$\begin{aligned}
\Gamma_{n>0} &= \frac{\Omega^2}{\gamma'}\frac{4\delta_{\mathrm{q}}^2 C + n^2\left(-\kappa^{7/2} + \kappa^4 + \kappa^3\right)C^3 + \left(n^2\kappa^4 + 2n\left[-\kappa^{3/2} + \kappa^2\right]\right)C^2}{4C^2\left[\delta_{\mathrm{q}} + \kappa^2\Delta_{\mathrm{A}}\right]^2 + \left[n\kappa^2 + 1\right]^2 C^2} && (6.24)\\
\Gamma_0 &= \frac{\Omega^2}{\gamma'}\frac{1}{C}. && (6.25)
\end{aligned}$$

Note that, in this approximation, the decay rate for a single qubit in $|1\rangle_1$ is the same regardless which qubit is connected to the waveguide. It is possible to set Γ_2 and Γ_1 equal to Γ_0 by choosing

$$\begin{aligned}
\Delta_{\mathrm{A}} &= \frac{\gamma'}{2\kappa^2}\sqrt{\left(-2\kappa^{7/2} + \kappa^4 + \kappa^3\right)C^2 + \kappa^4(C-1) + 1/2} && (6.26)\\
\delta_{\mathrm{q}} &= \gamma'^2\frac{4\left(\kappa^{5/2} - \kappa^4\right)C - 4\kappa^{5/2} - 3\sqrt{\kappa}}{16\kappa^{5/2}\Delta_{\mathrm{A}}}. && (6.27)
\end{aligned}$$

This eliminates the errors in the fidelity that stems from the different weights of the four qubit states due to the uneven decays. The effects on the fidelity and the success probability for the controlled phase gate are shown in Fig. (6.1) for different values of $\kappa = \eta$. A unity fidelity is observed for all three cases but the success probability experiences a significant drop off as the dipole moments of the two qubits are varied. This heralds the emergence of the subradiant effects discussed in Section (4.2.4), leading to a weaker interaction between the auxiliary emitter and the two qubits. The subradiant effects are enhanced even further when the position of the two qubits is varied in Section (6.2).

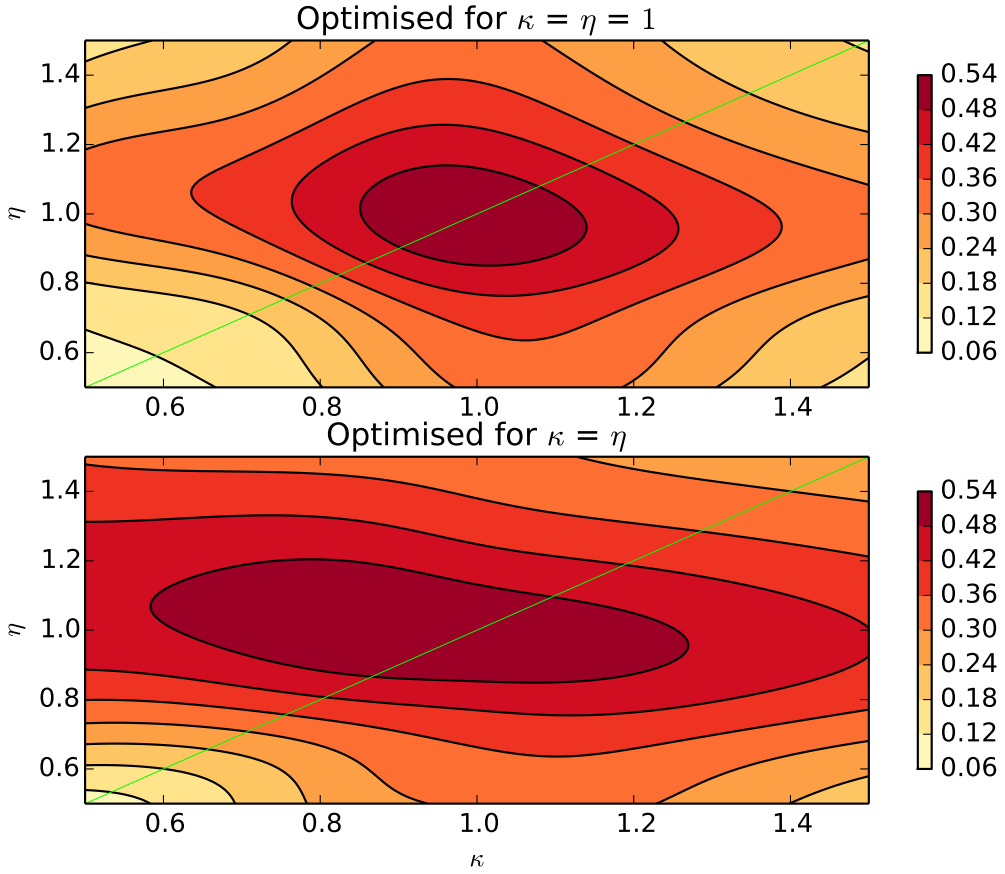

Figure 6.3: Contours of the success probability against the parametrization parameters of the dipole moments of the qubit emitters. This is done for the simply and completely optimised case, respectively. Fig. (6.2) is a cross section along the green diagonal line where $\kappa = \eta$. Note the enhancement of the success probability for the fully optimised case (lower panel) along the line where $\eta = 1$.

Setting $\kappa = 1$ in Eqs. (6.26) and (6.27) results in the following expressions

$$\left.\begin{aligned} \Delta_{\mathrm{A}} &= \frac{\gamma'}{2}\sqrt{C - 1/2} \\ \delta_{\mathrm{q}} &= -\frac{7\gamma'}{8\sqrt{C}} \end{aligned}\right\} \tag{6.28}$$

which optimises the fidelity for the simple case discussed in Chapter (5) when the terms of order $\mathcal{O}\left(C^{-3/2}\right)$ are included in the expressions for Δ_n and Γ_n. This makes it possible to remove the errors due to the uneven change in phase resulting from these higher order corrections and from the different weights of the qubit states simultaneously. Even higher corrections still exist; terms of order $\mathcal{O}\left(C^{-5/2}\right)$ lead to errors in the fidelity of order $\mathcal{O}\left(C^{-3}\right)$. More advanced methods a required to remove these errors, but the effects of these errors can be neglected for any realistic values of the cooperativity in W1 waveguides.
The detunings given by Eqs. (6.26) and (6.27) ensures that the fidelity will always be $F = 1$

when both qubits have the same dipole moment. They are not sufficient to keep this unity fidelity in the general case where $\kappa \neq \eta$. It has not been possible to find a method to optimise this case but there are several possible avenues for tackling this problem. These are discussed in Chapter (7). Using the detunings in Eqs. (6.26) and (6.27) does result in a near unit fidelity and high success probabilities for a wide range of values for κ and η. Fig. (6.3) and Fig. (6.4) show contours of the success probability and fidelity, respectively, as a function of κ and η for the fully and simply optimised cases. Both sets of detunings have a wide range of values for the parametrization constants allowing for a near unity fidelity (albeit the range is larger for the fully optimised case). The simply optimised case has a limit range of possible parametrization values that result in a maximised success probability, in contrast to the higher range for the fully optimised case.
There are three distinct choices of detunings with various effects on the fidelity and success probability, as is shown by Fig. (6.2). These choices are:

1. Surprisingly, using the completely unoptimised detunings $\Delta_{\mathrm{A}} = \gamma'\sqrt{C}$ and $\delta_{\mathrm{q}} = 0$ for specific values of κ ($\kappa \sim 0.7$ and $\kappa \sim 1.45$) will lead to $F \sim 1$ and a success probability comparable to that obtained from the completely optimised case. Values between these two has the highest success probability but with a high but sub-unity values for the fidelity.

2. The fully optimised case of Eqs. (6.26) and (6.27) that keeps a constant $F = 1$ for any value of $\kappa = \eta$. The success probability rapidly falls off as the strength of the qubit dipole moment is changed but this can be remedied by increasing the cooperativity C (see Fig. (6.1)). This choice is also useful for the situation where $\kappa \neq \eta$ with a high fidelity for a wide range of values for the two parametrization constants. This is shown in Fig. (6.3). It also has a larger freedom in the possible values κ and η that lead to a maximised success probability, compared to the simply optimised case.

3. The detunings in Eq. (6.28) lead to $F = 1$ for $\kappa = \eta = 1$ with a rapid drop off in the fidelity and a success probability that is strictly lower than for the completely optimised case. This set of detunings result in a narrower range of values for κ and η in order to obtain a high success probability, as is seen from Fig. (6.3).

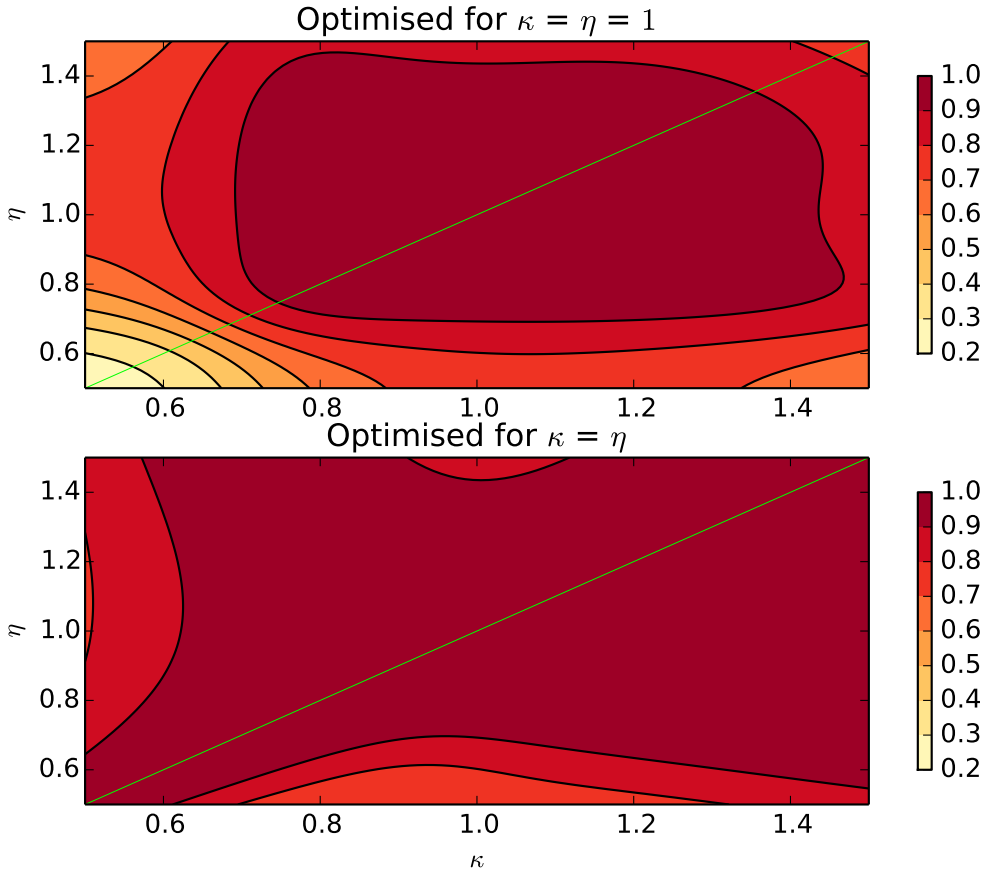

Figure 6.4: Contours of the fidelity against the parametrization parameters of the dipole moments of the qubit emitters. This is done for the simply and completely optimised case, respectively. Fig. (6.2) is a cross section along the green diagonal line where $\kappa = \eta$. Note the wide range of values for κ and η with a unity or near-unit fidelity in the optimised case (lower panel).

6.2 Variable Qubit Dipole Moment & Position

Quantum dots grown using the Stranski-Kastranov will in general be distributed randomly along the photonic crystal, leading to an imperfect spatial separation between the three emitters. This results in the introduction of destructive interference between the radiation fields for the three emitters, thereby lowering the interaction between them. It can, in principle, be possible to map the distribution of the quantum dots (e.g. using atomic-force micrography) in order to find three quantum dots with a mutual separation that satisfies the condition for constructive interference. Alternatively, it may be possible to build a bending waveguide between three randomly chosen quantum dots, thereby tailoring the spatial separation. Both of these methods may be infeasible to carry out in practise; the first relies on producing a lucky sample while the bending waveguide may be impractical to etch in practise. Is is therefore important to examine the effects of an imperfect position of the qubit quantum dots.

This section will discuss the negative effects of having three emitters embedded along a straight line in a W1 waveguide with an imperfect separation. The difference between the position $x_{\mathrm{k}} - x_{\mathrm{l}}$ of any two emitters has to fulfil:

$$k\left(x_{\mathrm{k}} - x_{\mathrm{l}}\right) = 2\pi m, \quad m \in \mathbb{N}, \tag{6.29}$$

in order to obtain full constructive interference between the radiation fields. Here k is the magnitude of the wave vector of the propagating photon. As a reminder, the total decay rate due to the dipole-dipole interaction is given by summing the contribution from the coherent (J^{nm} from Eq. (4.79)) and dissipative (γ^{nm} from Eq. (4.80)) interactions:

$$\Gamma^{\mathrm{kl}} = J^{\mathrm{kl}} + i\gamma^{\mathrm{kl}} = \gamma_0^{\mathrm{kl}} e^{-ik(x_{\mathrm{k}} - x_{\mathrm{l}})}, \quad \gamma_0^{\mathrm{kl}} = \frac{a d^{(\mathrm{k})} d^{(\mathrm{l})}}{\hbar \varepsilon_0 v_g} \omega_0, \tag{6.30}$$

where the complex exponential function describes the change in phase of the k'th quantum dots upon absorbing a photon emitted by the l'th quantum dot. If the requirement in Eq. (6.29) is fulfilled, then the dissipative dipole-dipole has the only contribution to the dynamics of the ground state. Varying the positions such the the requirement is broken will enhance the contribution from the coherent dipole-dipole interaction, which will lower the success probability, as will be shown below.
The origin will be placed at the position of the auxiliary quantum dot, while the positions of each emitter will be written as:

$$x_{\mathrm{q_k}} = x_{0,\mathrm{q_k}} + \delta x_{\mathrm{q_k}}, \tag{6.31}$$

where $x_{0,\mathrm{q_k}}$ is the ideal position of the k'th quantum dot and $\delta x_{\mathrm{q_k}}$ is the displaced distance to the actual position. This makes it possible to write the exponential functions in Eq. (6.30) in terms of only the displacements $\delta x_{\mathrm{q_k}}$. There are two cases pertaining to the position of he auxiliary emitter, depending on whether it is placed at the end of the chain or in the middle between the qubit emitters; both of these cases has been considered in the treatment below. In addition, the dipole moment of the two qubits are assumed to be different from that of the auxiliary emitter in the same manner as in Section (6):

$$d_{\mathrm{q_1}} = \kappa d_{\mathrm{A}}, \quad d_{\mathrm{q_2}} = \eta d_{\mathrm{A}}. \tag{6.32}$$

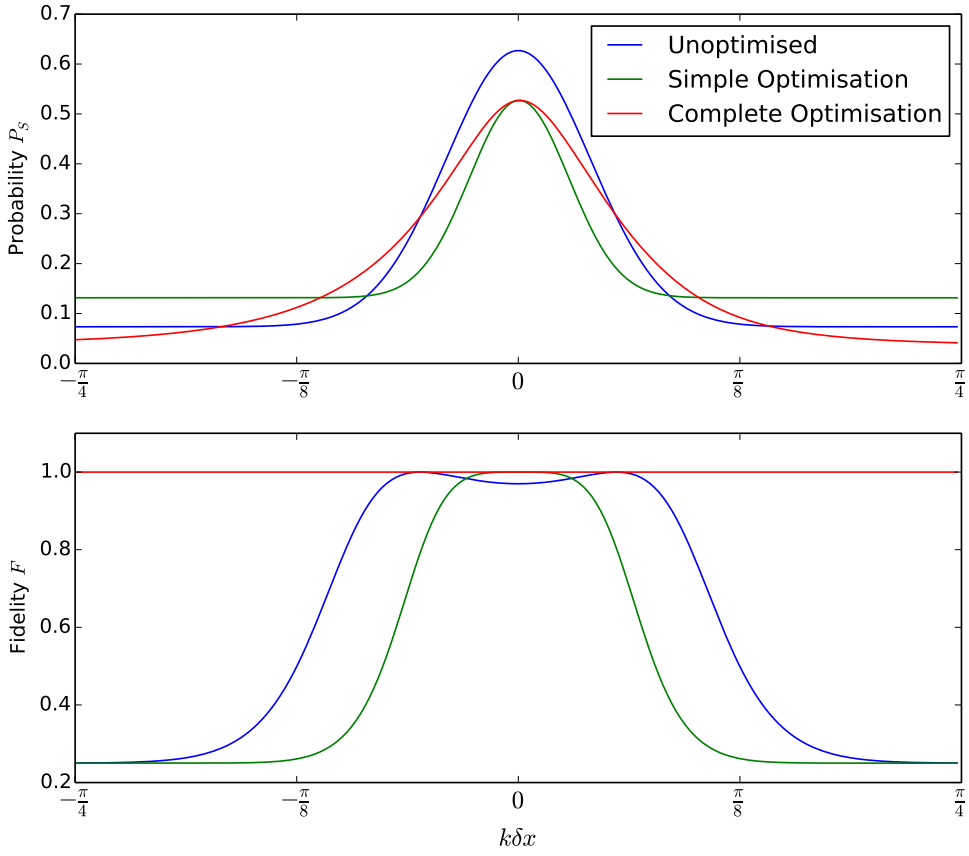

Figure 6.5: The success probability and fidelity plotted against the simultaneous displacement δx_{q} of both qubit quantum dots. This has been done with the detunings from the unoptimised and the simply optimised case previously discussed and for the completely optimised case from Eqs. (6.41) and (6.42). Note the unity fidelity for the completely optimised case and the low success probabilities for $k\delta x \gtrsim \pi/8$.

This leads to the following non hermitian Hamiltonian for $n = 2$:

$$\hat{H}_{\mathrm{NH}}\Big|_{n=2} = \begin{array}{c} \\ |11E\rangle \\ |e1f\rangle \\ |1ef\rangle \end{array} \begin{array}{c} \begin{array}{ccc} \langle 11E| & \langle e1f| & \langle 1ef| \end{array} \\ \begin{pmatrix} \Delta_{\mathrm{A}} - \frac{i}{2}\left(\gamma_A^{1\mathrm{D}} + \gamma'\right) & -\frac{i}{2}\kappa\gamma_A^{1\mathrm{D}} e^{ik\delta_{\mathrm{q},1}} & -\frac{i}{2}\eta\gamma_A^{1\mathrm{D}} e^{ik\delta_{\mathrm{q},2}} \\ -\frac{i}{2}\kappa\gamma_A^{1\mathrm{D}} e^{-ik\delta_{\mathrm{q},1}} & \delta_{\mathrm{q}} - \frac{i}{2}\left(\kappa^2\gamma_A^{1\mathrm{D}} + \gamma'\right) & -\frac{i}{2}\kappa\eta\gamma_A^{1\mathrm{D}} e^{ik(\delta x_{\mathrm{q},2} - \delta x_{\mathrm{q},1})} \\ -\frac{i}{2}\eta\gamma_A^{1\mathrm{D}} e^{-ik\delta_{\mathrm{q},2}} & -\frac{i}{2}\kappa\eta\gamma_A^{1\mathrm{D}} e^{ik(\delta x_{\mathrm{q},1} - \delta x_{\mathrm{q},2})} & \delta_{\mathrm{q}} - \frac{i}{2}\left(\eta^2\gamma_A^{1\mathrm{D}} + \gamma'\right) \end{pmatrix} \end{array} \tag{6.33}$$

where both qubits have the same detuning δ_{q}. This results in the familiar effective Hamiltonian:

$$\hat{H}_{\mathrm{eff}} = \sum_{n=0}^{2} \Delta_n \left|\mathrm{g}\right\rangle_{\mathrm{A}} \left\langle \mathrm{g}\right| \otimes \hat{P}_{\mathrm{n}}, \tag{6.34}$$

with the coefficients

$$\Delta_{n>0} = -\frac{\Omega^2}{\gamma'} \frac{4\tilde{\Delta}_{\mathrm{A}}\tilde{\delta}_{\mathrm{q}}^2 + \left[b_{H,n}\left(\delta x_{\mathrm{q},1}, \delta x_{\mathrm{q},2}, \kappa, \eta\right) C^3 + f_{H,n}\left(\kappa, \eta\right) C^2\right] \tilde{\delta}_{\mathrm{q}} + g_{H,n}\left(\kappa, \eta\right) C^2 \tilde{\Delta}_{\mathrm{A}}}{4\tilde{\delta}_{\mathrm{q}}^2 C^2 + h_n\left(\kappa, \eta\right) \tilde{\Delta}_{\mathrm{A}} \tilde{\delta}_{\mathrm{q}} C^2 + j_n\left(\kappa, \eta\right) \tilde{\Delta}_{\mathrm{A}}^2 C^2 + k_n\left(\kappa, \eta\right) C^2} \tag{6.35}$$

$$\Delta_0 = -\frac{\Omega^2}{\gamma'} \frac{\tilde{\Delta}_{\mathrm{A}}}{C^2}. \tag{6.36}$$

Note that $b_{H,n}\left(C, \delta x_{\mathrm{q},1} = 0, \delta x_{\mathrm{q},2} = 0, \kappa, \eta\right) = 0$, which recovers the Hamiltonian from Eq. (6.34), while the remaining functions in Eq. (6.35) are the same as in Section (6.1) and can be found in Appendix (B.2). The dynamics resulting from the effective Lindblad operators remain unchanged but the Lindblad coefficients are modified due to the imperfect qubit positions:

$$\hat{L}_{\mathrm{eff}}^{A} = \sum_{n=0}^{2} r_{\mathrm{n}}^{\mathrm{A}}\left(C, \delta x_{\mathrm{q},1}, \delta x_{\mathrm{q},2}, \kappa, \eta\right) \left|\mathrm{f}\right\rangle_{\mathrm{A}} \left\langle \mathrm{E}\right| \otimes \hat{P}_{\mathrm{n}} \tag{6.37}$$

$$\hat{L}_{\mathrm{eff}}^{q_j} = \sum_{n=1}^{2} r_{\mathrm{n}}^{\mathrm{qj}}\left(C, \delta x_{\mathrm{q},1}, \delta x_{\mathrm{q},2}, \kappa, \eta\right) \left|\mathrm{f}\right\rangle_{\mathrm{A}} \left\langle \mathrm{E}\right| \otimes \hat{P}_{\mathrm{n}}. \tag{6.38}$$

Placing the auxiliary emitter in the central position in the chain results in the same expressions as those listed above; the dynamics of the three emitters are thus unchanged when permuting the position of the auxiliary emitter. The position of the auxiliary emitter can become important by implementing the following modifications to the theory: this treatment assume that the dipole moments couple with the same strength to the forwards- and backwards propagating photon mode. The auxiliary quantum dot will only interact with one mode if it is placed at the end of the chain, while it interacts with both modes when placed in the middle. This can give rise to different dynamics, if its dipole moment couple differently to the two modes. The same holds for the qubits, which may exhibit more complicated dynamics depending on whether they are placed next to each other or are separated by the auxiliary emitter. Secondly, this treatment does not take loss of the propagating photon into account. Such a loss (which can, for instance, be caused if total internal reflection is not complete) may affect the dynamics differently, depending the distance that the photon has to propagate, in order to mediate the interaction between the two qubits. These two effects provide a natural extension for a further treatment of the proposal.

The imperfect qubit position will, just like the modified qubit dipole moments, only change the magnitude of the Hamiltonian- and Lindblad coefficients, but will leave the essential dynamics of the interaction unchanged. The implementation of the CZ-gate then follows the same form as in the previous sections. The modified decay rates are:

$$\Gamma_{n>0} = \frac{\Omega^2}{\gamma'} \frac{4\tilde{\delta}_{\mathrm{q}}^2 C + f_{\Gamma,n}\left(\delta x_{\mathrm{q},1}, \delta x_{\mathrm{q},2}, \kappa, \eta\right) C^3 + g_{\Gamma,n}\left(\delta x_{\mathrm{q},1}, \delta x_{\mathrm{q},2}, \kappa, \eta\right) C^2}{4\tilde{\delta}_{\mathrm{q}}^2 C^2 + h_n\left(\kappa, \eta\right) \tilde{\Delta}_{\mathrm{A}} \tilde{\delta}_{\mathrm{q}} C^2 + j_n\left(\kappa, \eta\right) \tilde{\Delta}_{\mathrm{A}}^2 C^2 + k_n\left(\kappa, \eta\right) C^2} \tag{6.39}$$

$$\Gamma_0 = \frac{\Omega^2}{\gamma'} \frac{1}{C}, \tag{6.40}$$

where the functions $f_{\Gamma,n}\left(\delta x_{\mathrm{q},1}, \delta x_{\mathrm{q},2}, \kappa, \eta\right)$ and $f_{\Gamma,n}\left(\delta x_{\mathrm{q},1}, \delta x_{\mathrm{q},2}, \kappa, \eta\right)$ are listed in Appendix (B.2).

The success probability and fidelity is calculated from Eq. (6.13) and (6.15), respectively, and are greatly inhibited by varying the position of the two qubit emitters, as can be seen in Fig. (6.5) for the different optimisation schemes employed. The success probability rapidly drops off for all three optimisations and reaches a minimum value at $k\delta x_{\mathrm{q,n}} \approx \pi/8$.

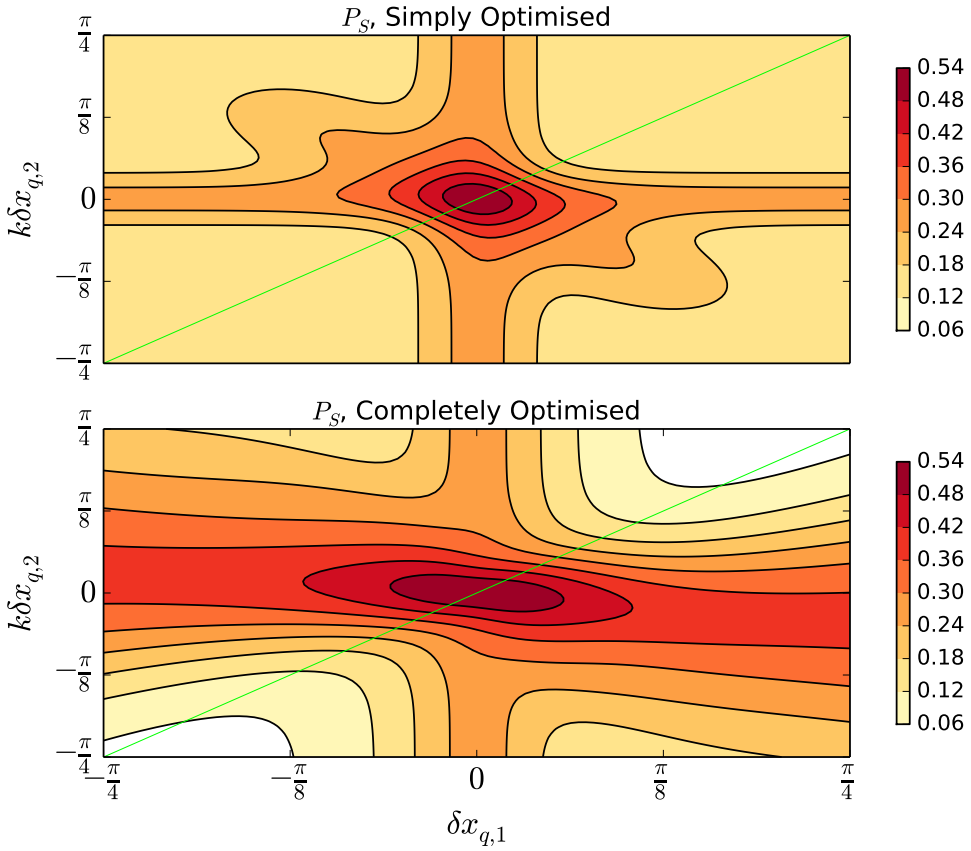

Figure 6.6: Contour plot of the success probability against the displacement of the two qubit emitters. The top panel show the simply optimised case with $\Delta_{\mathrm{A}} = \gamma'\sqrt{C-1/2}/2$ and $\delta_{\mathrm{q}} = -7\gamma'/8\sqrt{C}$, whereas the bottom panel show the situation for the completely optimised case from Eqs. (6.41) and (6.42). The green line show the diagonal where $\delta x_{\mathrm{q,1}} = \delta x_{\mathrm{q,2}}$, along which the optimisation has been carried out. The success probability remains high for displacements $k\delta x \lesssim \pi/8$.

It is possible to maximise the fidelity by setting:

$$\Delta_{\mathrm{A,n}} = \frac{\gamma'}{2\kappa^2}\sqrt{\left(-2\kappa^{7/2}\cos\left(k\delta x_{\mathrm{q,n}}\right)+\kappa^4+\kappa^3\right)C^2+\kappa^4\left(C-1\right)+1/2} \tag{6.41}$$

$$\delta_{\mathrm{q}} = \frac{\frac{\gamma'}{8}\left(4\left(\kappa^{3/2}\cos\left(k\delta x_{\mathrm{q,n}}\right)-\kappa^2\right)C+4\kappa^2+3\right)}{\kappa^{3/2}\sin\left(k\delta x_{\mathrm{q,n}}\right)C^2-\sqrt{\left(-2\kappa^{7/2}\cos\left(k\delta x_{\mathrm{q,n}}\right)+\kappa^4+\kappa^3\right)C^2+\kappa^4\left(C-1\right)+1/2}}, \tag{6.42}$$

which optimises the fidelity to $F = 1$ for the special case where both qubits are displaced by $\delta x_{\mathrm{q,n}}$ and share the same dipole moment through $\eta = \kappa$. The resulting success probability and fidelity are shown in Figs. (6.6) and (6.7), respectively, for a optimisation along the displacement of the first qubit and for the case where $\kappa = \eta = 1$. The fidelity is maximised along the diagonal line of $\delta x_{\mathrm{q,1}} = \delta x_{\mathrm{q,2}}$ and remains high within a displacement range of $k\delta x_{\mathrm{q,n}} \lesssim \pi/8$, but drops off when the displacements are outside of this range. The success probability, on the other hand, is only optimised along the chosen optimisation displacement of $\delta x_{\mathrm{q,1}}$ and has an unchanged and limited range of $k\delta x_{\mathrm{q,n}} \lesssim \pi/8$ along the displacement of the other qubit. Evaluating Eqs. (6.41)

and (6.42) for $\delta x_{\mathrm{q},2}$ will maximise the probability along the direction of the displacement of the second qubit, allowing for the ability to tailor the bit rate of the gate, depending on the spatial distribution of the quantum dots. Appendix (C) shows additional contour plots similar to those presented in this section. These are drawn for various values of κ and η and shows that the fidelity with the completely optimised detunings is very robust when the magnitude of the dipole moment of the qubits is changed. This robustness does not carry over to the success probability, which sees lower values for all the different sets of parametrisation parameters. The shape of the success probability profile is also heavily dependent on the values of κ and η but the general features remain the same: The probability is enhanced along the chosen qubit displacement for the detunings. It is thus possible to rotate each contour plot of the success probability by ninety degrees by evaluating Δ_{A} and δ_{q} along $\delta x_{\mathrm{q},2}$, as is seen from Figs. (C.9) and (C.10). This makes it possible to tailor the success probability depending on the exact distribution of the three quantum dots.

Fig. (6.5) shows the cross section of the contour plots along the highlighted diagonal line where $\delta x_{\mathrm{q},1} = \delta x_{\mathrm{q},2}$ for the aforementioned sets of detunings. This situation of the unoptimised case with $\Delta_{\mathrm{A}} = \gamma'\sqrt{C}$ and $\delta_{\mathrm{q}} = 0$ is also shown; This has the same general features as Fig. (6.2) for the case where only the qubit dipole moments were changed: The unoptimised and the simply optimised cases have a limited range with a unity or near-unity fidelity with a rapid drop-off in the success probability for all three sets of detunings. The maximum obtainable success probability changes between the three sets depending on the magnitude of the qubit displacement.
Both the success probability and the fidelity can attain high values for displacement that limited by range $k\delta x_{\mathrm{q,n}} \lesssim \pi/8$, with variations depending on the optimisation scheme (i.e. F is limited for both displacements for the simple optimisation, but is only limited along the displacement that is not optimised for the complete optimisation). This range corresponds to a maximal allowed displacement of $\delta x_{\mathrm{q,n}} \sim 18\mathrm{nm}$ for a refractive index of $n = 3.5$ and a wavelength of $\lambda = 1000\mathrm{nm}$ for the emitted light from an InAs quantum dot [13]. The typical in-plane size of quantum dots are typically in the range of $10 - 70\mathrm{nm}$, making the allowed displacement small compared to the in-plane size of the quantum dots. This may even allow small structural variations in the quantum dots themselves to reduce the success probability and fidelity; the treatment of these effects are beyond the scope of the work but can provide an interesting staring point for further treatment.

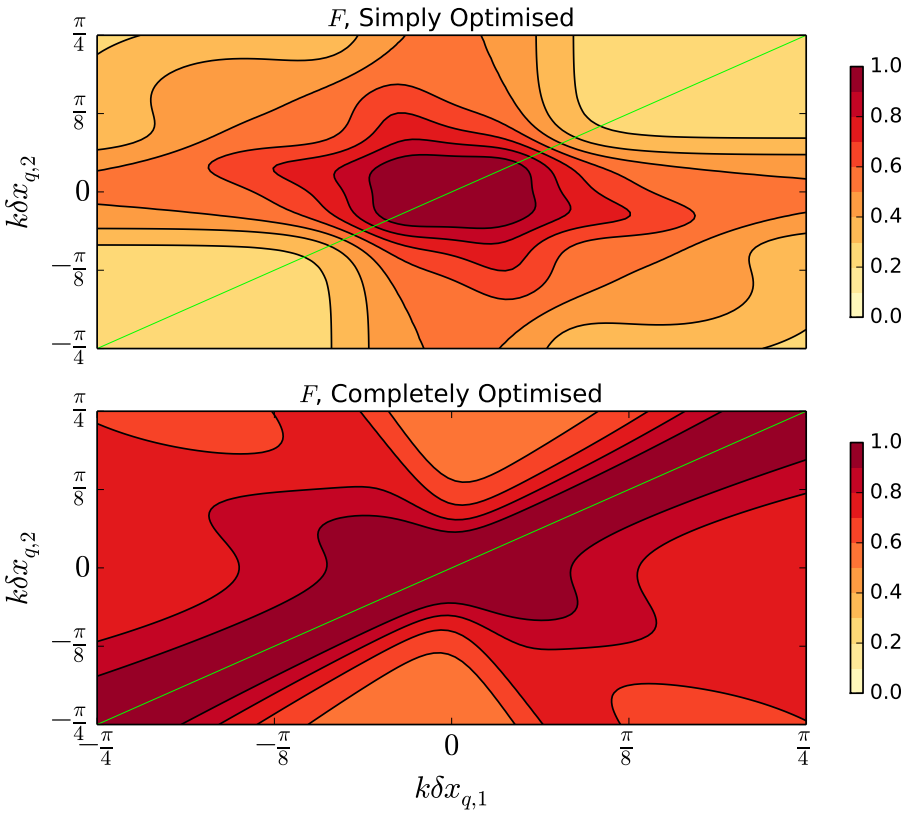

Figure 6.7: Contour plot of the fidelity against the displacement of the two qubit emitters. The top panel show the simply optimised case with $\Delta_{\mathrm{A}} = \gamma'\sqrt{C - 1/2}/2$ and $\delta_{\mathrm{q}} = -7\gamma'/8\sqrt{C}$, whereas the bottom panel show the situation for the completely optimised case from Eqs. (6.41) and (6.42). The green line show the diagonal where $\delta x_{\mathrm{q},1} = \delta x_{\mathrm{q},2}$, along which the optimisation has been carried out.

6.3 Conditions for the Adiabatic Treatment and Dephasing

The conditions for satisfying the validity of the adiabatic treatment and the suppression of dephasing processes can be carried out for the simplified case where both qubits are have the same dipole moment $\kappa = \eta$ and are displaced by the same amount from their ideal positions $\delta x_{\mathrm{q},1} = \delta x_{\mathrm{q},2} \equiv \delta x$. This derivation for a gate time t_{g} written only to leading order in C, where

$$\Delta_n \sim -\frac{\Omega^2}{\gamma'}\frac{1}{4\tilde{\Delta}_{\mathrm{A}}}, \tag{6.43}$$

leaving all the displacement- and κ dependence in the detuning Δ_{A} of the auxiliary quantum dot. Discarding the lowest order term in the argument for Δ_{A} yields:

$$\Delta_{\mathrm{A}} \underset{C\gg 1}{\approx} \frac{\gamma' C}{2\kappa^2}\sqrt{-2\kappa^{7/2}\cos\left(k\delta x\right) + \kappa^4 + \kappa^3 + \frac{\kappa^4}{C}}, \tag{6.44}$$

where the zeroth-order term has been discarded by rescaling the time scale. This results in a gate time that grows linear with the cooperativity:

$$t_{\mathrm{g}} = \frac{\pi}{|\Delta_2 - \Delta_{1,1} - \Delta_{1,2}|} = 2f^{-1}\left(\delta x, \kappa\right)\pi\frac{\gamma' C}{\Omega^2}, \tag{6.45}$$

where $f\left(\delta x, \kappa\right)$ is the constant of proportionality:

$$f\left(\delta x, \kappa\right) = \frac{1}{2\kappa^2}\sqrt{-2\kappa^{7/2}\cos\left(k\delta x\right) + \kappa^4 + \kappa^3 + \frac{\kappa^4}{C}}. \tag{6.46}$$

This is in contrast to the gate time in the ideal case that scaled as the square root of the cooperativity: $t_{\mathrm{g,I}} = 2\pi\sqrt{C}$.
The new scaling of the gate time requires a new choice for the drive field Ω in order to satisfy the adiabatic condition and to suppress the detrimental effect of dephasing processes. The adiabatic condition needs to satisfy:

$$\frac{\Delta_n^2}{\Omega^2} \ll 1 \Rightarrow \Omega \ll 4\Delta_{\mathrm{A}} = 2f\left(\delta x, \kappa\right)\gamma' C, \tag{6.47}$$

which can be satisfied by choosing a drive of:

$$\Omega \sim 2\pi a f^{-1}\left(\delta x, \kappa\right)\gamma' C, \quad a \ll 4\pi. \tag{6.48}$$

The value of a can be set to $a = 0.25$, as in Section (5.3.2) and is modified by the qubit displacement δx the qubit dipole moment κ through the function $f\left(\delta x, \kappa\right)$.
The effects of dephasing processes can be seen from Eq. (5.76): the maximum obtainable fidelity is significantly reduced. The aforementioned equation is rewritten here for convenience:

$$F_{\mathrm{Opt}} = \frac{1}{4} + \frac{3}{4}e^{-\gamma_{\mathrm{dp}}t_{\mathrm{g}}}, \tag{6.49}$$

where γ_{dp} is the dephasing rate. These effects can be minimised by setting the gate time to be shorter than the dephasing time $\gamma_{\mathrm{dp}}^{-1} \gg t_{\mathrm{g}}$:

$$\frac{\gamma_{\mathrm{dp}}}{4\pi\gamma'}\frac{f\left(\delta x, \kappa\right)}{a^2 C} \ll 1, \tag{6.50}$$

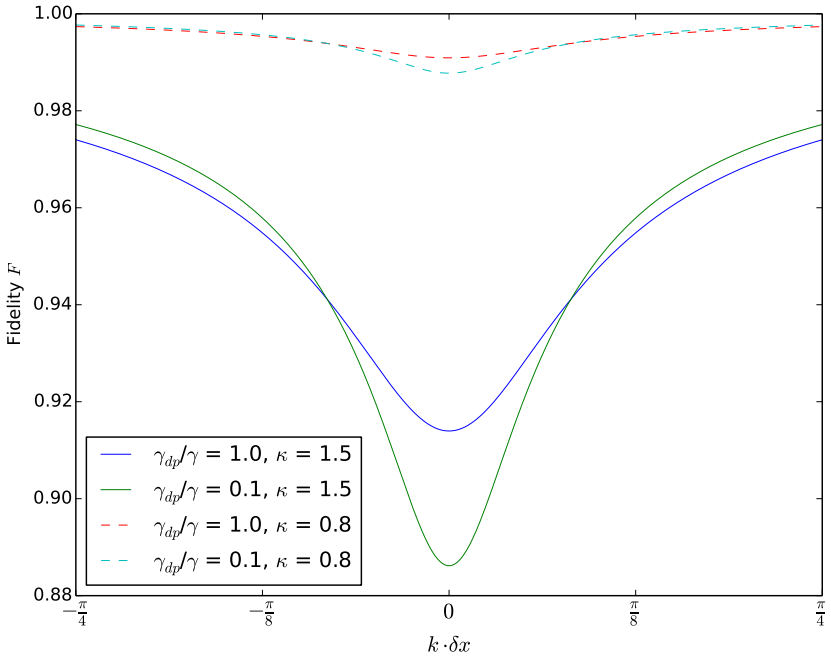

Figure 6.8: The fidelity plotted against $k\delta x$ for $C = 100$ for different values of κ and $\gamma_{\mathrm{dp}}/\gamma'$. Note how the dephasing induced errors decrease when the qubits are moved away from the auxiliary emitter.

leading to the same trade off between reducing the non-adiabatic errors or reducing detrimental effects from pure dephasing as in Section (5.3.2). This effect is shown in Fig. (6.8), with a smaller error when the qubits are moved in the same direction and when the dipole moments of the qubits are smaller than that of the emitter.

The detunings presented in Eqs. (6.41) and (6.42) gives the optimal choice due to the possibility to obtain a unit to near-unity fidelity for a wide range of values for the qubit dipole moment and position. In addition, setting the driving field as in Eq. (6.48) ensures that non-adiabatic errors are suppressed, even though this enhanced the impact on the gate operation from pure dephasing processes. The conditions outlined in this section provide the means to maximise the success probability of the gate through the simple optimisation schemes outlined in this section. Possibilities for enhancing these optimisation schemes exist, such that it may be possible to obtain a unity fidelity for all values of the aforementioned parameters. These possibilities are listed in Chapter (7).

Chapter 7

Conclusion and Outlook

7.1 Conclusion

The main subject of this thesis has been to examine the possibilities of implementing the controlled phase gate suggested by Borregaard et. al. [3] in a solid state environment. The basic idea has been to use the strong dipole-dipole interaction between three self-assembled quantum dots embedded in a nanophotonic waveguide. This has been done in order to control the dynamics of the three quantum emitters thereby producing the desired output state.

The dynamics of the physical system has been derived by adiabatically eliminating the excited states of the system when the auxiliary emitter is illuminated by a weak laser, yielding effective operators for the evolution of the ground states. This resulted in an effective Hamiltonian and a set of Lindblad operators describing the unitary and dissipative evolution, respectively. The evolution of these operators results in a controlled phase gate functionally identical to that proposed by Borregaard et al. This has been achieved by conditioning the gate upon measuring a specific ground state in the auxiliary emitter, as this emitter can only enter this state upon a successful gate operation. This eliminates detectable errors stemming from the dissipative evolution of the system and highlights one of the main strengths of this proposal: the gate has an integrated error detection, eliminating the need of implementing involved external quantum error correction protocols.

The dynamics of the gate are described through the effective Hamiltonian. This thesis has shown that this induces an effective AC Stark shift of the ground states of the system. This resulted in a dynamical phase change of the ground states that was used to implement the proposed CZ gate, when combined with a number of single qubit rotations. The success probability and fidelity of the gate were derived in order to quantify the effectiveness of the gate; both of these have been show to converge towards unity as the cooperativity of the system is increased. In addition, the ability to attain unity fidelity by standardising the effective decay rates of the system has been demonstrated. This standardisation results in the elimination of undetectable errors in the gate, namely errors resulting in the qubit states being weighted differently in time. This has been achieved by choosing a specific detuning of the laser field illuminating the auxiliary emitter. The conditions that are needed to be fulfilled in order to reduce the effect of non-adiabatic evolution has also been derived and the detrimental effects of pure dephasing processes has been described.

The effects of the emerging subradiance were examined by changing the physical parameters of the qubits, namely the dipole moments and their positions. Re-standardising the decay rates along the simple conditions of equal qubit dipole moments and positions has shown that this

proposal is reasonably robust against changes in both of the aforementioned parameters, with the ability to attain a unity to near-unity fidelity for a wide range of qubit dipole moments and positions. This robustness is limited to only the fidelity; the success probability undergoes a large drop off as the aforementioned parameters are changed. This is most pronounced for changes in the qubit position, demonstrating the large effects of the subradiant features of this proposal.

7.2 Outlook

There are several possible avenues for a further investigations into the proposal presented in this thesis. One could look into the permutation invariance. This can be implemented by letting the various emitter dipole moments couple differently to the backwards- and forwards propagating mode in the waveguide. In addition, the effects of photon loss in the waveguide may have an effect on the quality of the gate. Both of these additions may lead to changes depending on whether the auxiliary quantum dot is placed at the center or at either end of the quantum dot chain and can be implemented through the non-hermitian Hamiltonians governing the system. The resulting equations may be hard to treat analytically with the chosen laser scheme, leading to the next point.

The results for the non-ideal case in this thesis are derived for a simplified case where the two qubits are varied equally when compared to the auxiliary quantum dot. The effects of these quasi-complete optimisations on the completely non-ideal case have then been discussed. The main limitation for a full optimisation has, as previously mentioned, been computational complexity in the chosen method. One way to remedy this is to implement a numerical treatment of the completely non-ideal case in order to find a set of detunings that can standardise the decay rates. Alternatively, an analytical result for the completely non-ideal case may be obtained by introducing several perturbing lasers fields. One possible scheme is to use two lasers applied in succession of each other, where the first is nearly on resonance with the first qubit, while the second laser is nearly on resonance with the other qubit. This will result in separate effective operators for the two laser fields; the complete description of the dynamics can be achieved by a simple addition of these operators due to the nature of the formalised adiabatic elimination. This may lead to the ability of tailoring the coupling between the auxiliary quantum dot and either of the qubit dots independently, ultimately leading to a simplified scheme for standardising the decay rates.

Dephasing processes induce significant errors on the fidelity and are enhanced when the non-adiabatic errors are eliminated. The trade off between dephasing and non-adiabatic errors puts huge constraints on the usefulness of this proposal; it is then important to examine the possibilities of mitigating, or even removing, these errors and on how to simultaneously reduce both errors. Building upon this, a more complete description of dephasing can be carried out, as only pure dephasing has been considered in this work. Dephasing effects from phonons constitute are significant obstacle for experiment using quantum dots and photonic crystals. These effects may have a strong and detrimental effect on the controlled phase gate of this thesis and should thus de examined. In addition, the effects of dephasing of the excited states also need to be examined due to their dependence of the driving of the auxiliary emitter.

Appendix A

Effective Operator Formalism

This section will provide a derivation of the effective master equation and operators introduced in Section (2.1.4). The results and approach follows the procedure from [18]. The open system considered in this section can be divided into two distinct subspaces, which are connected by perturbative couplings. In addition, the system is considered to be Markovian. This makes is possible to describe the evolution of the density operator ρ through a master equation of the Lindblad form:

$$\dot{\rho} = -i\left[\hat{H}, \rho\right] + \sum_k \hat{L}_k \rho \hat{L}_k^\dagger - \frac{1}{2}\left(\hat{L}_k^\dagger \hat{L}_k \rho - \rho \hat{L}_k^\dagger \hat{L}_k\right), \tag{A.1}$$

where $\hat{H}$ is the Hamiltonian of the system and where each Lindblad operator $\hat{L}_k$ represents a source of decay. This can be reduced to an effective master equation by combining perturbation theory and adiabatic elimination fo the excited states. This reduced master equation only involves the ground state manifold:

$$\dot{\rho} = -i\left[\hat{H}_{\text{eff}}, \rho\right] + \sum_k \hat{L}^k_{\text{eff}} \rho \left(\hat{L}^k_{\text{eff}}\right)^\dagger - \frac{1}{2}\left(\left(\hat{L}^k_{\text{eff}}\right)^\dagger \hat{L}^k_{\text{eff}} \rho - \rho \left(\hat{L}^k_{\text{eff}}\right)^\dagger \hat{L}^k_{\text{eff}}\right), \tag{A.2}$$

with the effective Hamiltonian and Lindblad operator:

$$\hat{H}_{\text{eff}} = -\frac{1}{2}\hat{V}_- \left[\hat{H}_{\text{NH}}^{-1} + \left(\hat{H}_{\text{NH}}^{-1}\right)^\dagger\right] \hat{V}_+ + \hat{H}_g \tag{A.3}$$

$$\hat{L}^k_{\text{eff}} = \hat{L}_k \hat{H}_{\text{NH}}^{-1} V_+, \tag{A.4}$$

where V_+ (V_-) is the perturbative (de)excitation of the system and $\hat{H}_g$ is the ground state Hamiltonian. $\hat{H}_{\text{NH}}$ is the non-hermitian Hamiltonian of the quantum jump formalism:

$$\hat{H}_{\text{NH}} = \hat{H}_e - \frac{i}{2}\sum_k \hat{L}_k^\dagger \hat{L}_k, \tag{A.5}$$

with $\hat{H}_e$ being the excited state Hamiltonian. This formalism can be extended to systems with non-perturbative ground state Hamiltonians and containing several systems. The generalized effective Hamiltonian and Lindblad operator:

$$\hat{H}_{\text{eff}} = -\frac{1}{2}\sum_{f,l}\left[\hat{V}_-(t)\left(\hat{H}_{\text{NH}}^{(f,l)}\right)^{-1} V_+^{(f,l)(t)} + H.C.\right] + \hat{H}_g \tag{A.6}$$

$$\hat{L}^k_{\text{eff}} = \hat{L}_k \sum_{f,l}\left(\hat{H}_{\text{NH}}^{(f,l)}\right)^{-1} V_+^{(f,l)}(t), \tag{A.7}$$

where the sum over l runs over the different diagonal, non-perturbative ground states and f runs over the different perturbations or coupling fields.

A.1 Derivation of the Effective Operators

This section focuses on the derivation of the effective Hamiltonians and Lindblad used throughout this theses The derivation follows from [18].

A.1.1 Projection Operator Formalism

The projection operator formalism is used to structure the Hamiltonian into two separate subspaces. The total Hilbert space can be separated into a subspace for the ground states and a subspace for the excited state by the operators P_g and P_e, respectively. The projection operators fulfil $P_\mathrm{g} + P_\mathrm{e} = \mathbb{I}$ and $P_\mathrm{g}P_\mathrm{e} = 0$. The Hamiltonian is divided by:

$$\hat{H} = \hat{H}_g + \hat{H}_e + \hat{V}_+ + \hat{V}_-, \tag{A.8}$$

where $\hat{H}_e = P_\mathrm{g}\hat{H}P_\mathrm{g}$, $\hat{H}_e = P_\mathrm{e}\hat{H}P_\mathrm{e}$, $V_+ = P_\mathrm{e}\hat{H}P_\mathrm{g}$ and $\hat{V}_- = P_\mathrm{g}\hat{H}P_\mathrm{e}$. Note that $\hat{V}_+ = \hat{V}_-^\dagger$ and that $\hat{V} = \hat{V}_+ + \hat{V}_-$.
The excited states decay to the stable ground states such that the Lindblad operators can be written as $\hat{L}_k = P_\mathrm{g}\hat{L}_k P_\mathrm{e}$. There is no transition form the ground state manifold to the excited state manifold from spontaneous emission, which can be represented by writing $P_\mathrm{e}\hat{L}_k P_\mathrm{g} = 0$.

A.1.2 Non-Hermitian Time Evolution in the Quantum Jump Picture

The unitary and dissipative dynamics can be combined into a singe non-hermitian Hamiltonian $\hat{H}_{NH}$ in Eq. (A.5). This can be introduced into the master equation by noting that $\sum_k \hat{L}^k_\mathrm{eff}\left(\hat{L}^l_\mathrm{eff}\right)^\dagger = 2i\left(\hat{H}_\mathrm{NH} - \hat{H}_\mathrm{e}\right) = 2i\left(\hat{H}_\mathrm{NH} + \hat{H}_\mathrm{g} + \hat{V} - \hat{H}\right)$. Substituting this into the master equation given by Eq. (A.1) yields:

$$\dot{\rho} = -i\left[\hat{H}, \rho\right] + \sum_k \hat{L}^k_\mathrm{eff}\rho\left(\hat{L}^k_\mathrm{eff}\right)^\dagger - i\left(\left[\hat{H}_\mathrm{NH} + \hat{H}_\mathrm{g} + \hat{V} - \hat{H}\right]\rho - \rho\left[\hat{H}_\mathrm{NH} + \hat{H}_\mathrm{g} + \hat{V} - \hat{H}\right]\right) \tag{A.9}$$

$$= \sum_k \hat{L}^k_\mathrm{eff}\rho\left(\hat{L}^k_\mathrm{eff}\right)^\dagger - i\left(\left[\hat{H}_\mathrm{NH} + \hat{H}_\mathrm{g} + \hat{V}\right]\rho - \rho\left[\hat{H}_\mathrm{NH} + \hat{H}_\mathrm{g} + \hat{V}\right]\right). \tag{A.10}$$

The dynamics of the decaying excited states are mainly governed by the non-Hermitian Hamiltonian $\hat{H}_\mathrm{NH}$ for the case where the ground state interactions $\hat{H}_\mathrm{g}$ are much weaker than $\hat{H}_\mathrm{e}$.

A.1.3 Perturbation Theory in the Interaction Picture

The couplings between the subspaces $\hat{V}_\pm$ are assumed to be sufficiently weak in order to be described as perturbations of the evolution governed by the unperturbed Hamiltonian defined as $\hat{H}_0 = \hat{H}_\mathrm{g} + \hat{H}_\mathrm{NH}$. The perturbation theory is performed on the density matrix ρ in the interaction picture introduced in Section (2.1.3). The change to the interaction picture is performed using the operator:

$$\hat{O}(t) = \exp\left(-i\hat{H}_0 t\right) = \exp\left(-i\left(\hat{H}_\mathrm{g} + \hat{H}_\mathrm{NH}\right)t\right). \tag{A.11}$$

This makes the change to the interaction picture possible for the Hamiltonian $\hat{H}$, the density operator ρ and the Lindblad operator $\hat{L}^k_{\text{eff}}$. This is done using the transformed wavefunction $|\tilde{\psi}(t)\rangle$, which is defined by:

$$|\psi(t)\rangle = \hat{O}(t)\,|\tilde{\psi}(t)\rangle\,. \tag{A.12}$$

The time-dependent Schrödinger equation can then be transformed by:

$$i\frac{\mathrm{d}}{\mathrm{d}t}\left[|\psi(t)\rangle\right] = \hat{H}\,|\psi(t)\rangle \tag{A.13}$$

$$\Rightarrow i\frac{\mathrm{d}}{\mathrm{d}t}\left[\hat{O}(t)\,|\tilde{\psi}(t)\rangle\right] = \hat{H}'\hat{O}(t)\,|\tilde{\psi}(t)\rangle \tag{A.14}$$

$$\Rightarrow i\hat{O}(t)\frac{\mathrm{d}}{\mathrm{d}t}|\tilde{\psi}(t)\rangle = \left(\hat{H}'\hat{O}(t) - i\frac{\mathrm{d}}{\mathrm{d}t}\hat{O}(t)\right)|\tilde{\psi}(t)\rangle \tag{A.15}$$

$$\Rightarrow i\frac{\mathrm{d}}{\mathrm{d}t}|\tilde{\psi}(t)\rangle = \left(\hat{O}^{-1}(t)\,\hat{H}'\hat{O}(t) - i\hat{O}^{-1}(t)\frac{\mathrm{d}}{\mathrm{d}t}\hat{O}(t)\right)|\tilde{\psi}(t)\rangle \tag{A.16}$$

$$\Rightarrow i\frac{\mathrm{d}}{\mathrm{d}t}|\tilde{\psi}(t)\rangle = \left(\hat{O}^{-1}(t)\,\hat{H}'\hat{O}(t) + i\frac{\mathrm{d}}{\mathrm{d}t}\left[\hat{O}^{-1}(t)\right]\hat{O}(t)\right)|\tilde{\psi}(t)\rangle\,, \tag{A.17}$$

where $\hat{H}' = \hat{H}_0 + \hat{V}$. The change from Eq. (A.16) to (A.17) has been done using the following trick:

$$0 = \frac{\mathrm{d}\mathbb{1}}{\mathrm{d}t} = \frac{\mathrm{d}}{\mathrm{d}t}\left[\hat{O}^{-1}(t)\,\hat{O}(t)\right] = \frac{\mathrm{d}}{\mathrm{d}t}\left[\hat{O}^{-1}(t)\right]\hat{O}(t) + \hat{O}^{-1}(t)\frac{\mathrm{d}}{\mathrm{d}t}\hat{O}(t) \tag{A.18}$$

$$\Rightarrow \hat{O}^{-1}(t)\frac{\mathrm{d}}{\mathrm{d}t}\hat{O}(t) = -\frac{\mathrm{d}}{\mathrm{d}t}\left[\hat{O}^{-1}(t)\right]\hat{O}(t)\,, \tag{A.19}$$

where $\mathbb{1}$ is the identity operator. The transformed interaction Hamiltonian $\tilde{V}(t)$ from Eq. (A.16) is defined by:

$$\tilde{V}(t) = \hat{O}^{-1}(t)\left(\hat{H}_0 + \hat{V}\right)\hat{O}(t) - i\hat{O}^{-1}(t)\frac{\mathrm{d}}{\mathrm{d}t}\hat{O}(t) \tag{A.20}$$

$$= \hat{O}^{-1}(t)\left(\hat{H}_0 + \hat{V}\right)\hat{O}(t) - i\hat{O}^{-1}(t)\left(-i\hat{H}_0\right)\hat{O}(t) \tag{A.21}$$

$$= \hat{O}^{-1}(t)\,\hat{V}\hat{O}(t)\,. \tag{A.22}$$

The Hermitian conjugate is easily calculated:

$$\tilde{V}^\dagger = \hat{O}^\dagger(t)\,\tilde{V}\left(\hat{O}^{-1}(t)\right)^\dagger. \tag{A.23}$$

Note that this interaction Hamiltonian is not Hermitian, due to the non-unitary nature of $\hat{O}(t)$. The density operator ρ is transformed as:

$$\rho = |\psi(t)\rangle\langle\psi(t)| = \hat{O}(t)\,|\tilde{\psi}(t)\rangle\langle\tilde{\psi}(t)|\,\hat{O}^\dagger(t) = \hat{O}(t)\,\tilde{\rho}(t)\,\hat{O}^\dagger(t) \tag{A.24}$$

$$\Rightarrow \tilde{\rho}(t) = \hat{O}^{-1}(t)\,\rho\left(\hat{O}^\dagger(t)\right)^{-1}. \tag{A.25}$$

The Lindblad operator has the same form as $\hat{V}_-$, so the transformation to the interaction picture follows the same form as for $\hat{V}$:

$$\tilde{L}_k(t) = \hat{O}^{-1}(t)\,\tilde{L}_k(t)\,\hat{O}(t) \tag{A.26}$$

$$\tilde{L}^\dagger_k(t) = \hat{O}^\dagger(t)\,\tilde{L}^\dagger_k(t)\left(\hat{O}^{-1}(t)\right)^\dagger \tag{A.27}$$

The time derivative of the transformed density matrix is given by:

$$\dot{\tilde{\rho}} = -i\frac{\mathrm{d}}{\mathrm{d}t}\left[\hat{O}^{-1}(t)\,\rho\left(\hat{O}^{\dagger}(t)\right)^{-1}\right] \tag{A.28}$$

$$= \dot{O}(t)\,\rho\left(\hat{O}^{\dagger}(t)\right)^{-1} + \hat{O}^{-1}(t)\,\rho\left(\dot{O}^{\dagger}(t)\right)^{-1} + \hat{O}^{-1}(t)\,\dot{\rho}\left(\hat{O}^{\dagger}(t)\right)^{-1} \tag{A.29}$$

$$= i\hat{H}_0\hat{O}^{-1}(t)\,\rho\left(\hat{O}^{\dagger}(t)\right)^{-1} + \hat{O}^{-1}(t)\,\rho\left(-i\hat{H}_0^{\dagger}\right)\left(\hat{O}^{\dagger}(t)\right)^{-1} \tag{A.30}$$

$$+ \hat{O}^{-1}(t)\left[\sum_k \tilde{L}_k(t)\,\rho\tilde{L}_k^{\dagger}(t) - i\left(\left[\hat{H}_0+\hat{V}\right]\rho - \rho\left[\hat{H}_0+\hat{V}\right]\right)\right]\left(\hat{O}^{\dagger}(t)\right)^{-1}, \tag{A.31}$$

where the derivatives in the first two terms in Eq. (A.29) have been explicitly carried out and the full expression for the master equation from Eq. (A.1) have been substituted into the third term. The $\hat{H}_0$ terms cancel, which leaves:

$$\dot{\tilde{\rho}} = -i\hat{O}^{-1}(t)\left[\hat{V}\rho - \rho\hat{V}\right]\left(\hat{O}^{\dagger}(t)\right)^{-1} + \hat{O}^{-1}(t)\sum_k \tilde{L}_k(t)\,\rho\tilde{L}_k^{\dagger}(t)\left(\hat{O}^{\dagger}(t)\right)^{-1} \tag{A.32}$$

$$= -i\hat{O}^{-1}(t)\left(\hat{V}\left[\hat{O}(t)\,\hat{O}^{-1}(t)\right]\rho - \rho\left[\left(\hat{O}^{\dagger}(t)\right)^{-1}\hat{O}^{\dagger}(t)\right]\hat{V}\right)\left(\hat{O}^{\dagger}(t)\right)^{-1} \tag{A.33}$$

$$+ \hat{O}^{-1}(t)\sum_k \tilde{L}_k(t)\left[\hat{O}(t)\,\hat{O}^{-1}(t)\right]\rho\left[\left(\hat{O}^{-1}(t)\right)^{\dagger}\hat{O}^{\dagger}(t)\right]\tilde{L}_k^{\dagger}(t)\left(\hat{O}^{\dagger}(t)\right)^{-1} \tag{A.34}$$

$$= -i\left[\tilde{V}(t)\,\tilde{\rho}(t) - \tilde{\rho}(t)\,\tilde{V}^{\dagger}(t)\right] + \sum_k \tilde{L}_k(t)\,\tilde{\rho}(t)\,\tilde{L}_k^{\dagger}(t), \tag{A.35}$$

Eq. (A.32) by $\mathbb{1} = \hat{O}(t)\,\hat{O}^{-1}(t) = \hat{O}^{\dagger}(t)\left(\hat{O}^{-1}(t)\right)^{\dagger}$ a number of times in order to simplify the expression. These factors of $\mathbb{1}$ are shown in Eqs. (A.33) ans (A.34). This makes it possible to identify the operators $\tilde{\rho}, \tilde{V}(t), \tilde{V}^{\dagger}(t), \tilde{L}_k(t)$ and $\tilde{L}_k^{\dagger}(t)$, which yields Eq. (A.35).

The perturbative expansion of $\tilde{\rho}$ is written in terms of the small parameter ϵ:

$$\tilde{\rho}(t) \approx = \frac{1}{N}\left(\tilde{\rho}^{(0)}(t) + \epsilon\tilde{\rho}^{(1)}(t) + \epsilon^2\tilde{\rho}^{(2)}(t) + \ldots\right) \tag{A.36}$$

Plugging Eq. (A.36) into Eq. (A.35) results in a recursive expression for the reduced density operator by using that $\tilde{V}$ is a perturbative (de)excitation: $\tilde{V} \propto \epsilon$. This gives:

$$\dot{\tilde{\rho}}^{(n)}(t) = -i\left[\tilde{V}(t)\,\tilde{\rho}^{(n-1)}(t) - \tilde{\rho}^{(n-1)}(t)\,\tilde{V}^{\dagger}(t)\right] + \sum_k \tilde{L}_k(t)\,\tilde{\rho}^{(n)}(t)\,\tilde{L}_k^{\dagger}(t). \tag{A.37}$$

The first three orders of the recursive reduced density operator is thus:

$$\dot{\tilde{\rho}}^{(0)}(t) = \sum_k \tilde{L}_k(t)\,\tilde{\rho}^{(0)}(t)\,\tilde{L}_k^{\dagger}(t) \tag{A.38}$$

$$\dot{\tilde{\rho}}^{(1)}(t) = -i\left[\tilde{V}(t)\,\tilde{\rho}^{(0)}(t) - \tilde{\rho}^{(0)}(t)\,\tilde{V}^{\dagger}(t)\right] + \sum_k \tilde{L}_k(t)\,\tilde{\rho}^{(1)}(t)\,\tilde{L}_k^{\dagger}(t) \tag{A.39}$$

$$\dot{\tilde{\rho}}^{(2)}(t) = -i\left[\tilde{V}(t)\,\tilde{\rho}^{(1)}(t) - \tilde{\rho}^{(1)}(t)\,\tilde{V}^{\dagger}(t)\right] + \sum_k \tilde{L}_k(t)\,\tilde{\rho}^{(2)}(t)\,\tilde{L}_k^{\dagger}(t). \tag{A.40}$$

Decay processes can be neglected for orders $n \leq 1$ in the absence of initial excitations; the zeroth order is trivially in the ground state and attains no change due to spontaneous emission

events. This ensures that the first-order terms only evolves according to the drive terms; this evolution allows the higher order terms to have contributions from decay processes. This reduces Eqs. (A.38) through (A.40) to:

$$\dot{\tilde{\rho}}^{(0)}(t) = 0 \tag{A.41}$$

$$\dot{\tilde{\rho}}^{(1)}(t) = -i\left[\tilde{V}(t)\,\tilde{\rho}^{(0)}(t) - \tilde{\rho}^{(0)}(t)\,\tilde{V}^{\dagger}(t)\right] \tag{A.42}$$

$$\dot{\tilde{\rho}}^{(2)}(t) = -i\left[\tilde{V}(t)\,\tilde{\rho}^{(1)}(t) - \tilde{\rho}^{(1)}(t)\,\tilde{V}^{\dagger}(t)\right] + \sum_k \tilde{L}_k(t)\,\tilde{\rho}^{(2)}(t)\,\tilde{L}_k^{\dagger}(t)\,. \tag{A.43}$$

The projection operator formalism to separate the ground state evolution from the evolution of the excited states. The terms $P_{\mathrm{g}}\tilde{V}(t)\,\tilde{\rho}^{(0)}(t)$ in the equation for the first order terms will vanish, as they pick out non-physical de-excitations from the ground state. The ground state evolution is then given by:

$$P_{\mathrm{g}}\dot{\tilde{\rho}}^{(0)}(t)\,P_{\mathrm{g}} = P_{\mathrm{g}}\dot{\tilde{\rho}}^{(1)}(t)\,P_{\mathrm{g}} = 0 \tag{A.44}$$

$$P_{\mathrm{g}}\dot{\tilde{\rho}}^{(2)}(t)\,P_{\mathrm{g}} = -iP_{\mathrm{g}}\left[\tilde{V}(t)\,\tilde{\rho}^{(1)}(t) - \tilde{\rho}^{(1)}(t)\,\tilde{V}^{\dagger}(t)\right]P_{\mathrm{g}} + \sum_k P_{\mathrm{g}}\tilde{L}_k(t)\,P_{\mathrm{e}}\tilde{\rho}^{(2)}(t)\,P_{\mathrm{e}}\tilde{L}_k^{\dagger}(t)\,P_{\mathrm{g}}, \tag{A.45}$$

where the Lindblad operator has been written in the form $\tilde{L}_k = P_{\mathrm{g}}\tilde{L}_k P_{\mathrm{e}}$ in the last line. The evolution of the first order terms vanishes due to the lack of initial excitations. The identities $P_{\mathrm{g}}(P_{\mathrm{g}} + P_{\mathrm{e}}) = P_{\mathrm{g}} \cdot \mathbb{1} \Rightarrow P_{\mathrm{g}}P_{\mathrm{g}} = P_{\mathrm{g}}$ have also been used. The ground states are thus connected by unitary and dissipative processes of second order. Tvolution of the excited states can be simplified in a similar manner:

$$P_{\mathrm{e}}\dot{\tilde{\rho}}^{(0)}(t)\,P_{\mathrm{e}} = P_{\mathrm{e}}\dot{\tilde{\rho}}^{(1)}(t)\,P_{\mathrm{e}} = 0 \tag{A.46}$$

$$P_{\mathrm{e}}\dot{\tilde{\rho}}^{(2)}(t)\,P_{\mathrm{e}} = -iP_{\mathrm{g}}\left[\tilde{V}(t)\,\tilde{\rho}^{(1)}(t) - \tilde{\rho}^{(1)}(t)\,\tilde{V}^{\dagger}(t)\right]P_{\mathrm{g}}, \tag{A.47}$$

where the dissipative feeding term have not been included for the second-order evolution, as the excited states do not gain population from decay/spontaneous emission. The excited states dynamics are thus only driven by the interaction Hamiltonian $\tilde{V}(t)$, while interactions between the two subspaces are given by the terms $P_{\mathrm{e}}\dot{\tilde{\rho}}^{(1)}(t)\,P_{\mathrm{g}}$ and $P_{\mathrm{g}}\dot{\tilde{\rho}}^{(1)}(t)\,P_{\mathrm{g}}$.

A.1.4 Adiabatic Elimination of the Excited States

It is, in principle, possible to solve the second-order equations, but the calculations can be rather involved, even after having separated the various subspaces. This process can be simplified as the decaying excited states are essentially unpopulated. The evolution of these states can thus be adiabatically eliminated:

$$P_{\mathrm{e}}\dot{\tilde{\rho}}^{(2)}(t)\,P_{\mathrm{e}} \approx 0. \tag{A.48}$$

The dynamics of the second order term in Eq. (A.40) are approximated by the ground states of Eq. (A.43). An effective equation for $P_{\mathrm{e}}\tilde{\rho}^{(2)}(t)\,P_{\mathrm{e}}$ is acquired by formally integrating Eq. (A.47):

$$P_{\mathrm{e}}\tilde{\rho}^{(2)}(t) = -iP_{\mathrm{e}}\int_0^t \mathrm{d}t'\left[\tilde{V}(t')\,\tilde{\rho}^{(1)}(t') - \tilde{\rho}^{(1)}(t')\,\tilde{V}(t')\right]P_{\mathrm{e}}. \tag{A.49}$$

Integrating Eq. (A.38) gives an expression for $\tilde{\rho}^{(1)}(t)$:

$$\tilde{\rho}^{(1)}(t) = -i \int_0^t \mathrm{d}t' \left[\tilde{V}\left(t'\right) \tilde{\rho}^{(0)}\left(t'\right) - \tilde{\rho}^{(0)}\left(t'\right) \tilde{V}\left(t'\right) \right]. \tag{A.50}$$

This can be substituted into Eq. (A.49):

$$\left.\begin{aligned} P_{\mathrm{e}} \tilde{\rho}^{(2)}(t) P_{\mathrm{e}} = -P_{\mathrm{e}} \int_0^t \mathrm{d}t' \int_0^{t'} \mathrm{d}t'' \Big[& \tilde{V}\left(t'\right) \tilde{V}\left(t''\right) \tilde{\rho}^{(0)}\left(t''\right) - \tilde{V}\left(t'\right) \tilde{\rho}^{(0)}\left(t''\right) \tilde{V}^{\dagger}(t) \\ & - \tilde{V}\left(t''\right) \tilde{\rho}^{(0)}\left(t''\right) \tilde{V}^{\dagger}\left(t'\right) + \tilde{\rho}^{(0)}\left(t''\right) \tilde{V}^{\dagger}\left(t''\right) \tilde{V}^{\dagger}\left(t'\right) \Big] P_{\mathrm{e}} \end{aligned}\right\} \tag{A.51}$$

$$= P_{\mathrm{e}} \int_0^t \mathrm{d}t' \int_0^{t'} \mathrm{d}t'' \left[\tilde{V}\left(t'\right) \tilde{\rho}^{(0)}\left(t''\right) \tilde{V}^{\dagger}(t) + \tilde{V}\left(t''\right) \tilde{\rho}^{(0)}\left(t''\right) \tilde{V}^{\dagger}\left(t'\right) \right], \tag{A.52}$$

where the two terms of the form $P_{\mathrm{e}} \tilde{V}\left(t'\right) \tilde{V}\left(t''\right) \tilde{\rho}^{(0)}\left(t''\right) P_{\mathrm{e}}$ have been neglected, as $\tilde{V}\left(t'\right) \tilde{V}\left(t''\right)$ effectively is an excitation followed by an de-excitation of $\tilde{\rho}^{(0)}(t)$. $\tilde{\rho}^{(0)}(t)$ lives in the ground state subspace and has therefore no contribution to the excited state subspace. The two terms in Eq. (A.52) are to be substituted into the last term in Eq. (A.43). For the first two terms in Eq. (A.43):

$$P_{\mathrm{g}} \dot{\tilde{\rho}}^{(2)}(t) P_{\mathrm{g}} \Big|_{\mathrm{FirstTerms}} = -i P_{\mathrm{g}} \left[\tilde{V}(t) \tilde{\rho}^{(1)}(t) - \tilde{\rho}^{(1)}(t) \tilde{V}^{\dagger}(t) \right] P_{\mathrm{g}} \tag{A.53}$$

$$= -i \left\{ \begin{array}{l} P_{\mathrm{g}} \tilde{V}(t) \left[-i \int_0^t \mathrm{d}'t \left[\tilde{V}\left(t'\right) \tilde{\rho}^{(0)}\left(t'\right) - \tilde{\rho}^{(0)}\left(t'\right) \tilde{V}^{\dagger}\left(t'\right) \right] \right] P_{\mathrm{g}} \\ + P_{\mathrm{g}} \left[-i \int_0^t \mathrm{d}'t \left[\tilde{V}\left(t'\right) \tilde{\rho}^{(0)}\left(t'\right) - \tilde{\rho}^{(0)}\left(t'\right) \tilde{V}^{\dagger}\left(t'\right) \right] \right] \tilde{V}^{\dagger}(t) P_{\mathrm{g}} \end{array} \right\} \tag{A.54}$$

$$= -P_{\mathrm{g}} \tilde{V}(t) \int_0^t \mathrm{d}t' \left[\tilde{V}\left(t'\right) \tilde{\rho}^{(0)}\left(t'\right) \right] P_{\mathrm{g}} - P_{\mathrm{g}} \int_0^t \mathrm{d}t' \left[\tilde{\rho}^{(0)}(t) \tilde{V}^{\dagger}\left(t'\right) \right] P_{\mathrm{g}}, \tag{A.55}$$

where terms of the form $P_{\mathrm{g}} \tilde{V}(t) \tilde{\rho}^{(0)}(t) \tilde{V}^{\dagger}(t) P_{\mathrm{g}}$ have been neglected, as these terms describes (de)excitations between the sub spaces and therefore do not contribute to the ground state evolution. Combining Eqs. (A.55) and (A.52) yields:

$$\begin{aligned} P_{\mathrm{g}} \dot{\tilde{\rho}}^{(2)}(t) P_{\mathrm{g}} = & - P_{\mathrm{g}} \tilde{V}(t) \int_0^t \mathrm{d}t' \left[\tilde{V}\left(t'\right) \tilde{\rho}^{(0)}\left(t'\right) \right] P_{\mathrm{g}} - P_{\mathrm{g}} \int_0^t \mathrm{d}t' \left[\tilde{\rho}^{(0)}(t) \tilde{V}^{\dagger}\left(t'\right) \right] P_{\mathrm{g}} \\ & + P_{\mathrm{g}} \sum_k \tilde{L}_k(t) Pe \int_0^t \mathrm{d}t' \int_0^{t'} \mathrm{d}t'' \left[\tilde{V}\left(t'\right) \tilde{\rho}^{(0)}\left(t''\right) \tilde{V}^{\dagger}(t) + \tilde{V}\left(t''\right) \tilde{\rho}^{(0)}\left(t''\right) \tilde{V}^{\dagger}\left(t'\right) \right] P_{\mathrm{e}} \tilde{L}_k^{\dagger}(t) P_{\mathrm{g}}. \end{aligned} \tag{A.56}$$

The four terms in Eq. (A.56) are either Hamiltonian-like or Lindblad-like. They have the following form:

$$I_1 = P_{\mathrm{g}} \tilde{V}(t) \int_0^t \mathrm{d}t' \left[\tilde{V}(t') \tilde{\rho}^{(0)}(t') \right] P_{\mathrm{g}} \tag{A.57}$$

$$I_2 = \frac{1}{2} P_{\mathrm{e}} \int_0^t \mathrm{d}t' \int^{t'} \mathrm{d}t'' \left[\tilde{V}(t') \tilde{\rho}^{(0)}(t'') \tilde{V}^{\dagger}(t'') \right]. \tag{A.58}$$

These integrals can be solved by assuming that the interaction between the ground state subspaces to be perturbative, such that the ground state evolution is negligible as compared to the evolution of the excited states. The contribution to the evolution of the ground state subspace from $\hat{O}(t)$ can be found by:

$$P_{\mathrm{g}} \hat{O}(t) P_{\mathrm{g}} = P_{\mathrm{g}} \exp\left(-i \left[\hat{H}_{\mathrm{g}} + \hat{H}_{\mathrm{NH}} \right] t \right) P_{\mathrm{g}} \tag{A.59}$$

$$= P_{\mathrm{g}} \mathbb{1} P_{\mathrm{g}} + P_{\mathrm{g}} \left(-i \left[\hat{H}_{\mathrm{g}} + \hat{H}_{\mathrm{NH}} \right] t \right) P_{\mathrm{g}} + P_{\mathrm{g}} \left(- \left[\hat{H}_{\mathrm{g}} + \hat{H}_{\mathrm{NH}} \right]^2 t^2 \right) P_{\mathrm{g}} + \ldots \tag{A.60}$$

$$\approx P_{\mathrm{g}} \left(\mathbb{1} - i \hat{H}_{\mathrm{NH}} t + \left(-i \hat{H}_{\mathrm{NH}} t \right)^2 + \ldots \right) P_{\mathrm{g}} \tag{A.61}$$

$$= P_{\mathrm{g}} \mathbb{1} P_{\mathrm{g}}. \tag{A.62}$$

It is thus possible to set $\hat{O}(t) P_{\mathrm{g}} \simeq P_{\mathrm{g}}$ for a perturbative ground state interaction. I_1 then simplifies to:

$$I_1 = P_{\mathrm{g}} \tilde{V}(t) \int_0^t \mathrm{d}t' \left[\tilde{V}(t') \tilde{\rho}^{(0)}(t') \right] P_{\mathrm{g}} \tag{A.63}$$

$$= P_{\mathrm{g}} \hat{O}^{-1}(t) V \hat{O}(t) \int_0^t \mathrm{d}t' \left[\hat{O}^{-1}(t') V \hat{O}(t') \tilde{\rho}^{(0)}(t') \right] P_{\mathrm{g}} \tag{A.64}$$

$$\simeq P_{\mathrm{g}} V \hat{O}(t) \int_0^t \mathrm{d}t' \left[\hat{O}^{-1}(t') V P_{\mathrm{g}} \tilde{\rho}^{(0)}(t) \right] \tag{A.65}$$

$$= P_{\mathrm{g}} V (P_{\mathrm{e}} + P_{\mathrm{g}}) \hat{O}(t) \int_0^t \mathrm{d}t' \left[\hat{O}^{-1}(t') (P_{\mathrm{g}} + P_{\mathrm{e}}) V P_{\mathrm{g}} \tilde{\rho}^{(0)}(t) \right] \tag{A.66}$$

$$= P_{\mathrm{g}} \hat{V}_- \hat{O}(t) \int_0^t \mathrm{d}t' \left[\hat{O}^{-1}(t') \hat{V}_+ \tilde{\rho}^{(0)}(t) \right] P_{\mathrm{g}} \tag{A.67}$$

$$= P_{\mathrm{g}} \hat{V}_- \exp\left(-i \hat{H}_{\mathrm{NH}} t \right) \left[\left(i \hat{H}_{\mathrm{NH}} t \right)^{-1} \exp\left(i \hat{H}_{\mathrm{NH}} t \right) \right]_0^t \hat{O}^{-1}(t') \hat{V}_+ \tilde{\rho}^{(0)}(t) P_{\mathrm{g}} \tag{A.68}$$

$$\simeq P_{\mathrm{g}} \hat{V}_- \left(i \hat{H}_{\mathrm{NH}} \right)^{-1} \hat{V}_+ \tilde{\rho}^{(0)}(t) P_{\mathrm{g}}, \tag{A.69}$$

where the interaction Hamiltonian $\tilde{V}(t)$ have been transformed back to the Schrödinger picture. In addition, $P_{\mathrm{g}} V P_{\mathrm{e}} = P_{\mathrm{e}} V P_{\mathrm{g}} = 0$ have been used to simplify the expression. The density operator for the ground state thus evolves slowly and to second order in V. The factors of $\tilde{V}(t)$

and $\tilde{V}(t')$ will cause the interaction to have features of fourth order. This can be overcome by assuming that $\tilde{\rho}^{(0)}(t') \approx \tilde{\rho}^{(0)}(t)$.
The $t' = 0$ term have been dropped at the last equation, as it is detuned with respect to the $t' = t$ term due to the time dependence of $\exp\left(i\hat{H}_{\mathrm{NH}}t\right)$. The term arising from $t' = 0$ can be neglected due to its fast evolution, assuming that the evolution of the ground states is slow compared to that due to $\hat{H}_{\mathrm{NH}}$. The second integral of type I_1 is treated in the same manner and gives the Hermitian conjugate of Eq. (A.69):

$$I_{1,2} = P_{\mathrm{g}}\tilde{\rho}^{(0)}(t)\,\hat{V}_{-}\left(-i\hat{H}_{\mathrm{NH}}^{-1}\right)^{\dagger}\hat{V}_{+}P_{\mathrm{g}}. \tag{A.70}$$

The factor $\tilde{\rho}^{(0)}(t'')$ can be approximated as $\tilde{\rho}^{(0)}(t)$ in I_2 using the same argument as described above. The integrals in I_2 can then be separated as follows:

$$I_2 \simeq \frac{1}{2}P_{\mathrm{e}}\int_0^t \mathrm{d}t' \int^{t'} \mathrm{d}t''\left[\tilde{V}\left(t'\right)\tilde{\rho}^{(0)}(t)\,\tilde{V}^{\dagger}\left(t''\right)\right] \tag{A.71}$$

$$= \frac{1}{2}P_{\mathrm{e}}\int_0^t \mathrm{d}t'\left[\tilde{V}\left(t'\right)\right]\tilde{\rho}^{(0)}(t)\int_0^t \mathrm{d}t'\left[\tilde{V}^{\dagger}\left(t'\right)\right]P_{\mathrm{e}} \tag{A.72}$$

$$= \frac{1}{2}P_{\mathrm{e}}\int_0^t \mathrm{d}t'\left[\hat{O}^{-1}\left(t'\right)V\hat{O}\left(t'\right)\right]\tilde{\rho}^{(0)}(t)\int_0^t \mathrm{d}t'\left[\hat{O}^{\dagger}\left(t'\right)V\left(\hat{O}^{-1}\left(t'\right)\right)^{\dagger}\right]P_{\mathrm{e}} \tag{A.73}$$

$$= \frac{1}{2}P_{\mathrm{e}}\int_0^t \mathrm{d}t'\left[\hat{O}^{-1}\left(t'\right)V\left(P_{\mathrm{g}}+P_{\mathrm{e}}\right)\hat{O}\left(t'\right)\right]\tilde{\rho}^{(0)}(t)\int_0^t \mathrm{d}t'\left[\hat{O}^{\dagger}\left(t'\right)\left(P_{\mathrm{e}}+P_{\mathrm{g}}\right)V\left(\hat{O}^{-1}\left(t'\right)\right)^{\dagger}\right]P_{\mathrm{e}} \tag{A.74}$$

$$\simeq \frac{1}{2}\int_0^t \mathrm{d}t'\left[\hat{O}^{-1}\left(t'\right)\right]\hat{V}_{+}\tilde{\rho}^{(0)}(t)\,\hat{V}_{-}\int_0^t \mathrm{d}t'\left[\left(\hat{O}^{-1}\left(t'\right)\right)^{\dagger}\right] \tag{A.75}$$

$$\simeq \frac{1}{2}\left(i\hat{H}_{\mathrm{NH}}\right)^{-1}\hat{V}_{+}\tilde{\rho}^{(0)}(t)\,\hat{V}_{-}\left(-i\hat{H}_{\mathrm{NH}}^{-1}\right)^{\dagger}. \tag{A.76}$$

The second integral of type I_2 yields the same result. Eqs. (A.69), (A.70) and (A.76) are substituted into Eq. (A.56), which yields:

$$\left.\begin{aligned} P_{\mathrm{g}}\dot{\tilde{\rho}}^{(2)}(t)\,P_{\mathrm{g}} = &-P_{\mathrm{g}}\hat{V}_{-}\left[\left(i\hat{H}_{\mathrm{NH}}\right)^{-1}\tilde{\rho}^{(0)}(t)+\tilde{\rho}^{(0)}(t)\left(-i\hat{H}_{\mathrm{NH}}^{-1}\right)^{\dagger}\right]P_{\mathrm{g}}\hat{V}_{+} \\ &+P_{\mathrm{g}}\sum_k \tilde{L}_k(t)\left(i\hat{H}_{\mathrm{NH}}\right)^{-1}\hat{V}_{+}\tilde{\rho}^{(0)}(t)\,\hat{V}_{-}\left(-i\hat{H}_{\mathrm{NH}}^{-1}\right)^{\dagger}\tilde{L}_k^{\dagger}(t)\,P_{\mathrm{g}} \end{aligned}\right\} \tag{A.77}$$

The following relations are defined for a shorthand notation:

$$A(t) = -P_{\mathrm{g}}\hat{V}_{-}\left(i\hat{H}_{\mathrm{NH}}\right)^{-1}\tilde{\rho}^{(0)}(t)\,\hat{V}_{+}P_{\mathrm{g}} \tag{A.78}$$

$$B(t) = -P_{\mathrm{g}}\hat{V}_{-}\tilde{\rho}^{(0)}(t)\left(i\hat{H}_{\mathrm{NH}}^{\dagger}\right)^{-1}\hat{V}_{+}P_{\mathrm{g}} \tag{A.79}$$

$$C(t) = P_{\mathrm{g}}\sum_k \tilde{L}_k(t)\left(i\hat{H}_{\mathrm{NH}}\right)^{-1}\hat{V}_{+}\tilde{\rho}^{(0)}(t)\,\hat{V}_{-}\left(-i\hat{H}_{\mathrm{NH}}^{-1}\right)^{\dagger}\tilde{L}_k^{\dagger}(t)\,P_{\mathrm{g}} \tag{A.80}$$

It is useful to change the remaining operators back to the Schrödinger picture. The terms on the left hand side and the terms on the right hand side are treated separately separately for brevity. The left hand side of Eq. (A.77) is:

$$P_{\mathrm{g}}\dot{\tilde{\rho}}^{(2)}(t)\,P_{\mathrm{g}} = P_{\mathrm{g}}\left[\begin{array}{c}\dfrac{\mathrm{d}\hat{O}^{-1}(t)}{\mathrm{d}t}\rho^{(2)}\left(\hat{O}^{\dagger}(t)\right)^{-1} + \hat{O}^{-1}(t)\,\rho^{(2)}\dfrac{\mathrm{d}\left(\hat{O}^{\dagger}(t)\right)^{-1}}{\mathrm{d}t} \\ +\hat{O}^{-1}(t)\,\dot{\rho}^{(2)}\left(\hat{O}^{\dagger}(t)\right)^{-1}\end{array}\right]P_{\mathrm{g}} \tag{A.81}$$

$$= i\left(\hat{H}_{\mathrm{g}}\rho^{(0)} - \rho^{(0)}\hat{H}_{\mathrm{g}}\right) + \dot{\rho}^{(2)}\,, \tag{A.82}$$

where the relations $\hat{O}(t)\,P_{\mathrm{g}} \simeq P_{\mathrm{g}}$ and that $P_{\mathrm{g}}\hat{H}_0 P_{\mathrm{g}} = P_{\mathrm{g}}\hat{H}_{\mathrm{g}}P_{\mathrm{g}} + P_{\mathrm{g}}\hat{H}_{\mathrm{NH}}P_{\mathrm{g}} = \hat{H}_{\mathrm{g}}$ are needed in order to simplify the expression.
The first term on the right hand side of Eq. (A.77) is changed to the Schrödinger picture using $\hat{O}(t)\,P_{\mathrm{g}} \simeq P_{\mathrm{g}}$. It is useful to note that that $\hat{O}(t)$ commutes with $\hat{V}_-\hat{H}_{\mathrm{NH}}^{-1}\hat{V}_+$:

$$\hat{V}_-\hat{H}_{\mathrm{NH}}^{-1}\hat{V}_+ \propto |g\rangle\langle e|\cdot\left(\hat{H}_{\mathrm{e}} - \hat{L}_k^{\dagger}\hat{L}\right)^{-1}\cdot|e\rangle\langle g| \propto |g\rangle\langle e|e\rangle\langle e|e\rangle\langle g| = |g\rangle\langle g|\,. \tag{A.83}$$

Lindblad operators are proportional to $|g\rangle\langle e|$, which effectively gives $\hat{H}_{\mathrm{NH}} \propto |e\rangle\langle e|$. It is then easily seen that $\left[\hat{O}(t)\,,\hat{V}_-\hat{H}_{\mathrm{NH}}^{-1}\hat{V}_+\right] = 0$. The change to the Schrödinger picture can then be carried out:

$$A(t) = iP_{\mathrm{g}}\hat{V}_-\hat{H}_{\mathrm{NH}}^{-1}\hat{V}_+\hat{O}^{-1}(t)\,\rho^{(0)}\left(\hat{O}^{\dagger}(t)\right)^{-1}P_{\mathrm{g}} \tag{A.84}$$

$$= iP_{\mathrm{g}}\hat{O}^{-1}(t)\,\hat{V}_-\hat{H}_{\mathrm{NH}}^{-1}\hat{V}_+\rho^{(0)}\left(\hat{O}^{\dagger}(t)\right)^{-1}P_{\mathrm{g}} \tag{A.85}$$

$$\simeq iP_{\mathrm{g}}\hat{V}_-\hat{H}_{\mathrm{NH}}^{-1}\hat{V}_+\rho^{(0)}P_{\mathrm{g}}. \tag{A.86}$$

This expression is simplified by adding zero and splitting each term into two halves:

$$A(t) = iP_{\mathrm{g}}\hat{V}_-\hat{H}_{\mathrm{NH}}^{-1}\hat{V}_+\rho^{(0)}P_{\mathrm{g}} + iP_{\mathrm{g}}\hat{V}_-\left(\hat{H}_{\mathrm{NH}}^{-1}\right)^{\dagger}\hat{V}_+\rho^{(0)}P_{\mathrm{g}} - iP_{\mathrm{g}}\hat{V}_-\left(\hat{H}_{\mathrm{NH}}^{-1}\right)^{\dagger}\hat{V}_+\rho^{(0)}P_{\mathrm{g}} \tag{A.87}$$

$$= \frac{i}{2}P_{\mathrm{g}}\hat{V}_-\left[\hat{H}_{\mathrm{NH}}^{-1} + \left(\hat{H}_{\mathrm{NH}}^{-1}\right)^{\dagger}\right]\hat{V}_+\rho^{(0)}P_{\mathrm{g}} + \frac{i}{2}P_{\mathrm{g}}\hat{V}_-\left[\hat{H}_{\mathrm{NH}}^{-1} - \left(\hat{H}_{\mathrm{NH}}^{-1}\right)^{\dagger}\right]\hat{V}_+\rho^{(0)}P_{\mathrm{g}} \tag{A.88}$$

$$= -iP_{\mathrm{g}}\hat{H}'_{\mathrm{eff}}\rho^{(0)}P_{\mathrm{g}} + \frac{i}{2}P_{\mathrm{g}}\hat{V}_-\left[\hat{H}_{\mathrm{NH}}^{-1} - \left(\hat{H}_{\mathrm{NH}}^{-1}\right)^{\dagger}\right]\hat{V}_+\rho^{(0)}P_{\mathrm{g}}, \tag{A.89}$$

where $\hat{H}'_{\text{eff}} \equiv -\frac{1}{2}\hat{V}_- \left[\hat{H}_{\text{NH}}^{-1} + \left(\hat{H}_{\text{NH}}^{-1}\right)^\dagger\right] \hat{V}_+$. The last term in Eq. (A.89) is rewritten by multiplying by $\mathbb{1}$. In the following, any factor in a bracket multiplies to $\mathbb{1}$:

$$i\hat{V}_- \left[\hat{H}_{\text{NH}}^{-1} - \left(\hat{H}_{\text{NH}}^{-1}\right)^\dagger\right] \hat{V}_+ = \hat{V}_- \left[\left[\left(\hat{H}_{\text{NH}}^{-1}\right)^\dagger \left(\hat{H}_{\text{NH}}\right)^\dagger\right] \left[\hat{H}_{\text{NH}}^{-1}\hat{H}_{\text{NH}}\right] \hat{H}_{\text{NH}}^{-1} - \left(\hat{H}_{\text{NH}}^{-1}\right)^\dagger \left[\hat{H}_{\text{NH}}\hat{H}_{\text{NH}}^{-1}\right]\right] \hat{V}_+ \tag{A.90}$$

$$= i\hat{V}_- \left[\left(\hat{H}_{\text{NH}}^{-1}\right)^{-1} \cdot \left(\hat{H}_{\text{NH}}^{-1}\right)^\dagger \cdot \hat{H}_{\text{NH}}^{-1} - \left(\hat{H}_{\text{NH}}^{-1}\right)^{-1} \cdot \hat{H}_{\text{NH}} \cdot \hat{H}_{\text{NH}}^{-1}\right] \hat{V}_+ \tag{A.91}$$

$$= i\hat{V}_- \left(\hat{H}_{\text{NH}}^{-1}\right)^{-1} \left[\left(\hat{H}_{\text{e}} + \frac{i}{2}\sum_k \hat{L}_k^\dagger \hat{L}_k\right) - \left(\hat{H}_{\text{e}} - \frac{i}{2}\sum_k \hat{L}_k^\dagger \hat{L}_k\right)\right] \hat{H}_{\text{NH}}^{-1}\hat{V}_+ \tag{A.92}$$

$$= -\sum_k \hat{V}_- \left(\hat{H}_{\text{NH}}^{-1}\right)^{-1} \hat{L}_k^\dagger \hat{L}_k \hat{H}_{\text{NH}}^{-1}\hat{V}_+ \tag{A.93}$$

$$= -\sum_k \left(\hat{L}_{\text{eff}}^k\right)^\dagger \hat{L}_{\text{eff}}^k, \tag{A.94}$$

where the effective Lindblad operator is defined:

$$\hat{L}_{\text{eff}}^k \equiv \sum_k \hat{V}_- \hat{H}_{\text{NH}}^{-1} \hat{L}_k. \tag{A.95}$$

Eq. (A.89) can then be written as:

$$A\left(t\right) = -i\hat{H}'_{\text{eff}}\rho^{(0)} - \frac{1}{2}\sum_k \left(\hat{L}_{\text{eff}}^k\right)^\dagger \hat{L}_{\text{eff}}^k \rho^{(0)}. \tag{A.96}$$

Note that the time dependence vanishes. The second term on the right hand side of Eq. (A.77) is the Hermition conjugate of Eq. (A.96):

$$B\left(t\right) = i\rho^{(0)}\hat{H}'_{\text{eff}} - \frac{1}{2}\sum_k \rho^{(0)} \left(\hat{L}_{\text{eff}}^k\right)^\dagger \hat{L}_{\text{eff}}^k. \tag{A.97}$$

The third term on the right hand side of Eq. A.77 is rewritten by changing $\tilde{L}_{\text{eff}}^k\left(t\right)$ and $\tilde{\rho}^{(0)}\left(t\right)$ to the Schrödinger picture and by using that $\left[\hat{O}\left(t\right), \hat{V}_-\hat{H}_{\text{NH}}^{-1}\hat{V}_+\right] = 0$. This gives:

$$C\left(t\right) = P_{\text{g}} \sum_k \hat{O}^{-1}\left(t\right) \hat{L}_k \hat{O}\left(t\right) \left(i\hat{H}_{\text{NH}}\right)^{-1} \hat{V}_+ \hat{O}^{-1}\left(t\right) \rho^{(0)} \left(\hat{O}^{-1}\left(t\right)\right)^\dagger \hat{V}_- \left(-i\hat{H}_{\text{NH}}^{-1}\right)^\dagger \hat{O}^\dagger\left(t\right) \hat{L}_k^\dagger \left(\hat{O}^{-1}\left(t\right)\right)^\dagger P_{\text{g}} \tag{A.98}$$

$$\simeq P_{\text{g}} \sum_k \hat{L}_k \left(i\hat{H}_{\text{NH}}\right)^{-1} \hat{V}_+ \rho^{(0)} \hat{V}_- \left(-i\hat{H}_{\text{NH}}^{-1}\right)^\dagger \hat{L}_k^\dagger P_{\text{g}} \tag{A.99}$$

$$= \sum_k \hat{L}_{\text{eff}}^k \rho^{(0)} \left(\hat{L}_{\text{eff}}^k\right)^\dagger, \tag{A.100}$$

where the same definition for the effective Lindblad operator has been used as above. Eqs. (A.96), (A.97) and (A.100) for the right hand side of Eq. A.77 can now be collected together. An effective

equation for the time evolution for the reduced density operator of second order can be found by using Eq. (**??**) for the left hand side:

$$i\left[\hat{H}_{\mathrm{g}},\rho^{(0)}\right]+\dot{\rho}^{(2)}=\left\{\begin{array}{c}-i\left[\hat{H}'_{\mathrm{eff}},\rho^{(0)}\right]+\sum_k \hat{L}^k_{\mathrm{eff}}\rho^{(0)}\left(\hat{L}^k_{\mathrm{eff}}\right)^\dagger \\ -\frac{1}{2}\sum_k\left(\hat{L}^k_{\mathrm{eff}}\right)^\dagger\hat{L}^k_{\mathrm{eff}}\rho^{(0)}-\rho^{(0)}\frac{1}{2}\sum_k\left(\hat{L}^k_{\mathrm{eff}}\right)^\dagger\hat{L}^k_{\mathrm{eff}}\end{array}\right\} \tag{A.101}$$

This gives an effective equation of motion for the ground states

$$\dot{\rho}^{(2)}=-i\left[H_{\mathrm{eff}},\rho^{(0)}\right]+\sum_k\left(\hat{L}^k_{\mathrm{eff}}\rho^{(0)}\left(\hat{L}^k_{\mathrm{eff}}\right)^\dagger-\frac{1}{2}\left(\hat{L}^k_{\mathrm{eff}}\right)^\dagger\hat{L}^k_{\mathrm{eff}}\rho^{(0)}+\rho^{(0)}\left(\hat{L}^k_{\mathrm{eff}}\right)^\dagger\hat{L}^k_{\mathrm{eff}}\right), \tag{A.102}$$

where the effective Hamiltonian is defined as:

$$\hat{H}_{\mathrm{eff}}=\hat{H}'_{\mathrm{eff}}+\hat{H}_{\mathrm{g}}=-\frac{1}{2}\hat{V}_-\left[\hat{H}^{-1}_{\mathrm{NH}}+\left(\hat{H}^{-1}_{\mathrm{NH}}\right)^\dagger\right]\hat{V}_++\hat{H}_{\mathrm{g}}. \tag{A.103}$$

Eq. (A.101) is of the standard Lindblad form with the effective Hamiltonian $\hat{H}_{\mathrm{eff}}$ and effective Lindblad operator $\hat{L}^k_{\mathrm{eff}}$. These Lindblad operators describe second-order decay processes. Each consist of a weak excitation $\hat{V}_+$, an evolution between the excited states through $\hat{H}_{\mathrm{NH}}$ and subsequent decay $\hat{L}_k$.

Appendix B

Calculation of Effective Operators

The system considered in the thesis is governed by the non-hermitian Hamiltonian $\hat{H}_{\mathrm{NH}}$ that take both coherent and dissipative evolution of the quantum states into account. This Hamiltonian can be split into four different non-Hermitian Hamiltonians, depending on the number of qubits in state $|1\rangle_{\mathrm{q}}$:

$$\hat{H}_{\mathrm{NH}}\Big|_{n=2} = \begin{array}{c} \\ |11E\rangle \\ |e1f\rangle \\ |1ef\rangle \end{array} \begin{array}{c} \langle 11E| \\ \begin{pmatrix} \Delta_{\mathrm{A}} - \frac{i}{2}\left(\gamma_A^{1\mathrm{D}} + \gamma'\right) & -\frac{i}{2}\gamma_{Aq}^{1\mathrm{D}} & -\frac{i}{2}\gamma_{Aq}^{1\mathrm{D}} \\ -\frac{i}{2}\gamma_{Aq}^{1\mathrm{D}} & \delta_{\mathrm{q_1}} - \frac{i}{2}\left(\gamma_{q_1}^{1\mathrm{D}} + \gamma'\right) & -\frac{i}{2}\gamma_{qq}^{1\mathrm{D}} \\ -\frac{i}{2}\gamma_{Aq}^{1\mathrm{D}} & -\frac{i}{2}\gamma_{qq}^{1\mathrm{D}} & \delta_{\mathrm{q_1}} - \frac{i}{2}\left(\gamma_{q_2}^{1\mathrm{D}} + \gamma'\right) \end{pmatrix} \end{array} \begin{array}{c} \\ \langle e1f| \\ \\ \\ \\ \\ \end{array} \begin{array}{c} \\ \langle 1ef| \\ \\ \\ \\ \\ \end{array} \tag{B.1}$$

$$\hat{H}_{\mathrm{NH}}\Big|_{n=1,q_1} = \begin{array}{c} \\ |10E\rangle \\ |e0f\rangle \end{array} \begin{array}{c} \langle 10E| \\ \begin{pmatrix} \Delta_{\mathrm{A}} - \frac{i}{2}\left(\gamma_A^{1\mathrm{D}} + \gamma'\right) & -\frac{i}{2}\gamma_{Aq}^{1\mathrm{D}} \\ -\frac{i}{2}\gamma_{Aq}^{1\mathrm{D}} & \delta_{\mathrm{q_1}} - \frac{i}{2}\left(\gamma_{q_1}^{1\mathrm{D}} + \gamma'\right) \end{pmatrix} \end{array} \begin{array}{c} \\ \langle e0f| \\ \\ \\ \end{array} \tag{B.2}$$

$$\hat{H}_{\mathrm{NH}}\Big|_{n=1,q_2} = \begin{array}{c} \\ |01E\rangle \\ |0ef\rangle \end{array} \begin{array}{c} \langle 01E| \\ \begin{pmatrix} \Delta_{\mathrm{A}} - \frac{i}{2}\left(\gamma_A^{1\mathrm{D}} + \gamma'\right) & -\frac{i}{2}\gamma_{Aq}^{1\mathrm{D}} \\ -\frac{i}{2}\gamma_{Aq}^{1\mathrm{D}} & \delta_{\mathrm{q_2}} - \frac{i}{2}\left(\gamma_{q_2}^{1\mathrm{D}} + \gamma'\right) \end{pmatrix} \end{array} \begin{array}{c} \\ \langle 0ef| \\ \\ \\ \end{array} \tag{B.3}$$

$$\hat{H}_{\mathrm{NH}}\Big|_{n=0} = \left(\Delta_{\mathrm{A}} - \frac{i}{2}\left(\gamma_A^{1\mathrm{D}} + \gamma'\right)\right)|00E\rangle\langle 00E| \tag{B.4}$$

and includes the cases where either two, one or no qubit states are optically connected to the waveguide. Here $\gamma'_{\mathrm{A,q}}$ is the decay rate into the wave gudie for the auxiliary emiiter or for a qubit emitter, respectively. γ' is the nonradiative decay rate while γ_{Aq} and γ_{qq} are the two-emitter decay rates between the auxiliary- and qubit emitters, and between the two qubit emitters respectively. These rates are for decay into the guided mode in the waveguide Δ_{A} and δ_{q} are the detuning of the auxiliary and qubit emitters. The evolution of the system can be simplified using adiabatic elimination, which results in the effective master equation:

$$\dot{\rho} = -i\left[\hat{H}_{\mathrm{eff}}, \rho(t)\right] + \sum_{k,l}\hat{L}_{\mathrm{eff}}^{k}\rho(t)\left(\hat{L}_{\mathrm{eff}}^{l}\right)^{\dagger} - \frac{1}{2}\sum_{k,l}\left[\left(\hat{L}_{\mathrm{eff}}^{k}\right)^{\dagger}\hat{L}_{\mathrm{eff}}^{l}\rho(t) + \rho(t)\left(\hat{L}_{\mathrm{eff}}^{k}\right)^{\dagger}\hat{L}_{\mathrm{eff}}^{l}\right] \tag{B.5}$$

$$\hat{H}_{\mathrm{eff}} = -\frac{1}{2}\hat{V}_{-}\left[\hat{H}_{\mathrm{NH}}^{-1} + \left(\hat{H}_{\mathrm{NH}}^{-1}\right)^{\dagger}\right]\hat{V}_{+} + \hat{H}_{\mathrm{g}} \tag{B.6}$$

$$\hat{L}_{\mathrm{eff}}^{k} = \hat{L}_k\hat{H}_{\mathrm{NH}}^{-1}\hat{V}_{+}. \tag{B.7}$$

B.1 Two qubits in the ground state

The calculations for deriving the effective operators in Eqs. (B.6) and (B.7) are shown below in the ideal case where the coupling constants of the three emitters are equal, the detuning of the two qubit emitters are $\delta_{q_1} = 0$ and the emitters are placed in the constructive interference zones to maximize the effects of superradiance. This causes all the decay rates to the guided mode in Eqs. (B.1) trough (B.4) to be equal to γ_A and will be denote γ^{1D} throughout this section.
The inverse of $\hat{H}_{NH}$ can then be calculated, where the each element is given by:

$$\hat{H}_{NH}^{-1}[k,l] = \frac{(-1)^{k+l} \cdot \det\left(\hat{H}_{NH,k,l}\right)}{\det\left(\hat{H}_{NH}\right)}, \tag{B.8}$$

where det is the determinant and $\hat{H}_{NH,k,l}$ is the complimentary matrix to the matrix element $\hat{H}_{NH}[k,l]$. The only relevant contribution to the dynamics of the gate comes from three matrix elements in the first row contribute, as these are the terms that $\hat{V}_+$ picks out. These terms can be formally extracted using the projection operator $\hat{P}_2 = |11\rangle_q \langle 11|$. The three terms are:

$$\hat{H}_{NH,j}^{-1}[1,1] = \frac{2\left(2\gamma^{1D} + \gamma'\right)}{2\Delta_A\left[2\gamma^{1D} + \gamma'\right] - i\left[3\gamma^{1D}\gamma' + \gamma'^2\right]} |E\rangle_A \langle E| \otimes |11\rangle_q \langle 11| \tag{B.9}$$

$$= \frac{2\left(\gamma^{1D} + \gamma'\right)\left[2\Delta_A\left(2\gamma^{1D} + \gamma'\right) + i\left(3\gamma^{1D}\gamma' + \gamma'^2\right)\right]}{4\Delta_A^2\left[2\gamma^{1D} + \gamma'\right]^2 + \left[3\gamma^{1D}\gamma' + \gamma'^2\right]^2} |E\rangle_A \langle E| \otimes |11\rangle_q \langle 11| \tag{B.10}$$

$$\tag{B.11}$$

$$= \frac{1}{\gamma'} \frac{2(2C+1)\left[2\frac{\Delta_A}{\gamma'}(2C+1) + i(3C+1)\right]}{\left(2\frac{\Delta_A}{\gamma'}\right)^2 [2C+1]^2 + [3C+1]^2} |E\rangle_A \langle E| \otimes |11\rangle_q \langle 11| \tag{B.12}$$

$$\hat{H}_{NH,j}^{-1}[2,1] = -\frac{2\gamma^{1D}}{2\Delta_A\left[2\gamma^{1D} + \gamma\right] - i\left[3\gamma^{1D}\gamma' + \gamma'^2\right]} |f\rangle_A \langle E| \otimes |e1\rangle_q \langle 11| \tag{B.13}$$

$$\tag{B.14}$$

$$= -\frac{1}{\gamma'} \frac{2C\left[2\frac{\Delta_A}{\gamma'}(2C+1) + i(3C+1)\right]}{\left(2\frac{\Delta_A}{\gamma'}\right)^2 [2C+1]^2 + [3C+1]^2} |f\rangle_A \langle E| \otimes |e1\rangle_q \langle 11| \tag{B.15}$$

$$\hat{H}_{NH,j}^{-1}[3,1] = -\frac{2\gamma^{1D}}{2\Delta_A\left[2\gamma^{1D} + \gamma'\right] - i\left[3\gamma^{1D}\gamma' + \gamma'^2\right]} |f\rangle_A \langle E| \otimes |1e\rangle_q \langle 11| \tag{B.16}$$

$$\tag{B.17}$$

$$= -\frac{1}{\gamma'} \frac{2C\left[2\frac{\Delta_A}{\gamma'}(2C+1) + i(3C+1)\right]}{\left(2\frac{\Delta_A}{\gamma'}\right)^2 [2C+1]^2 + [3C+1]^2} |f\rangle_A \langle E| \otimes |1e\rangle_q \langle 11|, \tag{B.18}$$

where the cooperativity $C = \gamma^{1D}/\gamma'$ has been introduced. The cooperativity is related to the $\beta-$factor introduced in Section (3.1.2) by:

$$C = \frac{1}{\beta^{-1} - 1}. \tag{B.19}$$

Only Eq. (B.12) is needed to calculate the effective Hamiltonian:

$$\hat{H}_{\text{eff},2} = -\frac{1}{2}\hat{V}_{-}\left[\hat{H}_{\text{NH}}^{-1} + \left(\hat{H}_{\text{NH}}^{-1}\right)^{\dagger}\right]\hat{V}_{+} \tag{B.20}$$

$$= \Delta_2 \left|\mathrm{g}\right\rangle_{\mathrm{A}} \langle g| \otimes \hat{P}_2, \tag{B.21}$$

where the energy shift Δ_2 is defined as:

$$\Delta_2 = -\frac{\Omega^2}{\gamma'}\frac{\Delta_{\mathrm{A}}}{\gamma'}\frac{(2C+1)^2}{\left(2\frac{\Delta_{\mathrm{A}}}{\gamma'}\right)^2(2C+1)^2 + (3C+1)^2}. \tag{B.22}$$

The effective Lindblad operators are readily calculated:

$$\hat{L}_{\text{eff}}^{\mathrm{A},2} = \hat{L}^{\mathrm{A},2}\hat{H}_{\text{NH}}^{-1}\hat{V}_{+} = r_{\mathrm{A},2}\left|\mathrm{f}\right\rangle_{\mathrm{A}}\langle \mathrm{g}| \otimes \hat{P}_2 \tag{B.23}$$

$$\hat{L}_{\text{eff}}^{\mathrm{q_j},2} = \hat{L}^{\mathrm{q_j},2}\hat{H}_{\text{NH}}^{-1}\hat{V}_{+} = r_{\mathrm{q_j},2}\left|\mathrm{f}\right\rangle_{\mathrm{A}}\langle \mathrm{g}| \otimes \hat{P}_2, j = 1, 2, \tag{B.24}$$

where the Lindblad coefficients for the decay of the auxiliary emitter $r_{\mathrm{A},2}$ and the qubits $r_{\mathrm{q}_j,2}$ are given by:

$$r_{\mathrm{A},2} = \sqrt{\gamma^{1\mathrm{D}} + \gamma'}\frac{\Omega}{\gamma'}\frac{(2C+1)\left[2\frac{\Delta_{\mathrm{A}}}{\gamma'}(2C+1) + i(3C+1)\right]}{\left(2\frac{\Delta_{\mathrm{A}}}{\gamma'}\right)^2[2C+1]^2 + [3C+1]^2} \tag{B.25}$$

$$r_{\mathrm{q}_j,2} = -\sqrt{\gamma^{1\mathrm{D}}}\frac{\Omega}{\gamma'}\frac{C\left[2\frac{\Delta_{\mathrm{A}}}{\gamma'}(2C+1) + i(3C+1)\right]}{\left(2\frac{\Delta_{\mathrm{A}}}{\gamma'}\right)^2[2C+1]^2 + [3C+1]^2}. \tag{B.26}$$

Note that $r_{\mathrm{q}_1,2} = r_{\mathrm{q}_2,2}$ in this ideal case.

B.1.1 One qubit in the ground state

The two 2×2 sub matrices in Eqs. (B.2) ans (B.3) represent the case when only the first or the second qubit is in the optical ground state. These two sub matrices are, in the ideal case considered here, equal. The two terms that are picked out by $\hat{V}_{+}$ are:

$$\hat{H}_{\text{NH},j}^{-1}[k,k] = \frac{2\left(\gamma^{1\mathrm{D}} + \gamma'\right)}{2\Delta_{\mathrm{A}}\left[\gamma^{1\mathrm{D}} + \gamma'\right] - i\left[\gamma^{1\mathrm{D}}\gamma' + \gamma'^2\right]}\left|\mathrm{E}\right\rangle_{\mathrm{A}}\langle \mathrm{E}| \otimes \hat{P}_{1\mathrm{j}} \tag{B.27}$$

$$= \frac{2\left(\gamma^{1\mathrm{D}} + \gamma'\right)\left[2\Delta_{\mathrm{A}}/\gamma'\left(\gamma^{1\mathrm{D}} + \gamma'\right) + i\left(2\gamma^{1\mathrm{D}} + \gamma'\right)\right]}{4\Delta_{\mathrm{A}}^2\left[\gamma^{1\mathrm{D}} + \gamma'\right]^2 + \left(2\gamma^{1\mathrm{D}} + \gamma'\right)^2}\left|\mathrm{E}\right\rangle_{\mathrm{A}}\langle \mathrm{E}| \otimes \hat{P}_{1\mathrm{j}} \tag{B.28}$$

$$= \frac{1}{\gamma'}\frac{2(C+1)\left[2\Delta_{\mathrm{A}}/\gamma'(C+1) + i(2C+1)\right]}{\left(2\frac{\Delta_{\mathrm{A}}}{\gamma'}\right)^2[C+1]^2 + [2C+1]^2}\left|\mathrm{E}\right\rangle_{\mathrm{A}}\langle \mathrm{E}| \otimes \hat{P}_{1\mathrm{j}} \tag{B.29}$$

$$\hat{H}_{\text{NH},j}^{-1}[k+1,k] = -\frac{2\gamma^{1\mathrm{D}}}{2\Delta_{\mathrm{A}}\left[\gamma^{1\mathrm{D}} + \gamma'\right] - i\left[\gamma^{1\mathrm{D}}\gamma' + \gamma'^2\right]}\left|\mathrm{f}\right\rangle_{\mathrm{A}}\langle \mathrm{E}| \otimes \left|\{\mathrm{e_j}\}\right\rangle_{\mathrm{q_j}}\langle\{1_{\mathrm{j}}\}| \tag{B.30}$$

$$= -\frac{1}{\gamma'}\frac{2C\left[(2\Delta_{\mathrm{A}}/\gamma')(C+1) + i(2C+1)\right]}{\left(2\frac{\Delta_{\mathrm{A}}}{\gamma'}\right)^2[C+1]^2 + [2C+1]^2}\left|\mathrm{f}\right\rangle_{\mathrm{A}}\langle \mathrm{E}| \otimes \left|\{\mathrm{e_j}\}\right\rangle_{\mathrm{q_j}}\langle\{1_{\mathrm{j}}\}|, \tag{B.31}$$

where $\hat{P}_{1\mathrm{j}}$ is the projection operator when only qubit j is in the grounds state, $|\{\mathrm{e_j}\}\rangle_{\mathrm{q_j}}$ ($|\{1\}\rangle_{\mathrm{q_j}}$) is the excited state (optical ground state) for qubit j with the other qubit in state $|0\rangle$. The effective Hamiltonian is in this case given by:

$$\hat{H}_{\mathrm{eff},1j} = \Delta_1 |\mathrm{g}\rangle_{\mathrm{A}} \langle \mathrm{g}| \otimes \hat{P}_{1,\mathrm{j}}, \tag{B.32}$$

with the coefficient:

$$\Delta_1 = -\frac{\Omega^2}{\gamma'}\frac{\Delta_{\mathrm{A}}}{\gamma'}\frac{(C+1)^2}{\left(2\frac{\Delta_{\mathrm{A}}}{\gamma'}\right)^2[C+1]^2 + [2C+1]^2}. \tag{B.33}$$

The Lindblad operators are given by:

$$\hat{L}_{\mathrm{eff}}^{\mathrm{A},1j} = \hat{L}^{\mathrm{A},1j}\hat{H}_{\mathrm{NH}}^{-1}\hat{V}_+ = r_{\mathrm{A},1j} |\mathrm{f}\rangle_{\mathrm{A}} \langle \mathrm{g}| \otimes \hat{P}_{1\mathrm{j}} \tag{B.34}$$

$$\hat{L}_{\mathrm{eff}}^{\mathrm{q_j},1} = \hat{L}^{\mathrm{q_j},1}\hat{H}_{\mathrm{NH}}^{-1}\hat{V}_+ = r_{\mathrm{q_j},1} |\mathrm{f}\rangle_{\mathrm{A}} \langle \mathrm{g}| \otimes \hat{P}_{1\mathrm{j}}, \tag{B.35}$$

with coefficients

$$r_{\mathrm{A},1} = \sqrt{\gamma^{1\mathrm{D}} + \gamma'}\frac{\Omega}{\gamma'}\frac{(C+1)\left[2\Delta_{\mathrm{A}}/\gamma'\,(C+1) + i\,(2C+1)\right]}{\left(2\frac{\Delta_{\mathrm{A}}}{\gamma'}\right)^2[C+1]^2 + [2C+1]^2} \tag{B.36}$$

$$r_{\mathrm{qj},1} = -\sqrt{\gamma^{1\mathrm{D}}}\frac{\Omega}{\gamma'}\frac{C\left[(2\Delta_{\mathrm{A}}/\gamma')\,(C+1) + i\,(2C+1)\right]}{\left(2\frac{\Delta_{\mathrm{A}}}{\gamma'}\right)^2[C+1]^2 + [2C+1]^2}. \tag{B.37}$$

B.1.2 No qubits in the ground state

This case is particularly simple, as it only involves the single element in Eq. (B.4). The inverse is then

$$\hat{H}_{\mathrm{NH},j}^{-1}[1,1] = \frac{2}{2\Delta_{\mathrm{A}} - i\left[\gamma^{1\mathrm{D}} + \gamma'\right]} |\mathrm{E}\rangle_{\mathrm{A}} \langle \mathrm{E}| \otimes \hat{P}_0 \tag{B.38}$$

$$= \frac{2\left(2\Delta_{\mathrm{A}} + i\left[\gamma^{1\mathrm{D}} + \gamma'\right]\right)}{4\Delta_{\mathrm{A}}^2 + \left[\gamma^{1\mathrm{D}} + \gamma'\right]^2} |\mathrm{E}\rangle_{\mathrm{A}} \langle \mathrm{E}| \otimes \hat{P}_0 \tag{B.39}$$

$$= \frac{2}{\gamma'}\frac{2\frac{\Delta_{\mathrm{A}}}{\gamma'} + i\,[C+1]}{\left(2\frac{\Delta_{\mathrm{A}}}{\gamma'}\right)^2 + [C+1]^2} |\mathrm{E}\rangle_{\mathrm{A}} \langle \mathrm{E}| \otimes \hat{P}_0. \tag{B.40}$$

The corresponding matrix element for the effective Hamiltonian is:

$$\hat{H}_{\mathrm{eff},0} = \Delta_0 |\mathrm{g}\rangle_{\mathrm{A}} \langle \mathrm{g}| \otimes \hat{P}_0, \tag{B.41}$$

where the coefficient is defined as:

$$\Delta_0 = -\frac{\Omega^2}{\gamma'}\frac{\Delta_{\mathrm{A}}}{\gamma'}\frac{1}{\left(2\frac{\Delta_{\mathrm{A}}}{\gamma'}\right)^2 + (C+1)^2}. \tag{B.42}$$

The single Lindblad operator is in this case given by:

$$\hat{L}_{\mathrm{eff}}^{\mathrm{A},0} = \hat{L}^{\mathrm{A},0}\hat{H}_{\mathrm{NH}}^{-1}\hat{V}_+ = r_{\mathrm{A},0} |\mathrm{f}\rangle_{\mathrm{A}} \langle \mathrm{g}| \otimes \hat{P}_0, \tag{B.43}$$

where

$$r_{\mathrm{A},0} = \sqrt{\gamma^{1\mathrm{D}} + \gamma'}\frac{\Omega}{\gamma'}\frac{2\frac{\Delta_\mathrm{A}}{\gamma'} + i\left(C+1\right)}{\left(2\frac{\Delta_\mathrm{A}}{\gamma'}\right)^2 + \left[C+1\right]^2}. \tag{B.44}$$

These effective operators derived above can be written in a compact by summing over the number n of qubits in the ground state:

$$\hat{H}_{\mathrm{eff}} = \sum_{n=0}^{2} -\frac{\Omega^2}{\gamma'}\frac{\Delta_\mathrm{A}}{\gamma'}\frac{\left(nC+1\right)^2}{\left(2\frac{\Delta_\mathrm{A}}{\gamma'}\right)^2\left(nC+1\right)^2 + \left(\left[n+1\right]C+1\right)^2}\left|\mathrm{g}\right\rangle_\mathrm{A}\left\langle\mathrm{g}\right| \otimes \hat{P}_\mathrm{n} \tag{B.45}$$

$$= \sum_{n=0}^{2} \Delta_n \left|\mathrm{g}\right\rangle_\mathrm{A}\left\langle\mathrm{g}\right| \otimes \hat{P}_\mathrm{n} \tag{B.46}$$

$$\hat{L}_{\mathrm{eff}}^{A} = \sum_{n=0}^{2} \sqrt{C+1}\frac{\Omega}{\sqrt{\gamma'}}\left(nC+1\right)\frac{2\frac{\Delta_\mathrm{A}}{\gamma'}\left(nC+1\right) + i\left(\left[n+1\right]C+1\right)}{\left(2\frac{\Delta_\mathrm{A}}{\gamma'}\right)^2\left(nC+1\right)^2 + \left(\left[n+1\right]C+1\right)^2}\left|\mathrm{f}\right\rangle_\mathrm{A}\left\langle\mathrm{g}\right| \otimes \hat{P}_\mathrm{n} \tag{B.47}$$

$$= \sum_{n=0}^{2} r_{\mathrm{A},n}\left|\mathrm{f}\right\rangle_\mathrm{A}\left\langle\mathrm{g}\right| \otimes \hat{P}_\mathrm{n} \tag{B.48}$$

$$\hat{L}_{\mathrm{eff}}^{q_j} = \sum_{n=1}^{2} -\sqrt{C}\frac{\Omega}{\sqrt{\gamma'}}C\frac{2\frac{\Delta_\mathrm{A}}{\gamma'}\left(nC+1\right) + i\left(\left[n+1\right]C+1\right)}{\left(2\frac{\Delta_\mathrm{A}}{\gamma'}\right)^2\left(nC+1\right)^2 + \left(\left[n+1\right]C+1\right)^2}\left|\mathrm{f}\right\rangle_\mathrm{A}\left\langle\mathrm{g}\right| \otimes \hat{P}_\mathrm{n} \tag{B.49}$$

$$= \sum_{n=1}^{2} r_{\mathrm{q}_j,n}\left|\mathrm{f}\right\rangle_\mathrm{A}\left\langle\mathrm{g}\right| \otimes \hat{P}_\mathrm{n} \tag{B.50}$$

B.1.3 Inclusion of $\delta_{\mathrm{q_j}}$

The coefficients for the effective operators for $\hat{H}_{\mathrm{eff}}$, $\hat{L}_{\mathrm{eff}}^{A}$ and $\hat{L}_{\mathrm{eff}}^{q_j}$ for a non-zero qubit detuning $\delta_{\mathrm{q_j}}$ will be listed below under the assumption that $\delta_{\mathrm{q_1}} = \delta_{\mathrm{q_2}}$. The calculations follow the same procedure as in the preceding section. Only the operators for $n = 2$ and $n = 1$ will be shown, as the $n = 0$ case is unchanged:

$$\Delta_{n>0} = \frac{-\frac{\Omega^2}{\gamma'}\left[\tilde{\Delta}_\mathrm{A}\left(nC+1\right)^2 + \tilde{\delta}_\mathrm{q}\left(4\tilde{\Delta}_\mathrm{A}\delta_\mathrm{q} + nC^2\right)\right]}{\left(2\tilde{\Delta}_\mathrm{A}\right)^2\left(nC+1\right)^2 + \left(\left[n+1\right]C+1\right)^2 + 8n\tilde{\Delta}_\mathrm{a}\tilde{\delta}_\mathrm{q}C^2 + \left[16\tilde{\Delta}_\mathrm{A}^2 + 4\left(C+1\right)^2\right]\tilde{\delta}_\mathrm{q}^2} \tag{B.51}$$

$$r_{\mathrm{A},n>0} = \frac{\frac{\Omega\sqrt{C+1}}{\sqrt{\gamma'}}\left[\left(nC+1\right)\cdot\alpha_n\left(C\right) + 2\tilde{\delta}_\mathrm{q}\left[4\tilde{\delta}_\mathrm{q} + nC^2\right] + 4i\left(C+1\right)\tilde{\delta}_\mathrm{q}^2\right]}{\left(2\tilde{\Delta}_\mathrm{A}\right)^2\left(nC+1\right)^2 + \left(\left[n+1\right]C+1\right)^2 + 8n\tilde{\Delta}_\mathrm{a}\tilde{\delta}_\mathrm{q}C^2 + \left[16\tilde{\Delta}_\mathrm{A}^2 + 4\left(C+1\right)^2\right]\tilde{\delta}_\mathrm{q}^2} \tag{B.52}$$

$$r_{\mathrm{q}_j,n} = \frac{-\frac{\Omega\sqrt{C}C}{\sqrt{\gamma'}}\left(\left[2\tilde{\Delta}_\mathrm{A}\left(nC+1\right)^2 + i\left(\left[n+1\right]C+1\right)\right] + 2\tilde{\delta}_\mathrm{q}C\left[1+C+2i\tilde{\Delta}_\mathrm{A}\right]\right)}{\left(2\tilde{\Delta}_\mathrm{A}\right)^2\left(nC+1\right)^2 + \left(\left[n+1\right]C+1\right)^2 + 8n\tilde{\Delta}_\mathrm{a}\tilde{\delta}_\mathrm{q}C^2 + \left[16\tilde{\Delta}_\mathrm{A}^2 + 4\left(C+1\right)^2\right]\tilde{\delta}_\mathrm{q}^2} \tag{B.53}$$

where α_n in Eq. (B.52) is defined as:

$$\alpha_n\left(C,n\right) = 2\tilde{\Delta}_\mathrm{A}\left(nC+1\right) + i\left(\left[n+1\right]C+1\right) \tag{B.54}$$

The Lindblad coefficients in Eqs. (B.52) and (B.53) result in the following effective decay rates:

$$\Gamma_{n>0} = \frac{\Omega^2}{\gamma'} \frac{4C\left[\tilde{\delta}_{\mathrm{q}}^2 + nC\right]}{\left(2\tilde{\Delta}_{\mathrm{A}}\right)^2 (nC+1)^2 + ([n+1]\,C+1)^2 + 8n\tilde{\Delta}_{\mathrm{a}}\tilde{\delta}_{\mathrm{q}}C^2 + \left[16\tilde{\Delta}_{\mathrm{A}}^2 + 4\,(C+1)^2\right]\tilde{\delta}_{\mathrm{q}}^2}. \tag{B.55}$$

B.2 Variable Qubit Dipole Moments & Positions

The coefficients will be listed below for a non-zero qubit detuning $\delta_{\mathrm{q_j}}$ and where the dipole moments for the qubit emitters differ from the auxiliary emitter by:

$$d_{\mathrm{q_1}} = \kappa d_{\mathrm{A}}, \quad d_{\mathrm{q_2}} = \eta d_{\mathrm{A}}, \tag{B.56}$$

and where the n'th qubit can be displaced from its ideal position by $\delta x_{\mathrm{q,n}}$. This results in the following expressions for the energy shifts Δ_n and decay rates Γ_n, for $n > 0$:

$$\Delta_{n>0} = -\frac{\Omega^2}{\gamma'} \frac{4\tilde{\Delta}_{\mathrm{A}}\tilde{\delta}_{\mathrm{q}}^2 + \left[b_{H,n}\left(\delta x_{\mathrm{q},1}, \delta x_{\mathrm{q},2}, \kappa, \eta\right) C^3 + f_{H,n}\left(\kappa,\eta\right) C^2\right]\tilde{\delta}_{\mathrm{q}} + g_{H,n}\left(\kappa,\eta\right) C^2 \tilde{\Delta}_{\mathrm{A}}}{4\tilde{\delta}_{\mathrm{q}}^2 C^2 + h_n\left(\kappa,\eta\right)\tilde{\Delta}_{\mathrm{A}}\tilde{\delta}_{\mathrm{q}} C^2 + j_n\left(\kappa,\eta\right)\tilde{\Delta}_{\mathrm{A}}^2 C^2 + k_n\left(\kappa,\eta\right) C^2} \tag{B.57}$$

$$\Gamma_{n>0} = \frac{\Omega^2}{\gamma'} \frac{4\tilde{\delta}_{\mathrm{q}}^2 C + f_{\Gamma,n}\left(\delta x_{\mathrm{q},1}, \delta x_{\mathrm{q},2}, \kappa, \eta\right) C^3 + g_{\Gamma,n}\left(\delta x_{\mathrm{q},1}, \delta x_{\mathrm{q},2}, \kappa, \eta\right) C^2}{4\tilde{\delta}_{\mathrm{q}}^2 C^2 + h_n\left(\kappa,\eta\right)\tilde{\Delta}_{\mathrm{A}}\tilde{\delta}_{\mathrm{q}} C^2 + j_n\left(\kappa,\eta\right)\tilde{\Delta}_{\mathrm{A}}^2 C^2 + k_n\left(\kappa,\eta\right) C^2}. \tag{B.58}$$

These expressions are used in Chapters (6.1) (for the case where $\delta x_{\mathrm{q},1} = \delta x_{\mathrm{q},2} = 0$) and (6.2) in order to describe the dynamics of the ground states. The various functions in the numerator for Eqs. (B.57) and (B.58) are given by:

$$b_{H,n}\left(\delta x_{\mathrm{q},1}, \delta x_{\mathrm{q},2}, \kappa, \eta\right) = 4\kappa^2\eta^2\left[\cos^2\left(\delta x_{\mathrm{q},1} - \delta x_{\mathrm{q},2}\right) + \sin\left(\delta x_{\mathrm{q},1} - \delta x_{\mathrm{q},2}\right)\sin\left(\delta x_{\mathrm{q},1} + \delta x_{\mathrm{q},2}\right) - 1\right] \tag{B.59}$$

$$f_{H,n}\left(\kappa,\eta\right) = -\kappa^2 - \eta^2 \tag{B.60}$$

$$g_{H,n}\left(\kappa,\eta\right) = -\left(\kappa^2+\eta^2\right)^2 \tag{B.61}$$

$$g_{\Gamma,n}\left(\delta x_{\mathrm{q},1}, \delta x_{\mathrm{q},2}, \kappa, \eta\right) = -2\left[\kappa^{3/2}\cos\left(\delta x_{\mathrm{q},1}\right) + \eta^{3/2}\cos\left(\delta x_{\mathrm{q},2}\right) + \kappa^2 + \eta^2\right] + \left(\kappa^2+\eta^2\right)^2 \tag{B.62}$$

with the last function defined as:

$$f_{\Gamma,n}\left(\delta x_{\mathrm{q},1}, \delta x_{\mathrm{q},2}, \kappa, \eta\right) = \left\{\begin{array}{l} \left(\kappa^2+\eta^2\right)^2 + \kappa^3 + \eta^3 + 2\left(\kappa\eta\right)^{3/2}\cos\left(\delta x_{\mathrm{q},1} - \delta x_{\mathrm{q},2}\right) \\ -2\kappa^{3/2}\eta^2\left[-\cos\left(\delta x_{\mathrm{q},1} - \delta x_{\mathrm{q},2}\right)\cos\left(\delta x_{\mathrm{q},2}\right) + \sin\left(\delta x_{\mathrm{q},1} - \delta x_{\mathrm{q},2}\right)\sin\left(\delta x_{\mathrm{q},2}\right)\right] \\ -2\kappa^{3/2}\left[2\eta^2\cos\left(\delta x_{\mathrm{q},1}\right) + \kappa^2\cos\left(\delta x_{\mathrm{q},1}\right)\right] \\ -2\eta^{3/2}\kappa^2\left[-\cos\left(\delta x_{\mathrm{q},1} - \delta x_{\mathrm{q},2}\right)\cos\left(\delta x_{\mathrm{q},1}\right) + \sin\left(\delta x_{\mathrm{q},1} - \delta x_{\mathrm{q},2}\right)\sin\left(\delta x_{\mathrm{q},1}\right)\right] \\ -2\eta^{3/2}\left[2\kappa^2\cos\left(\delta x_{\mathrm{q},2}\right) + \eta^2\cos\left(\delta x_{\mathrm{q},2}\right)\right] \end{array}\right\} \tag{B.63}$$

The shared functions in the denominator of Eqs. (B.57) and (B.58) are defined as:

$$h_n\left(\kappa,\eta\right) = 8\left(\kappa^2+\eta^2\right) \tag{B.64}$$

$$j_n\left(\kappa,\eta\right) = 4\left(\kappa^2+\eta^2\right)^2 \tag{B.65}$$

$$k_n\left(\kappa,\eta\right) = \left(\kappa^2+\eta^2\right)^2 + 2\left(\kappa^2+\eta^2\right) + 1. \tag{B.66}$$

Appendix C

Additional Contour Plots

This section provides additional plots of the contours for the success probability and fidelity as a function of the displacements of the two qubits. These are plotted for a variety of combinations of qubit dipole moments by changing the value of κ and η. The detunings used for the simply optimised case are:

$$\Delta_{\mathrm{A}} = \frac{\gamma'}{2}\sqrt{C - \frac{1}{2}} \tag{C.1}$$

$$\delta_{\mathrm{q}} = -\frac{7\gamma'}{8\sqrt{C}}, \tag{C.2}$$

while the detunings employed in the complete optimisation are:

$$\Delta_{\mathrm{A,n}} = \frac{\gamma'}{2\kappa^2}\sqrt{\left(-2\kappa^{7/2}\cos\left(k\delta x_{\mathrm{q,n}}\right) + \kappa^4 + \kappa^3\right)C^2 + \kappa^4\left(C-1\right) + 1/2} \tag{C.3}$$

$$\delta_{\mathrm{q}} = \frac{\frac{\gamma'}{8}\left(4\left(\kappa^{3/2}\cos\left(k\delta x_{\mathrm{q,n}}\right) - \kappa^2\right)C + 4\kappa^2 + 3\right)}{\kappa^{3/2}\sin\left(k\delta x_{\mathrm{q,n}}\right)C^2 - \sqrt{\left(-2\kappa^{7/2}\cos\left(k\delta x_{\mathrm{q,n}}\right) + \kappa^4 + \kappa^3\right)C^2 + \kappa^4\left(C-1\right) + 1/2}} \tag{C.4}$$

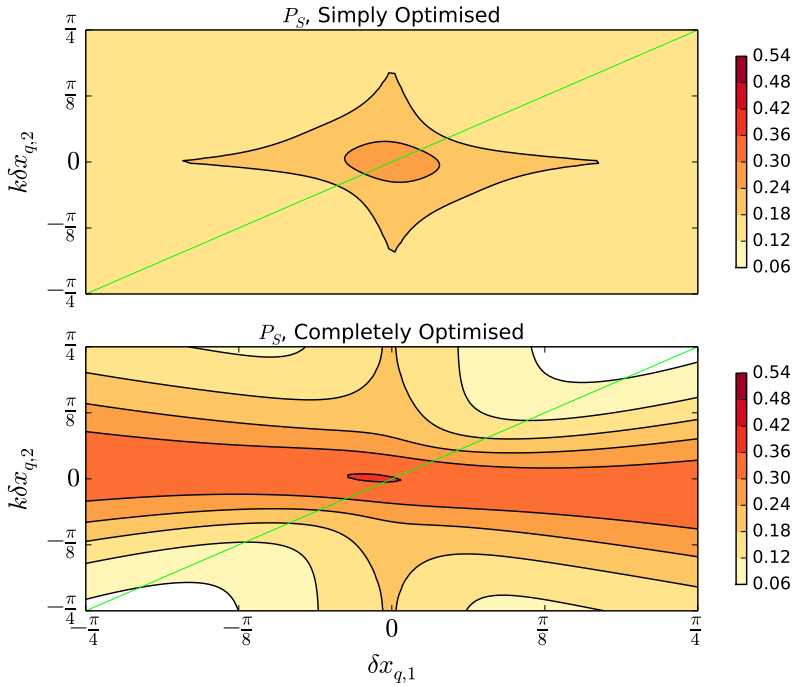

Figure C.1: Plot of the contours for the success probability as a function of the displacement of the two qubits for $\kappa = \eta = 1.3$. Note the massively lowered success probability compared to the case where $\kappa = \eta = 1$

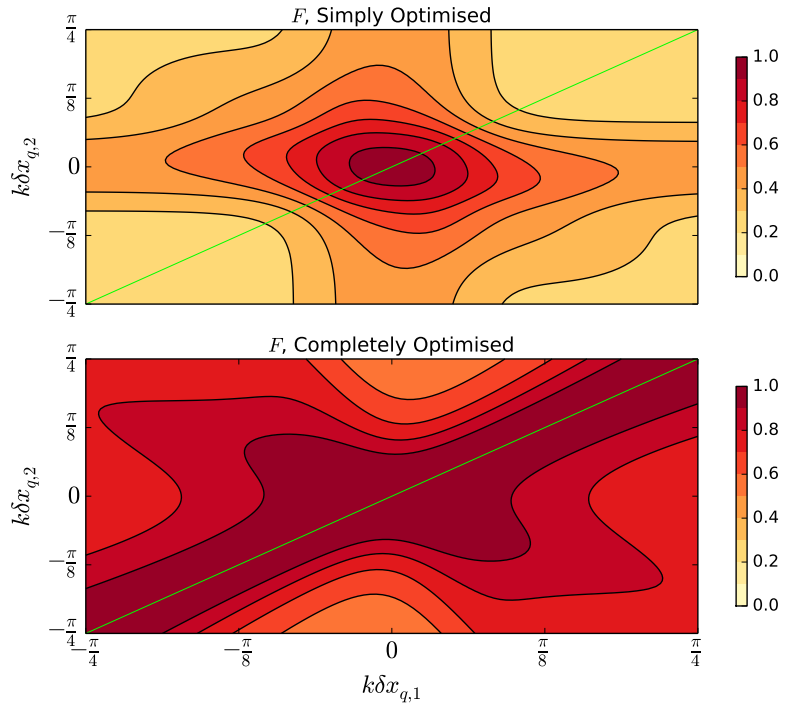

Figure C.2: Plot of the contours for the fidelity as a function of the displacement of the two qubits for $\kappa = \eta = 1.3$.

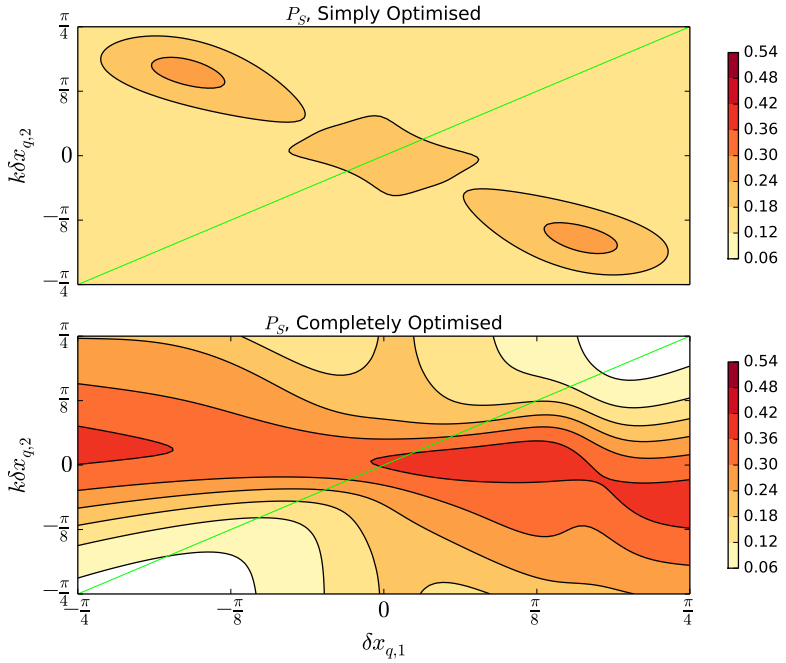

Figure C.3: Plot of the contours for the success probability as a function of the displacement of the two qubits for $\kappa = \eta = 0.75$.

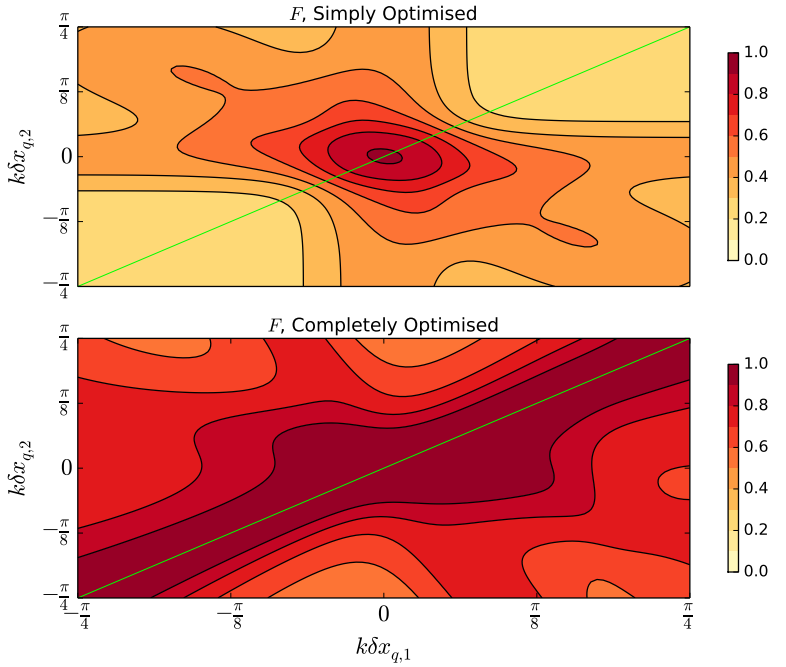

Figure C.4: Plot of the contours for the fidelity as a function of the displacement of the two qubits for $\kappa = \eta = 0.75$.

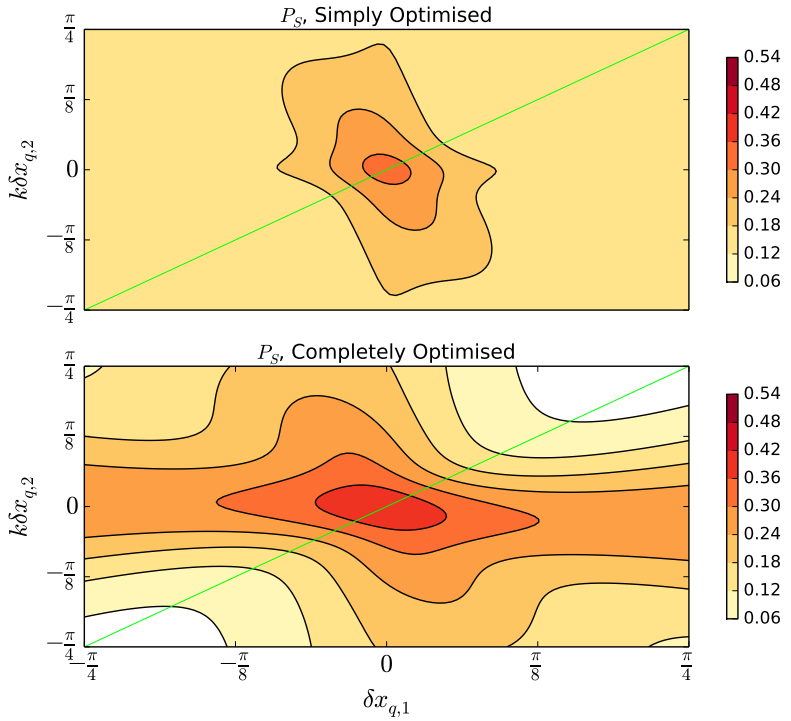

Figure C.5: Plot of the contours for the success probability as a function of the displacement of the two qubits for $\kappa = 1.3$ and $\eta = 0.75$.

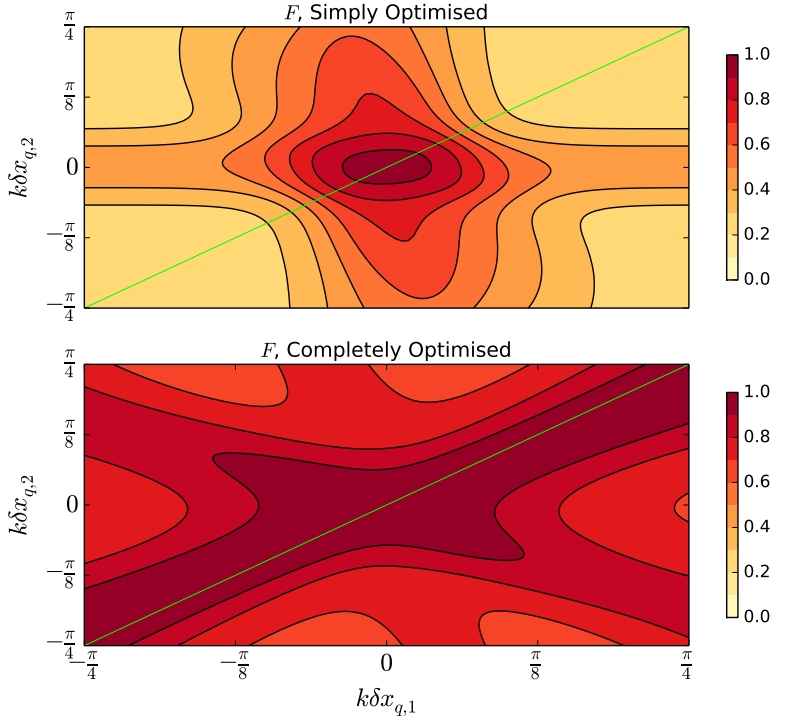

Figure C.6: Plot of the contours for the fidelity as a function of the displacement of the two qubits for $\kappa = 1.3$ and $\eta = 0.75$.

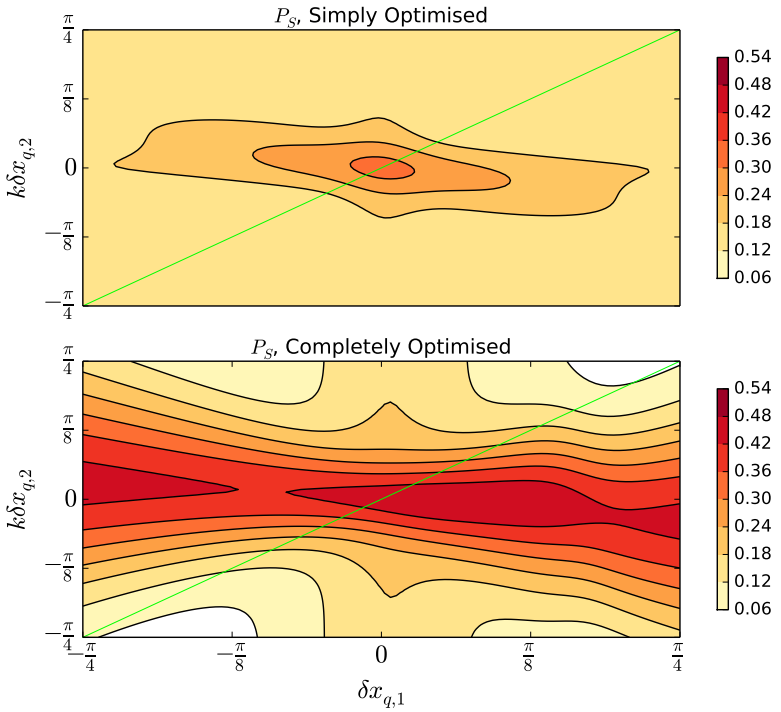

Figure C.7: Plot of the contours for the success probability as a function of the displacement of the two qubits for $\kappa = 0.75$ and $\eta = 1.3$.

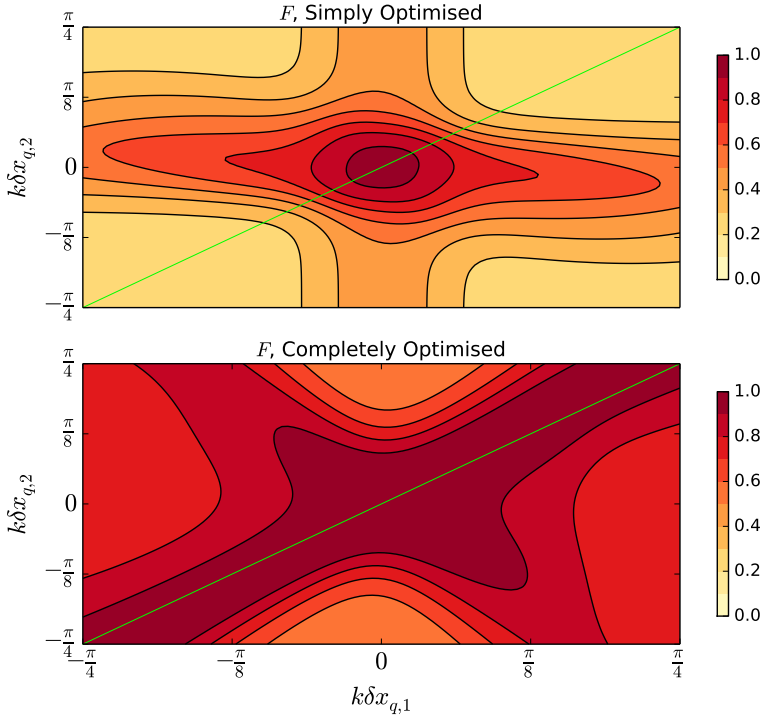

Figure C.8: Plot of the contours for the fidelity as a function of the displacement of the two qubits for $\kappa = 0.75$ and $\eta = 1.3$.

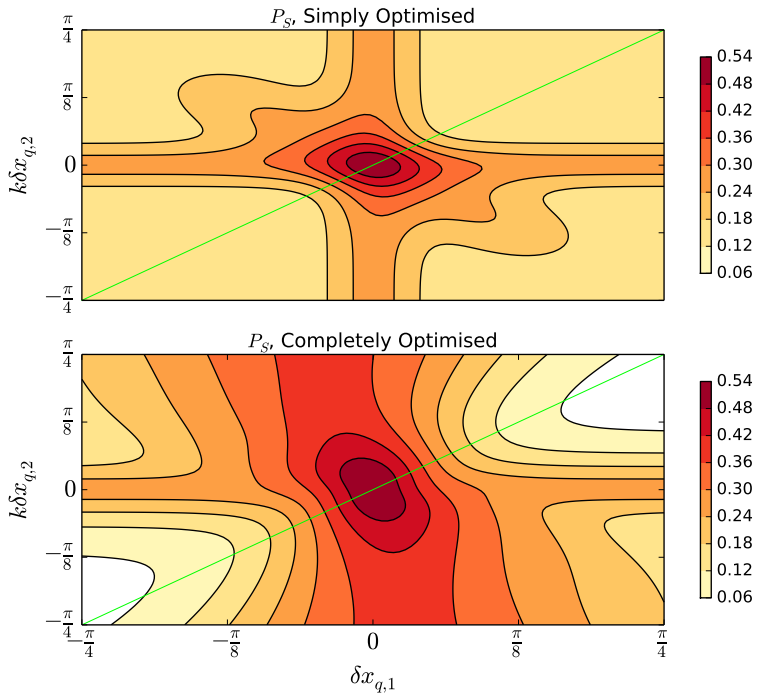

Figure C.9: Plot of the contours for the success probability as a function of the displacement of the two qubits for $\kappa = \eta = 1$. The completely optimising detunings are here evaluated along $\delta x_{\mathrm{q_w}}$, thereby maximising the success probability along this displacement.

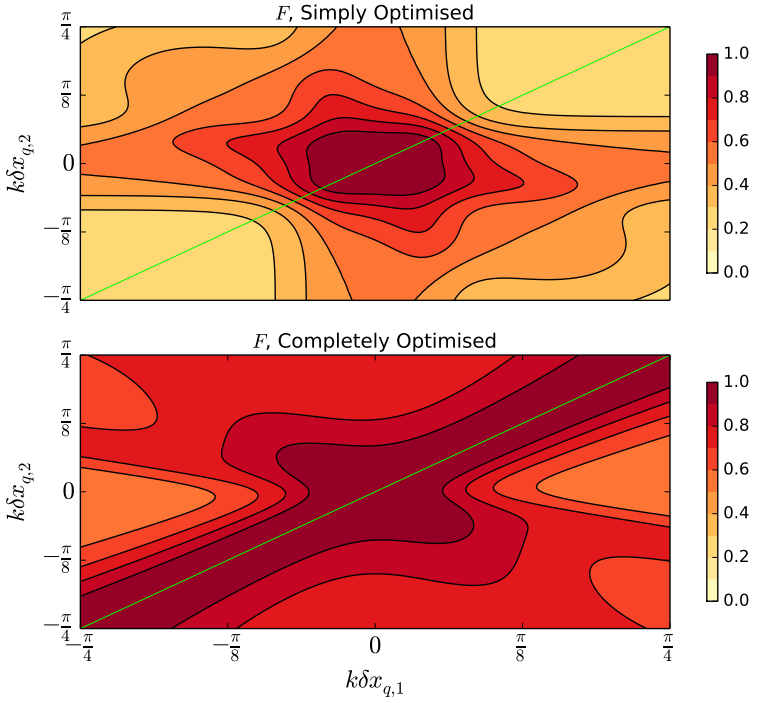

Figure C.10: Same as Fig. (C.10), but for the fidelity.

Appendix D

Solving The Effective Master Equation

The dynamics of an open quantum mechanical system can be described well by the master equation for the density operator:

$$\dot{\rho} = i\left[\hat{H}, \rho\right] + \sum_{k,l} \hat{L}_k \rho \hat{L}_l^\dagger - \frac{1}{2}\sum_{k,l}\left[\hat{L}_k^\dagger \hat{L}_k \rho - \rho \hat{L}_k^\dagger \hat{L}_k\right], \tag{D.1}$$

where $\hat{H}$ is the Hamiltonian for the system and $\hat{L}_k$ is the Lindblad operator describing a source of decay. This assumes that the dynamics of the system is Markovian. The system of equations that can be extracted from Eq. (D.1) will often be large and can be cumbersome to solve. These systems of equations can be simplified by adiabatically eliminating rapidly evolving excited states, resulting in an effective master equation:

$$\dot{\rho} = i\left[\hat{H}_{\text{eff}}, \rho\right] + \sum_{k,l}\left(\hat{L}_{\text{eff}}^k\right)^\dagger \rho \hat{L}_{\text{eff}}^k - \frac{1}{2}\sum_{k,l}\left[\left(\hat{L}_{\text{eff}}^k\right)^\dagger \hat{L}_{\text{eff}}^l \rho - \rho\left(\hat{L}_{\text{eff}}^k\right)^\dagger \hat{L}_{\text{eff}}^l\right], \tag{D.2}$$

where the effective operators are given by:

$$\hat{H}_{\text{eff}} = -\frac{1}{2}\hat{V}_-\left[\hat{H}_{\text{NH}}^{-1} + \left(\hat{H}_{\text{NH}}^{-1}\right)^\dagger\right]\hat{V}_+ + \hat{H}_{\text{g}} \tag{D.3}$$

$$\hat{L}_{\text{eff}}^k = \hat{L}_k \hat{H}_{\text{NH}}^{-1}\hat{V}_+. \tag{D.4}$$

Here $\hat{V}_+$ ($\hat{V}_-$) is a weak (de)excitation laser field and $\hat{H}_{\text{NH}} = \hat{H}_{\text{e}} - \frac{i}{2}\sum_{k,l}\hat{L}_k^\dagger \hat{L}_l$ is the non-Hermitian Hamiltonian of the quantum jump formalism, with $\hat{H}_{\text{e}}$ being the Hamiltonian of the excited state manifold and $\hat{H}_{\text{g}}$ for the ground state manifold. The following sections will show the derivation of the system of equations describing the dynamics of the system discussed in this work.

D.1 The Effective Operators

The effective operators are derived in Appendix (B) and have the general form:

$$\hat{H}_{\text{eff}} = \sum_{n=0}^{2} \Delta_n \left|\text{g}\right\rangle_{\text{A}} \left\langle\text{g}\right| \otimes \hat{P}_{\text{n}} \tag{D.5}$$

$$\hat{L}_{\text{eff}}^A = \sum_{n=0}^{2} r_{\text{A},n} \left|\text{f}\right\rangle_{\text{A}} \left\langle\text{g}\right| \otimes \hat{P}_{\text{n}} \tag{D.6}$$

$$\hat{L}_{\text{eff}}^{q_j} = \sum_{n=1}^{2} r_{\text{q}_j,n} \left|\text{f}\right\rangle_{\text{A}} \left\langle\text{g}\right| \otimes \hat{P}_{\text{n}}, \tag{D.7}$$

where Pn projects onto the states where there are n qubits in state $|1\rangle$:

$$\hat{P}_2 = |11\rangle_{\mathrm{q}} \langle 11| \tag{D.8}$$

$$\hat{P}_{1,1} = |01\rangle_{\mathrm{q}} \langle 01| \tag{D.9}$$

$$\hat{P}_{1,2} = |10\rangle_{\mathrm{q}} \langle 10| \tag{D.10}$$

$$\hat{P}_0 = |00\rangle_{\mathrm{q}} \langle 00| . \tag{D.11}$$

The gate in question is conditioned on measuring the state of the auxiliary quantum dot to be in state $|\mathrm{g}\rangle_{\mathrm{A}}$, so the second term in Eq. (D.2) will not contribute to the success probability or the fidelity of the gate and can thus be omitted from the following discussion. An arbitrary input state for the qubits of the form $|\psi(t)\rangle = c_{00}(t)|00\rangle_{\mathrm{q}} + c_{01}(t)|01\rangle_{\mathrm{q}} + c_{10}(t)|10\rangle_{\mathrm{q}} + c_{11}(t)|11\rangle_{\mathrm{q}}$ is considered for the following. The density matrix is given by $\rho = |\psi\rangle\langle\psi| = \sum_{mn} \rho_n^m(t)|m\rangle\langle n|$, where $\rho_n^m(t) = c_m(t)\, c_n(t)^*$ with $m, n = \{00, 01, 10, 11\}$. The coherent part of the effective master equation is given by:

$$-i\left[\hat{H}_{\mathrm{eff}}, \rho\right] = -i\sum_{n=0}^{2} \Delta_n \left(\hat{P}_{\mathrm{n}}\rho - \rho\hat{P}_{\mathrm{n}}\right) \tag{D.12}$$

$$\begin{aligned}
= \; & -i\Delta_0 \left(\rho_{00}^{00}|00\rangle_{\mathrm{q}}\langle 00| + \rho_{01}^{00}|00\rangle_{\mathrm{q}}\langle 01| + \rho_{10}^{00}|00\rangle_{\mathrm{q}}\langle 10| + \rho_{11}^{00}|00\rangle_{\mathrm{q}}\langle 11| \right. && \text{(D.13)}\\
& \left. -\rho_{00}^{00}|00\rangle_{\mathrm{q}}\langle 00| - \rho_{00}^{01}|01\rangle_{\mathrm{q}}\langle 00| - \rho_{00}^{10}|10\rangle_{\mathrm{q}}\langle 00| - \rho_{00}^{11}|11\rangle_{\mathrm{q}}\langle 00| \right) && \text{(D.14)}\\
& -i\Delta_{1,1} \left(\rho_{00}^{01}|01\rangle_{\mathrm{q}}\langle 00| + \rho_{01}^{01}|01\rangle_{\mathrm{q}}\langle 01| + \rho_{10}^{01}|01\rangle_{\mathrm{q}}\langle 10| + \rho_{11}^{01}|01\rangle_{\mathrm{q}}\langle 11| \right. && \text{(D.15)}\\
& \left. -\rho_{01}^{00}|00\rangle_{\mathrm{q}}\langle 01| - \rho_{01}^{01}|01\rangle_{\mathrm{q}}\langle 01| - \rho_{01}^{10}|10\rangle_{\mathrm{q}}\langle 01| - \rho_{01}^{11}|11\rangle_{\mathrm{q}}\langle 01| \right) && \text{(D.16)}\\
& -i\Delta_{1,2} \left(\rho_{00}^{10}|10\rangle_{\mathrm{q}}\langle 00| + \rho_{01}^{10}|10\rangle_{\mathrm{q}}\langle 01| + \rho_{10}^{10}|10\rangle_{\mathrm{q}}\langle 10| + \rho_{11}^{10}|10\rangle_{\mathrm{q}}\langle 11| \right. && \text{(D.17)}\\
& \left. -\rho_{10}^{00}|00\rangle_{\mathrm{q}}\langle 10| - \rho_{10}^{01}|01\rangle_{\mathrm{q}}\langle 10| - \rho_{10}^{10}|10\rangle_{\mathrm{q}}\langle 10| - \rho_{10}^{11}|11\rangle_{\mathrm{q}}\langle 10| \right) && \text{(D.18)}\\
& -i\Delta_2 \left(\rho_{00}^{11}|11\rangle_{\mathrm{q}}\langle 00| + \rho_{01}^{11}|11\rangle_{\mathrm{q}}\langle 01| + \rho_{10}^{11}|11\rangle_{\mathrm{q}}\langle 10| + \rho_{11}^{11}|11\rangle_{\mathrm{q}}\langle 11| \right. && \text{(D.19)}\\
& \left. -\rho_{11}^{00}|00\rangle_{\mathrm{q}}\langle 11| - \rho_{11}^{01}|01\rangle_{\mathrm{q}}\langle 11| - \rho_{11}^{10}|10\rangle_{\mathrm{q}}\langle 11| - \rho_{11}^{11}|11\rangle_{\mathrm{q}}\langle 11| \right) . && \text{(D.20)}
\end{aligned}$$

All possible no-jump terms in the dissipative part of Eq. (D.2) are listed here for convenience $\{\}$ denotes that there is an additional term where A and $\mathrm{q_k}$ have been interchanged. All off the following expressions are multiplied by $\otimes|\mathrm{g}\rangle_{\mathrm{A}}\langle\mathrm{g}|$. The dissipative no-jump terms for $n = 2$ are given by, where k, l denotes a term corresponding to either the first or the second qubit:

$$\left(\hat{L}_{\mathrm{A2}}^{\mathrm{Eff}}\right)^{\dagger} \hat{L}_{\mathrm{A2}}^{\mathrm{Eff}}\rho = \left|r_2^{\mathrm{A}}\right|^2 \left(\rho_{00}^{11}|11\rangle_{\mathrm{q}}\langle 00| + \rho_{01}^{11}|11\rangle_{\mathrm{q}}\langle 01| + \rho_{10}^{11}|11\rangle_{\mathrm{q}}\langle 10| + \rho_{11}^{11}|11\rangle_{\mathrm{q}}\langle 11|\right) \tag{D.21}$$

$$\rho\left(\hat{L}_{\mathrm{A2}}^{\mathrm{Eff}}\right)^{\dagger} \hat{L}_{\mathrm{A2}}^{\mathrm{Eff}} = \left|r_2^{\mathrm{A}}\right|^2 \left(\rho_{11}^{00}|00\rangle_{\mathrm{q}}\langle 11| + \rho_{11}^{01}|01\rangle_{\mathrm{q}}\langle 11| + \rho_{11}^{10}|10\rangle_{\mathrm{q}}\langle 11| + \rho_{11}^{11}|11\rangle_{\mathrm{q}}\langle 11|\right) \tag{D.22}$$

$$\left(\hat{L}_{\mathrm{q_k2}}^{\mathrm{Eff}}\right)^{\dagger} \hat{L}_{\mathrm{q_l2}}^{\mathrm{Eff}}\rho = r_{2,\mathrm{k}}^{\mathrm{q}} \left(r_{2,\mathrm{l}}^{\mathrm{q}}\right)^* \left(\rho_{00}^{11}|11\rangle_{\mathrm{q}}\langle 00| + \rho_{01}^{11}|11\rangle_{\mathrm{q}}\langle 01| + \rho_{10}^{11}|11\rangle_{\mathrm{q}}\langle 10| + \rho_{11}^{11}|11\rangle_{\mathrm{q}}\langle 11|\right) \tag{D.23}$$

$$\rho\left(\hat{L}_{\mathrm{q_k2}}^{\mathrm{Eff}}\right)^{\dagger} \hat{L}_{\mathrm{q_l2}}^{\mathrm{Eff}} = r_{2,\mathrm{k}}^{\mathrm{q}} \left(r_{2,\mathrm{l}}^{\mathrm{q}}\right)^* \left(\rho_{11}^{00}|00\rangle_{\mathrm{q}}\langle 11| + \rho_{11}^{01}|01\rangle_{\mathrm{q}}\langle 11| + \rho_{11}^{10}|10\rangle_{\mathrm{q}}\langle 11| + \rho_{11}^{11}|11\rangle_{\mathrm{q}}\langle 11|\right) \tag{D.24}$$

$$\left\{\left(\hat{L}_{\mathrm{A2}}^{\mathrm{Eff}}\right)^{\dagger} \hat{L}_{\mathrm{q_k2}}^{\mathrm{Eff}}\rho\right\} = r_2^{\mathrm{A}} \left(r_{2,\mathrm{k}}^{\mathrm{q}}\right)^* \left(\rho_{00}^{11}|11\rangle_{\mathrm{q}}\langle 00| + \rho_{01}^{11}|11\rangle_{\mathrm{q}}\langle 01| + \rho_{10}^{11}|11\rangle_{\mathrm{q}}\langle 10| + \rho_{11}^{11}|11\rangle_{\mathrm{q}}\langle 11|\right) \tag{D.25}$$

$$\left\{\rho\left(\hat{L}_{\mathrm{A2}}^{\mathrm{Eff}}\right)^{\dagger} \hat{L}_{\mathrm{q_k2}}^{\mathrm{Eff}}\right\} = r_2^{\mathrm{A}} \left(r_{2,\mathrm{k}}^{\mathrm{q}}\right)^* \left(\rho_{11}^{00}|00\rangle_{\mathrm{q}}\langle 11| + \rho_{11}^{01}|01\rangle_{\mathrm{q}}\langle 11| + \rho_{11}^{10}|10\rangle_{\mathrm{q}}\langle 11| + \rho_{11}^{11}|11\rangle_{\mathrm{q}}\langle 11|\right) \tag{D.26}$$

The dissipative terms when only the first qubit is optically connected to the waveguide are given by

$$\left(\hat{L}^{\mathrm{Eff}}_{\mathrm{A1},1}\right)^{\dagger}\hat{L}^{\mathrm{Eff}}_{\mathrm{A1},1}\rho = \left|r^{\mathrm{A}}_{1,1}\right|^2\left(\rho^{10}_{00}\left|10\right\rangle_{\mathrm{q}}\left\langle 00\right| + \rho^{10}_{01}\left|10\right\rangle_{\mathrm{q}}\left\langle 01\right| + \rho^{10}_{10}\left|10\right\rangle_{\mathrm{q}}\left\langle 10\right| + \rho^{10}_{11}\left|10\right\rangle_{\mathrm{q}}\left\langle 11\right|\right) \tag{D.27}$$

$$\rho\left(\hat{L}^{\mathrm{Eff}}_{\mathrm{A1},1}\right)^{\dagger}\hat{L}^{\mathrm{Eff}}_{\mathrm{A1},1} = \left|r^{\mathrm{A}}_{1,1}\right|^2\left(\rho^{00}_{10}\left|00\right\rangle_{\mathrm{q}}\left\langle 10\right| + \rho^{01}_{10}\left|01\right\rangle_{\mathrm{q}}\left\langle 10\right| + \rho^{10}_{10}\left|10\right\rangle_{\mathrm{q}}\left\langle 10\right| + \rho^{11}_{10}\left|11\right\rangle_{\mathrm{q}}\left\langle 10\right|\right) \tag{D.28}$$

$$\left(\hat{L}^{\mathrm{Eff}}_{\mathrm{q1},1}\right)^{\dagger}\hat{L}^{\mathrm{Eff}}_{\mathrm{q1},1}\rho = \left|r^{\mathrm{q}}_{1,1}\right|^2\left(\rho^{10}_{00}\left|10\right\rangle_{\mathrm{q}}\left\langle 00\right| + \rho^{10}_{01}\left|10\right\rangle_{\mathrm{q}}\left\langle 01\right| + \rho^{10}_{10}\left|10\right\rangle_{\mathrm{q}}\left\langle 10\right| + \rho^{10}_{11}\left|10\right\rangle_{\mathrm{q}}\left\langle 11\right|\right) \tag{D.29}$$

$$\rho\left(\hat{L}^{\mathrm{Eff}}_{\mathrm{q1},1}\right)^{\dagger}\hat{L}^{\mathrm{Eff}}_{\mathrm{q1},1} = \left|r^{\mathrm{q}}_{1,1}\right|^2\left(\rho^{00}_{10}\left|00\right\rangle_{\mathrm{q}}\left\langle 10\right| + \rho^{01}_{10}\left|01\right\rangle_{\mathrm{q}}\left\langle 10\right| + \rho^{10}_{10}\left|10\right\rangle_{\mathrm{q}}\left\langle 10\right| + \rho^{11}_{10}\left|11\right\rangle_{\mathrm{q}}\left\langle 10\right|\right) \tag{D.30}$$

$$\left\{\left(\hat{L}^{\mathrm{Eff}}_{\mathrm{A1},1}\right)^{\dagger}\hat{L}^{\mathrm{Eff}}_{\mathrm{q1},1}\rho\right\} = r^{\mathrm{A}}_{1,1}\left(r^{\mathrm{q}}_{1,1}\right)^{*}\left(\rho^{10}_{00}\left|10\right\rangle_{\mathrm{q}}\left\langle 00\right| + \rho^{10}_{01}\left|10\right\rangle_{\mathrm{q}}\left\langle 01\right| + \rho^{10}_{10}\left|10\right\rangle_{\mathrm{q}}\left\langle 10\right| + \rho^{10}_{11}\left|10\right\rangle_{\mathrm{q}}\left\langle 11\right|\right) \tag{D.31}$$

$$\left\{\rho\left(\hat{L}^{\mathrm{Eff}}_{\mathrm{A1},1}\right)^{\dagger}\hat{L}^{\mathrm{Eff}}_{\mathrm{q1},1}\right\} = r^{\mathrm{A}}_{1,1}\left(r^{\mathrm{q}}_{1,1}\right)^{*}\left(\rho^{00}_{10}\left|00\right\rangle_{\mathrm{q}}\left\langle 10\right| + \rho^{01}_{10}\left|01\right\rangle_{\mathrm{q}}\left\langle 10\right| + \rho^{10}_{10}\left|10\right\rangle_{\mathrm{q}}\left\langle 10\right| + \rho^{11}_{10}\left|11\right\rangle_{\mathrm{q}}\left\langle 10\right|\right) \tag{D.32}$$

The terms corresponding to the case where only the second qubit is connected can be written down by setting $r^{\mathrm{A}}_{1,1} \to r^{\mathrm{A}}_{1,2}$ and $r^{\mathrm{q}}_{1,1} \to r^{\mathrm{q}}_{1,2}$. The contributions to the effective master equation for the case where $n = 0$ are:

$$\left(\hat{L}^{\mathrm{Eff}}_{\mathrm{A0}}\right)^{\dagger}\hat{L}^{\mathrm{Eff}}_{\mathrm{A0}}\rho = \left|r^{\mathrm{A}}_{0}\right|^2\left(\rho^{00}_{00}\left|00\right\rangle_{\mathrm{q}}\left\langle 00\right| + \rho^{00}_{01}\left|00\right\rangle_{\mathrm{q}}\left\langle 01\right| + \rho^{00}_{10}\left|00\right\rangle_{\mathrm{q}}\left\langle 10\right| + \rho^{00}_{11}\left|00\right\rangle_{\mathrm{q}}\left\langle 11\right|\right)\otimes\left|\mathrm{g}\right\rangle_{\mathrm{A}}\left\langle \mathrm{g}\right| \tag{D.33}$$

$$\rho\left(\hat{L}^{\mathrm{Eff}}_{\mathrm{A0}}\right)^{\dagger}\hat{L}^{\mathrm{Eff}}_{\mathrm{A0}} = \left|r^{\mathrm{A}}_{0}\right|^2\left(\rho^{00}_{00}\left|00\right\rangle_{\mathrm{q}}\left\langle 00\right| + \rho^{01}_{00}\left|01\right\rangle_{\mathrm{q}}\left\langle 00\right| + \rho^{10}_{00}\left|10\right\rangle_{\mathrm{q}}\left\langle 00\right| + \rho^{11}_{00}\left|11\right\rangle_{\mathrm{q}}\left\langle 00\right|\right)\otimes\left|\mathrm{g}\right\rangle_{\mathrm{A}}\left\langle \mathrm{g}\right| \tag{D.34}$$

Any jump term in Eq. (D.2) for any of the four non-hermitian Hamiltonians take the following form:

$$\hat{L}_k\rho\hat{L}_l^{\dagger} \propto r^{\mathrm{k}}_{\mathrm{n}}\left(r^{\mathrm{l}}_{\mathrm{n}}\right)^{*}\rho_{ee}. \tag{D.35}$$

The initialization scheme presented in Section (3.3) ensures that the population of the excited states of the quantum dots is nearly empty. The effects of the jump terms can thus be neglected in this work. The Lindblad coefficients can be used to define the following decay rates:

$$\Gamma_0 \equiv \left|r^{\mathrm{A}}_{0}\right|^2 \tag{D.36}$$

$$\Gamma_{1,1} \equiv \left|r^{\mathrm{A}}_{1,1}\right|^2 + \left|r^{\mathrm{q}}_{1,1}\right|^2 + r^{\mathrm{A}}_{1,1}\left(r^{\mathrm{q}}_{1,1}\right)^{*} + r^{\mathrm{q}}_{1,1}\left(r^{\mathrm{A}}_{1,1}\right)^{*} \tag{D.37}$$

$$\Gamma_{1,2} \equiv \left|r^{\mathrm{A}}_{1,2}\right|^2 + \left|r^{\mathrm{q}}_{1,2}\right|^2 + r^{\mathrm{A}}_{1,2}\left(r^{\mathrm{q}}_{1,2}\right)^{*} + r^{\mathrm{q}}_{1,2}\left(r^{\mathrm{A}}_{1,2}\right)^{*} \tag{D.38}$$

$$\Gamma_2 \equiv \left.\begin{array}{l}\left|r^{\mathrm{A}}_{2}\right|^2 + \left|r^{\mathrm{q}}_{2,1}\right|^2 + \left|r^{\mathrm{q}}_{2,1}\right|^2 + r^{\mathrm{q}}_{2,1}\left(r^{\mathrm{q}}_{2,2}\right)^{*} + r^{\mathrm{q}}_{2,2}\left(r^{\mathrm{q}}_{2,1}\right)^{*} \\ + r^{\mathrm{A}}_{2}\left(r^{\mathrm{q}}_{2,1}\right)^{*} + r^{\mathrm{A}}_{2}\left(r^{\mathrm{q}}_{2,1}\right)^{*} + r^{\mathrm{q}}_{2,1}\left(r^{\mathrm{A}}_{2}\right)^{*} + r^{\mathrm{q}}_{2,2}\left(r^{\mathrm{A}}_{2}\right)^{*}\end{array}\right\} \tag{D.39}$$

The equations of motion for the system can now be found by projecting onto the effective master equation, which results in sixteen differential equations of the form:

$$\dot{\rho}^{x}_{y} = i\left(\Delta_y - \Delta_x\right)\rho^{x}_{y}\left(t\right) - \frac{1}{2}\left(\Gamma_x + \Gamma_y\right)\rho^{x}_{y}\left(t\right), \quad x, y = \left\{\underset{n=0}{00}, \underset{n=1}{01}, \underset{n=1}{10}, \underset{n=2}{11}\right\}, \tag{D.40}$$

where the notation underneath each element in the definition of x and y indicates the number of qubits in $\left|1\right\rangle_{\mathrm{q}}$. This equation has a straightforward solution:

$$\rho^{y}_{x}\left(t\right) = \rho^{y}_{x}\left(t=0\right)e^{i\left(\Delta_y - \Delta_x\right)t}e^{-\frac{1}{2}\left(\Gamma_x + \Gamma_y\right)t}. \tag{D.41}$$

The off-diagonal elements has has a dynamical change in phase set by the energy shifts Δ_n and are exponentially decaying set by various sums of the decay rates in Eqs. (D.37) through (D.39), while the only time evolution for the diagonal elements is an exponential decay set by Γ_n.

Bibliography

[1] M. Arcari et al. Near-Unity Coupling Efficiency of a Quantum Emitter to a Photonic Crystal Waveguide. Phys. Rev. Lett., 113:093603, Aug 2014.

[2] M. D. Barrett et al. Deterministic Quantum Teleportation of Atomic Qubits. Nature, 249:737–739, Jun 2004.

[3] J. Borregaard, P. Kómár, E. M. Kessler, A. S. Sørensen, and M. D. Lukin. Heralded Quantum Gates with Integrated Error Detection in Optical Cavities. Phys. Rev. Lett., 114:110502, Mar 2015.

[4] H. Bruus and K. Flensberg. Many-body quantum theory in condensed matter physics - an introduction. Oxford University Press, 2004.

[5] J. I. Cirac and P. Zoller. Quantum Computations with Cold Trapped Ions. Phys. Rev. Lett., 74:4091–4094, May 1995.

[6] J. Dalibard, Y. Castin, and K. Mølmer. Wave-function approach to dissipative processes in quantum optics. Phys. Rev. Lett., 68:580–583, Feb 1992.

[7] D. P. DiVincenzo. The Physical Implementation of Quantum Computation. Fortschritte der Physik, 48(9-11):771–783, 2000.

[8] J. Dreiser, M. Atatüre, C. Galland, T. Müller, A. Badolato, and A. Imamoglu. Optical investigations of quantum dot spin dynamics as a function of external electric and magnetic fields. Phys. Rev. B, 77:075317, Feb 2008.

[9] H. T. Dung, L. Knöll, and D.-G. Welsch. Resonant dipole-dipole interaction in the presence of dispersing and absorbing surroundings. Phys. Rev. A, 66:063810, Dec 2002.

[10] J. Eisert and M. M. Wolf. Quantum computing. In Handbook of nature-inspired and innovative computing, pages 253–286. Springer US, 2006.

[11] R. P. Feynman. Simulating Physics with Computers. International Journal of Theoretical Physics, 21:467–488, June 1982.

[12] N. Gisin, G. Ribordy, W. Tittel, and H. Zbinden. Quantum cryptography. Rev. Mod. Phys., 74:145–195, Mar 2002.

[13] P. Lodahl, S. Mahmoodian, and S. Stobbe. Interfacing single photons and single quantum dots with photonic nanostructures. Rev. Mod. Phys., 87:347–400, May 2015.

[14] K. H. Madsen, S. Ates, J. Liu, A. Javadi, S. M. Albrecht, I. Yeo, S. Stobbe, and P. Lodahl. Efficient out-coupling of high-purity single photons from a coherent quantum dot in a photonic-crystal cavity. Phys. Rev. B, 90:155303, Oct 2014.

[15] G. E. Moore. Cramming more components onto integrated circuits. Electronics, 38, April 1965.

[16] L. Novotny and B. Hecht. Principles of Nano-Optics. Cambridge University Press, 2006.

[17] J. Preskill. Lecture notes for physics 229: Quantum information and computation, 1998.

[18] F. Reiter and A. S. Sørensen. Effective operator formalism for open quantum systems. Phys. Rev. A, 85:032111, Mar 2012.

[19] R. Rudgley. The Lost Civilizations of the Stone Age. A Touchstone Book. Free Press, 2000.

[20] J. Sakurai and J. Napolitano. Modern Quantum Mechanics. Addison-Wesley, 2011.

[21] J. M. Smith, P. A. Dalgarno, R. J. Warburton, A. O. Govorov, K. Karrai, B. D. Gerardot, and P. M. Petroff. Voltage Control of the Spin Dynamics of an Exciton in a Semiconductor Quantum Dot. Phys. Rev. Lett., 94:197402, May 2005.

[22] Y. A. Vlasov et al. Active control of slow light on a chip with photonic crystal waveguides. Nature, 438:65–69, Nov 2005.

[23] C. P. Williams. Quantum Gates, pages 51–122. Springer London, London, 2011.

[24] P. Yao, V. Manga Rao, and S. Hughes. On-chip single photon sources using planar photonic crystals and single quantum dots. Laser & Photonics Reviews, 4(4):499–516, 2010.